
**Università degli Studi di Palermo**

**SCUOLA POLITECNICA**

Dipartimento di Ingegneria Civile, Ambientale, Aerospaziale, dei Materiali

Dottorato in Ingegneria Civile e Ambientale

Materiali

ciclo XXVI

Coor.: Prof. Orazio Giuffrè


**PH.D. THESIS**

# 3D fractional viscoelasticity with applications to structural engineering


Candidato:

**Ing. Gioacchino Alotta**

Relatori:

**Ch.mo Prof. Mario Di Paola**

**Ch.mo Prof. Alan C.F. Cocks**
**(*University of Oxford*)**

**Dr. Olga Barrera**
**(*University of Oxford*)**



**S.S.D. ICAR/08**

# 3D fractional viscoelasticity with applications to structural engineering

Ph.D thesis submitted to the University of Palermo

by

***Alotta Gioacchino***

Dipartimento di Ing. Civile Ambientale, Aerospaziale, dei Materiali
Università degli Studi di Palermo
Scuola Politecnica
Viale delle Scienze, Ed. 8 - 90128 Palermo

ALOTTA GIOACCHINO
Palermo, January 2016
e-mail:gioacchino.alotta@unipa.it
e-mail:gioacalo@gmail.com

Thesis of the Ph.D. course in *Civil and Environmental Engineering - Materials (Ingegneria Civile e Ambientale - Materiali)*
Dipartimento di Ingegneria Civile, Ambientale, Aerospaziale, dei Materiali
Università degli Studi di Palermo
Scuola Politecnica
Viale delle Scienze, Ed.8 - 90128 Palermo, ITALY

Written in LaTeX
Examples and figures made with *Wolfram Mathematica*©

# Contents

# List of Figures

# Introduction

## Aims and reasons

The main purpose of this thesis is to provide a tool for the analysis of engineering components that are made of viscoelastic materials. Indeed it is well known that in the field of civil, mechanical and aerospace engineering viscoelastic materials are more and more used; a classical example are polymeric materials, used for composites panel, pultruded beam or other applications, that because of their micro-structure exhibit evident viscoelastic behavior, but also soils, asphalt mixtures, wood and many other materials are surely viscoelastic. Moreover in the last decades great importance have been assuming in the field of biomechanics the mechanical modeling of biological tissues, such as bones, arteries and many others; this "materials" have a strong viscoelastic behavior as polymers have.
Viscoelastic materials are characterized by the dual phenomena of the creep and relaxation; in the first, the strain increases with time when a constant stress is applied, while in the second the stress decreases with time when a constant strain is applied. Then viscoelastic materials are time dependent materials, usually in literature it is referred to them as rate-dependent materials; in contrast with purely elastic materials, for the viscoelastic material the time variable must be taken into account in the analysis. Moreover, viscoelastic materials have memory; in other words the actual state (stresses/strains) depends not only of the current strain/stress but also on the past states.
The correct definition of the stresses and strains in engineering components made of viscoelastic materials can not disregard the viscoelastic properties of the material at hands, otherwise the structural design of the component would lead to erroneous results with consequences for the reliability and durability of the component itself and then consequences for the human life.

## Mathematical tools

In solid mechanics, viscoelastic materials have been modeled for decades with an approach involving classical differential calculus; that is, the stress-strain relationship involves integer order integro-differential operators. The creep and relaxation laws of these mechanical models involve exponential functions. This classical approach allows a relatively easy manipulation of governing equations; however, in contrast with the behavior of real materials that have a long *fading* memory, these models have short memory, or can have long memory if many mechanical parameters are introduced with consequent difficulties in the fitting of experimental data.
It is well known from the beginning of the twentieth century that experimental results of creep and relaxation tests are well fitted by power law type functions and not by exponential; starting from this fact, the use of the fundamental law of linear viscoelasticity, that is the Boltzmann superposition principle, in conjunction with power law creep and relaxation functions, leads to stress-strain relationship in terms of real order integro-differential operators, that are usually labeled as *fractional* derivatives and integrals; the branch of mathematics that study this operators is called *Fractional calculus*. With this approach, the fitting of experimental data is easier because involves few parameters and the mechanical model is able to reproduce both the short and long term behavior of the viscoelastic material at hands. However, the use this approach implies the need of an initial effort to learn how to manipulate fractional operators and fractional differential equations; in the author's opinion this effort is not big as it could appear at first glance.

## 3D fractional viscoelasticity

Fractional viscoelasticity has been widely studied from a theoretical points of way both by mathematicians and engineers; many experimental results of 1D tests are available in literature and they confirm that in 1D conditions fractional viscoelasticity is the best approach to model the behavior of viscoelastic materials. Advantages have been demonstrated by researchers also when the problem involves stochastic loading of the system. However, 1D models are not enough when there is the need is to study real engineering components. The fitting of 3D experimental tests needs the definition of a proper 3D constitutive law as well as the structural analysis of complex shaped engineering components. In the last years some 3D fractional viscoelastic models have

been proposed, but never the behavior is investigated in simple 3D conditions and in real applications. For these reasons in this thesis a series of linear isotropic 3D fractional viscoelastic models is proposed and their behavior is investigated by considering ideal creep and relaxation tests in 3D conditions. These models constitutes the most simple fractional models that can be defined and from the theoretical point of view they represents a benchmark to learn how to manipulate such a kind of model. Of course a complete description of real material behavior should include anisotropicity, when effectively present, and hyperelasticity that is present in many polymers and biological tissues, but it useful to start with something simple to increase gradually the difficulty of the problem.

## The finite element method

The definition of 3D constitutive models, however, is not enough to predict the distribution and the history of strain and stress in a complex shaped component; indeed, already the elastic solution can be obtained only in a few very simple cases. For this reason, in order to model real engineering components as fractional viscoelastic, the model of fractional viscoelasticity must be implemented in finite element framework. Many researchers, in fact, are attracted by fractional viscoelasticity, but any of the available commercial finite element software contains in its material library the possibility to characterize the constitutive behavior as fractional viscoelastic. For this reason, in this thesis this issue has been addressed.
The finite elements type definitions in terms of spatial discretization already available in literature are also good for fractional viscoelasticity; then the only efforts has been devoted to the time discretization in order to allows the finite element software to numerically integrate the governing equations in both explicit and implicit (with the Newton-Raphson method) schemes; user material subroutine codes have been obtained and provided. One problem that came out from the implementation is due to the fading memory of the fractional viscoelastic models that implies the needs to memorize all the history of stress and/or strain for each integration point of the finite element model; for this reason the amount of memory required to run an analysis could be prohibitive, but it shown that it is already possible to run analysis for models discretized with a large number of finite elements and with a large number of time increments by using normal computer.

In this work the implementation has been tested in the finite element software Abaqus 6.14, but the implementation is possible in other software that allows the definition of user material by mean of subroutines.

## Organization of the thesis

The thesis is subdivided in five main chapters and an appendix. The appendix contains the definition of some integral transforms and of some special functions that become of everyday use when one works with the fractional calculus.
The first chapter shows basic concepts and definitions of fractional calculus and provide some tools useful to manipulate and solve fractional differential equation, that is mainly the integral transform of fractional operators.
Chapter 2 introduces basic concepts of linear viscoelasticity and 1D fractional viscoelasticity. Chapter 3 is devoted to the formulation of 3D fractional viscoelastic models and the study of their behavior.
Chapter 4 deals with the implementation of 3D fractional viscoelasticity in a finite element framework.
Finally, Chapter 5 shows some applications of fractional viscoelasticity:

- propose of fractionally damped Tajimi-Kanai model (a single degree of freedom oscillator) useful to generate earthquake acceleration histories as filtered white noise;
- formulation of Euler-Bernoulli and Timoshenko fractional viscoelastic beam and a fitting of experimental test on a pultruded bar with the fractional viscoelastic Timoshenko beam model;
- application of fractional viscoelasticity to model damping of non-local Timoshenko beam discretized with the finite element model;
- 3D finite element analysis of a UHMWPE (Ultra-High Molecular Weight PolyEthylene) knee replacement bearing.

# Chapter 1

# Fractional calculus

This chapter introduces the main concepts of the *Fractional calculus*, a branch of mathematical analysis that studies the generalization of integer order integro-differential operators. In particular in this chapter the fractional operators are introduced and discussed, focusing the attention on that operators that are useful for the understanding of subsequent chapters: the Grünwald-Letnikov fractional integral and derivative, the Riemann-Liouville fractional integral and derivative and the Caputo fractional derivative. Furthermore, some of the main properties (semigroup rule, Leibniz rule,..) and the application of the integral transforms (introduced in Appendix A) to the fractional operators are discussed.
Obviously there exists more fractional operators and many more theoretical aspects then those considered in this chapter, but here the author limited itself to the treatment of what is related to fractional viscoelasticity that is the main topic of the following chapters. Many others informations on fractional calculus can be found in [60, 74, 75, 81].

## 1.1 Some history about fractional calculus

The basic idea of the fractional calculus, that is the generalization of the differential operators to allow non-integer order of differentiation/integration, is old as the differential calculus itself. The first mathematician to hypothesize the possibility to define this kind of operators was Leibniz in his letters to L'Hôpital (1695) and to Wallis (1697); in those letters Leibiniz discussed the possibility of considering differentials and derivatives of order 1/2.

The first derivative of non-integer order was defined by Euler (1738) that observed that the evaluation of the derivative of a power function $f(t) = t^a$ has a meaning also for non integer order of derivation. Then in 1822 Fourier suggested the idea to use the equality

$$\frac{d^p f(x)}{dx^p} = \frac{1}{2\pi} \int_{-\infty}^{\infty} \lambda^p d\lambda \int_{-\infty}^{\infty} f(t) \cos(\lambda x - t\lambda + p\pi/2) dt \tag{1.1}$$

to extend the concept of derivative to non-integer order. This was the first definition for derivative of arbitrary order.
However the history of that fractional calculus that has been developed so far began with a paper of Abel (1823) in which the following integral equation was solved:

$$\int_a^x \frac{\varphi(t)}{(x-t)^\mu} dt = f(x), \qquad x > a,\ 0 < \mu < 1 \tag{1.2}$$

This equation was not solved with the intention of defining fractional integrals or derivatives, however the integral in the left hand side is what later will be identified as the integral of order $1 - \mu$ of $\varphi(t)$ and then the inversion of this equation leads to the fractional differentiation.
A great contribution to fractional calculus came in the years between 1832 and 1837 from Liouville, that may be considered the real creator of the theory of fractional integro-differentiation. In fact his first contribution was to extend the $n - th$ derivative of the exponential function

$$\frac{d^n}{dt^n} e^{at} = a^n e^a t \tag{1.3}$$

with $n \in \mathbb{N}$, to a non integer order of derivation as follows

$$\frac{d^\alpha}{dt^\alpha} e^{at} = a^\alpha e^a t, \qquad \alpha \in \mathbb{R} \tag{1.4}$$

At this point, by expanding the generic function $f(t)$ as a series of exponential $f(t) = \sum_{k=0}^{\infty} c_j e^{a_j t}$, the fractional derivative is easily defined using the rule (1.4):

$$\left(D^\alpha f\right)(t) = \sum_{k=0}^{\infty} c_j a_j^\alpha e^{a_j t} \tag{1.5}$$

Another idea of Liouville was to define the fractional derivative as a limit of a difference quotient

$$D^{\alpha} f(t) = \lim_{h \to 0} \frac{(\Delta_h^{\alpha} f)(t)}{h^{\alpha}} \tag{1.6}$$

This idea was no further developed by Liouville, but it was reconsidered by Grünwald (1867) and Letnikov (1868) that now give the name to one of the known definition of fractional integral/derivative.
Another important contribution to the initial development of fractional calculus was that of Riemann; he arrived to the following expression for fractional integration

$$\frac{1}{\Gamma(\alpha)} \int_0^x \frac{\varphi(t)}{(x-t)^{1-\alpha}} dt, \qquad x > 0 \tag{1.7}$$

This definition has become one of the most important definition of fractional integral; later was unified with another integral definition of Liouville by Sonin and now is known as the Riemann-Liouville fractional integral.
As already mentioned above, subsequently Grünwald and Letnikov developed the idea of fractional differentiation as limit of a difference quotient and demonstrated some important properties of the fractional operators such as the semigroup property. Many others mathematician gave their contribution to the development of fractional calculus; among all of them the italian mathematician Caputo deserves to be reminded because in 1967 provided another definition of fractional derivative that has proved to be very useful in some engineering applications.

## 1.2 Fractional derivatives and integrals

Classical derivatives and integrals are characterized by the fact that the order $n$ of derivation or integration is integer, that is $n \in \mathbb{N}$. On the other hand, although the improper adjective *fractional* seems to refer to fraction and then to rational numbers, fractional operators are characterized by arbitrary order of derivation or integration $\alpha$, then $\alpha \in \mathbb{C}$. However for the purpose of this manuscript it is sufficient to consider real order derivatives and integrals, then to avoid confusion in the following it will not be considered complex order derivatives and integrals, even though all the properties also hold for complex order derivatives.

Following the notation of Davis, in the next sections fractional derivatives and integrals of a function $f(t)$ will be denoted as

$$\left({}_aD_t^{\alpha} f\right)(t) \tag{1.8a}$$

$$\left({}_aI_t^{\alpha} f\right)(t) = \left({}_aD_t^{-\alpha} f\right)(t) \tag{1.8b}$$

where $a$ and $t$ are the lower and upper bound of integration, respectively.
A *fractional differential equation* is an equation that contains one or more fractional derivatives; a *fractional integral equation* is an equation that contains one or more fractional integrals. In general, a *fractional order system* involves fractional differential and/or integral equations.
In the subsequent sections the main definitions of fractional integro-differential operators are introduced; moreover the integral transforms of them are presented.

### 1.2.1 The Grünwald-Letnikov definition

As mentioned in the previous section, Grünwald and Letnikov developed a definition of fractional derivative based on the generalization of a difference quotient; this definition is suitable for both integration and derivation of arbitrary order. In order to give a single definition including both integration and derivation, the generalized integer order derivatives and integrals definition will be unified first, then extended to the arbitrary order.
We start from the definition of first derivative of a function $f(t)$ as a limit of difference quotient

$$\frac{df(t)}{dt} = \lim_{\Delta t \to 0} \frac{f(t) - f(t - \Delta t)}{\Delta t} \tag{1.9}$$

By applying this definition two and three times the second and third order derivatives are obtained, respectively:

$$\frac{d^2 f(t)}{dt^2} = \lim_{\Delta t \to 0} \frac{f(t) - 2f(t - \Delta t) + f(t - 2\Delta t)}{\Delta t^2} \tag{1.10a}$$

$$\frac{d^3 f(t)}{dt^3} = \lim_{\Delta t \to 0} \frac{f(t) - 3f(t - \Delta t) + 3f(t - 2\Delta t) - f(t - 3\Delta t)}{\Delta t^3} \tag{1.10b}$$

For the generic order of derivation $n$:

$$\frac{d^n f(t)}{dt^n} = \lim_{\Delta t \to 0} \Delta t^{-n} \sum_{k=0}^{n} (-1)^k \binom{n}{k} f(t - k\Delta t) \tag{1.11}$$

where $\binom{n}{k}$ are the binomial coefficients defined as

$$\binom{n}{k} = \frac{n!}{(n-k)!k!} \tag{1.12}$$

In order to unify (1.11) with the corresponding formula for integration of order $n$, it is convenient to define the $n-th$ derivative in a limited range; to do this it is sufficient to choose $\Delta t_N = (t-a)/N$, with $a$ lower limit of the range and $N$ number of intervals contained in the range considered. If the unrestricted limit (1.11) exists, the restricted limit exists as well and they are equal; moreover, since $\binom{n}{k} = 0$ for $k > n$, the $n-th$ derivative may be rewritten as

$$\frac{d^n f(t)}{dt^n} = \lim_{\Delta t_N \to 0} \Delta t_N^{-n} \sum_{k=0}^{N-1} (-1)^k \binom{n}{k} f(t - k\Delta t_N) = \lim_{N \to \infty} \left(\frac{t-a}{N}\right)^{-n} \sum_{k=0}^{N-1} (-1)^k \binom{n}{k} f\left[t - k\left(\frac{t-a}{N}\right)\right] \tag{1.13}$$

Now the same procedure is repeated to define the integral of order $n$; we start from the first order integral defined as Riemann summation

$$\frac{d^{-1} f(t)}{[d(t-a)]^{-1}} = \int_a^t f(t)dt = \lim_{\Delta t \to 0} \Delta t \sum_{k=0}^{N-1} f(t - k\Delta t) \tag{1.14}$$

The integral has the meaning of the area under the curve $f(t)$ evaluated as a sum of the area $\Delta t f(t)$ of $N$ rectangles. If we apply this definition twice and three times to evaluate second and third order integrals, the following equations are obtained:

$$\frac{d^{-2} f(t)}{[d(t-a)]^{-2}} = \lim_{\Delta t \to 0} \Delta t^2 \sum_{k=0}^{N-1} (k+1) f(t - k\Delta t) \tag{1.15a}$$

$$\frac{d^{-3}f(t)}{[d(t-a)]^{-3}} = \lim_{\Delta t\to 0} \Delta t^3 \sum_{k=0}^{N-1} \frac{(k+1)(k+2)}{2} f(t-k\Delta t) \tag{1.15b}$$

For the generic $n-th$ order of integration

$$\frac{d^{-n}f(t)}{[d(t-a)]^{-n}} = \lim_{\Delta t\to 0} \Delta t^n \sum_{k=0}^{N-1} \binom{k+n-1}{k} f(t-k\Delta t) = \lim_{N\to\infty} \left(\frac{t-a}{N}\right)^n \sum_{k=0}^{N-1} \binom{k+n-1}{k} f\left[t-k\left(\frac{t-a}{N}\right)\right] \tag{1.16}$$

Comparison of Eqs. (1.13) and (1.16) reveals that, apart from the sign outside $n$, they differ only for the binomial coefficient; however it can be demonstrated that

$$(-1)^k \binom{n}{k} = \binom{k-n-1}{k} \tag{1.17}$$

and since the sign of $n$ has to be changed switching from integral to derivative, equality (1.17) makes Eqs. (1.13) and (1.16) identical, then the two definition are unified.
In order to extend the formula (1.13), or equivalently (1.16), to arbitrary order $\alpha$ it is needed to generalize the binomial coefficient to allow the substitution of $n \in \mathbb{N}$ with $\alpha \in \mathbb{C}$; to do this we make use of Euler gamma function in the place of factorials, as follows

$$\binom{k-\alpha-1}{k} = \frac{(k-\alpha-1)!}{(-\alpha-1)!k!} = \frac{\Gamma(k-\alpha)}{\Gamma(-\alpha)\Gamma(k+1)} \tag{1.18}$$

By using relationship (1.18) the Grünwald-Letnikov (GL) fractional derivative can be written as

$$\left({}_aD_t^{\alpha} f\right)(t) = \lim_{\Delta t\to 0} \Delta t^{-\alpha} \sum_{k=0}^{N-1} \lambda_k f(t-k\Delta t) \tag{1.19}$$

where as usual $\Delta t = (t-a)/N$ and

$$\lambda_k = \frac{\Gamma(k-\alpha)}{\Gamma(-\alpha)\Gamma(k+1)} \tag{1.20}$$

A further simplification on the coefficients $\lambda_k$ based on Euler gamma function properties leads to

$$\lambda_k = \frac{k-1-\alpha}{k}\lambda_{k-1}, \qquad \lambda_0 = 1 \tag{1.21}$$

Eq. (1.21) allows to evaluate coefficients $\lambda_k$ in a recursive way; this can be useful for the numerical implementation of the fractional derivative, especially when working with softwares in which Euler gamma function is not implemented. Details on how to obtain Eq. (1.21) can be found in [86].
Obviously, if $\alpha < 0$ Eq. (1.19) becomes a fractional integral; moreover if $\alpha \in \mathbb{Z}$ Eq. (1.19) reduces to discretized integer order integrals or derivatives.
Finally, the GL definition of fractional derivative is very useful mainly for two reasons:

- The derivatives of the function $f(t)$ do not appear in it; only the values of the function itself are needed to evaluate the GL fractional derivative.
- It is easy to implement in numerical codes and then permits to get numerical solution to fractional derivatives and integrals.

### 1.2.2 Riemann-Liouville fractional operators

Riemann-Liouville (RL) definition of fractional integrals can be derived by generalization of the Cauchy formula for multiple integrals; this formula allows to evaluate a multiple integral as a single convolution integral

$$\left({}_aI_t^n f\right)(t) = \int_a^t \int_a^{\tau_1} \cdots \int_a^{\tau_{n-1}} f(\tau_n) d\tau_n \cdots d\tau_2 d\tau_1 = \frac{1}{(n-1)!}\int_a^t f(\tau)(t-\tau)^{n-1} d\tau \tag{1.22}$$

For the generalization of Eq. (1.22) it is sufficient to use Euler gamma function and to substitute $n \in \mathbb{N}$ with $\alpha \in \mathbb{C}$:

$$\left({}_aI_t^\alpha f\right)(t) = \frac{1}{\Gamma(\alpha)}\int_a^t f(\tau)(t-\tau)^{\alpha-1} d\tau \tag{1.23}$$

Eq. (1.23) is the *Riemann-Liouville fractional integral* of order $\alpha$; in particular this

one is called the *left sided*, because the lower bound $a$ is fixed while the upper bound is the variable $t$. The *right sided Riemann-Liouville fractional integral* is defined with a fixed upper bound $b$ and a variable lower bound:

$$\left({}_tI_b^\alpha f\right)(t) = \frac{1}{\Gamma(\alpha)} \int_t^b f(\tau)(\tau - t)^{\alpha-1} d\tau \tag{1.24}$$

Usually the left sided and right sided RL integrals are labeled as $I_{a^+}^\alpha$ and $I_{b^-}^\alpha$, respectively. If $a \to -\infty$ and $b \to \infty$ the left and the right RL fractional integrals are usually denoted as $I_+^\alpha$ and $I_-^\alpha$, respectively.
The *Riemann-Liouville fractional derivative* is easily obtained from the RL fractional integral considering that the derivative of order $\alpha$ can be obtained as the derivative of order $n$ of the integral of order $n - \alpha$; this approach leads to the following expression for the *left* and *right-sided* RL fractional derivatives, respectively:

$$\left({}_aD_t^\alpha f\right)(t) = \frac{1}{\Gamma(n-\alpha)} \frac{d^n}{dt^n} \int_a^t \frac{f(\tau)}{(t-\tau)^{\alpha-n+1}} d\tau \tag{1.25a}$$

$$\left({}_tD_b^\alpha f\right)(t) = \frac{(-1)^n}{\Gamma(n-\alpha)} \frac{d^n}{dt^n} \int_t^b \frac{f(\tau)}{(\tau-t)^{\alpha-n+1}} d\tau \tag{1.25b}$$

As for the integrals, the left sided and right sided RL derivatives are labeled as $D_{a^+}^\alpha$ and $D_{b^-}^\alpha$, respectively; if $a \to -\infty$ and $b \to \infty$ the left and the right RL fractional derivatives are usually denoted as $D_+^\alpha$ and $D_-^\alpha$, respectively.
Note that the definitions provided in this section use the backward difference $(t - \tau)$; if the forward differences $(t + \tau)$ are used instead, the obtained operator are known as *Weil fractional integrals and derivatives*.
One of the main characteristic of the RL derivative is that the derivative of a constant is not zero:

$${}_aD_t^\alpha c = \frac{c(t-a)^{-\alpha}}{\Gamma(1-\alpha)} \tag{1.26}$$

### 1.2.3 Riesz fractional integrals and derivatives

The generalizations of fractional integrals to the whole real axis are the *Riesz fractional integral* $I^\alpha$ and *Riesz complementary fractional integral* $H^\alpha$; they are defined as

$$\left(I^\alpha f\right)(t) = \frac{1}{2\nu_c(\alpha)} \int_{-\infty}^{\infty} f(\tau)|t-\tau|^{\alpha-1} d\tau \tag{1.27a}$$

$$(H^{\alpha} f)(t) = \frac{1}{2\nu_s(\alpha)} \int_{-\infty}^{\infty} f(\tau)\mathrm{sgn}(t-\tau)|t-\tau|^{\alpha-1} d\tau \tag{1.27b}$$

where $\nu_c(\alpha) = \Gamma(\alpha)\cos(\alpha\pi/2)$ and $\nu_s(\alpha) = \Gamma(\alpha)\sin(\alpha\pi/2)$. By means of some simple considerations, Riesz fractional integrals can be related to RL fractional integrals:

$$(I^{\alpha} f)(t) = \frac{1}{2\cos\left(\frac{\alpha\pi}{2}\right)} \left[(I_{+}^{\alpha} f)(t) + (I_{-}^{\alpha} f)(t)\right] \tag{1.28a}$$

$$(H^{\alpha} f)(t) = \frac{1}{2\sin\left(\frac{\alpha\pi}{2}\right)} \left[(I_{+}^{\alpha} f)(t) - (I_{-}^{\alpha} f)(t)\right] \tag{1.28b}$$

As for the RL definitions, starting from the Riesz fractional integrals it is possible to define the *Riesz fractional derivative* $D^{\alpha}$ and the *Riesz complementary fractional derivative* $\tilde{D}^{\alpha}$:

$$(D^{\alpha} f)(t) = \frac{1}{2\nu_c(-\alpha)} \int_{-\infty}^{\infty} \frac{f(t-\tau) - f(t)}{|\tau|^{\alpha+1}} d\tau \tag{1.29a}$$

$$\left(\tilde{D}^{\alpha} f\right)(t) = \frac{1}{2\nu_s(-\alpha)} \int_{-\infty}^{\infty} \frac{f(t-\tau) - f(t)}{|\tau|^{\alpha+1}} \mathrm{sgn}(\tau) d\tau \tag{1.29b}$$

As for the integrals, Riesz fractional derivative are strictly related to RL fractional derivative:

$$(D^{\alpha} f)(t) = -\frac{1}{2\cos\left(\frac{\alpha\pi}{2}\right)} \left[(D_{+}^{\alpha} f)(t) + (D_{-}^{\alpha} f)(t)\right] \tag{1.30a}$$

$$\left(\tilde{D}^{\alpha} f\right)(t) = -\frac{1}{2\sin\left(\frac{\alpha\pi}{2}\right)} \left[(D_{+}^{\alpha} f)(t) - (D_{-}^{\alpha} f)(t)\right] \tag{1.30b}$$

It is worth noticing that definitions of Riesz integrals and derivatives are valid for $\Re(\alpha) \neq 1, 3, 5, \ldots$.

### 1.2.4 Caputo's fractional derivative

Riemann-Liouville definitions of fractional derivatives and integrals has been very important for the development of the fractional calculus theory, especially for applications in pure mathematics. However for for practical applications the pure mathematical approach need to be revised. In fact fractional

derivatives appear in many applications, especially in the field of viscoelasticity and hereditary materials (that is the application of this thesis); these applications need the formulation of initial conditions (conditions in the lower terminal $a$) in order to solve the governing differential equations of fractional order. However RL approach leads to initial conditions in terms of initial values of the fractional derivatives, but unfortunately these have not physical meaning and can not be known a priori. To overcome this problem one can think to consider as lower terminal of the derivative $-\infty$ instead of a finite value $a$, but this strategy does not allow to study transient problem.
A solution to this problem was proposed by the italian mathematician Michele Caputo, that gave another definition of fractional derivative:

$$\left({}_a^C D_t^\alpha f\right)(t) = \frac{1}{\Gamma(\alpha - n)} \int_a^t \frac{f^{(n)}(\tau)}{(t-\tau)^{\alpha+1-n}} d\tau \tag{1.31}$$

where $n - 1 < \alpha < n$. When using definition (1.31), initial conditions in terms of integer order derivatives are obtained and this make Caputo's fractional derivative suitable for applications in real physical problems.
If $\alpha \to n$ the Caputo's derivative reduces to classical integer order derivatives; moreover the Caputo fractional derivative of a constant is zero as integer order derivative. In certain cases, putting $a = -\infty$ in both Caputo and RL definitions and when the function $f(t)$ has a certain behavior for $t \to -\infty$, the Caputo and RL fractional derivative give the same result. Also the same result is achieved for $f(0) = 0$ when $a = 0$.

## 1.3 Examples of fractional derivatives

In this section fractional derivative of some simple functions are reported. In particular here the fractional derivative of the Unitstep function, a power law function and a trigonometric function are shown.

### 1.3.1 Fractional derivative of the Unitstep function

The *Unitstep* function $U(t)$ is a function defined as

$$U(t) = \begin{cases} 0 & t < 0 \\ 1 & t > 0 \end{cases} \tag{1.32}$$

The RL fractional derivative of this function is:

$$(D^{\alpha}_{0+}U)(t) = \frac{t^{-\alpha}}{\Gamma(1-\alpha)} \tag{1.33}$$

Form Fig. 1.1 it is possible to appreciate that for $\alpha = 0$ the differintegration

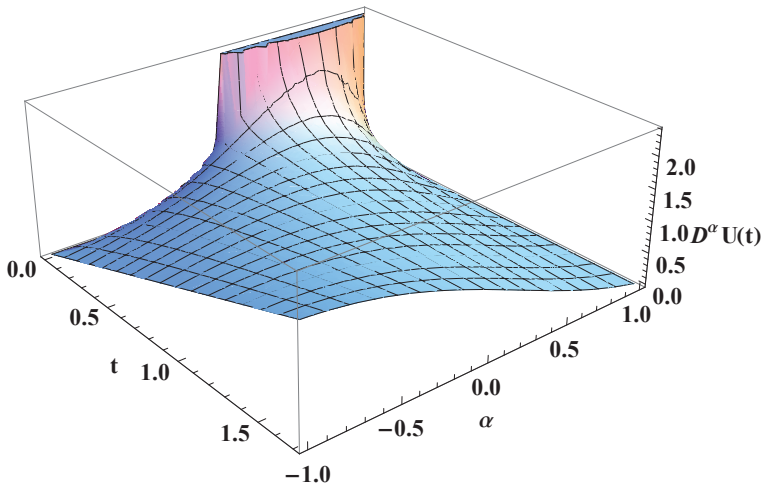


**Figure 1.1:** 3D plot of RL fractional derivative of the Unitstep function for $t > 0$ and oerder of differintegration $-1 \leq \alpha \leq 1$.

gives the function $U(t)$ itself, for $\alpha = 1$ gives the first order derivative (Dirac Delta function $\delta(t)$) and for $\alpha = -1$ the results is the first order integral of the function $U(t)$, that is the ramp function; for real values of $\alpha$ the results of the differintegration is a power law of real order, then something intermediate between the ramp and $U(t)$ $(-1 < \alpha < 0)$ or something intermediate between $U(t)$ and $\delta(t)$ $(0 < \alpha < 1)$.

### 1.3.2 Fractional derivative of a power law function

Consider a power law function $(t-a)^{\beta}$ with $\beta \in \mathbb{R}$ and $a > 0$. The RL fractional derivative is:

$$D^{\alpha}_{a^+}(t-a)^{\beta} = \frac{\Gamma(\beta+1)}{\Gamma(\beta-\alpha+1)}(t-a)^{\beta-\alpha} \tag{1.34}$$

According to Eq. (1.34) the fractional derivative of a power law function is still a power law function, whose power is the difference between the original power of the function $f(t)$ and the order of derivation.

### 1.3.3 Fractional derivative of $\sin(\omega t)$

The RL fractional derivative $D^{\alpha}_{a^+}$ of trigonometric functions gives results in terms of the so called *hypergeometric* functions; however focusing the attention far from the lower terminal of the derivative $a$, the fractional derivative of a trigonometric function is still a trigonometric function. This is confirmed by the fact that if we choose as lower terminal of the derivative $-\infty$, hypergeometric functions do not appear and trigonometric function appear instead; if we consider the function $\sin(\omega t)$, with $\omega \in \mathbb{R}$, its RL fractional derivative gives:

$$D^{\alpha}_{+} \sin(\omega t) = \omega^{\alpha} \sin\left(\omega t + \frac{\pi\alpha}{2}\right) \tag{1.35}$$

The operation of derivation on the $\sin(\omega t)$ function give another sinusoidal function with a different phase that depends on the order of differintegration $\alpha$ and with a different amplitude that depends on $\omega$ and $\alpha$. In particular, by considering $\omega = 1$, the amplitude remains the same and only the phase change, as it is possible to see in Fig. 1.2:

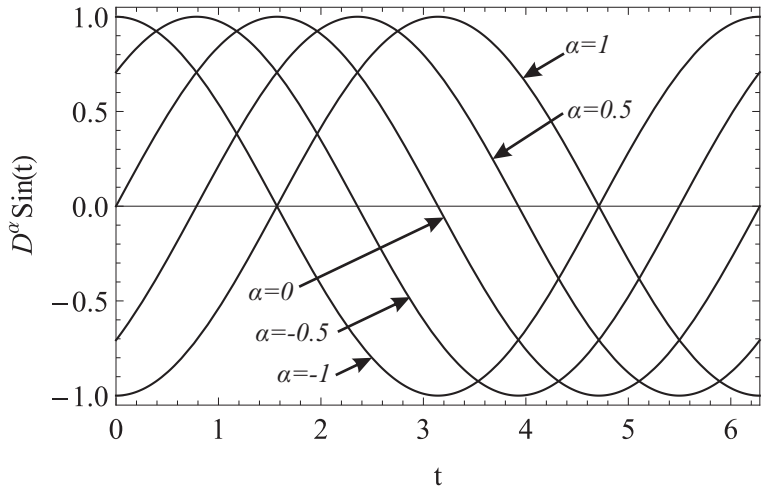


**Figure 1.2:** Plot of RL fractional derivative of $sin(t)$ for different values of the order of differintegration $\alpha$.

## 1.4 Properties of fractional integrals and derivatives

In this section *linearity*, *Leibniz* rule and *semigroup* rule for fractional operators are discussed.

- **Linearity.** Fractional operators are linear operators; this property can be demonstrated for each of the definitions of fractional integrals and derivatives; here the linearity is proved just for the left RL fraction derivative. Consider two function $f(t)$ and $g(t)$ and two complex numbers $\lambda$ and $\mu$ and definition (1.25a):

$$D^{\alpha}_{a^+}\left(\lambda f(t)+\mu g(t)\right)=\frac{1}{\Gamma(n-\alpha)}\frac{d^n}{dt^n}\int_a^t\frac{\lambda f(\tau)+\mu g(\tau)}{(t-\tau)^{\alpha-n+1}}d\tau=$$
$$\frac{\lambda}{\Gamma(n-\alpha)}\frac{d^n}{dt^n}\int_a^t\frac{f(\tau)}{(t-\tau)^{\alpha-n+1}}d\tau+\frac{\mu}{\Gamma(n-\alpha)}\frac{d^n}{dt^n}\int_a^t\frac{g(\tau)}{(t-\tau)^{\alpha-n+1}}d\tau=$$

$$\lambda D^{\alpha}_{a^+}f(t)+\mu D^{\alpha}_{a^+}g(t) \quad (1.36)$$

- **Leibniz rule.** This rule allows to evaluate the $n-th$ derivative of the product of two functions and can be extended to non integer order derivation. In the case of $n-th$ integer order derivative Leibniz rule is expressed as follows:

$$\frac{d^n}{dt^n}\left(f(t)g(t)\right)=\sum_{k=0}^{n}\binom{n}{k}f^{(k)}(t)g^{(n-k)}(t) \quad (1.37)$$

An extension of Eq. (1.37) is valid for all the definitions of fractional derivative introduced above; the proof is very long and here is not reported for brevity. Leibniz rule for fractional derivative is expressed as follows:

$$D^{\alpha}_{a^+}\left(f(t)g(t)\right)=\sum_{k=0}^{\infty}\binom{\alpha}{k}f^{(k)}(t)\left(D^{\alpha-k}_{a^+}g\right)(t) \quad (1.38)$$

Obviously Eq. (1.38) is not applicable because the summation contains infinite terms. Then the summation is truncated, resulting in the following form of the Leibniz rule:

$$D^{\alpha}_{a^+}\left(f(t)g(t)\right)=\sum_{k=0}^{n}\binom{\alpha}{k}f^{(k)}(t)\left(D^{\alpha-k}_{a^+}g\right)(t)-R^{\alpha}_{n}(t) \quad (1.39)$$

where $n > \alpha + 1$ and $R_n^\alpha(t)$ is a *remainder* that can be evaluated as follows:

$$R_n^\alpha(t) = \frac{1}{n!\Gamma(-\alpha)} \int_a^t (t-\tau)^{-\alpha-1} g(\tau) d\tau \int_\tau^t f^{(n+1)}(\xi)(\tau-\xi)^n d\xi \quad (1.40)$$

If $n \to \infty$ then $R_n^\alpha(t) \to 0$ and Eq. (1.39) reduces to Eq. (1.38).

- **Semigroup rule.** Semigroup rule allows to combine multiple operation of derivation and/or integration. By considering a function $f(t)$, integrable for the orders $\alpha$ and $\beta$ with $\Re(\alpha) > 0$ and $\Re(\beta) > 0$, the semigroup rule can be demonstrated for both the left and the right-sided integrals:

$$\left[I_{a^+}^\alpha \left(I_{a^+}^\beta f\right)\right](t) = \left[I_{a^+}^\beta \left(I_{a^+}^\alpha f\right)\right](t) = \left(I_{a^+}^{\alpha+\beta} f\right)(t) \quad (1.41a)$$

$$\left[I_{b^-}^\alpha \left(I_{b^-}^\beta f\right)\right](t) = \left[I_{b^-}^\beta \left(I_{b^-}^\alpha f\right)\right](t) = \left(I_{b^-}^{\alpha+\beta} f\right)(t) \quad (1.41b)$$

For $\alpha > 0$:

$$\left[D_{a^+}^\alpha \left(I_{a^+}^\alpha f\right)\right](t) = f(t) \quad (1.42a)$$

$$\left[D_{b^-}^\alpha \left(I_{b^-}^\alpha f\right)\right](t) = f(t) \quad (1.42b)$$

As it happens for the classical differential calculus, commutation of the operations of derivation and integration is not valid

$$\left[I_{a^+}^\alpha \left(D_{a^+}^\alpha f\right)\right](t) \neq f(t) \quad (1.43a)$$

$$\left[I_{b^-}^\alpha \left(D_{b^-}^\alpha f\right)\right](t) \neq f(t) \quad (1.43b)$$

Another form of the rule is

$$\left[D_{a^+}^\alpha \left(I_{a^+}^\beta f\right)\right](t) = \left(D_{a^+}^{\alpha-\beta} f\right)(t) \quad (1.44a)$$

$$\left[D_{b^-}^\alpha \left(I_{b^-}^\beta f\right)\right](t) = \left(D_{b^-}^{\alpha-\beta} f\right)(t) \quad (1.44b)$$

with $\Re(\alpha) > \Re(\beta) > 0$. Finally, if $\Re(\alpha) > 0$ and $n \in \mathbb{N}$:

$$\frac{d^n}{dt^n}\left(D_{a^+}^\alpha f\right)(t) = \left(D_{a^+}^{\alpha+n} f\right)(t) \quad (1.45a)$$

$$\frac{d^n}{dt^n}\left(D_{b^-}^\alpha f\right)(t) = (-1)^n \left(D_{b^-}^{\alpha+n} f\right)(t) \quad (1.45b)$$

## 1.5 Laplace transform of fractional derivatives and integrals

In this section Laplace transforms of fractional operators introduced in the previous sections are reported; the proofs are often long and here are not reported for brevity; more details on how the relationships presented here are obtained can be found in Podlubny.

### 1.5.1 Laplace transform of Riemann-Liouville fractional operators

We start with the Laplace transform of the RL fractional integral oforder $\alpha > 0$; this can be easily found by noting that RL integral (1.23) is neither else than a convolution integral; then applying the rule (A.12) for the Laplace transform of the convolution, it can be proved that

$$\mathcal{L}\left\{\left(I_{0^+}^{\alpha} f\right)(t); s\right\} = s^{-\alpha} F_{\mathcal{L}}(s) \tag{1.46}$$

Eq. (1.46) is obtained for fractional integrals in the range $0 \div t$, because the rule (A.12) holds true for convolution in the same range; this could appear as a limitation, but it is not, because any RL integral with the generic lower terminal $a \neq 0$ can be reduced to an integral in the range $0 \div t$ by performing some change of variables and/or making use of particular functions such as the Unitstep function U(t).
The Laplace transform of RL fractional derivative is slightly different because it contains initial values of the fractional derivatives of the function at hand:

$$\mathcal{L}\left\{\left(D_{0^+}^{\alpha} f\right)(t); s\right\} = s^{\alpha} F_{\mathcal{L}}(s) - \sum_{k=0}^{n-1} s^{k} \left[\left(D_{0^+}^{\alpha-k-1} f\right)(t)\right]_{t=0} \tag{1.47}$$

where $n - 1 < \alpha < n$. The applicability of Eq. (1.47) to fractional differential equations is limited, for practical applications, by the presence in it of the values of fractional derivatives at $t = 0$ that have not physical meaning.

### 1.5.2 Laplace transform of Grünwald-Letnikov fractional operators

In [75] it has been demonstrated that GL discrete fractional integrals and derivatives can be reduced to convolution integrals similar to RL fractional operators; this allows to use the same strategy used in the previous section to

obtain Laplace transform of GL operators.
For the GL fractional integral:

$$\mathcal{L}\left\{\left(D_{0^+}^{-\alpha} f\right)(t); s\right\} = s^{-\alpha} F_{\mathcal{L}}(s) \tag{1.48}$$

with $\alpha > 0$. For the GL fractional derivative:

$$\mathcal{L}\left\{\left(D_{0^+}^{\alpha} f\right)(t); s\right\} = \frac{f(0)}{s^{1-\alpha}} + \frac{1}{s^{1-\alpha}}\left(sF(s) - f(0)\right) = s^{\alpha} F_{\mathcal{L}}(s) \tag{1.49}$$

In spite of the validity of Laplace transform of GL integrals (Eq. (1.48)) for any $\alpha > 0$, Laplace transform of GL derivative of order $\alpha > 1$ does not exist, then Eq. (1.49) is valid only for $0 < \alpha < 1$.

### 1.5.3 Laplace transform of Caputo fractional derivative

Laplace transform of Caputo fractional derivative has the same structure of Laplace transform of RL fractional derivative

$$\mathcal{L}\left\{\left({}_{0}^{C}D_{t}^{\alpha} f\right)(t); s\right\} = s^{\alpha} F_{\mathcal{L}}(s) - \sum_{k=0}^{n-1} s^{\alpha-k-1} f^{(k)}(0) \tag{1.50}$$

The fundamental difference is that, differently from Eq. (1.47) (Laplace transform of RL fractional derivative), in Eq. (1.50) the values of the function $f(t)$ and of its integer order derivatives appear; these terms have a clear physical meaning when we try to solve fractional differential equation with physical applications and then can be known a priori. For this reason Caputo fractional derivative is preferable for the description of some physical phenomena.

## 1.6 Fourier transform of fractional operators

In some cases it is convenient to use Fourier transform instead of Laplace transform in the study of fractional differential equations; this can be true for example when investigating the stationary behavior of dynamical systems such as fractional damped oscillators. The proofs of the relationships presented in this section are not reported an can be found in Podlubny.

### 1.6.1 Fourier transform of fractional integrals

The procedure to obtain the Fourier transform of fractional integrals is analogous to the one used in the case of Laplace transform, that is the use of the property of the Fourier transform of convolution. With this strategy, by considering the left RL fractional integral with lower terminal $a = -\infty$ we obtain:

$$\mathcal{F}\left\{\left(I_{+}^{\alpha} f\right)(t); \omega\right\} = (-i\omega)^{-\alpha} F_{\mathcal{F}}(\omega) \tag{1.51}$$

Eq. (1.51) is valid also for GL fractional integral and Caputo fractional integral, both with lower terminal $a = -\infty$, because in this case they coincide with RL fractional integral. The Fourier transform of right RL fractional integral $I_{-}^{\alpha}$ is:

$$\mathcal{F}\left\{\left(I_{-}^{\alpha} f\right)(t); \omega\right\} = (i\omega)^{-\alpha} F_{\mathcal{F}}(\omega) \tag{1.52}$$

For simplicity sake, Eqs. (1.51) and (1.52) can be written in one equation:

$$\mathcal{F}\left\{\left(I_{\pm}^{\alpha} f\right)(t); \omega\right\} = (\mp i\omega)^{-\alpha} F_{\mathcal{F}}(\omega) \tag{1.53}$$

With the aid of Eqs. (1.53) and (1.28) and considering that

$$(\mp i\omega)^{-\alpha} = \left[\cos\left(\frac{\alpha\pi}{2}\right) \pm i\,\mathrm{sgn}(\omega)\sin\left(\frac{\alpha\pi}{2}\right)\right]|\omega|^{-\alpha} \tag{1.54}$$

the Fourier transform of Riesz integrals can be easily found:

$$\mathcal{F}\left\{\left(I^{\alpha} f\right)(t); \omega\right\} = |\omega|^{-\alpha} F_{\mathcal{F}}(\omega) \tag{1.55a}$$

$$\mathcal{F}\left\{\left(H^{\alpha} f\right)(t); \omega\right\} = i\,\mathrm{sgn}(\omega)|\omega|^{-\alpha} F_{\mathcal{F}}(\omega) \tag{1.55b}$$

### 1.6.2 Fourier transform of fractional derivatives

By setting $a = -\infty$ in left RL, GL and Caputo fractional derivatives, these three definitions are equivalent; then the following relationship for the Fourier transform of the fractional derivative is valid for all of them:

$$\mathcal{F}\left\{\left({}_{-\infty}D_{t}^{\alpha} f\right)(t); \omega\right\} = (-i\omega)^{\alpha} F_{\mathcal{F}}(\omega) \tag{1.56}$$

For the right RL fractional derivative:

$$\mathcal{F}\left\{\left({}_tD_{\infty}^{\alpha}f\right)(t);\omega\right\} = (i\omega)^{\alpha}F_{\mathcal{F}}(\omega) \tag{1.57}$$

Using Eqs. (1.56) and (1.57) and taking into account Eq. (1.54) the following expressions for the Fourier transform of Riesz derivatives are obtained:

$$\mathcal{F}\left\{\left(D^{\alpha}f\right)(t);\omega\right\} = |\omega|^{\alpha}F_{\mathcal{F}}(\omega) \tag{1.58a}$$

$$\mathcal{F}\left\{\left(\tilde{D}^{\alpha}f\right)(t);\omega\right\} = -i\,\mathrm{sgn}(\omega)|\omega|^{\alpha}F_{\mathcal{F}}(\omega) \tag{1.58b}$$

## 1.7 Mellin transform of fractional operators

In some cases, the study and the solution of fractional differential equations can be conveniently done with the aid of Mellin transform, then it is important to know Mellin transform of fractional operators.

### 1.7.1 Mellin transform of RL fractional integral

The Mellin transform of RL fractional integral can be found for the case in which the lower terminal $a = 0$. Using the change of variable $\tau = t\xi$ it is possible to write:

$$\left({}_0I_t^{\alpha}f\right)(t) = \frac{1}{\Gamma(\alpha)}\int_0^t (t-\tau)^{\alpha-1}f(\tau)d\tau = \frac{t^{\alpha}}{\Gamma(\alpha)}\int_0^1 (1-\xi)^{\alpha-1}f(t\xi)d\xi = \frac{t^{\alpha}}{\Gamma(\alpha)}\int_0^{\infty} f(t\xi)g(\xi)d\xi \tag{1.59}$$

where

$$g(t) = \begin{cases} (1-t)^{\alpha-1} & (0 \le t < 1) \\ 0 & (t \ge 1) \end{cases} \tag{1.60}$$

The Mellin transform of $g(t)$ gives the Euler beta function:

$$\mathcal{M}\left\{g(t);\gamma\right\} = B(\alpha,\gamma) = \frac{\Gamma(\alpha)\Gamma(\gamma)}{\Gamma(\alpha+\gamma)} \tag{1.61}$$

At this point using property (A.53) and Eqs. (1.59) and (1.61) the following relationship for the Mellin transform of RL integral is obtained:

$$\mathcal{M}\left\{\left({}_0I_t^{\alpha}f\right)(t);\gamma\right\} = \frac{\Gamma(1-\gamma-\alpha)}{\Gamma(1-\gamma)}F_{\mathcal{M}}(\gamma+\alpha) \tag{1.62}$$

### 1.7.2 Mellin transform of RL fractional derivative

Consider $0 \leq n-1 < \alpha < n$. According to the definition (1.23) of left RL fractional derivative we can write

$$\left({}_0D_t^{\alpha}f\right)(t) = \frac{d^n}{dt^n}\left({}_0D_t^{-n+\alpha}f\right)(t) \tag{1.63}$$

By assuming $g(t) = \left({}_0D_t^{-n+\alpha}f\right)(t)$ it is possible to use property (A.54) of the Melin transform of integer order derivatives; moreover using the rule (1.62) we obtain:

$$\begin{aligned}
\mathcal{M}\left\{\left({}_0D_t^{\alpha}f\right)(t);\gamma\right\} =& \mathcal{M}\left\{\frac{d^n}{dt^n}\left({}_0D_t^{-n+\alpha}f\right)(t);\gamma\right\} = \mathcal{M}\left\{g^{(n)}(t);\gamma\right\} \\
&= \sum_{k=0}^{n-1}\frac{\Gamma(1-\gamma+k)}{\Gamma(1-\gamma)}\left[g^{(n-k-1)}(t)t^{\gamma-k-1}\right]_0^{\infty} \\
&\quad + \frac{\Gamma(1-\gamma+n)}{\Gamma(1-\gamma)}G_{\mathcal{M}}(\gamma-n) \\
&= \sum_{k=0}^{n-1}\frac{\Gamma(1-\gamma+k)}{\Gamma(1-\gamma)}\left[\frac{d^{n-k-1}}{dt^{n-k-1}}({}_0D_t^{\alpha-n}f)(t)t^{(\gamma-k-1)}\right]_0^{\infty} \\
&\quad + \frac{\Gamma(1-\gamma+n)\Gamma(1-\gamma+n-n+\alpha)}{\Gamma(1-\gamma)\Gamma(1-\gamma+n)}F_{\mathcal{M}}(\gamma-n+n-\alpha) \\
&= \sum_{k=0}^{n-1}\frac{\Gamma(1-\gamma+k)}{\Gamma(1-\gamma)}\left[\left({}_0D_t^{\alpha-k-1}f\right)(t)t^{\gamma-k-1}\right]_0^{\infty} \\
&\quad + \frac{\Gamma(1-\gamma+\alpha)}{\Gamma(1-\gamma)}F_{\mathcal{M}}(\gamma-\alpha)
\end{aligned} \tag{1.64}$$

If $0 < \alpha < 1$ then Eq. (1.64) reduces to

$$\mathcal{M}\left\{\left({}_0D_t^{\alpha}f\right)(t);\gamma\right\} = \left[\left({}_0D_t^{\alpha-1}f\right)(t)t^{\gamma-1}\right]_0^{\infty} + \frac{\Gamma(1-\gamma+\alpha)}{\Gamma(1-\gamma)}F_{\mathcal{M}}(\gamma-\alpha) \tag{1.65}$$

Eq. (1.64) can be further simplified if $f(t)$ and $\Re(\gamma)$ are such that the limits in square brackets at $t = 0$ and $t = \infty$ in give zero and in this case:

$$\mathcal{M}\left\{\left({}_0D_t^{\alpha} f\right)(t);\gamma\right\} = \frac{\Gamma(1-\gamma+\alpha)}{\Gamma(1-\gamma)} F_{\mathcal{M}}(\gamma-\alpha) \tag{1.66}$$

### 1.7.3 Mellin transform of Riesz operators

Following the approach used to obtain Mellin transform of RL integrals, it is possible to obtain the Mellin transform of the Riesz integral and the complementary Riesz integral. In order to do this, it is necessary to distinguish between the even and odd part $u(t)$ and $v(t)$ of the function $f(t)$ at hand; in the end the following expressions are obtained:

$$\mathcal{M}\left\{\left(I^{\alpha} f\right)(t);\omega\right\} = \mathcal{M}\left\{I^{\alpha}\left(u(t)+v(t)\right);\gamma\right\} = \frac{\nu_c(\gamma)}{\nu_c(\gamma+\alpha)} U_{\mathcal{M}}(\gamma+\alpha) + \frac{\nu_s(\gamma)}{\nu_s(\gamma+\alpha)} V_{\mathcal{M}}(\gamma+\alpha) \tag{1.67a}$$

$$\mathcal{M}\left\{\left(H^{\alpha} f\right)(t);\omega\right\} = \mathcal{M}\left\{H^{\alpha}\left(u(t)+v(t)\right);\gamma\right\} = \frac{\nu_c(1-\gamma-\alpha)}{\nu_c(1-\gamma)} U_{\mathcal{M}}(\gamma+\alpha)\tan\left(\frac{\pi}{2}\gamma\right) - \frac{\nu_s(1-\gamma-\alpha)}{\nu_s(1-\gamma)} V_{\mathcal{M}}(\gamma+\alpha)\cot\left(\frac{\pi}{2}\gamma\right) \tag{1.67b}$$

With the same approach used for the Mellin transform of RL derivatives it is also possible to find Mellin transform of Riesz derivative and complementary Riesz derivative; as in the case of the Mellin transform of Riesz derivative, it is necessary to distinguish between the even and odd part $u(t)$ and $v(t)$ of the function $f(t)$ at hand; in the end the following expressions are obtained:

$$\mathcal{M}\left\{\left(D^{\alpha} f\right)(t);\omega\right\} = \mathcal{M}\left\{D^{\alpha}\left(u(t)+v(t)\right);\gamma\right\} = -\sum_{k=0}^{n-1} \frac{\Gamma(1-\gamma-k)}{\Gamma(1-\gamma)} \left[\left(D^{\alpha-k-1} f\right)(t) t^{\gamma-k-1}\right]_0^{\infty} - \frac{\nu_c(\gamma)}{\nu_c(\gamma-\alpha)} U_{\mathcal{M}}(\gamma-\alpha) - \frac{\nu_s(\gamma)}{\nu_s(\gamma-\alpha)} V_{\mathcal{M}}(\gamma-\alpha) \tag{1.68a}$$

$$\mathcal{M}\left\{\left(\tilde{D}^{\alpha}f\right)(t);\omega\right\} = \mathcal{M}\left\{\tilde{D}^{\alpha}\left(u(t)+v(t)\right);\gamma\right\} = - \sum_{k=0}^{n-1} \frac{\Gamma(1-\gamma-k)}{\Gamma(1-\gamma)}\left[\left(\tilde{D}^{\alpha-k-1}f\right)(t)t^{\gamma-k-1}\right]_0^{\infty} + \frac{\nu_c(1-\gamma+\alpha)}{\nu_c(1-\gamma)}U_{\mathcal{M}}(\gamma-\alpha)\tan\left(\frac{\pi}{2}\gamma\right) - \frac{\nu_s(1-\gamma+\alpha)}{\nu_s(1-\gamma)}V_{\mathcal{M}}(\gamma-\alpha)\cot\left(\frac{\pi}{2}\gamma\right) \tag{1.68b}$$

If $f(t)$ and $\Re(\gamma)$ are such that in Eqs. (1.68) the limits a t $t=0$ and $t=\infty$ give zero then

$$\mathcal{M}\left\{\left(D^{\alpha}f\right)(t);\omega\right\} = \mathcal{M}\left\{D^{\alpha}\left(u(t)+v(t)\right);\gamma\right\} = - \frac{\nu_c(\gamma)}{\nu_c(\gamma-\alpha)}U_{\mathcal{M}}(\gamma-\alpha) - \frac{\nu_s(\gamma)}{\nu_s(\gamma-\alpha)}V_{\mathcal{M}}(\gamma-\alpha) \tag{1.69a}$$

$$\mathcal{M}\left\{\left(\tilde{D}^{\alpha}f\right)(t);\omega\right\} = \mathcal{M}\left\{\tilde{D}^{\alpha}\left(u(t)+v(t)\right);\gamma\right\} = + \frac{\nu_c(1-\gamma+\alpha)}{\nu_c(1-\gamma)}U_{\mathcal{M}}(\gamma-\alpha)\tan\left(\frac{\pi}{2}\gamma\right) - \frac{\nu_s(1-\gamma+\alpha)}{\nu_s(1-\gamma)}V_{\mathcal{M}}(\gamma-\alpha)\cot\left(\frac{\pi}{2}\gamma\right) \tag{1.69b}$$

### 1.7.4 Mellin transform of Caputo fractional derivative

Consider $0 \leq n-1 < \alpha < n$. By denoting $h(t) = f^{(n)}(t)$ and using properties (A.54) and (1.62) it is possible to write

$$\begin{aligned}\mathcal{M}\left\{\left({}_0^C D_t^{\alpha}f\right)(t);\gamma\right\} =& \mathcal{M}\left\{\left({}_0D_t^{\alpha-n}f^{(n)}\right)(t);\gamma\right\} = \mathcal{M}\left\{\left({}_0D_t^{\alpha-n}h\right)(t);\gamma\right\} \\ =& \frac{\Gamma(1-s-(n-\alpha))}{\Gamma(1-\gamma)}H_{\mathcal{M}}(s+n-\alpha) \\ =& \sum_{k=0}^{n-1}\frac{\Gamma(1-\gamma-n+\alpha+k)}{\Gamma(1-\gamma)}\left[f^{(n-k-1)}(t)t^{\gamma+n-\alpha-k-1}\right]_0^{\infty} \\ &+ \frac{\Gamma(1-\gamma+\alpha)}{\Gamma(1-\gamma)}F_{\mathcal{M}}(\gamma-\alpha)\end{aligned} \tag{1.70}$$

$$= \sum_{k=0}^{n-1} \frac{\Gamma(\alpha-k-\gamma)}{\Gamma(1-\gamma)} \left[ f^{(k)}(t) t^{\gamma-\alpha+k} \right]_0^\infty + \frac{\Gamma(1-\gamma+\alpha)}{\Gamma(1-\gamma)} F_{\mathcal{M}}(\gamma-\alpha)$$

If $0 < \alpha < 1$ Eq. (1.70) reduces to

$$\mathcal{M}\left\{ \left( {}_0^C D_t^\alpha f \right)(t); \gamma \right\} = \frac{\Gamma(\alpha-\gamma)}{\Gamma(1-\gamma)} \left[ f(t) t^{\gamma-\alpha} \right]_0^\infty + \frac{\Gamma(1-\gamma+\alpha)}{\Gamma(1-\gamma)} F_{\mathcal{M}}(\gamma-\alpha) \tag{1.71}$$

If the function $f(t)$ and $\Re(\gamma)$ are such that in Eq.(1.70) the limits at $t = 0$ and $t = \infty$ give zero then

$$\mathcal{M}\left\{ \left( {}_0^C D_t^\alpha f \right)(t); \gamma \right\} = \frac{\Gamma(1-\gamma+\alpha)}{\Gamma(1-\gamma)} F_{\mathcal{M}}(\gamma-\alpha) \tag{1.72}$$

## 1.8 Conclusions

In this chapter the main concepts regarding fractional calculus have been shown; in particular the main definitions of fractional derivatives and integrals have been introduced and integral transforms of these operators have been obtained. The definitions shown in the previous section are useful to understand the mathematical development of fractional viscoelasticity, but it is to be emphasized that others definitions of fractional operators exist. Moreover, integral transforms of fractional operators have been introduced in order to give some tool useful to solve fractional differential equations. The reader that wants to go deeper inside the fractional calculus can refer to [60, 74, 75, 81]; for an innovative techniques useful to solve fractional differential equations with the aid of Mellin transform one can consult [4, 14, 15, 28].

# Chapter 2

# Linear viscoelasticity

In this chapter the main concepts of linear viscoelasticity will be introduced, starting from the classical approach of classical viscoelasticity that models viscoelastic behaviour by combining elastic and viscous models; further, the fundamental principle of linear viscoelasticity, the *Boltzmann superposition principle* will be discussed; finally fractional viscoelasticity will be introduced and discussed.

## 2.1 Preliminary concepts

Viscoelastic materials are those materials that exhibit a mechanical behavior intermediate between those of elastic solids and viscous fluids. Solids are characterized by the fact that they have their own shape; in particular elastic solids are those solids which experience deformations proportional to external applied loads through a material parameter, the modulus of elasticity, and that return to their initial configuration once the loads are removed. Fluids, instead, do not possess an own shape and are characterized by the fact that the internal stress is proportional to the deformation gradient through the so-called viscosity, a parameter of the liquid itself; in particular for Newtonian fluids the viscosity is a constant that does not depend on the gradient of deformation. Because of the presence of the viscous part in their behavior, mechanical behavior of viscoelastic materials is time dependent.
Many materials exhibit viscoelastic behavior: polymers, biological tissues, bones, asphalt mixtures, concrete, soils and also some kind of rocks. For this reason in civil and industrial construction the characterization of viscoelastic

properties of materials is very important because allows to predict long terms effects of loads that if neglected can lead to erroneous design of engineering components and structures.
The time dependent nature of the mechanical behavior of viscoelastic material imposes to take into account into viscoelastic models of the time variable. For this reason in viscoelasticity usually the terms *stress history* and *strain history* take place instead of the simple stress and strain and time dependent entity, such as relaxation and creep function, are taken into account instead of the simple elastic moduli used in linear elasticity.

## 2.2 Basic concepts of linear viscoelasticity

In this section some basic concepts of linear viscoelasticity are introduced; firstly the attention will be focused on the creep and relaxation functions, then using those definitions the Boltzmann superposition principle will be obtained.

### 2.2.1 Creep and relaxation functions

Creep and relaxation are two phenomena typical of viscoelastic materials; in particular, the creep is the evolution of the strain that increases when a constant stress is applied to the material, while the relaxation is the evolution of the stress that decreases when a constant strain is applied. Each of these phenomena can be described by a corresponding function, the creep and the relaxation functions. They are able to completely describe the time dependent behavior of viscoelastic materials and are also involved in their constitutive laws.
The creep function $C(t)$ is the response in terms of strain history to an applied constant unitary stress history $\sigma(t) = U(t)$, where $U(t)$ is the unitstep function. Since we are limiting ourselves to linear viscoelasticity, if the applied constant stress is not unitary the obtained strain is simply obtained as:

$$\varepsilon(t) = C(t)\sigma_0 \tag{2.1}$$

where $\sigma_0$ is the constant applied stress. The function $C(t)$ is monotonically increasing and depends on the material at hands; moreover $C(t) = 0$ for $t < 0$. A typical creep function is depicted in Fig. 2.1.
The relaxation function $R(t)$ is the response in terms of stress history to an

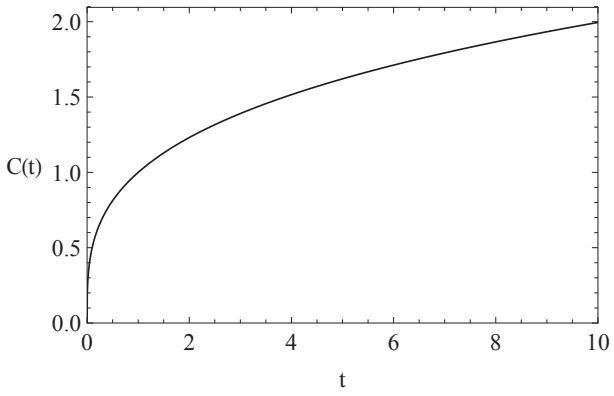


**Figure 2.1:** Typical creep function for a viscoelastic material.

applied constant unitary strain history $\varepsilon(t) = U(t)$. In linear viscoelasticity:

$$\sigma(t) = R(t)\varepsilon_0 \tag{2.2}$$

where$\varepsilon_0$ is the constant applied strain. The function $R(t)$ is monotonically decreasing and depends on the material at hand; like the creep function, $R(t) = 0$ for $t < 0$. A typical relaxation function is depicted in Fig. 2.2.

The properties of the Creep and Relaxation function to be null for $t < 0$ estab-

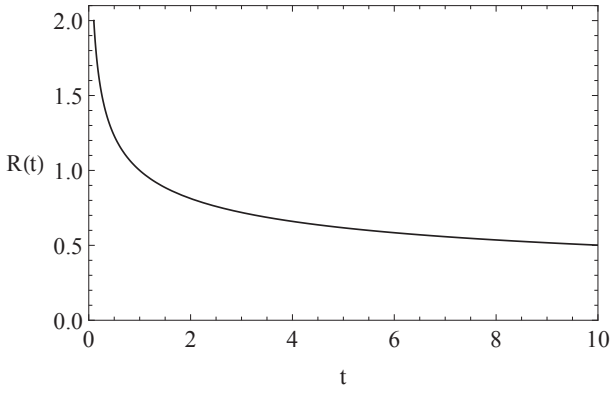


**Figure 2.2:** Typical relaxation function for a viscoelastic material.

lish an important characteristic of viscoelastic models: the effect does not anticipate the cause, then viscoelastic models are non-anticipative systems and obey to the concept of causality.

### 2.2.2 The Boltzmann superposition principle

Consider an ideal test in which a tensile stress is applied to a linear viscoelastic material. At the time $t = t_1 > 0$ a stress of magnitude $\Delta\sigma_1$ is applied; at the time $t = t_2 > t_1$ the stress is instantaneously increased to the value $\Delta\sigma_1 + \Delta\sigma_2$; this history of stress can be written as follows:

$$\sigma(t) = \Delta\sigma_1 U(t - t_1) + \Delta\sigma_2 U(t - t2) \tag{2.3}$$

The presence of the unitstep function $U(t)$ in Eq. (2.3) suggests that in $t_1$ and in $t_2$ the history of the applied stress has two jumps, than it is discontinuous, as shown in Fig. 2.3(a). In the range $0 \leq t \leq t_1$ the applied stress is zero

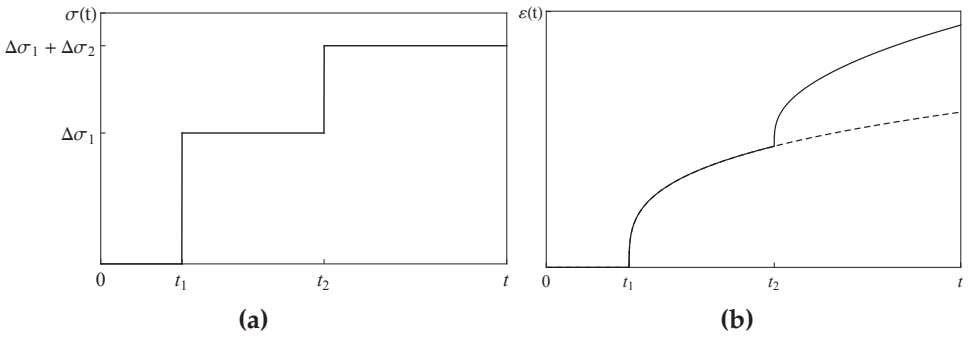


**Figure 2.3:** Applied stress history (a) and response in terms of strain history (b).

and nothing happens; in the range $t_1 < t \leq t_2$, the applied stress is $\Delta\sigma_1$, then the response in terms of strain history can be evaluated by applying Eq. (2.1); finally, for $t \geq t_2$ the applied stress is $\Delta\sigma_1 + \Delta\sigma_2$ and since the material is linear, it is possible to superimpose the responses due to the two stresses $\Delta\sigma_1$ and $\Delta\sigma_2$ considered separately, that is:

$$\varepsilon(t) = \Delta\sigma_1 C(t - t_1) + \Delta\sigma_2 C(t - t_2) \tag{2.4}$$

Since $C(t - t_1) = 0$ for $t < t_1$, in Eq. (2.4) $\varepsilon(t) = 0$ for $t < t_1$ and in the range $t_1 < t \leq t_2$ only the stress $\Delta\sigma_1$ contribute to the strain as it is shown in Fig. 2.3(b).
The same approach described above can be used with $n$ jumps in the stress history; in this case the response in terms of strain history can be written as

$$\varepsilon(t) = \sum_{k=1}^{n} \Delta\sigma_k C(t - t_k) \tag{2.5}$$

Eq. (2.5) express the superposition principle that is valid in linear viscoelasticity.
If the applied stress history is continuous, it can be discretized as a series of steps of duration $\Delta t$ in which the stress is constant; if $\Delta t \to 0$ then $\Delta\sigma \to d\sigma$ and summation (2.5) becomes an integral:

$$\varepsilon(t) = \int_0^t d\sigma(\tau)C(t-\tau) = \int_0^t \dot{\sigma}(\tau)C(t-\tau)d\tau \tag{2.6}$$

Eq. (2.6) is a convolution integral that gives the response in terms of stain history to a certain applied stress history and represents the integral formulation of viscoelasticity. It is evident that at every time instant the strain depends on all the past stress history; moreover if $\sigma(0) \neq 0$ it is necessary to add another term in Eq. (2.6):

$$\varepsilon(t) = \int_0^t \dot{\sigma}(\tau)C(t-\tau)d\tau + \sigma(0)C(t) \tag{2.7}$$

It is possible to define a dual formulation of the integral formulation of viscoelasticity; in order to do this, it is necessary to consider an ideal test in which the strain is applied to the viscoelastic material. Using the same approach as above the following formulation is obtained:

$$\sigma(t) = \int_0^t \dot{\varepsilon}(\tau)R(t-\tau)d\tau + \varepsilon(0)R(t) \tag{2.8}$$

Integrals in Eqs. (2.7) and (2.8) are often labeled as Boltzmann integral from the mathematician that studied them; often they are also labeled as "hereditary" integrals because of the dependence that the output $\varepsilon(t)$ (or $\sigma(t)$) has of the all past history of the input $\sigma(t)$ (or $\varepsilon(t)$).
Boltzmann integrals are also useful to find a relationship between the creep and relaxation functions; to this purpose, consider to apply to a linear viscoelastic material a stress history $\sigma(t)$ with $\sigma(0) = 0$; if we suppose to know the creep function $C(t)$, by means of Eq. (2.7) it is possible to obtain the response in terms of strain history $\varepsilon(t)$. If we also suppose to know the relaxation function $R(t)$, by using the response $\varepsilon(t)$ in Eq. (2.8), the initially imposed stress history $\sigma(t)$ is obtained. By performing Laplace transform of (2.7) and (2.8) and remembering properties (A.10) and (A.6), the following relationships in Laplace domain are obtained:

$$\sigma_{\mathcal{L}}(s) = s\varepsilon_{\mathcal{L}}(s)R_{\mathcal{L}}(s) \qquad \varepsilon_{\mathcal{L}}(s) = s\sigma_{\mathcal{L}}(s)C_{\mathcal{L}}(s) \tag{2.9}$$

that with simple manipulation give:

$$R_{\mathcal{L}}(s)C_{\mathcal{L}}(s) = \frac{1}{s^2} \tag{2.10}$$

Eq. (2.10) states that one of the creep or relaxation function can be obtained once the other is already known; this is a very important result because allows to perform only one test to characterize the behavior of a linear viscoelastic material both in creep and in relaxation.

## 2.3 Classical viscoelastic models

In this section the main aspects of classical viscoelastic models and some basic concepts of linear viscoelasticity are introduced.

### 2.3.1 The elastic and the viscous model

As already mentioned in the previous section, classic viscoelastic models are obtained by means of the combination of linear elastic and viscous models. The linear elastic model is the the so called Hooke's law in which the stress is linearly proportional to the strain:

$$\sigma = E\varepsilon \tag{2.11}$$

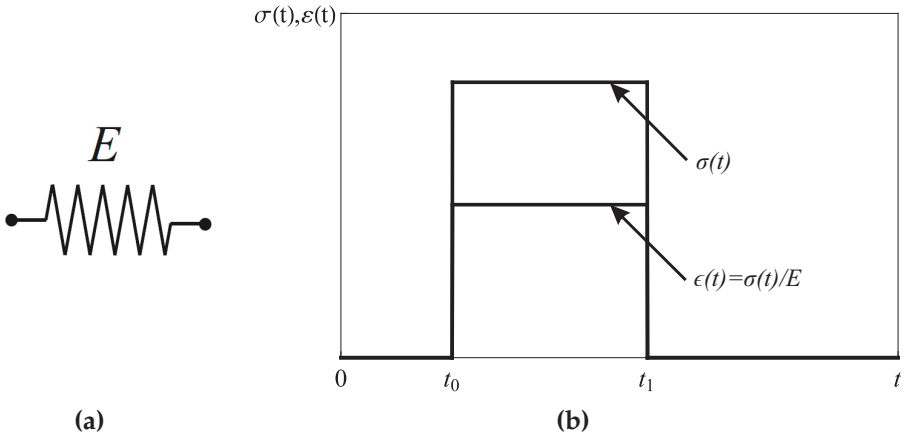


**Figure 2.4:** The spring or Hooke model (a); constant applied stress and obtained strain (b).

where $\sigma(t)$ is the stress, $\varepsilon(t)$ is the strain and $E$ is the Young modulus, that measure the attitude of a material to be strained under the application of some stress; the higher is the Young modulus greater has to be the stress to induce a given strain or smaller is the strain to induce a given stress. The stress is a force per unit area, then it has the dimension of a pressure (Pascal); the strain is an elongation per unit length then it is adimensional then the Young modulus has the same dimension of the stress. Usually the Hooke model is represented as a spring as depicted in Fig. 2.4(a).
As for the viscous model, the Newton-Petroff model is usually used; the constitutive law of this model is:

$$\sigma(t) = \eta\dot{\varepsilon}(t) \tag{2.12}$$

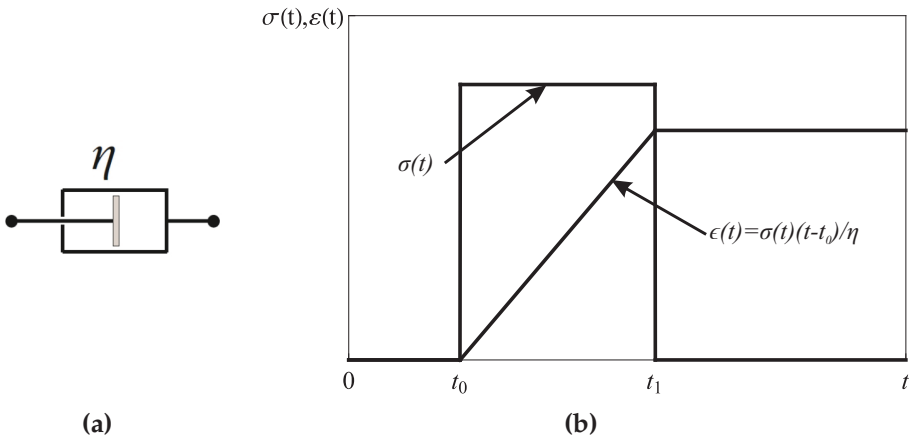


**Figure 2.5:** The dashpot or Newton-Petroff model (a); constant applied stress and obtained strain (b).

where $\eta$ is the viscosity of the fluid and the dot means first time derivative. The viscosity $\eta$ plays a role analogue to the Young modulus because if it is higher a smaller strain rate $\dot{\varepsilon}(t)$ is needed to obtain a given stress. Differently from the Young modulus, the dimension of $\eta$ is a stress multiplied for time and the dimension of the strain rate is the inverse of time.The Newton-Petroff model is represented as a dashpot as depicted in Fig. 2.5(a).
Although the structures of the two laws above are very similar, they describe very different behavior; in fact the Hooke law does not depend on time, any stress/strain applied to the solid immediately causes a correspondent strain/

stress and when the cause is removed also the consequence immediately disappears (see Fig. 2.4(b)). This also means that the Hooke material is able to store the work done by external load and to give it back when the loads are removed, without any loss of energy. The Newton-Petroff model, instead, is not able to store energy and all the work done by the external load is transformed into heat; as a consequence, the viscous fluid flows and does not return on the initial configuration when the loads are removed, as shown in Fig. 2.5(b). For this reason this model is usually used to represent the damping or dissipation of materials.
The Hooke and the Newton-Petroff models are mathematical models that represent ideal solid and ideal fluid. Although some materials can be modeled with very satisfactory approximation with one of this ideal behavior, as for example many metals in their linear elastic range, in the real world neither of the limiting behavior above described exist; indeed, all real materials combine properties of those limit cases and for this reason in classical viscoelasticity they are modeled as combinations of springs and dashpots.

### 2.3.2 Maxwell and Kelvin-Voigt models

The most simple classical viscoelastic models are the Maxwell model and the Kelvin-Voigt (KV) model; the first is constituted by a spring and a dashpot in series while the second is a spring connected in parallel with a dashpot, as depicted in Fig. 2.6.

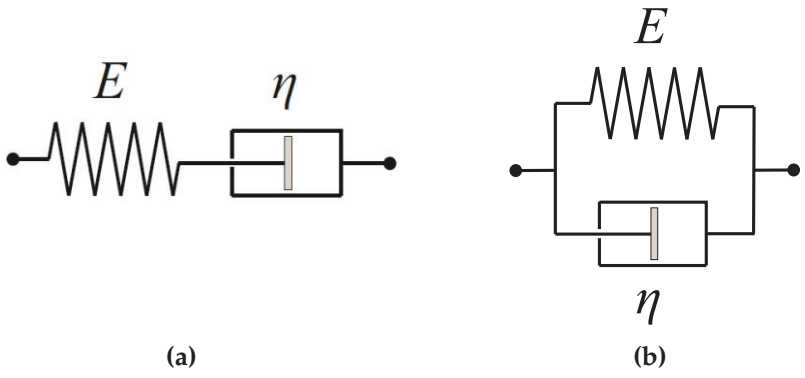


**Figure 2.6:** Maxwell model (a); KV model(b).

These models are the basis of viscoelasticity and are discussed in the following.

### Maxwell model

This model is characterized by the fact the both the spring and the dashpot in it experience the same stress, while the strain is the sum of the strains of the spring and of the dashpot; it is possible to take advantage of these conditions to obtain the constitutive equation of the model. In order to do this, the strain of the spring will be labeled as $\varepsilon_e(t)$ while the total strain simply $\varepsilon(t)$. The previous conditions in analytical form are the following:

$$\sigma(t) = E\varepsilon_e(t), \qquad \sigma(t) = \eta\left(\varepsilon(t) - \varepsilon_e(t)\right) \tag{2.13}$$

Combining the two expressions the constitutive equation is easily obtained:

$$\dot{\sigma}(t) + \frac{E}{\eta}\sigma(t) = E\dot{\varepsilon}(t) \tag{2.14}$$

In order to find the creep and the relaxation function Eq. (2.14) has to be solved once by imposing an unitary constant stress $\sigma(t) = U(t)$ and once by imposing an unitary strain $\varepsilon = U(t)$; alternatively one of the function can be found solving the constitutive equation and the other can be found with the aid of Eq. (2.10). The following expressions are obtained:

$$C(t) = \frac{t}{\eta} + \frac{1}{E} \tag{2.15a}$$

$$R(t) = Ee^{-\frac{E}{\eta}t} \tag{2.15b}$$

Eqs. (2.15) are depicted in Fig. 2.7; although the relaxation function is acceptable to fit experimental data (but it is not the best fitting possible for many viscoelastic material), the creep function is in contrast with the experimental evidence, because the strain increases linearly indefinitely. For this reason this model is not suitable to reproduce the mechanical behavior of real viscoelastic material.

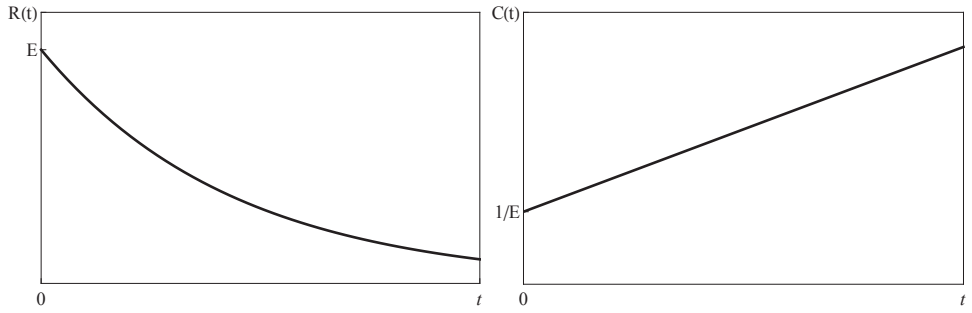


**Figure 2.7:** Creep (a) and relaxation (b) functions for the Maxwell model.

**Kelvin-Voigt model**

This model is the dual of the Maxwell one; since the elements are connected in parallel, they experience the same strain while the applied stress is the sum of the stresses on the spring $\sigma_e(t)$ and on the dashpot $\sigma_\eta(t)$:

$$\sigma_e(t) = E\varepsilon(t), \qquad \sigma_\eta(t) = \eta\dot{\varepsilon}(t) \tag{2.16}$$

Considering that the total stress is the sum of the two aliquots in Eq. (2.16), the following constitutive equation is obtained:

$$\dot{\varepsilon}(t) + \frac{E}{\eta}\varepsilon(t) = \frac{\sigma(t)}{\eta} \tag{2.17}$$

As in the case of the Maxwell model, the creep and relaxation can be easily found from the constitutive equation and are the following:

$$C(t) = \frac{1}{E}\left(1 - e^{-\frac{E}{\eta}t}\right) \tag{2.18a}$$

$$R(t) = E + \eta\delta(t) \tag{2.18b}$$

It is worth noticing that in Eq. (2.18b) $\eta\delta(t)$ does not contribute to the relaxation function itself but it is not negligible when we use the relaxation function in the Boltzmann integral. Differently from the Maxwell model, in this case the creep function can be considered acceptable to fit experimental data, although it is not the best choice for the correct fitting; the relaxation function, instead, is totally in disagreement with experiments, because it is constant, as

it is possible to see in Fig. 2.8.

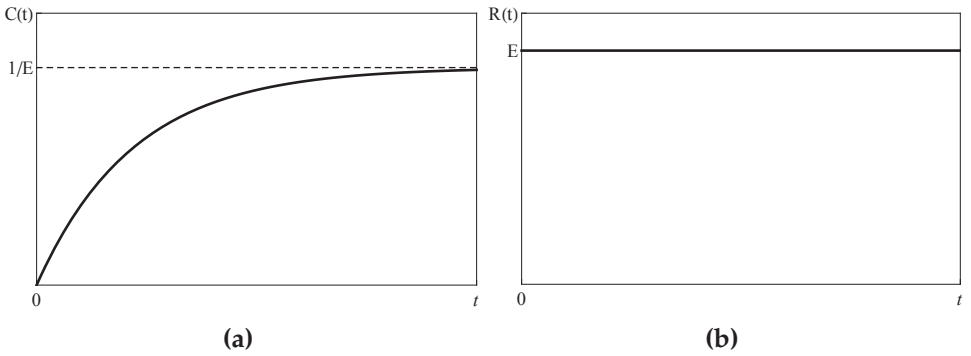


**Figure 2.8:** Creep (a) and relaxation (b) functions for the KV model.

The Maxwell and the KV are not able to reproduce both the creep and relaxation behavior; indeed, the Maxwell model is acceptable only to simulate the relaxation while the KV model is acceptable only to reproduce the creep behavior. For this reason other viscoelastic models constituted by more elements have been developed. These models are discussed in the following section.

### 2.3.3 Other classical viscoelastic models

Using more then two simple elements it is possible to define viscoelastic mechanical models that are able to reproduce both the creep and the relaxation behavior; by changing the way the springs and the dashpots are linked, different viscoelastic behavior can be obtained. The most simple of these models are the Zener models or Standard Linear Solid (SLS) models, depicted in Fig. 2.9. The constitutive equations of these two models are the following:

$$\dot{\sigma}(t) + \frac{E_2}{\eta}\sigma(t) = (E_1 + E_2)\dot{\varepsilon}(t) + \frac{E_1 E_2}{\eta}\varepsilon(t) \tag{2.19a}$$

$$\dot{\sigma}(t) + \frac{E_1 + E_2}{\eta}\sigma(t) = E_1\dot{\varepsilon}(t) + \frac{E_1 E_2}{\eta}\varepsilon(t) \tag{2.19b}$$

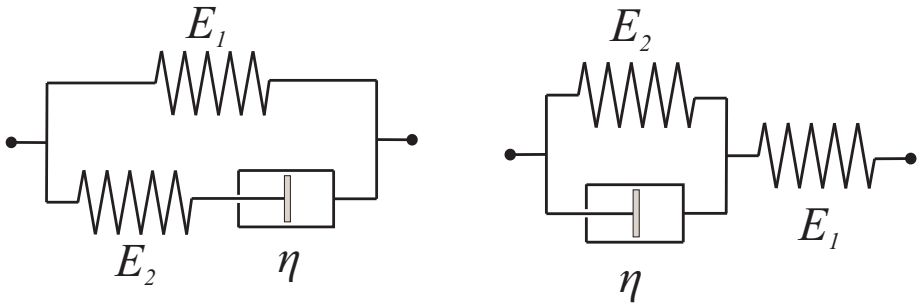


**Figure 2.9:** Standard linear solid models: model correspondent to Eq. (2.19a) (a), model correspondent to Eq. (2.19b) (b).

The creep and relaxation functions can be easily evaluated; for the model **(a)**:

$$C(t) = \frac{1}{E_1}\left(1 - \frac{E_2\, e^{-\frac{E_1 E_2}{(E_1+E_2)\eta}t}}{E_1 + E_2}\right) \tag{2.20a}$$

$$R(t) = E_1 + E_2 e^{-\frac{E_2}{\eta}t} \tag{2.20b}$$

whereas for the model **(b)**:

$$C(t) = \frac{1}{E_2}\left(\frac{E_1 + E_2}{E_1} - e^{-\frac{E_2}{\eta}t}\right) \tag{2.21a}$$

$$R(t) = \frac{E_1}{E_1 + E_2}\left(E_2 + E_1\, e^{-\frac{E_1+E_2}{\eta}t}\right) \tag{2.21b}$$

All the response of these model are governed by exponential functions, that ensure acceptable approximation of the creep and relaxations functions, especially when short term responses have to be simulated. Furthermore, these models have only three parameters each and then the best fitting of experimental results is still easy to perform. However, when simulation of long term behavior is needed these models are not enough accurate. For this reason viscoelastic models with more than three elements exists; the generic constitutive equation of these models is:

$$\sum_{k=0}^{n} a_k \frac{d^k}{dt^k}\sigma(t) = \sum_{k=0}^{m} b_k \frac{d^k}{dt^k}\varepsilon(t) \tag{2.22}$$

In Eq. (2.22) $a_k$ and $b_k$ are coefficients that depend on the mechanical parameters of springs and dashpots; when $n$ and $m$ increase, the accuracy of the model improves both in the short and in long term behavior. This is due to the fact that real viscoelastic materials exhibit power law type creep and relaxation functions; since the models of Eq. (2.22) have exponential type creep and relaxation functions, a good fitting of experimental data can be performed only with the superposition of many exponential functions, and then using models with many elements. However, many elements in the model means many coefficients to be defined with the best fitting of the experimental results; this can leads to practical difficulties in performing the best fitting and sometimes also to unexpected results.
Despite all the disadvantages classical viscoelastic models are still used for some engineering application, for the simplicity of mathematical manipulation and also for the ease in the implementation in finite element software, but many researcher of the field in the last decades switched their attention to something more rigorous and consistent with experimental results, that is fractional viscoelasticity.

## 2.4 Linear fractional viscoelasticity

In the previous section it has been shown how classical viscoelastic models are inadequate to properly simulate the behavior of real viscoelastic material. Fractional viscoelasticity overcomes the main disadvantages of classical viscoelasticity, as it will be shown in the following.

### 2.4.1 The experimental evidence

As mentioned above, many viscoelastic materials are characterized by creep and relaxation function that are well fitted by power law type functions; this fact has been confirmed by many researcher throughout the 20th century, but before it was believed that viscoelastic material could be characterized by exponential type functions as the classical model suggested.
The first that suggested the possibility to characterize viscoelastic materials with power law functions was P.G. Nutting; he performed many experimental test on viscoelastic materials (creep and relaxation tests) and in the end he arrived to two conclusions: 1) creep and relaxation functions are will fitted by power law functions; 2) the Hooke and the Newton law are particular cases of a more general constitutive law of solids.

In his paper of 1921 [73] he states that for the materials he tested he found two characteristics: for a given stress, the displacement is proportional to the power law of the time variable; for a given time instant the displacement is proportional to the power law of the applied force. Based on these results he postulated what he called "a new general law of deformation" for the description of the creep of solids:

$$s = at^n F^m \tag{2.23}$$

where $s$ is the displacement, $F$ is the constant applied force, $a$, $n$ and $m$ are material parameters; $n$ and $m$ are independent of $F$, $s$ and $a$ but depend on the temperature. The behavior of the Hooke law can be obtained from Eq. (2.23) by setting $m = 1$ and $n = 0$, whereas the behavior of the Newton law can be obtained by setting $n = m = 1$. Nutting found that the typical value of $n$ are in the range $0.2 \div 0.9$, while the values of $m$ lie in the range $0.75 \div 3.5$. For material that exhibit a solid behavior the values of $n$ is close to zero, while for materials which behavior is similar to fluids the value of $n$ is close to the unity, as for example for materials near the melting temperature.
After the experience of Nutting many researcher of the field confirmed his results; following these results, other researcher had the idea to use the fractional calculus to describe the mechanical behavior of viscoelastic material; the link between the law of Nutting and fractional viscoelasticity will be explained in the following sections.

### 2.4.2 The springpot element and the fractional constitutive law

In his paper Nutting introduced a law for the creep of viscoelastic materials that can be particularized to the limiting behavior of the Hooke law and the Newton law. Following this idea, in the twentieth century some researchers proposed a viscoelastic constitutive law in terms of fractional derivative, with order of derivation in the range $0 \div 1$; in this way when the order of derivation reach the limiting values of 0 and 1 the Hooke law and the Newton law are obtained, respectively, extending the idea of Nutting.
The first to hypothesize such a kind of constitutive law were Scott Blair G. W. and Caffyn J.E. [83]; they introduced a constitutive law containing the RL fractional derivative:

$$\sigma(t) = E(D^{\alpha}_{0^+}\varepsilon)(t) \tag{2.24}$$

where $0 \leq \alpha \leq$ and $E > 0$ are material parameters; moreover they introduced a symbol corresponding to this law and they gave it a name: the *springpot*, that

is something intermediate between the spring and the dashpot. The springpot is depicted in Fig. 2.10. Another author, A. N. Gerasimov [54], formulated a similar expression in which the only difference is the use of the Caputo's fractional derivative instead of the RL one:

$$\sigma(t) = k({}^{C}D_{+}^{\alpha}\varepsilon)(t) \tag{2.25}$$

where $0 \leq \alpha \leq 1$ and $k > 0$ are material parameters. If $\varepsilon(t) \leq 0$ for $t \leq 0$, then the RL derivative in Eq. (2.25) and Caputo derivative in Eq. (2.24) coincide, then the two formulation are equivalent.
A slightly different formulation was introduced by G.L. Slonimsky [85]:

$$\varepsilon(t) = \frac{1}{k}(I_{+}^{\alpha}\sigma)(t) \tag{2.26}$$

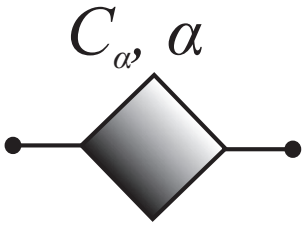


**Figure 2.10:** The springpot model.

As previously, $0 \leq \alpha \leq 1$ and $k > 0$ are material parameters. If $\varepsilon(t) \leq 0$ for $t \leq 0$, this formulation coincide with the first two. $E$ and $k$ assume the meaning of generalized viscosity; in the following this generalized viscosity will be denoted as $C_\alpha$. Then the fractional constitutive law of the springpot element can be expressed in the following equivalent ways

$$\sigma = C_\alpha({}^{C}D_{+}^{\alpha}\varepsilon)(t) \tag{2.27a}$$

$$\varepsilon(t) = \frac{1}{C_\alpha}(I_{+}^{\alpha}\sigma)(t) \tag{2.27b}$$

It is to be noted that $C_\alpha$ is not a usual coefficient and usually it is considered an anomalous coefficient; its dimension depends on the other parameter of the material $\alpha$, indeed as the dimension of the Young modulus is $Pa$ (Pascal, $= N/m^2$) and the dimension of the viscosity $\eta$ is $Pasec$, the dimension of $C_\alpha$ is $Pasec^\alpha$.

Since the Caputo derivative and RL integral reduce to integer order operators if $\alpha$ reaches integer values, the constitutive law of the springpot reduces to the Hooke one or the Newton one. This concepts is well summarize in Fig. 2.11

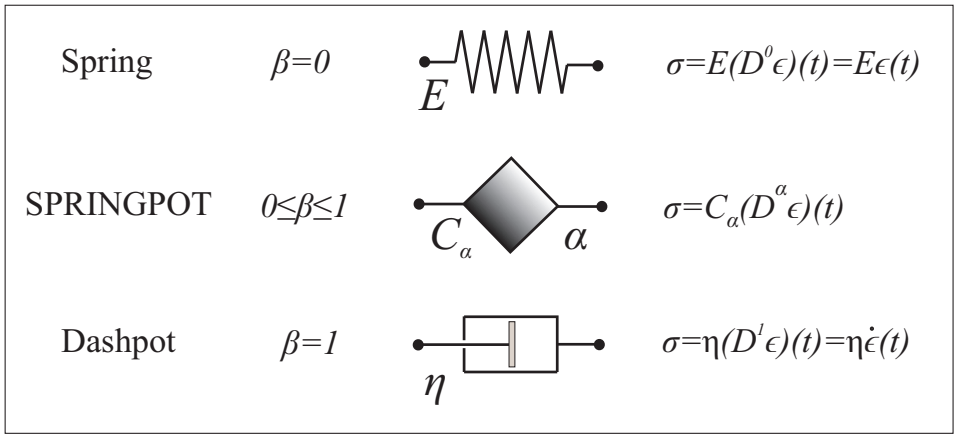


**Figure 2.11:** The springpot model and its particular cases.

It is to be emphasized that Eqs. (2.27) are not defined arbitrarily; indeed they descend directly from the Boltzmann superposition principle when power law creep and relaxation functions are assumed. In this way, the theory of fractional viscoelasticity is founded on solid basis and the link between power law functions and fractional derivatives is set rigorously.

### 2.4.3 The integral formulation of fractional viscoelasticity

In order to obtain fractional constitutive laws, the power law creep and relaxation functions have to be arranged like in the following:

$$C(t) = \frac{t^{\alpha}}{C_{\alpha}\Gamma(1+\alpha)} \tag{2.28a}$$

$$R(t) = \frac{C_{\alpha}t^{-\alpha}}{\Gamma(1-\alpha)} \tag{2.28b}$$

These functions are depicted in Fig. 2.12 for the different values of the parameter $\alpha$ and for $C_{\alpha} = 1$.

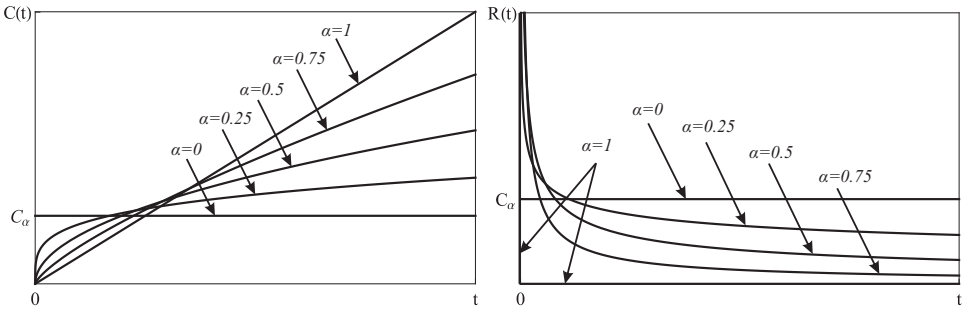


**Figure 2.12:** Creep (a) and relaxation (b) functions of the springpot for $C_\alpha = 1$ and different values of $\alpha$.

We start by considering the formulation (2.8) of the Boltzmann superposition principle and the relaxation function (2.28b):

$$\sigma(t) = \frac{C_\alpha}{\Gamma(1-\alpha)} \int_0^t \dot{\varepsilon}(\tau)(t-\tau)^{-\alpha} d\tau = C_\alpha ({}^{C}D_{0^+}^{\alpha} \varepsilon)(t) \tag{2.29}$$

By using the formulation (2.7) and the creep function (2.28a) instead:

$$\varepsilon(t) = \frac{1}{C_\alpha \Gamma(1+\alpha)} \int_0^t \dot{\sigma}(\tau)(t-\tau)^{\alpha} d\tau \tag{2.30}$$

integrating by parts and using property (A.66) of the Euler gamma function:

$$\begin{aligned} \varepsilon(t) &= \frac{\alpha}{C_\alpha \Gamma(1+\alpha)} \int_0^t \sigma(\tau)(t-\tau)^{\alpha-1} d\tau \\ &= \frac{1}{C_\alpha \Gamma(\alpha)} \int_0^t \sigma(\tau)(t-\tau)^{\alpha-1} d\tau = \frac{1}{C_\alpha} (I_{0^+}^{\alpha} \sigma)(t) \end{aligned} \tag{2.31}$$

From the Equations above, it is evident that by using power law creep and relaxation function in the Boltzmann superposition principle, fractional derivatives or integrals appears in the stress-strain relationship, because these operators are neither else than convolution integrals with power law kernel.
The use of the Euler gamma function in the creep and relaxation functions is not casual, but it is useful to respect the relationship between the creep and relaxation function in the Laplace domain; indeed, by performing Laplace transform of creep function (2.28a):

$$C_{\mathcal{L}}(s) = \mathcal{L}\{C(t); s\} = \mathcal{L}\left\{ \frac{t^{\alpha}}{C_\alpha \Gamma(1+\alpha)}; s \right\} = \frac{s^{-1-\alpha}}{C_\alpha} \tag{2.32}$$

while for the Laplace transform of the relaxation function (2.28b):

$$R_{\mathcal{L}}(s) = \mathcal{L}\left\{R(t); s\right\} = \mathcal{L}\left\{\frac{C_\alpha t^{-\alpha}}{\Gamma(1-\alpha)}; s\right\} = C_\alpha s^{-1+\alpha} \tag{2.33}$$

and then by multiplying the two Laplace transform:

$$C_{\mathcal{L}}(s)R_{\mathcal{L}}(s) = \frac{s^{-1-\alpha}}{C_\alpha} C_\alpha s^{-1+\alpha} = \frac{1}{s^2} \tag{2.34}$$

Eq. (2.34) demonstrate that the way the power law functions in Eqs. (2.28) have been arranged is consistent with the Boltzmann superposition principle, because condition (2.10) is respected. Note that without the Euler gamma functions in the definitions of $C(t)$ and $R(t)$ the product between their Laplace transform would give

$$C_{\mathcal{L}}(s)R_{\mathcal{L}}(s) = \frac{\Gamma(1-\alpha)\Gamma(1+\alpha)}{s^2}$$

violating the condition (2.10).
Note that the validity of the relationship (2.34) for the springpot model implies that with only two parameters it is possible to characterize a viscoelastic material both in relaxation and creep phases; for more details see [39].

## 2.5 The physical meaning of fractional viscoelasticity

Fractional viscoelasticity has some unquestionable advantages, but in the past its application has encountered some obstacles because of the lack of physical meaning of the fractional derivative of the strain (or of the fractional integral of the stress). Indeed, while the integer order derivatives or integrals of a function have a well known meaning, the fractional derivatives and integrals still lack of geometrical interpretation. However, in the field of viscoelasticity some researchers have been able to give to the fractional constitutive law a mechanical description in terms of particular combinations of simple classical elements, springs and dashpots, and then to give it a physical meaning.
In the past this issue was tackled by Schiessel and Blumen [82] and by Heymans and Bauwens [58] with their hierarchical models; in the last year the problem was also faced by Di Paola research group [36–38, 41] that defined the mechanical model of fractional viscoelasticity. In the following sections these models will be briefly discussed.

### 2.5.1 The hierarchical models

These models are characterized by the fact that some pattern is always repeated; the models of Schiessel and Blumen [82] for example is constituted by a series of Maxwell model connected like in the Fig. 2.13.

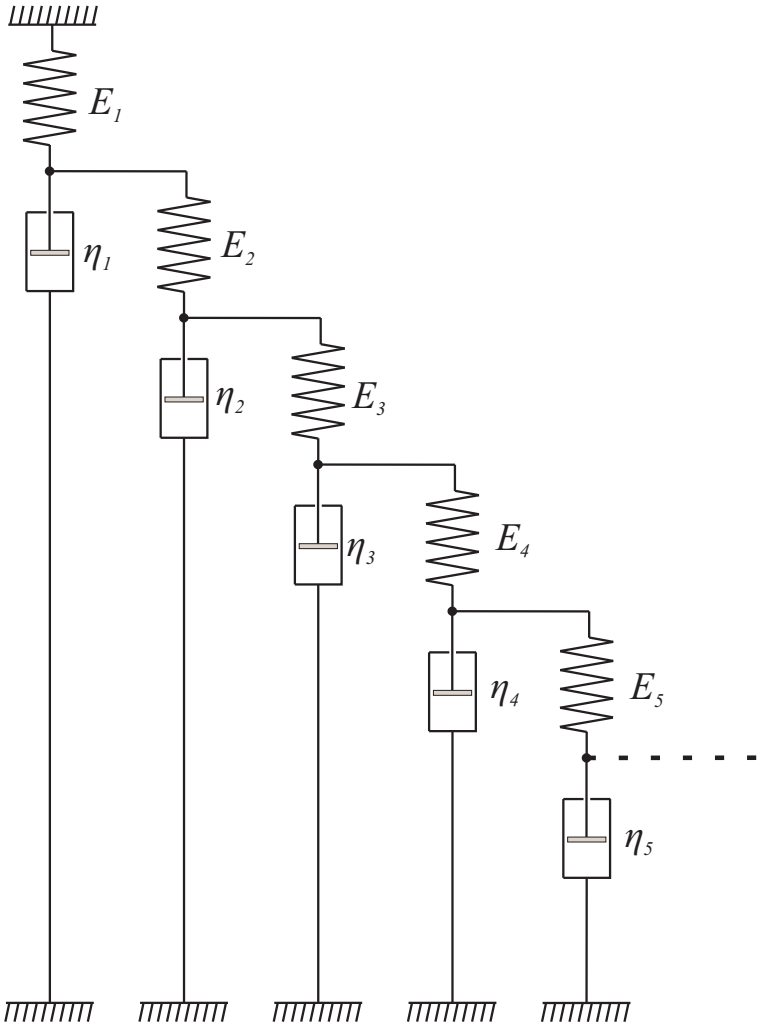


**Figure 2.13:** Schiessel and Blumen hierarchical model.

If the Young moduli and the viscosities are chosen as the following

$$E_j = \frac{1}{2j-1}\frac{\Gamma(\beta)}{\Gamma(1-\beta)}\frac{\Gamma(j+1-\beta)}{\Gamma(j-1-\beta)}E_1 \tag{2.35a}$$

$$\eta_j = \frac{2\Gamma(\beta)}{\Gamma(1-\beta)}\frac{\Gamma(j+1-\beta)}{\Gamma(j+\beta)}\eta_1 \tag{2.35b}$$

then the constitutive law of the springpot is obtained.
The same authors proposed another model based on the fractal Sierpinski triangle; this model simulates the chain network of many polymers and is constituted by a self-similar structure of springs and dashpot, as depicted in Fig. 2.14

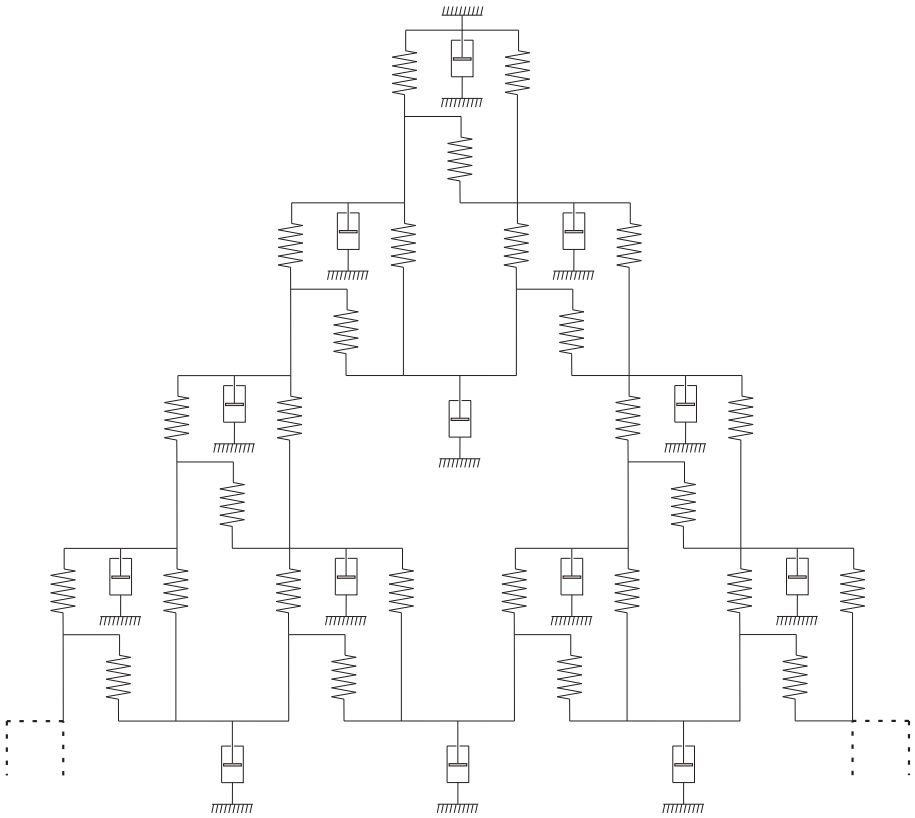

**Figure 2.14:** Schiessel and Blumen self-similar model.

As the previous one, this model exhibit power law creep and relaxation functions, then is able to reproduce the features of fractional viscoelasticity.
Heymans and Bauwens [58] proposed a fractal model constituted of KV models that form a self-similar tree structure; the model is representative of the mechanism generated by the chain structure of the polymers. The model is depicted in Fig. 2.15.

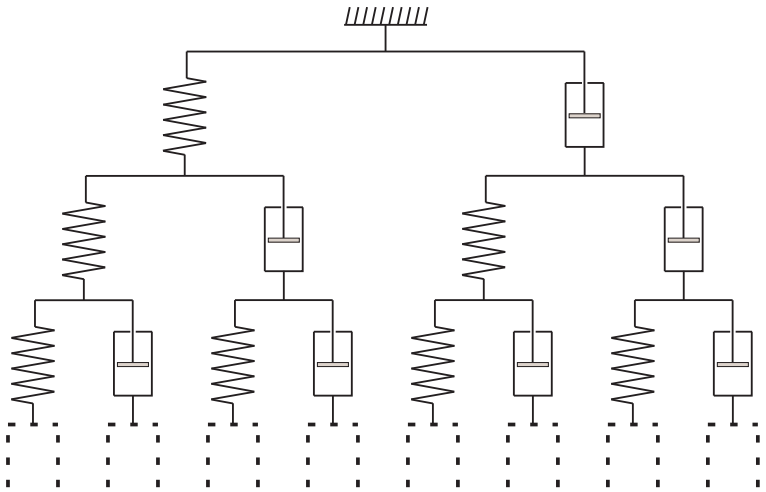

**Figure 2.15:** Heymans and Bauwens fractal model.

Also this model is able to reproduce power law creep and relaxation functions and then the constitutive law of the springpot.

### 2.5.2 The mechanical model of fractional viscoelasticity

In the early eighties Bagley and Torvik [11] showed how the fractional derivative naturally arises when particular mechanical models are studied.
Their original model was represented by a thin massless plate resting on a Newtonian viscous half-space (see Fig. 2.16(a)); they investigated the shear stress exerted by the Newtonian fluid on the plate when the plate is moved with a prescribed speed $\dot{u}(t)$. The Newtonian fluid is characterized by uniform viscosity $\eta_0$ and uniform mass density $\rho_0$. The governing equation of the motion of the fluid column with area $A = 1$ is the following:

$$\rho_0 \ddot{u}(z,t) = \eta_0 \frac{\partial^2 \dot{u}(z,t)}{\partial z^2} \tag{2.36}$$

By imposing the boundary conditions $u(\infty, t) = 0$ and $\dot{u}(0, t) = \dot{u}(t)$ the following solution is obtained:

$$\sigma(t) = \sqrt{\rho_0 \eta_0} ({}^{C}D_{0^+}^{3/2} u)(t) \tag{2.37}$$

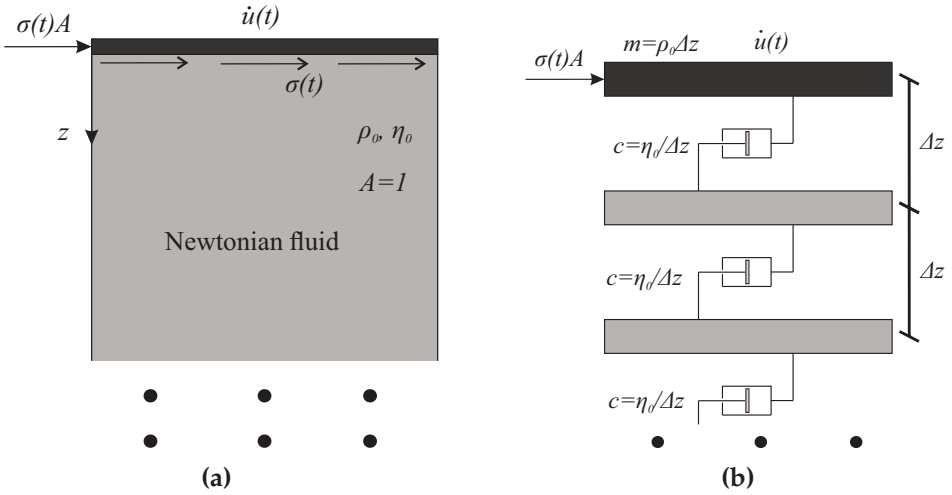


**Figure 2.16:** Original Bagley and Torvik model (a) and discretized version (b).

Eq. (2.37) shows that the mechanical of Fig. 2.16(a) does not yield a viscoelastic rheologic model, since the order of derivation is not in the range $0 \div 1$ and it may be considered a visco-inertial system. The discretized version of Fig. (2.16(b)), for $\Delta z \to 0$, leads to the same results of the continuous counterpart.
In order to obtain a viscoelastic behavior this model has to be modified as shown in Fig. 2.17(b), that has been labeled as visco-elastic (VE) model. In this case a nondimensional $z$ coordinate is introduced and the unitary strain $\gamma(z, t)$ instead of the displacement $u(z, t)$ is considered. If $\eta_V(z) = \eta_{V0}$ and $G_V(z) = G_{V0}$ the governing equation of this model is:

$$\eta_0 \dot{\gamma}(z, t) = G_0 \frac{\partial^2 \gamma(z, t)}{\partial z^2} \tag{2.38}$$

that leads to the following relationship between applied stress and the strain at $z = 0$:

$$\sigma(t) = \sqrt{G_{V0} \eta_{V0}} ({}^{C}D_{0^+}^{1/2} \gamma)(t) \tag{2.39}$$

Since the order of the fractional derivative in the range $0 \div 1$, this model describe a fractional viscoelastic constitutive behavior. The same result can be achieved with a model specular to the VE model, that is depicted in Fig. 2.17(a) and is usually labeled as elasto-viscous (EV) model, simply by setting constant stiffness of the bed of springs and constant viscosity of the viscous layer.

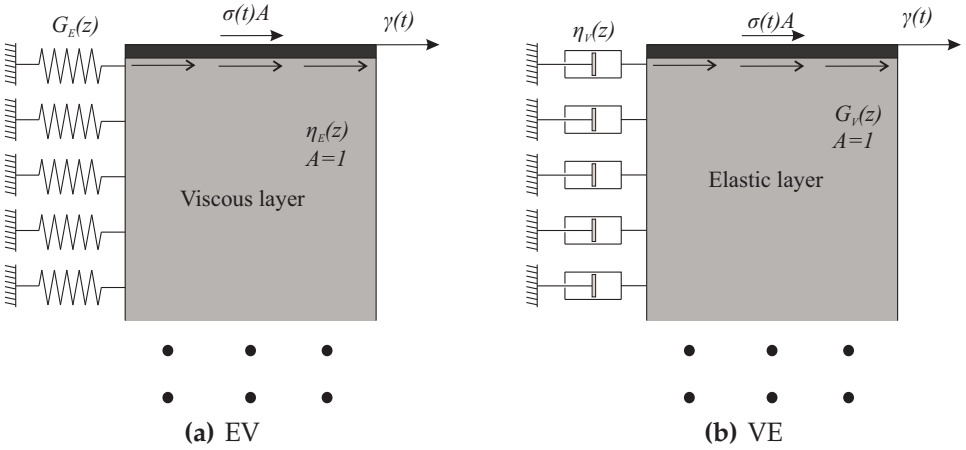


**(a)** EV **(b)** VE

**Figure 2.17:** Modified Bagley and Torvik elasto-viscous (EV) model (a) and visco-elastic (VE) model (b).

However these models are not satisfactory, because permit to obtain only a particular case of fractional viscoelasticity, that is the case with order of derivation $\alpha = 1/2$. But experimental tests reveal that viscoelastic material can have very different values of the order of derivation in the range $0 \div 1$. Then to obtain a more general results these models have been further improved by Di Paola [41]. In order to do so, variable viscosities and stiffness along the coordinate $z$ are defined; for the EV material ($\alpha \in [0, 1/2]$):

$$G_E(z) = \frac{G_0}{\Gamma(1+\beta)} z^{-\beta}, \qquad \eta_E(z) = \frac{\eta_0}{\Gamma(1-\beta)} z^{-\beta} \tag{2.40}$$

while for the VE material ($\alpha \in [1/2, 1]$):

$$G_V(z) = \frac{G_0}{\Gamma(1-\beta)} z^{-\beta}, \qquad \eta_V(z) = \frac{\eta_0}{\Gamma(1+\beta)} z^{-\beta} \tag{2.41}$$

where $G_0$ and $\eta_0$ are reference values. The governing equations of the systems of Fig. 2.17 are:

$$EV: \quad \frac{\partial}{\partial z}\left[\eta_E(z)\frac{\partial \dot{\gamma}(z,t)}{\partial z}\right] = G_E(z)\gamma(z,t) \tag{2.42a}$$

$$VE: \quad \frac{\partial}{\partial z}\left[G_V(z)\frac{\partial \gamma(z,t)}{\partial z}\right] = \eta_V(z)\dot{\gamma}(z,t) \tag{2.42b}$$

The solutions to these equations can be easily found in the Laplace domain; indeed, the Laplace transform of Eqs. (2.42) are Bessel equations, then the solution $\gamma(z,s)$ involves modified Bessel function of the first and second kind, denoted $I_\alpha(\cdot)$ and $K_\beta(\cdot)$, respectively, and defined in Eqs. (A.98) and (A.99). The solutions in the Laplace domain for the EV case is:

$$\gamma_{\mathcal{L}}(z,s) = z^\alpha\left[B_{E1}I_\alpha\left(\frac{z}{\sqrt{\tau_E(\beta)s}}\right) + B_{E2}K_\alpha\left(\frac{z}{\sqrt{\tau_E(\beta)s}}\right)\right] \tag{2.43}$$

where $\tau_E(\beta) = -\eta_0\Gamma(\beta)/(\Gamma(-\beta)G_0)$ and $\alpha = (1-\beta)/2$; for the VE case instead:

$$\gamma_{\mathcal{L}}(z,s) = z^\alpha\left[B_{V1}I_\alpha\left(z\sqrt{\tau_E(\beta)s}\right) + B_{V2}K_\alpha\left(z\sqrt{\tau_E(\beta)s}\right)\right] \tag{2.44}$$

with $\tau_V(\beta) = -\eta_0\Gamma(-\beta)/(\Gamma(\beta)G_0)$ and $\alpha = (1+\beta)/2$. The constant $B_{Ei}$ and $B_{Vi}$ are obtained from the following boundary conditions:

$$EV: \quad \begin{cases} \lim\limits_{z\to 0}\eta_E(z)\dfrac{\partial \dot{\gamma}(z,t)}{\partial z} = \sigma(0,t) = \sigma(t) \\ \lim\limits_{z\to\infty}\gamma(z,t) = 0 \end{cases} \tag{2.45a}$$

$$VE: \quad \begin{cases} \lim\limits_{z\to 0}G_V(z)\dfrac{\partial \gamma(z,t)}{\partial z} = \sigma(0,t) = \sigma(t) \\ \lim\limits_{z\to\infty}\gamma(z,t) = 0 \end{cases} \tag{2.45b}$$

By making inverse Laplace transform of Eqs. (2.43) and (2.44) the constitutive law of the springpot is obtained:

$$EV: \quad \gamma(t) = \frac{1}{C_E(\alpha)}(I^\alpha_{0^+}\sigma)(t) \tag{2.46a}$$

$$VE: \quad \gamma(t) = \frac{1}{C_V(\alpha)}(I^{\alpha}_{0^+}\sigma)(t) \tag{2.46b}$$

where $C_E(\alpha)$ and $C_V(\alpha)$ are defined as following:

$$C_E(\alpha) = \frac{G_0\Gamma(\alpha)2^{2\alpha-1}}{\Gamma(2-2\alpha)\Gamma(1-\alpha)}\tau_E(\beta)^{\alpha} \tag{2.47a}$$

$$C_V(\alpha) = \frac{G_0\Gamma(1-\alpha)2^{1-2\alpha}}{\Gamma(2-2\alpha)\Gamma(1-\alpha)}\tau_V(\beta)^{\alpha} \tag{2.47b}$$

An interesting characteristic of the mechanical models in Fig. 2.17 is that the motion is not transmitted indefinitely along the $z$ coordinate; this allows to discretize the models in the way depicted in Fig. 2.18 by considering a finite number of elements.

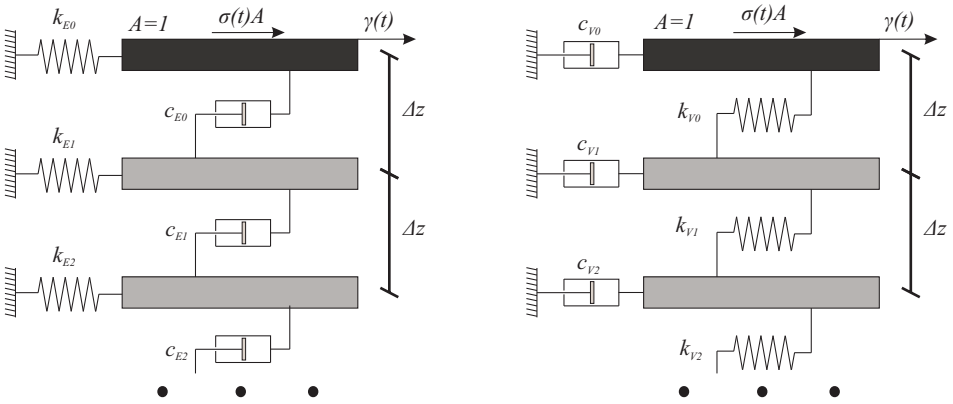


**(a)** EV **(b)** VE

**Figure 2.18:** Modified Bagley and Torvik elasto-viscous model (a) and viscoelastic model (b): discretized counterparts.

For the EV model, the coefficients of the springs and of the dashpots are defined, accordingly to the continuous counterpart, as:

$$k_{Ej} = \frac{G_0}{\Gamma(1+\alpha)}z_j^{-\alpha}\Delta z, \qquad c_{Ej} = \frac{\eta_0}{\Gamma(1-\alpha)}\frac{z_j^{-\alpha}}{\Delta z} \tag{2.48}$$

whereas for the VE model:

$$k_{Vj} = \frac{G_0}{\Gamma(1-\alpha)}\frac{z_j^{-\alpha}}{\Delta z}, \qquad c_{Vj} = \frac{\eta_0}{\Gamma(1+\alpha)}z_j^{-\alpha}\Delta z \tag{2.49}$$

To obtain the response of the upper lamina, which corresponds with the response of the springpot, it is necessary to write the equilibrium equations of all the laminae considered; for the $j-th$ lamina:

$$EV: \quad k_{Ej}\gamma_j(t) + c_{Ej-1}\Delta\dot{\gamma}_{j-1}(t) - c_{Ej}\Delta\dot{\gamma}_j(t) = 0, \quad j = 1,2,...,\infty \tag{2.50a}$$

$$VE: \quad c_{Vj}\dot{\gamma}_j(t) + k_{Vj-1}\Delta\dot{\gamma}_{j-1}(t) - k_{Vj}\Delta\dot{\gamma}_j(t) = 0, \quad j = 1,2,...,\infty \tag{2.50b}$$

then if the model is constituted by $n$ laminae, a system of $n$ coupled ordinary differential equations is obtained. The advantage is that the system can be decoupled by a modal analysis obtaining $n$ uncoupled differential equation of the first order that are very easy to solve; in this way it is possible to construct comparison solutions also for cases in which the input is very complicate. Accurate results are obtained with a high number of laminae, such as $n = 1000 \div 1500$ for observation times of some tens of seconds; longer is the observation time higher must be the number $n$ to obtain accurate results.
Finally note that the discretized VE model is perfectly equivalent to the Schiessel and Blumen of Fig. 2.13. More details can be found in [36–38, 41].

## 2.6 Conclusions

In this chapter basic concepts for linear viscoelasticity have been introduced and then applied for deriving the fractional viscoelasticity law, that is the constitutive law of the so-called springpot; moreover it has been shown how the behavior of the springpot can be reproduced by classical viscoelastic models only by taking into account a great number (theoretically infinite) of classical elements, namely springs and dashpots.
However, the 1D law is not enough if one wants to apply the fractional viscoelasticity to real engineering components; indeed, the evaluation of the stress and strain fields in real engineering components needs the definition of a proper 3D constitutive law; this issue will be addressed in the next chapter.

# Chapter 3

# 3D fractional viscoelasticity

In the previous chapter, the fractional viscoelasticity has been introduced for 1D problems. Nowadays, many polymers and other viscoelastic materials are used in many applications, from engineering to biomechanics; then, in order to replace expensive experimental tests with numerical simulation, there is the need to define accurate 3D models; the parameters of these models can be found by the best fitting procedure on experimental tests of simple shaped specimen. In this chapter a linear fractional viscoelastic 3D model is defined; others 3D fractional viscoelastic models have been proposed in literature with both small strain and large strain formulations, but never the 3D behavior of these models is investigated or at least shown by means of creep or relaxation tests in 3D conditions, or by analyzing the behavior of the viscoelastic Poisson's ratio, see for example [50, 53, 59]. For this reason, in this chapter, once the 3D fractional viscoelastic model is introduced, the 3D behavior is investigated through creep and relaxation tests and by means of the viscoelastic Poisson's ratio in creep and in relaxation; moreover the thermodynamic consistency of the model is discussed in order to find restrictions on the values of the parameters.

## 3.1 3D fractional constitutive law

In this section we introduce the isotropic 3D fractional model of the springpot; the model is intended to be isotropic throughout the deformation, hence it is assumed that the effects due to memory do not alter the material symmetries. However, concepts outlined in the following are valid also for the other frac-

tional models mentioned above.
The constitutive model is obtained by means of a generalization of the elastic constitutive law (Hooke's Law); in that case only two parameters are required to define the whole stiffness (or compliance) matrix of the material and these two parameters can be chosen as Young's modulus and Poisson's ratio. In this case, we choose to write the stiffness matrix in terms of the shear modulus and Bulk modulus, because of their clear physical meaning (deviatoric and volumetric parts of the stiffness). The terms of the stiffness matrix $\boldsymbol{D}$ can be written as follows:

$$D_{ijkh} = \left(K - \frac{2}{3}G\right)\delta_{ij}\delta_{kh} + G\left(\delta_{ik}\delta_{jh} + \delta_{ih}\delta_{jk}\right) \tag{3.1}$$

where $K = \frac{E}{3(1-2\nu)}$ is the Bulk modulus, $G$ is the shear modulus, $\delta_{ij}$ is the Kronecker symbol, $E$ is Young's modulus and $\nu$ is Poisson's ratio.
In order to generalize the elastic laws and obtain a fractional viscoelastic constitutive model, it is sufficient to substitute shear modulus and Bulk modulus with appropriate relaxation functions; we choose to consider both the deviatoric part (shear relaxation function) and the volumetric part (Bulk relaxation function) as follows:

$$G(t) = \frac{G_\alpha t^{-\alpha}}{\Gamma(1-\alpha)} \tag{3.2a}$$

$$K(t) = \frac{K_\beta t^{-\beta}}{\Gamma(1-\beta)} \tag{3.2b}$$

where $K_\alpha$, $G_\beta$, $\alpha$ and $\beta$ are parameters of the deviatoric and volumetric relaxation functions respectively.
By assuming relaxation functions with the form of Eqs. (3.2), a four parameter mechanical model is obtained. The strain-stress relationship can be obtained simply by applying the Boltzmann superposition principle:

$$\boldsymbol{\sigma}(t) = \int_0^t \boldsymbol{R}(t-\tau)\dot{\boldsymbol{\varepsilon}}d\tau \tag{3.3}$$

where $\boldsymbol{R}(t)$ is the relaxation matrix and $\boldsymbol{\sigma}(t)$ and $\boldsymbol{\varepsilon}(t)$ are the stress and strain tensors, respectively. The relaxation matrix $\boldsymbol{R}(t)$ can be written in the same way as the stiffness matrix of Eq. (3.1) in which $G$ is substituted with $G(t)$ of Eq. (3.2a) and $K$ is substituted with $K(t)$ of Eq. (3.2b). In some cases, application of Eq. (3.3) is difficult because of the presence of the Mittag-Leffler function in the relaxation function (fractional Maxwell and SLS models): the

convolution with this function as kernel in-fact leads to a summation of infinite fractional derivatives. This problem may be overcome by using the inverse relationship, namely the convolution in terms of creep functions (Eq. (2.6)).
The inverse relationship of Eq. (3.3) is obtained by applying the dual form of Boltzmann's superposition principle:

$$\boldsymbol{\varepsilon}(t) = \int_0^t \boldsymbol{C}(t-\tau)\dot{\boldsymbol{\sigma}}(\tau)d\tau \tag{3.4}$$

In order to use Eq. (3.4) we need to obtain the creep matrix $\boldsymbol{C}(t)$ by using Eq. (2.10) (adapted for the 3D case). $\boldsymbol{C}(t)$ is evaluated by performing a Laplace transformation of the relaxation matrix and evaluating its inverse in the Laplace domain:

$$\hat{\boldsymbol{C}}(s) = \frac{\hat{\boldsymbol{R}}^{-1}(s)}{s^2} \tag{3.5}$$

By taking the inverse Laplace transform of $\hat{\boldsymbol{C}}(s)$ in Eq. (3.5) the creep matrix can be written as:

$$C_{ijkh} = \left(\frac{\bar{K}(t)}{9} - \frac{\bar{G}(t)}{6}\right)\delta_{ij}\delta_{kh} + \bar{G}(t)\left(\delta_{ik}\delta_{jh} - \frac{\delta_{ih}\delta_{jk}}{2}\right) \tag{3.6}$$

where $\bar{K}(t)$ and $\bar{G}(t)$ are creep functions of the volumetric and deviatoric parts, respectively, and are analogous to Eq. (2.28b):

$$\bar{G}(t) = \frac{t^\alpha}{G_\alpha \Gamma(1+\alpha)} \tag{3.7a}$$

$$\bar{K}(t) = \frac{t^\beta}{K_\beta \Gamma(1+\beta)} \tag{3.7b}$$

Note that in both Eqs. (3.1) and (3.6) the shear strain is considered as the engineering shear strain, e.g. $\gamma_{12} = 2\varepsilon_{12}$.
In the SLS models, both the creep and the relaxation functions contain Mittag-Leffler functions, then using Eq. (3.4) is not a viable strategy. In this case we write directly the governing equations separating the volumetric and deviatoric contributions and then summing the contributions; obviously, since the volumetric and deviatoric relaxation and creep functions have the same structures of Eq. (3.26), the equations for the two contributions are perfectly analogous to Eq. (3.26). This is the easiest way to obtain governing equations

for the 3D fractional models.
In some applications it could be necessary to define anisotropic viscoelastic models; this is for example the case of fiber reinforced composites with polymeric matrices, especially when the fiber have a prevalent orientation. Indeed most of the fibers used in the composites may be considered as elastic, while polymeric matrices exhibit a considerable viscoelastic behavior (pultruded bars); for this reason the mechanical properties are different between the direction along the fibers and the directions orthogonal to fibers and anisotropic constitutive model are required. As in elasticity the number of mechanical constant increases with the increasing level of anisotropy, in viscoelasticity for anisotropic models more than two relaxation (or creep) functions must be defined. Once again, this leads to the need to use simple fractional viscoelastic models and not very complicate ones in order to have the smallest number of mechanical parameters to be defined.

## 3.2 Behavior of the 3D springpot model

In this section the behavior of the 3D springpot model is analyzed in creep and relaxation tests focusing the attention on the Poisson's ratio and on the evolution of the stresses and the strains in 3D conditions.

### 3.2.1 Poisson's ratio

One of the most important aspects of 3D viscoelastic models is the behavior of the ratio of the lateral contraction to the elongation, i.e. the viscoelastic Poisson ratio. In fact, it is well known that during the infinitesimal deformation of any real viscoelastic material, the lateral contraction is a time-dependent (or equivalently frequency-dependent) function. Among all studies devoted to the viscoelastic Poisson's ratio, the works of Lakes and Tschoegl are of particular interest. In the paper [89] some concepts about viscoelastic Poisson's ratio are clarified: first, it is shown that the viscoelastic Poisson's ratio depends on the test performed, then viscoelastic Poissson's ratio is different in creep and in relaxation test; then it is shown, by means of correspondence principles [49], that the viscoelastic counterpart of the elastic Poisson's ratio is the viscoelastic Poisson's ratio in relaxation and not in creep; finally, it is shown how to switch between Poisson's ratio in creep and in relaxation. In the paper [64] the same results are achieved; moreover, in the papers [63, 64] it is shown that the viscoelastic Poisson's ratio can increase or decrease with

time; indeed, most polymers for example exhibit an increasing Poisson ratio because of the fact that the volumetric part of stress relaxes much less than the deviatoric part, but material with a particular microscopic structure can behave the opposite way; furthermore, in the paper [64] it is demonstrated that the viscoelastic Poisson's ratio need not be monotonic with time.
As it is shown in the following 3D fractional constitutive models are able to reproduce both an increasing and a decreasing viscoelastic Poisson's ratio. To this purpose the viscoelastic Poisson ratio is evaluated from an ideal creep test and an ideal relaxation test.

**Poisson's ratio in creep**

The Poisson ratio is evaluated in an ideal creep test on a viscoelastic cube; only one face of the cube is fixed only in the normal direction and in the opposite face the cube is loaded by a constant normal stress $\sigma_0$; using the springpot model of Fig. 2.10 considering the creep functions specified in Eqs. (3.7):

$$\begin{aligned} \nu_C(t) = -\frac{\varepsilon_T(t)}{\varepsilon_L(t)} = -\frac{\left(\frac{\bar{K}(t)}{9} - \frac{\bar{G}(t)}{6}\right)\sigma_0 U(t)}{\left(\frac{\bar{K}(t)}{9} + \frac{\bar{G}(t)}{3}\right)\sigma_0 U(t)} = \\ -\frac{\frac{t^\beta}{9K_\beta\Gamma(1+\beta)} - \frac{t^\alpha}{6G_\alpha\Gamma(1+\alpha)}}{\frac{t^\beta}{9K_\beta\Gamma(1+\beta)} + \frac{t^\alpha}{3G_\alpha\Gamma(1+\alpha)}} = \frac{-2+3at^{\alpha-\beta}}{2\left(1+3at^{\alpha-\beta}\right)} \end{aligned} \tag{3.8}$$

where $\varepsilon_L(t) = \left(\frac{\bar{K}(t)}{9} + \frac{\bar{G}(t)}{3}\right) U(t)$ and $\varepsilon_T(t) = \left(\frac{\bar{K}(t)}{9} - \frac{\bar{G}(t)}{6}\right) U(t)$ are the longitudinal and transverse strain, respectively, $U(t)$ is the unit step function and $a = \frac{K_\beta\Gamma(1+\beta)}{G_\alpha\Gamma(1+\alpha)} > 0$ and the subscript $C$ of $\nu_C(t)$ stands for creep. If $\alpha = \beta$, the Poisson ratio is constant over time:

$$\nu_C(t) = \bar{\nu} = \frac{-2G_\alpha + 3K_\beta}{2(G_\alpha + 3K_\beta)} \tag{3.9}$$

Note that Eq. (3.8) can be written in this form because, since in creep all the components of the stress vector are unitstep functions (the longitudinal one is a unitstep function, while the others are zero), the convolution (3.4) reduces to a product between $\boldsymbol{C}(t)$ and $\boldsymbol{\sigma}(t)$ and then both $\varepsilon_L(t)$ and $\varepsilon_T(t)$ can be simply written in terms of volumetric and deviatoric creep functions.
If $\alpha \neq \beta$, the Poisson ratio varies in time and it has limit values at $t = 0$ and $t = \infty$, as summarized in the Table 3.2.

| | $t=0$ | $t=\infty$ |
|---|---|---|
| $\alpha > \beta$ | $\nu = -1$ | $\nu = 1/2$ |
| $\alpha = \beta$ | $\nu(t) = \frac{-2G_\alpha + 3K_\beta}{2(G_\alpha + 3K_\beta)}$ | |
| $\beta > \alpha$ | $\nu = 1/2$ | $\nu = -1$ |

**Table 3.1:** Limiting values for the Poisson ratio in a creep test.

Note that both the value have to be evaluated as a limit. The main consequences of these results are:

- If $\alpha > \beta$, the material exhibits a Poisson ratio of -1 at $t = 0$, then its behavior gradually changes until it becomes incompressible for large values of $t$.
- If $\beta > \alpha$, the material is incompressible at $t = 0$, then its behavior gradually changes until it exhibits a negative Poisson ratio for large values of $t$.

**Poisson's ratio in relaxation**

The Poisson ratio can also be evaluated for an ideal relaxation test on a cube with the same boundary conditions of the creep test; on the face opposite the fixed one, a normal constant displacement is applied. In this case the longitudinal strain is imposed while the transverse strain is unknown; in order to obtain it we simply need to write Eq. (3.3) and assume that the transverse components of the stress are both zero. Since $\varepsilon_T(t)$ is not constant as $\varepsilon_L(t) = \varepsilon_0 U(t)$ is, relationship (3.3) does not simplify in a simple product between $\boldsymbol{R}(t)$ and $\boldsymbol{\varepsilon}(t)$, then determine an expression of the Poisson ratio in relaxation in terms of the relaxation functions is not straightforward. In (citare) a relationship between the two ratios has been found:

$$\nu_C(t) = \frac{\int_0^t \nu_R(t-\tau)\dot{C}_{11}(\tau)d\tau}{C_{11}(t)} \tag{3.10}$$

where $C_{11}(t)$ is the term in position $1-1$ of the creep matrix that in this case is $C_{11}(t) = \frac{\bar{K}(t)}{9} + \frac{\bar{G}(t)}{3}$. In order to find $\nu_R(t)$ Laplace transform can be used, but inversion of the Laplace transform of $\nu_R(t)$ to the time domain is very

difficult. Only in the case when $\alpha = \beta$ the transverse strain $\varepsilon_T(t)$ is constant during the relaxation test and is equal to:

$$\varepsilon_T(t) = -\frac{-2G(t) + 3K(t)}{2(G(t) + 3K(t))}\varepsilon_0 U(t) \qquad (\alpha = \beta) \tag{3.11}$$

where $\varepsilon_0$ is the amplitude of the superimposed strain. Since $\varepsilon_L(t) = \varepsilon_0 U(t)$ the Poisson ratio is

$$\nu_R(t) = -\frac{-2G(t) + 3K(t)}{2(G(t) + 3K(t))} \qquad (\alpha = \beta) \tag{3.12}$$

that form the equality $\alpha = \beta$ reduces to:

$$\nu_R(t) = \bar{\nu} = -\frac{-2G_\alpha + 3K_\beta}{2(G_\alpha + 3K_\beta)} \qquad (\alpha = \beta) \tag{3.13}$$

The Poisson ratio in relaxation when $\alpha \neq \beta$ can be found in another way. The longitudinal stress $\sigma_L(t)$ can be decomposed into its deviatoric and volumetric components; the volumetric component of the longitudinal stress is

$$\sigma_L^{(v)}(t) = \frac{I_1}{3} = \frac{\sigma_L(t)}{3} \tag{3.14}$$

being $I_1$ the first invariant of stress; the deviatoric component of the stress is instead

$$\sigma_L^{(d)}(t) = \sigma_L(t) - \sigma_L^{(v)}(t) = \frac{2}{3}\sigma_L(t) \tag{3.15}$$

On the other hand, by considering the constitutive law (3.3), $\sigma_L^{(v)}(t)$ and $\sigma_L^{(d)}(t)$ are written as:

$$\sigma_L^{(v)}(t) = K_\beta \left(D_{0^+}^{\beta} \varepsilon_V\right)(t) \tag{3.16a}$$

$$\sigma_L^{(d)}(t) = \frac{4}{3} G_\alpha \left[D_{0^+}^{\alpha}(\varepsilon_L - \varepsilon_T)\right](t) \tag{3.16b}$$

Since from Eqs. (3.14) and (3.15) descends that $\sigma_L^{(d)}(t) = 2\sigma_L^{(v)}$, by considering Eqs. (3.16) the following equation is obtained:

$$\frac{4}{3} G_\alpha \left[D_{0^+}^{\alpha}(\varepsilon_L - \varepsilon_T)\right](t) = 2K_\beta \left(D_{0^+}^{\beta} \varepsilon_V\right)(t) \tag{3.17}$$

This equation can be solved in the Laplace domain using properties (1.50) and (A.87) and gives the following results for the Poisson's ratio:

$$\nu_R(t) = \begin{cases} \frac{1}{2} - \frac{3}{2} E_{\alpha-\beta}\left(-\frac{3K_\beta}{G_\alpha} t^{\alpha-\beta}\right) & \alpha > \beta \\ -1 + \frac{3}{2} E_{\beta-\alpha}\left(-\frac{G_\alpha}{3K_\beta} t^{\beta-\alpha}\right) & \beta > \alpha \end{cases} \tag{3.18}$$

As expected, the expression for $\nu(t)$ is not the same as for the creep test; however since, for $c > 0$, $E_\lambda(-ct^\lambda) \to 1$ for $t \to 0$ and $E_\lambda(-ct^\lambda) \to 0$ for $t \to \infty$, the general trend and limiting values still hold, hence observations made above for the creep test are still valid; in particular for $\alpha = \beta$ the Poisson ratio assumes the same constant value $\bar{\nu}$ of Eq. (3.9).

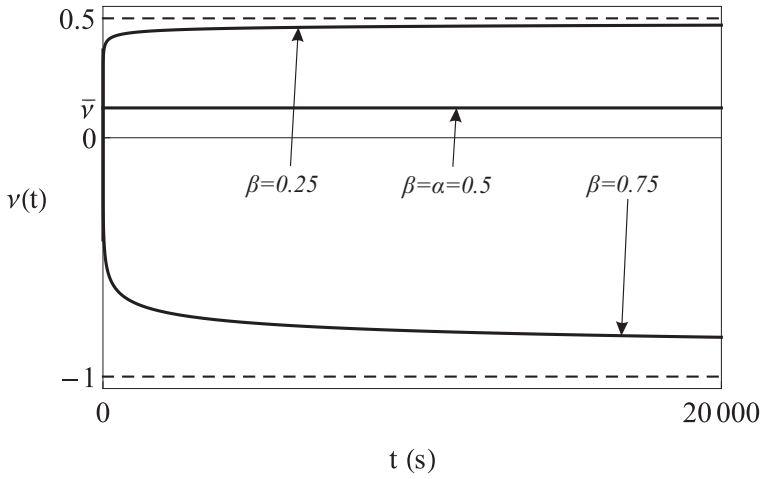


**Figure 3.1:** Poisson's ratio in relaxation test for the 3D springpot model for $K_\beta = 1$, $G_\alpha = 1$, $\alpha = 0.5$ and different values of $\beta$.

In Fig. 3.1 it is shown the viscoelastic Poisson ratio in a creep test for fixed $\alpha = 0.5$ and different values of $\beta$; from this Figure it is possible to appreciate that the proposed 3D model is able to produce different trends in the behavior of the viscoelastic Poisson ratio.
The single springpot model considered here produces prescribed limits at $t = 0$ and $t = \infty$, depending on the relative values of $\alpha$ and $\beta$.
By using more complex fractional viscoelastic models (shown in Fig. 3.5) it is possible to obtain different asymptotic trends of the viscoelastic Poisson ratio. It is also possible to use different fractional viscoelastic models for the deviatoric and volumetric contributions and changing the values of the parameters

many different behaviors can be obtained; basically it is possible to obtain any initial value and any asymptotic trends ($t \to \infty$) in the range $-1 \div 0.5$.

### 3.2.2 Creep and relaxation behavior

The influence of the Poisson ratio, and then of the relative values of $\alpha$ and $\beta$, can be analyzed also by monitoring the normal components of stress and strain in ideal creep and relaxation tests in 3D conditions.
To this purpose, an ideal creep test in the same conditions of the previous section is considered; in this case the final value of the applied stress $\sigma_0 = 1\ MPa$ is reached with a linear ramp of duration $t_0$, as depicted in Fig.3.2(a).

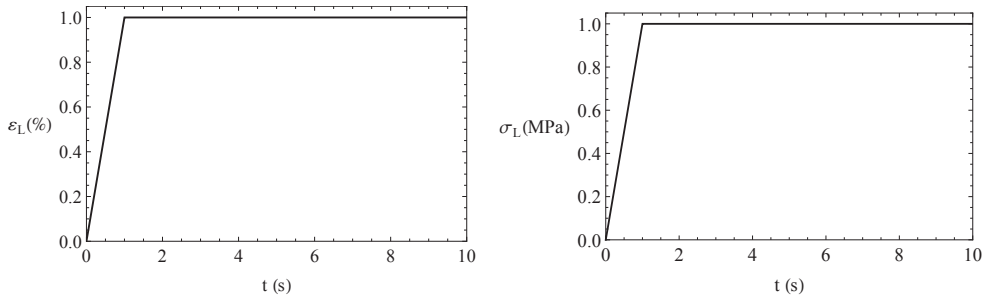


**Figure 3.2:** Applied strain (a) and stress (b) for the 3D springpot model; $t_0 = 1\ s$.

Then the applied stress history $\sigma(t)$ and the resulting strain $\varepsilon_L(t)$ and $\varepsilon_T(t)$ can be written as follows:

$$\sigma(t) = \frac{\sigma_0}{t_0}\left[t - (t-t_0)U(t-t_0)\right] \tag{3.19a}$$

$$\varepsilon_L(t) = \frac{\sigma_0}{t_0}\left[\frac{t^{\beta+1} - (t-t_0)^{\beta+1}U(t-t_0)}{9K_\beta\Gamma(2+\beta)} + \frac{t^{\alpha+1} - (t-t_0)^{\alpha+1}U(t-t_0)}{3G_\alpha\Gamma(2+\alpha)}\right] \tag{3.19b}$$

$$\varepsilon_T(t) = \frac{\sigma_0}{t_0}\left[\frac{t^{\beta+1} - (t-t_0)^{\beta+1}U(t-t_0)}{9K_\beta\Gamma(2+\beta)} - \frac{t^{\alpha+1} - (t-t_0)^{\alpha+1}U(t-t_0)}{6G_\alpha\Gamma(2+\alpha)}\right] \tag{3.19c}$$

The value of $\alpha$ is fixed, while different $\beta$ values are considered. The evolution of the longitudinal and transverse strain is monitored and reported in Fig. 3.3. From these figures it is clear that the while the behavior of the longitudinal

strain is affected only in the amplitude, the transverse strain can even radically change its behavior depending on the relative values of $\alpha$ and $\beta$; indeed, if $\beta > \alpha$ the amplitude of the transverse strain decrease even if the longitudinal one increase. The values of $\alpha$ and $\beta$ affect also the stresses; in order to

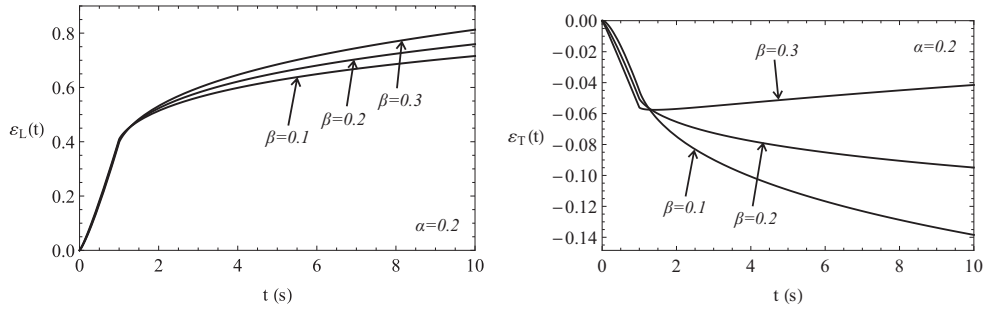


**Figure 3.3:** Evolution of longitudinal (a) and transverse (b) strain for the 3D springpot model in a creep test, with fixed $\alpha$ and various values of $\beta$, for $K_\beta = 1\ MPa\ s^\beta$ and $G_\alpha = 1\ MPa\ s^\alpha$.

analyze this influence, a relaxation behavior on a cube is considered. The cube has all faces but one fixed in the normal direction and in the free face a normal displacement is applied; with these boundary conditions the transverse strain is zero, but the transverse stress is not zero. The free face is strained reaching the final value of the strain $\varepsilon_0 = 1\%$ of by a linear ramp, as depicted in Fig. 3.2(b). The applied strain and the obtained stress are expressed as follows:

$$\varepsilon(t) = \frac{\varepsilon_0}{t_0}\left[t - (t-t_0)U(t-t_0)\right] \tag{3.20a}$$

$$\sigma_L(t) = \frac{\varepsilon_0}{t_0}\left[K_\beta \frac{t^{1-\beta} - (t-t_0)^{1-\beta}U(t-t_0)}{\Gamma(2-\beta)} + \frac{4G_\alpha}{3}\frac{t^{1-\alpha} - (t-t_0)^{1-\alpha}U(t-t_0)}{\Gamma(2-\alpha)}\right] \tag{3.20b}$$

$$\sigma_T(t) = \frac{\varepsilon_0}{t_0}\left[K_\beta \frac{t^{1-\beta} - (t-t_0)^{1-\beta}U(t-t_0)}{\Gamma(2-\beta)} - \frac{2G_\alpha}{3}\frac{t^{1-\alpha} - (t-t_0)^{1-\alpha}U(t-t_0)}{\Gamma(2-\alpha)}\right] \tag{3.20c}$$

While the behavior of the longitudinal stress is slightly affected by the relative values $\alpha$ and $\beta$ and it is always decreasing with time, the transverse stress can increase or decrease with time, in particular if $\beta > \alpha$ the transverse stress increases instead of decreasing as one expects.

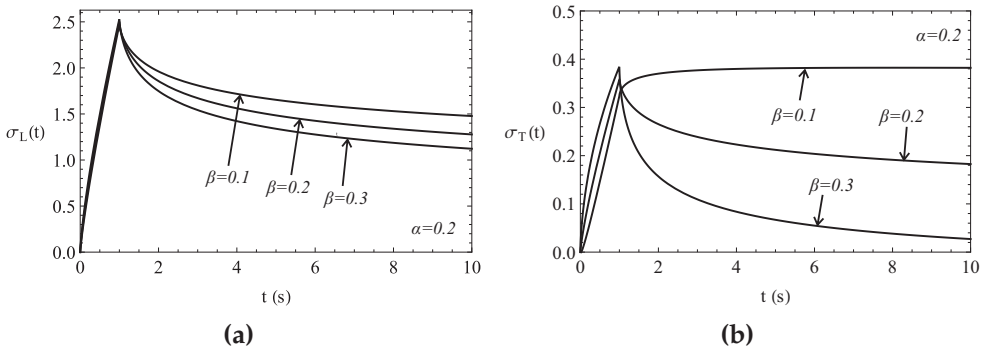


**Figure 3.4:** Evolution of longitudinal (a) and transverse (b) stress for the 3D springpot model in a relaxation test, with fixed $\alpha$ and various values of $\beta$, for $K_\beta = 1\ MPa\ s^\beta$ and $G_\alpha = 1\ MPa\ s^\alpha$.

The results of Figs. 3.3 and 3.4 have shown the flexibility of the 3D springpot model in which the order of the power law for creep (and relaxation) volumetric and deviatoric functions can have different values; however these are only theoretical behaviors and in some cases they can be not so intuitive, as for example when $\beta > \alpha$. For this reason, one way to validate what ranges of the mechanical parameters are valid is to study whether the model is thermodynamically consistent or not. This issue will be addressed later on.

## 3.3 Multi-element fractional viscoelastic models

Although the power law creep and relaxations functions of the springpot are often good to fit experimental data, sometimes the springpot model is not fully satisfactory in practical applications for different reasons:

- some viscoelastic materials exhibit an instantaneous strain when loaded, while the creep law of the springpot is zero for $t = 0$;
- the creep functions $C(t)$ is monotonically increasing in the range $0 \div \infty$ and goes to $\infty$ for $t \to \infty$, but in some cases it is desirable a finite value asymptote in the creep law; this is for example the case of the volumetric part of the strain in a the creep test, because with the pure power law the volume of the specimen would go to zero (compression) or to $\infty$ (tension) as the time goes to infinity, leading to an evident paradox;

- the relaxation function $R(t)$ diverges in $t = 0$; this can generate difficulties in the fitting of relaxation tests when, in order to simplify the procedure, the ramp is reasonably neglected because it lasts very short in comparison with the duration of the entire test;
- the relaxation function $R(t)$ is monotonically decreasing and goes to zero for $t \to \infty$, but some materials experience a residual stress, so that the relaxation law needs to exhibit an asymptotic limit different from zero for $t \to \infty$.

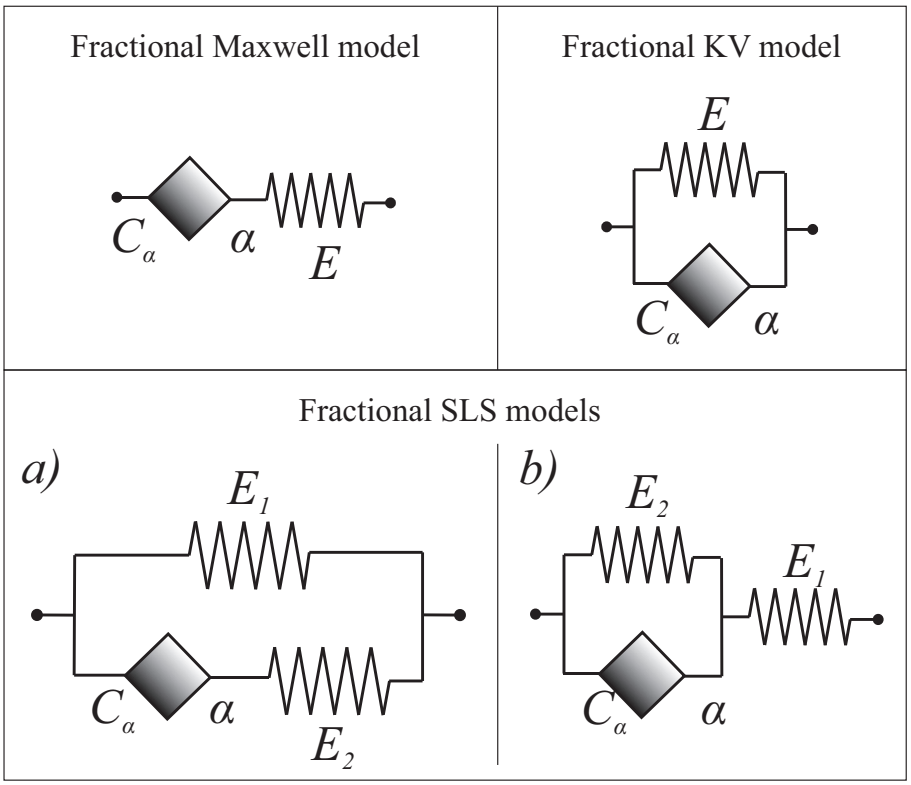


**Figure 3.5:** Fractional viscoelastic multi-elements models.

For these reasons in many engineering applications, researchers prefer to use the springpot in combinations with other classical elements; usually the springpot is used with springs as substitute of the dashpot in classical models; in this way the generalizations of classical viscoelastic models are obtained: the frac-

tional Maxwell model, the fractional KV model, the fractional SLS models and so on. The most used of these models are depicted in Fig. 3.5. As an a example the fractional Maxwell model has been used to reproduce the behavior of asphalt mixtures [27] and of polyethylene for human joint substitutions [56], the fractional KV is used to model the behavior of lumped degrees of freedom structures with fractional damping term ([10], [35]), while the SLS models are used to model arteries ([20]) and other biological tissues ([24, 26, 61]).
For the models depicted in Fig.3.5 the governing equations and the creep and relaxation functions are reported in the following.

**Fractional Maxwell model.**

This is a three parameters mechanical model. The creep and relaxations function of the fractional Maxwell model have an finite value different from zero at the origin, while at $\infty$ they behave as the springpot functions:

$$\left(D^{\alpha}\sigma\right)(t) + \frac{E}{C_{\alpha}}\sigma(t) = E\left(D^{\alpha}\varepsilon\right)(t) \tag{3.21a}$$

$$R(t) = E\,E_{\alpha}\left(-\frac{E}{C_{\alpha}}t^{\alpha}\right); \qquad C(t) = \frac{1}{E} + \frac{t^{\alpha}}{C_{\alpha}\Gamma(1+\alpha)} \tag{3.21b}$$

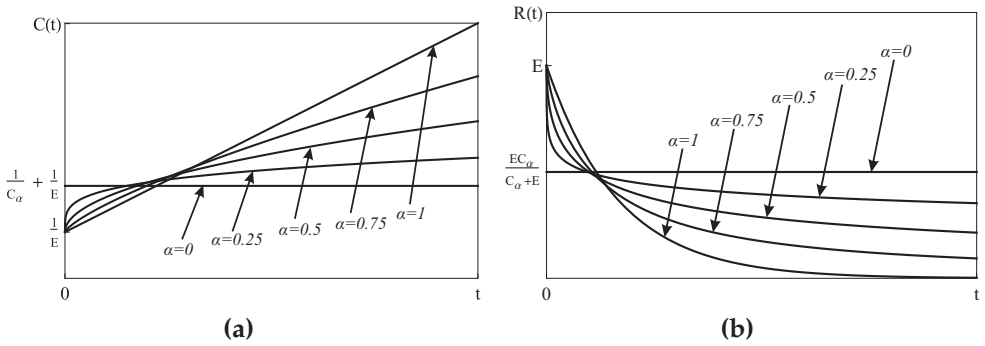


**Figure 3.6:** Creep (a) and relaxation (b) functions of fractional Maxwell model for various value of $\alpha$.

**Fractional Kelvin-Voigt model.**

This is a three parameters mechanical model. The KV model has creep and relaxation functions that asymptotically tend to a finite value different from

zero for $t \to \infty$, but at the origin they behave like the springpot functions:

$$\sigma(t) = C_\alpha \left({}_0^C D_t^\alpha \varepsilon\right)(t) + E\varepsilon(t) \tag{3.22a}$$

$$R(t) = E + \frac{C_\alpha t^{-\alpha}}{\Gamma(1-\alpha)}; \qquad C(t) = \frac{1}{E}\left(1 - E_\alpha\left(-\frac{E}{C_\alpha}t^\alpha\right)\right) \tag{3.22b}$$

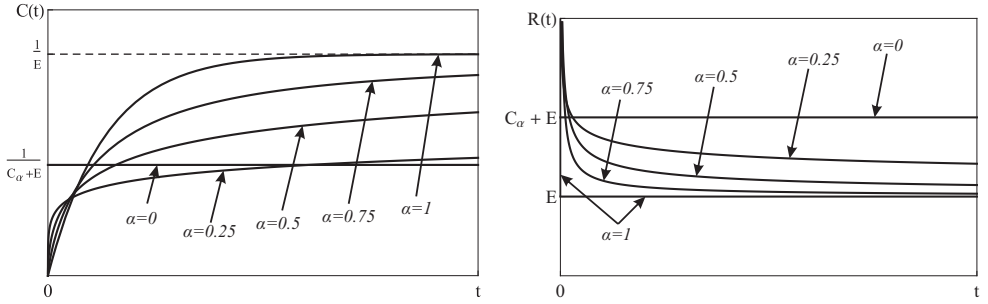


**Figure 3.7:** Creep (a) and relaxation (b) functions of fractional KV model for various value of $\alpha$.

**Fractional SLS model a).**

This is a four parameters mechanical model. This model and the subsequent ensure finite values in both the relaxation and creep functions and for both the value at $t = 0$ and for $t \to \infty$; then they overcome all critical points reported at the beginning of this section for the springpot model:

$$\sigma(t) + \frac{C_\alpha}{E_2}\left(D^\alpha \sigma\right)(t) = E_1\varepsilon(t) + \frac{C_\alpha(E_1+E_2)}{E_2}\left(D^\alpha \varepsilon\right)(t) \tag{3.23}$$

$$R(t) = E_1 + E_2 E_\alpha\left(-\frac{E_2}{C_\alpha}t^\alpha\right) \tag{3.24a}$$

$$C(t) = \frac{1}{E_1} - \frac{E_2}{E_1(E_1+E_2)}E_\beta\left[-\frac{E_1E_2}{(E_1+E_2)C_\alpha}t^\alpha\right] \tag{3.24b}$$

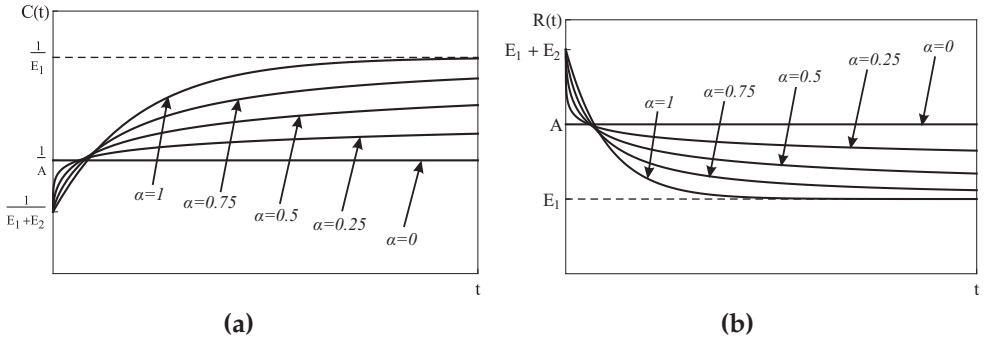


**(a)** **(b)**

**Figure 3.8:** Creep (a) and relaxation (b) functions of fractional SLS a) model for various value of $\alpha$.

**Fractional SLS model b).**

This is a four parameters mechanical models. For this model the same considerations of the previous model are valid:

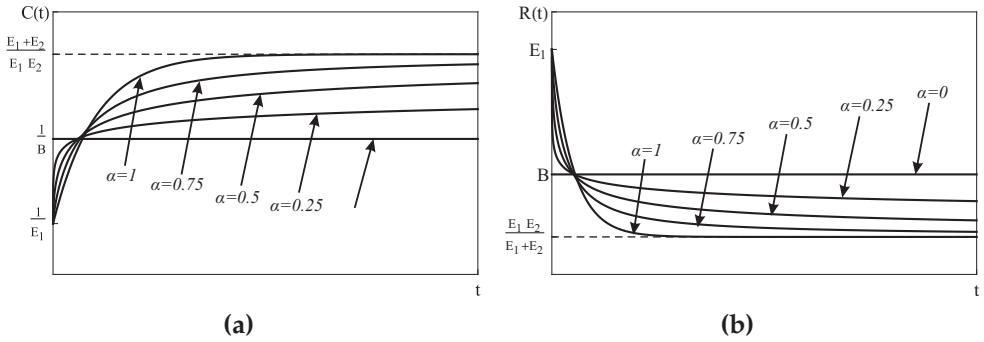


**(a)** **(b)**

**Figure 3.9:** Creep (a) and relaxation (b) functions of fractional SLS a) model for various value of $\alpha$.

$$\sigma(t) + \frac{C_\alpha}{E_1 + E_2} \left(D^\alpha \sigma\right)(t) = \frac{E_1 E_2}{E_1 + E_2} \varepsilon(t) + \frac{C_\alpha E_1}{E_1 + E_2} \left(D^\alpha \varepsilon\right)(t) \tag{3.25}$$

$$R(t) = \frac{E_1}{E_1 + E_2} \left[ E_1 E_\alpha \left( -\frac{E_1 + E_2}{C_\alpha} t^\alpha \right) + E_2 \right] \tag{3.26a}$$

$$C(t) = \frac{1}{E_2}\left[\frac{E_1 + E_2}{E_1} - E_\alpha\left(-\frac{E_2}{C_\alpha}t^\alpha\right)\right] \tag{3.26b}$$

In Fig. 3.8 $A = (C_\alpha E_2 + C_\alpha E_1 + E_1 E_2)/(C_\alpha + E_2)$, while in Fig. 3.9 $B = [E_1(E_2 + C_\alpha)]/(E_1 + E_2 + C_\alpha)$.
The values of the instantaneous $E_0$ and long-term $E_\infty$ moduli for the springpot and the multielement fractional models are summarized in Table 3.2.

| | $E_0$ | $E_\infty$ |
|---|---|---|
| Springpot | $\infty$ | 0 |
| F. Maxwell | $E$ | 0 |
| F. KV | $\infty$ | $E$ |
| F. SLS a) | $E_1 + E_2$ | $E_1$ |
| F. SLS b) | $E_1$ | $\frac{E_1 E_2}{(E_1+E_2)}$ |

**Table 3.2:** Instantaneous and long term moduli for fractional viscoelastic models

By observing Tab. 3.2 it is evident that fractional SLS (FSLS) models are the most adjustable; indeed, by changing the parameters of the springs different combinations of $E_1$ and $E_2$ can be obtained. It is worth noticing that since property (A.78) holds true for the Mittag-Leffler function $E_\alpha(\cdot)$, when $\alpha = 1$ the creep and relaxation functions for the fractional models reduce to the creep and relaxation functions of the correspondent classical models, where exponential functions appear instead of Mittag-Leffler one.

### 3.3.1 Generalized fractional viscoelastic models

Theoretically it is possible to use fractional models with more elements than the models of Fig. 3.5; in this way it is possible to obtain slightly different behaviors, but no other improvements can be achieved about the critical points listed for the springpot model. To the limit it is also possible to generalize Eq. (2.22):

$$\sum_{k=0}^{n} a_k (D^{\alpha_k}\sigma)(t) = \sum_{k=0}^{m} b_k (D^{\beta_k}\varepsilon)(t) \tag{3.27}$$

The creep and relaxation functions for these kind of model are expressed as sum of Mittag-Leffler functions.
However a fractional viscoelastic model with more than three simple elements

(with at least one being the springpot) is not justified, especially if the fractional viscoelasticity is adopted to decrease the number of mechanical parameters in the model; moreover, in order to work with 3D viscoelasticity, more than one creep function or relaxation function are needed, then the number of mechanical parameters to be defined increases even more. In the light of these considerations, the author opinion is that the models mentioned above are sufficient for most of the applications of viscoelasticity, then in the formulations of the 3D fractional viscoelasticity only the models depicted in Fig. 3.5 are taken into account.

## 3.4 Multi-element 3D fractional models

In some cases when the best fitting of the experimental data is obtained with one of the model of Fig. 3.5, 3D models can be defined also starting from one of them, as already mentioned in Sec. 3.2. The main difference between the multi-element models and the springpot are the instantaneous and long term moduli; indeed for the springpot the afore mentioned moduli are 0 and $\infty$, respectively, and this values for some materials can be not adequate. In the case of 3D models the instantaneous and long term Bulk and shear moduli affect the instantaneous and long-term behavior of the Poisson's ratio, as summarized in the following:

- Fractional 3D Maxwell model:

$$\nu(0) = \frac{-2G + 3K}{2(G + 3K)} \tag{3.28a}$$

$$\nu(\infty) = \begin{cases} 0,5 & \beta < \alpha \\ -1 & \beta > \alpha \\ \frac{-2G_\alpha + 3K_\beta}{2(G_\alpha + 3K_\beta)} & \beta = \alpha \end{cases} \tag{3.28b}$$

- Fractional 3D KV model:

$$\nu(0) = \begin{cases} -1 & \beta < \alpha \\ 0,5 & \beta > \alpha \\ \frac{-2G_\alpha + 3K_\beta}{2(G_\alpha + 3K_\beta)} & \beta = \alpha \end{cases} \tag{3.29a}$$

$$\nu(\infty) = \frac{-2G + 3K}{2(G + 3K)} \tag{3.29b}$$

- Fractional 3D SLS a) model:

$$\nu(0) = \frac{-2(G_1 + G_2) + 3(K_1 + K_2)}{2\left[(G_1 + G_2)1 + 3(K_1 + K_2)\right]} \tag{3.30a}$$

$$\nu(\infty) = \frac{-2G_1 + 3K_1}{2(G_1 + 3K_1)} \tag{3.30b}$$

- Fractional 3D SLS b) model:

$$\nu(0) = \frac{-2G_1 + 3K_1}{2(G_1 + 3K_1)} \tag{3.31a}$$

$$\nu(\infty) = \frac{-2\frac{G_1 G_2}{G_1 + G_2} + 3\frac{K_1 K_2}{K_1 + K_2}}{2(\frac{G_1 G_2}{G_1 + G_2} + 3\frac{K_1 K_2}{K_1 + K_2})} \tag{3.31b}$$

It is worth noticing that when then instantaneous and the long term moduli have finite values, the values of the viscoelastic Poisson's ratio at 0 and $\infty$ are not determined by the relative values of $\alpha$ and $\beta$, but only from the values of the elastic moduli; this means that in those cases the properties of the viscoelastic element of the model only affect the way the viscoelastic Poisson's ratio evolves from 0 to $\infty$, but they do not affect the fact that $\nu(t)$ is increasing or decreasing with the time.
It has to be remarked that different behavior can be obtained also by combining different viscoelastic models for the deviatoric and the volumetric contributions; these cases are not analyzed here, but it has to be taken into account that a fitting procedure can leads to adopt different models for the two contributions.

## 3.5 Thermodynamic consistency of the 3D fractional models

Any constitutive model of material behaviour must be thermodynamically consistent. The thermodynamic consistency of viscoelastic materials with memory have been demonstrated by many authors (see for example [21, 23]); Bagley and Torvik [12] found the thermodynamic restrictions on the values of the parameters of a fractional SLS viscoelastic models by making use of concepts as dissipation rated and stored energy; recently, Adolfsson [1] found

thermodynamic restrictions on the relaxation function of a fractional viscoelastic material based on the mechanical analogy between the springpot and the Maxwell chain, that is a mechanical model constituted by a number of classical Maxwell model in parallel. In the light of these works, the 1D springpot model is for sure thermodynamically consistent; however, working in 3D conditions it has been found that the behavior can be very weird and not intuitive when $\alpha \neq \beta$. Then in the following the admissibility of the reciprocal values of parameters $\alpha$ and $\beta$ that the determine the behavior of the viscoelastic Poisson's ratio is investigated.

### 3.5.1 The Bagley and Torvik study

Thermodynamic consistency of fractional viscoelastic models has been examined by Bagley and Torvik [12] that based their analysis on the following form of 1D constitutive equation:

$$\sigma(t) + A(D^{\gamma}\sigma)(t) = B\varepsilon(t) + C(D^{\lambda}\varepsilon)(t) \tag{3.32}$$

Note that the original notation has been changed to avoid confusion with the present notation. The thermodynamic consistency is usually investigated by imposing to the model non-negative internal work (elastic energy stored in the solid) and non-negative rate of energy dissipation and verifying if these two conditions can be fulfilled by the model, and if so what restrictions apply to its parameters in order to respect the conditions. In classical models the internal work is related to the stored energy in the solid, then to the elastic part of strain, while the dissipated energy is related to the viscous part of the strain. However, differently form classical models, in fractional viscoelasticity is not possible to distinguish between elastic and inelastic strain; this is due to the the fact that the springpot model contains in itself the features of both springs and dashpots, as shown with the hierarchical and the mechanical models of fractional viscoelasticity. Then in order to investigate the thermodynamic consistency of their model, in the paper [12] the authors apply a sinusoidal history of strain and analyze the system behaviour after the transient has decayed. In the stationary condition the stress is also sinusoidal and by means of the complex modulus in the frequency (Fourier) domain it is possible to relate the signs of the internal work and of the dissipate energy to the mechanical parameters of the model. With this strategy they obtained the following restrictions on the parameters of the model:

$$A \geq 0 \tag{3.33a}$$

$$B > 0 \tag{3.33b}$$

$$C > 0 \tag{3.33c}$$

$$\frac{C}{A} \geq B \tag{3.33d}$$

$$\gamma = \lambda \tag{3.33e}$$

By comparing Eq. (3.32) with Eq. (3.25) we recognize that they are equivalent if:

$$A = \frac{C_\beta}{E_1 + E_2}; \quad B = \frac{E_1 E_2}{E_1 + E_2}; \quad C = \frac{C_\beta E_1}{E_1 + E_2}; \quad \gamma = \lambda \tag{3.34}$$

Then conditions (3.33a)-(3.33d) for the model described in(3.25) are automatically satisfied if the coefficients $E_1$, $E_2$ and $C_\beta$ are positive; condition (3.33e) is implicitly satisfied because the same order of derivation was assumed for the derivative of the stress and the strain in Eq. (3.25). The concepts outlined above are also valid for a 3D model because as in [12], the same restrictions apply independently to the deviatoric and the volumetric material functions. Furthermore, the procedure does not impose any restrictions on the relationship between the two parameters ($\alpha$, $\beta$), which relationship determine the behavior of the viscoelastic Poisson ratio. Eq.(3.32) can be compared also with Eq. (3.23) and the same conclusions are reached, then both the SLS models presented in this chapter are thermodynamical consistent (provided that the coefficients are positive). These results have been obtained for the particular case of the SLS models of Fig. 3.5; however in the author opinion it is important to find restrictions that apply to the mechanical parameters of simple 3D springpot model; this issue is addressed in the next section.

### 3.5.2 Validation of the values of $\alpha$ and $\beta$ of the 3D springpot model

Thermodynamic restrictions on the values of $\alpha$ and $\beta$ can be investigated working with state functions and in particular with the concept of free energy and dissipation rates. The specific Helmotz free energy $\psi$ is a thermodynamic state function whose gradient with respect to the actual value of strain $\varepsilon$ gives the measured stress; it represent the energy stored in the solid, that is what in elasticity is defined as elastic energy. The rate of free energy can be expressed as follows:

$$\dot{\psi} = \dot{u} - T\dot{s} \tag{3.35}$$

where $\dot{u}$ is the rate of specific internal energy, $T$ is the the absolute temperature and $\dot{s}$ is the entropy production. The second principle of thermodynamics states that $\dot{s} \geq \dot{q}/T$, being $\dot{q}$ the rate of change of specific thermal energy, or simply the rate of thermal energy exchange. It is to be emphasized that:

- The rate of change of specific internal energy is related to the rate of the specific mechanical work done on the system and on the thermal energy exchange, then $\dot{u} = \dot{w}_{ext} + \dot{q}$.
- Introducing the entropy production rate due to irreversible transformations labeled as $\dot{s}^{(i)} \geq 0$, that is related to the dissipated energy, the second principle of thermodynamics can be written as $\dot{s} = \dot{q}/T + \dot{s}^{(i)}$.

By performing these two substitutions in Eq. (3.35) we get:

$$\dot{\psi} = \dot{w}_{ext} + \dot{q} - T\left(\dot{q}/T + \dot{s}^{(i)}\right) = \dot{w}_{ext} - D(t) \tag{3.36}$$

where $D(t) = T\dot{s}$ denotes the dissipation rate. When we apply to the viscoelastic solid a strain or stress history, in Eq. (3.36) the external work rate is known and can be evaluated as $\dot{w}_{ext} = \sigma(t)\dot{\varepsilon}(t)$; if it is possible to define also the free energy rate then also the dissipation rate can be evaluated from Eq. (3.36). Unfortunately the free energy is not uniquely defined unless a rheological model with well defined and distinct elastic and viscous phases is available, as it is so in classical viscoelasticity; in fractional viscoelasticity the only possibility to distinguish between elastic and viscous phases is to make use of the discretized versions of the mechanical models described at the end of the previous chapter, but the number of elements to be taken into account is very high and depends also on the observation time and on the input on the system; for these reasons this strategy is not applicable. However, in the paper [25] the mechanical models of fractional viscoelasticity have been used to prove that the correct form of the free energy function for the fractional viscoelastic material is the one proposed by Stavermann and Schwartzl (citare) and defined as:

$$\psi_{SS} = \frac{1}{2}\int_{\infty}^{t}\int_{\infty}^{t} R(2t - \tau_1 - \tau_2)\varepsilon'(\tau_1)\varepsilon'(\tau_2)d\tau_1 d\tau_2 \tag{3.37}$$

where $R(\cdot)$ is the relaxation function as usual and the pedex $SS$ stands for Stavermann and Schwartzl. By using Eq. (3.37) in Eq. (3.36), the following expression for the dissipation rate is obtained:

$$D(t) = -\frac{1}{2}\int_{\infty}^{t}\int_{\infty}^{t} \dot{R}(2t - \tau_1 - \tau_2)\varepsilon'(\tau_1)\varepsilon'(\tau_2)d\tau_1 d\tau_2 \tag{3.38}$$

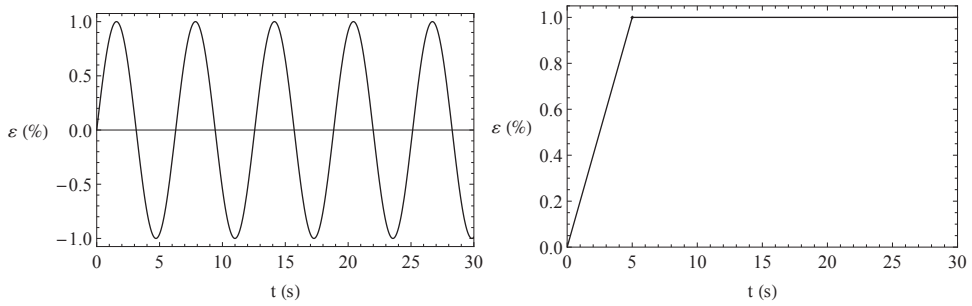


**Figure 3.10:** Applied strain histories for the evaluation of free energy and dissipation rate with Eqs. (3.39): sinusoidal (a) and constant with initial linear ramp (b).

For the particular case of the springpot Eqs. (3.37) and (3.38) read as follow:

$$\psi_{SS} = \frac{1}{2C_\alpha \Gamma(\alpha)} \int_\infty^t \int_\infty^t (2t - \tau_1 - \tau_2)^{-\alpha} \varepsilon'(\tau_1) \varepsilon'(\tau_2) d\tau_1 d\tau_2 \tag{3.39a}$$

$$D(t) = -\frac{\alpha}{C_\alpha \Gamma(\alpha)} \int_\infty^t \int_\infty^t (2t - \tau_1 - \tau_2)^{-\alpha-1} \varepsilon'(\tau_1) \varepsilon'(\tau_2) d\tau_1 d\tau_2 \tag{3.39b}$$

Eqs. (3.39) should be first applied to the 1D springpot model and then to the 3D springpot model; however the main reason to use Eqs. (3.39) is to validate the range of values of $\alpha$ and $\beta$, then the validation is made directly for the 3D model. In this case in order to evaluate the free energy and the dissipation rate it is needed to take all the components of stress and strain into account from both the volumetric and deviatoric contributions. Limitations on the relationship between $\alpha$ and $\beta$ can be found by enforcing the condition that $\psi(t) \geq 0 \quad \forall t$ and $D(t) \geq 0 \quad \forall t$. However the analytical solution of the double integrals in Eqs. (3.39) is not straightforward hence numerical integration has been performed. Eqs. (3.39) have been evaluated by considering a large range of values of $\alpha$ and $\beta$; the other mechanical parameters ($G_\alpha$ and $K_\beta$) are chosen positive. Two histories of strains have been applied as shown in Fig. 3.10: a) sinusoidal; b) relaxation with initial linear ramp. For simplicity here we show only results with the following values: 1) $\alpha = \beta = 0.5$; 2) $\alpha = 0.5, \beta = 0.25$; 3) $\alpha = 0.5, \beta = 0.75$. Fig. 3.11 shows the specific dissipation rate (dissipation rate per unit volume), while Fig. 3.12 show s the specific free energy function for the two applied strain histories of Fig. 3.10. Figs. 3.11

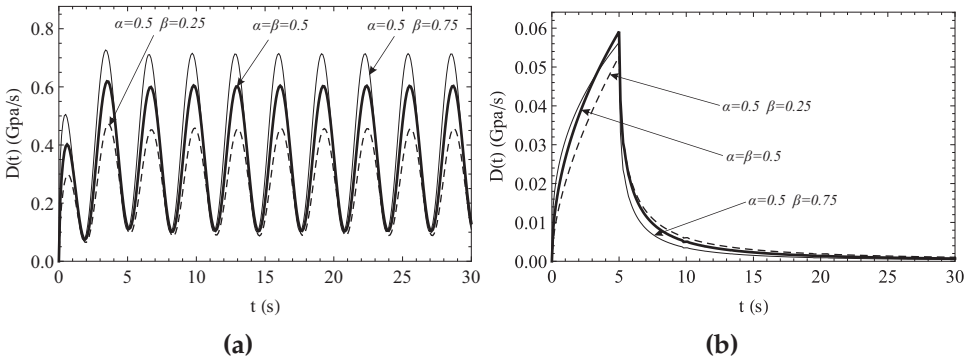


**Figure 3.11:** Dissipation rates for the applied strain of Fig. 3.10 evaluated with Eq. (3.39b): sinusoidal (a) and constant with initial linear ramp (b).

and 3.12 show that the dissipation rate and the free energy function are non-negative whatever the relationship between the values of $\alpha$ and $\beta$ is. From this evidence it has to be concluded that the 3D fractional viscoelastic models are thermodynamically consistent independently of the relationship between $\alpha$ and $\beta$; this means that both an increasing and a decreasing viscoelastic Poisson's ratio are possible for 3D fractional constitutive models that hence are suitable to represent both behaviors. The thermodynamic consistency of the

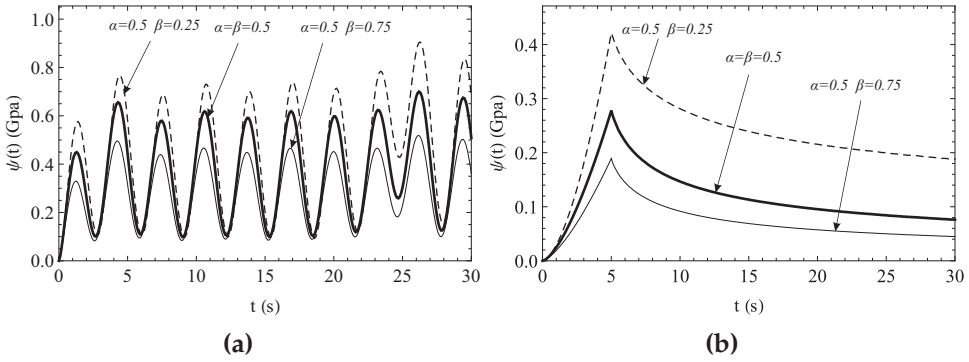


**Figure 3.12:** Free energy for the applied strain of Fig. 3.10 evaluated with Eq. (3.39a): sinusoidal (a) and constant with initial linear ramp (b).

multielement fractional viscoelastic models descend directly from the thermodynamic consistency of the springpot; indeed by adding one or more springs,

in series or in parallel, to the springpot, no dissipation is added to model; moreover springs are mechanical elements able to store only positive energy, then they can not make the free energy function negative. For these reasons it is possible to state that all the fractional viscoelastic models considered here are thermodynamically consistent.

## 3.6 Conclusions

In this chapter a 3D viscoelastic isotropic model based on the fractional viscoelasticity has been proposed. The model is defined by means of two relaxation (or creep) functions that are assumed power law functions as the simple 1D springpot. The behavior of the model has been explored in terms of the viscoelastic Poisson's ratio in creep and in relaxation and by means of creep and relaxation tests in 3D conditions; the thermodynamic consistency of such a model has also been investigated in order to find eventual restrictions on the parameters $\alpha$ and $\beta$, which relationship determine the behavior, increasing or decreasing with time, of the Poisson's ratios in creep and in relaxation; it has been found that no restrictions apply to the values of $\alpha$ and $\beta$ and this is in agreement with reality because there exist both material with increasing Poisson's ratio and material with decreasing Poisson's ratio.
In the same way the 3D springpot model has been defined, it is possible to define other 3D models based on multielement fractional viscoelastic models; the advantage of these models is that they have well defined instantaneous and/or long term moduli. The thermodynamic consistency of these model descends directly from that one of the springpot model.
Of course, these models are not able to reproduce the behavior of all viscoelastic materials; indeed, for some materials the memory affects the symmetry and then makes a material anisotropic; also, many materials experience, as well as viscoelasticity, the feature of hyperelasticity. For these reasons these models are not resolutive for viscoelasticity problems, but they constitute a first step to learn how to manipulate and control their behavior and in the future it is for sure needed more complicate mechanical models to take into account of all phenomenon that a material experiences. Moreover, the definition of a mechanical model is not enough to allow researcher and enginner to use it, then in the next chapter the implementation of these model in a finite element framework is addressed.

# Chapter 4

# Numerical implementation of 3D fractional viscoelasticity

The formulation of proper constitutive models to reproduce the behavior of viscoelastic materials is of great importance for design and prediction of the life of engineering components; however, in the field of engineering this is not enough. Indeed, when working with a real complex shaped components the analysis of stress and/or of strain can not be conducted without the aid of some advanced tool such as the Finite Element Method (FEM). For this reason, in order to make the 3D model of fractional viscoelasticity usable by engineers it has to implemented in a finite element framework. In this chapter routines are obtained for the fractional models presented in the previous chapter; moreover the stability of the integration scheme is analyzed and some examples performed with the Finite Element (FE) software Abaqus are presented.

## 4.1 Basic concepts on the finite element method

The finite element method is the most known and efficient methods to find the solution to problems of solid mechanics. The method is based on the spatial discretization of a continuum body in a finite number of elements. For the sake of simplicity, in the following the basic concepts of FEM are recalled referring to an elastic problem.
Consider the generic elastic solid of Fig. 5.26(a), characterized by the volume $V$, the free surface $S_F$ and the constrained surface $S_C$. The solid is loaded with body forces $\boldsymbol{P}$ and surface traction $\boldsymbol{T}$ on the free surface $S_F$. The analytical

problem of elasticity is governed by fifteen differential equation:

$$\begin{cases} \boldsymbol{C}^T\boldsymbol{\sigma} = \boldsymbol{P} & \text{Equilibrium (3)} \\ \boldsymbol{C}\boldsymbol{u} = \boldsymbol{\varepsilon} & \text{Compatibility (6)} \\ \boldsymbol{\sigma} = \boldsymbol{D}\boldsymbol{\varepsilon} & \text{Constitutive law (6)} \end{cases} \tag{4.1}$$

with the following boundary conditions:

$$\begin{cases} \boldsymbol{C}_n^T\boldsymbol{\sigma} = \boldsymbol{T} & \text{in } S_V \\ \boldsymbol{u} = \bar{\boldsymbol{u}} & \text{in } S_C \end{cases} \tag{4.2}$$

where $\boldsymbol{C}^T$ and $\boldsymbol{C}$ are the equilibrium and compatibility matrix, respectively, containing partial differential operators with respect to $x$, $y$, $z$; $\boldsymbol{u}$ is the displacement vector, $\boldsymbol{D}$ is the stiffness matrix, $\bar{\boldsymbol{u}}$ are prescribed displacement and $\boldsymbol{n}$ is the outgoing normal vector to the free surface. For the Kirchoff theorem the solution is unique, but it can be really found only in some special cases or by introducing some simplifying hypothesis, such as for example the De Saint-Venant hypothesis for the beams.

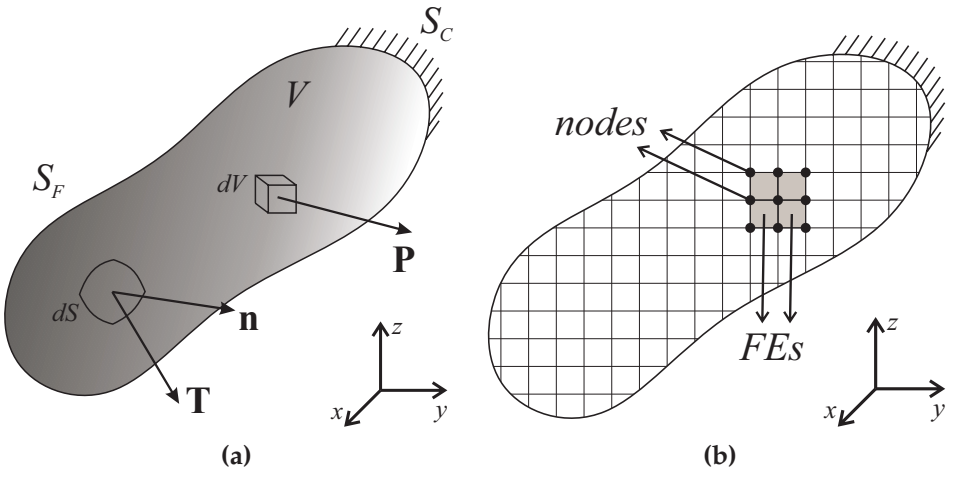


**Figure 4.1:** Generic elastic body (a); FEM discretization (b).

In order to find an approximate solution, the FEM considers a discretized domain of the body as shown in Fig. 5.26(b); the number of degree of freedom (DOF) of such a system is equal to the sum of the number of DOF of each

node. The displacement field $\boldsymbol{u}$ inside the domain of each FE is obtained by interpolating the nodal displacements $\boldsymbol{d_e}$ by means of shape functions:

$$\boldsymbol{u} = \boldsymbol{N}\ \boldsymbol{d_e} \tag{4.3}$$

where $\boldsymbol{N}$ is the shape functions matrix; shape functions are usually chosen as polynomial. By using Eq. (4.3) in the compatibility equation Eq. (4.1), the following relationship is obtained:

$$\boldsymbol{\varepsilon} = \boldsymbol{B}\ \boldsymbol{d_e} \tag{4.4}$$

where $\boldsymbol{B} = \boldsymbol{C}\ \boldsymbol{N}$ is the matrix containing the derivatives of the shape functions and is usually labeled as compatibility matrix of the FE model. The nodal displacement vector $\boldsymbol{d_e}$ of the single FE must be related to the the global nodal displacement vector $\boldsymbol{d_g}$ that contains displacements of all the nodes of the system; this is possible by means of connectivity matrices $\boldsymbol{L_e}$:

$$\boldsymbol{d_e} = \boldsymbol{L_e}\ \boldsymbol{d_g} \tag{4.5}$$

To enforce the equilibrium of the system it is necessary to equate the work of internal forces with the work of external forces for any admissible change of configuration characterized by the virtual strain field $\boldsymbol{\delta\varepsilon}$ and the virtual displacement field $\boldsymbol{\delta u}$. For the continuum solid of Fig.5.26(a):

$$\int_V \boldsymbol{\delta\varepsilon}^T \boldsymbol{\sigma} dV = \int_V \boldsymbol{\delta u}^T \boldsymbol{P} dV + \int_{S_F} \boldsymbol{\delta u}^T \boldsymbol{T} dS \tag{4.6}$$

For the discretized solid of Fig. 5.26(b) Eq. (4.6) can be written as:

$$\sum_{i=1}^{N_e} \int_{V_e} \boldsymbol{\delta\varepsilon}^T \boldsymbol{\sigma} dV = \sum_{i=1}^{N_e} \int_{V_e} \boldsymbol{\delta u}^T \boldsymbol{P} dV + \sum_{i=1}^{N_f} \int_{S_f} \boldsymbol{\delta u}^T \boldsymbol{T} dS \tag{4.7}$$

where $N_e$ is the number of FEs, $V_e$ is the volume of the generic FE, $N_f$ is the number of FEs that have a face on the free surface of the solid and $S_f$ is the free surface of the generic FE. By using Eq. (4.3), (4.4) and (4.5), the variations of the strain and of the displacement fields and the stress field are written as follows:

$$\delta\boldsymbol{\varepsilon} = \boldsymbol{B}\boldsymbol{L_e}\delta\boldsymbol{d_g} \tag{4.8a}$$

$$\delta\boldsymbol{u} = \boldsymbol{N}\boldsymbol{L_e}\delta\boldsymbol{d_g} \tag{4.8b}$$

$$\boldsymbol{\sigma} = \boldsymbol{D}\boldsymbol{B}\boldsymbol{L_e}\boldsymbol{d_g} \tag{4.8c}$$

Substituting Eqs. (4.8) in Eq (4.7) leads to:

$$\delta \boldsymbol{d}_g^T \left\{ \sum_{i=1}^{N_e} \left( \int_{V_e} \boldsymbol{L}_e^T \boldsymbol{B}^T \boldsymbol{D} \boldsymbol{B} \boldsymbol{L}_e dV \right) \boldsymbol{d}_g - \sum_{i=1}^{N_e} \int_{V_e} \boldsymbol{L}_e^T \boldsymbol{N}^T \boldsymbol{P} dV - \sum_{i=1}^{N_f} \int_{S_f} \boldsymbol{L}_e^T \boldsymbol{N}^T \boldsymbol{T} dS \right\} = 0 \quad (4.9)$$

that in more compact form reads:

$$\delta \boldsymbol{d}_g^T \left\{ \boldsymbol{K} \boldsymbol{d}_g - \boldsymbol{F}_V - \boldsymbol{F}_S \right\} = 0 \quad (4.10)$$

where:

$$\boldsymbol{K} = \sum_{i=1}^{N_e} \int_{V_e} \boldsymbol{L}_e^T \boldsymbol{B}^T \boldsymbol{D} \boldsymbol{B} \boldsymbol{L}_e dV \quad (4.11a)$$

$$\boldsymbol{F}_V = \sum_{i=1}^{N_e} \int_{V_e} \boldsymbol{L}_e^T \boldsymbol{N}^T \boldsymbol{P} dV \quad (4.11b)$$

$$\boldsymbol{F}_S = \sum_{i=1}^{N_f} \int_{S_f} \boldsymbol{L}_e^T \boldsymbol{N}^T \boldsymbol{T} dS \quad (4.11c)$$

In Eqs. (4.11) $\boldsymbol{K}$ is the stiffness matrix, $\boldsymbol{F}_V$ is the nodal loads vector corresponding to the body forces $\boldsymbol{P}$ and $\boldsymbol{F}_S$ is the nodal loads vector corresponding to the surface traction $\boldsymbol{T}$. Eq. (4.10) must be valid for any admissible change of configuration described by the virtual nodal displacements vector $\delta \boldsymbol{d}_g$; then, by denoting $\boldsymbol{F} = \boldsymbol{F}_V + \boldsymbol{F}_S$:

$$\boldsymbol{K} \boldsymbol{d}_g = \boldsymbol{F} \quad (4.12)$$

Once the stiffness matrix and external loads are known, displacements $\boldsymbol{d}_g$ can be easily evaluated from Eq. (4.12).
Integrals in Eqs. (4.11) are usually solved numerically with the aid of the Gauss integration rule (or Gauss quadrature), that reduce one integral in a summation of a few products and then reduce the computation time; for this reason each FE contains some so-called Gauss points (or simply integration points) which number and position depends on the order of the polynomial of the shape functions (citare un libro sul FEM).
The Gauss integration is especially important when the material is nonlinear or time dependent; in those cases the solution cannot be found in one step by inverting Eq. (4.12), but in most of the cases many steps are involved and the

integrals in Eq. (4.11b) have to be evaluated at every step. With the aid of the Gauss integration the analysis time is decreased drastically.

## 4.2 Implicit and explicit integration schemes

When a time-dependent or a nonlinear material is considered, at every time step the value of the stress must be evaluated for every integration point, then suitable and efficient integration schemes have to be defined. The most used integration schemes can be subdivided in two great classes: *explicit* and *implicit* integration methods.

### 4.2.1 Explicit methods

Explicit methods allows to evaluate the state of the system at a later time from the state of the system at the current time. Consider Eq. (4.13):

$$\dot{x}(t) = f(x(t), t) \tag{4.13}$$

In order to find a numerical solution of Eq. (4.13), the time variable $t$ is discretized in $n$ time steps of length $\Delta t$. At the generic time $t_k = k\Delta t$ the equation is written as:

$$\dot{x}_k = f(x_k, t_k) \tag{4.14}$$

Approximation of the first time derivative with forward Euler method as $\dot{x}_k = (x_{k+1} - x_k)/\Delta t$ gives

$$\frac{x_{k+1} - x_k}{\Delta t} = f(x_k, t_k) \tag{4.15}$$

and then:

$$x_{k+1} = x_k + \Delta t f(x_k, t_k) \tag{4.16}$$

The method is called explicit because the solution for each consecutive step is written explicitly in terms of the past state of the system. The advantage of this method is that no iteration is needed through each time increment, however the method is conditionally stable and in some cases it needs very small time step $\Delta t$.

**Example**

Consider the first order differential equation:

$$\begin{cases} \dot{x}(t) + ax^2(t) = f(t) \\ x(0) = x_0 \end{cases} \tag{4.17}$$

Discretization with the forward Euler method gives:

$$\frac{x_{k+1} - x_k}{\Delta t} + ax_k^2 = f_k \tag{4.18}$$

The solution at the time step $k+1$ is easily found as:

$$x_{k+1} = x_k + (f_k - ax_k^2)\Delta t \tag{4.19}$$

### 4.2.2 Implicit methods

With implicit methods the solution of the system at a late time is found by solving an equation that involves both the later time and the current time. Consider Eq. (4.14); if $\dot{x}_k$ is approximated with the backward Euler method as

$$\dot{x}_k = \frac{x_k - x_{k-1}}{\Delta t} \tag{4.20}$$

the discretized equation becomes:

$$\frac{x_k - x_{k-1}}{\Delta t} = f(x_k, t_k) \tag{4.21}$$

and then:

$$x_k = x_{k-1} + \Delta t f(x_k, t_k) \tag{4.22}$$

Eq. (4.22) is said to be implicit in $x_k$ because it appears on both side of the equation. The advantage of this method is that it is unconditionally stable, then the time step can be larger than that used in explicit integration; however at each time step Eq. (4.22) has to be solved and then each time step is computationally more expensive than a time step in explicit methods.

**Example**

Consider the same first order differential equation considered above; discretization with backward Euler method gives:

$$\frac{x_k - x_{k-1}}{\Delta t} a x_k^2 = f_k \tag{4.23}$$

and rearranging:

$$a x_k^2 + \frac{x_k}{\Delta t} - (f_k + \frac{x_{k-1}}{\Delta t}) = 0 \tag{4.24}$$

Eq. (4.24) is a quadratic equation, then there exist two roots for it:

$$x_k = \frac{-\frac{1}{\Delta t} \pm \sqrt{\frac{1}{\Delta t^2} + 4a\left(f_k + \frac{x_{k-1}}{\Delta t}\right)}}{2a} \tag{4.25}$$

The correct solution is chosen based on the values of $x_{k-1}$ ($x_0$ at the first step) and $f_k$. In most of the cases the equation to be solved is not as simple as Eq. (4.24), then no analytical solution is available. For this reason so-called root finding algorithms are used; the most efficient and used of these algorithms is the Newton-Raphson that is briefly explained in the next section.

### 4.2.3 The Newton-Raphson algorithm

The Newton-Raphson algorithm is able to find iteratively the solution to the equation $f(x) = 0$; suppose the correct solution is $\bar{x}$. In the first iteration an estimate $x_1$ of the solution must be defined arbitrarily; the correct solution can be defined as $\bar{x} = x_1 + e_1$, where $e_1 = \bar{x} - x_1$ is the distance between the correct and the tentative solution. Since by definition $f(\bar{x}) = 0$, by using linear approximation:

$$f(\bar{x}) = f(x_1 + e_1) = f(x_1) + e_1 f'(x_1) = 0 \tag{4.26}$$

that gives an estimate of $e_1$:

$$e_1 \approx -\frac{f(x_1)}{f'(x_1)} \tag{4.27}$$

With $e_1$ it is possible to evaluate an improved estimate of $\bar{x}$, namely $x_2$:

$$\bar{x} = x_1 + e_1 \approx x_1 - \frac{f(x_1)}{f'(x_1)} \tag{4.28a}$$

$$x_2 = x_1 + e_1 = x_1 - \frac{f(x_1)}{f'(x_1)} \tag{4.28b}$$

At this point the procedure is repeated:

$$e_2 = -\frac{f(x_2)}{f'(x_2)} \tag{4.29a}$$

$$x_3 = x_2 + e_2 = x_2 - \frac{f(x_2)}{f'(x_2)} \tag{4.29b}$$

The procedure ends when the difference between $x_n$ and $x_{n-1}$ is smaller than a prescribed tolerance. This method is often called tangent method because of the geometric interpretation shown in Fig. 4.2. The Newton method works well when a sufficiently good first estimate is defined; it is not so, or if the function is oscillating near the root, Newton method can lead to the wrong solution or converge very slowly.

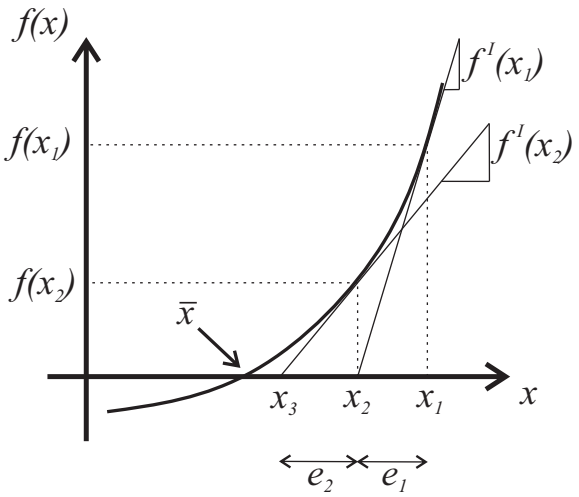


**Figure 4.2:** The Newton-Raphson method.

When applied to a FEM problem, the Newton method does not need an initial guess estimate because equilibrium equations can be used to guide the procedure. Consider a nonlinear system in the configuration $u_0$ with applied load $F_0$. If a load increment $\Delta F$ is applied, the new applied load is $F_1$; in

order to find the corresponding displacement $u_1$ a residual $R_0$ is defined as difference between the internal and applied forces:

$$R_0 = I_0 - F_1 = -\Delta F \tag{4.30}$$

Using linear approximation, the first tentative $u_1$, labeled as $u_{1,1}$, is evaluated as:

$$u_{1,1} = u_0 - \frac{R_0}{K_0} \tag{4.31}$$

where $K_0$ is the tangent stiffness, usually labeled as Jacobian, in the configuration $u_0$. The tangent stiffness $K_{1,1}$ and the internal force $I_{1,1}$ are evaluated in the configuration $u_{1,1}$; with these quantities a new residual $R_{1,1}$ and a new tentative $u_1$, labeled as $u_{1,2}$ are evaluated:

$$R_{1,1} = I_{1,1} - F_1 \tag{4.32a}$$

$$u_{1,2} = u_{1,1} - \frac{R_{1,1}}{K_{1,1}} \tag{4.32b}$$

The solution is stopped when $R_{1,n}$ and/or $u_{1,n} - u_{1,n-1}$ are smaller than prescribed tolerances. The geometric interpretation of this procedure is shown in Fig. 4.3.

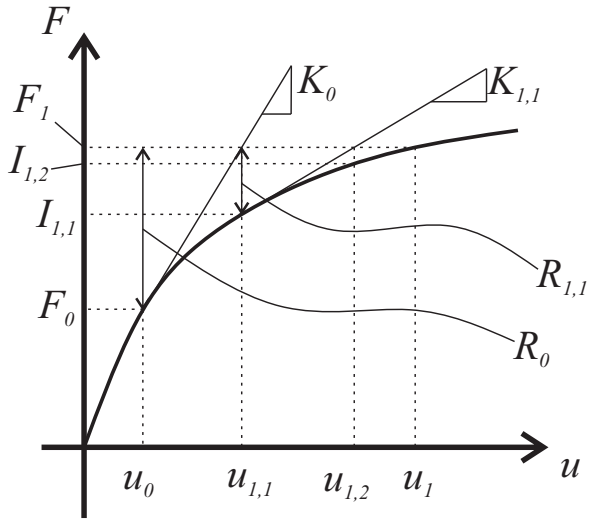


**Figure 4.3:** The Newton-Raphson method in FEM analysis.

When a multi degree of freedom (MDOF) is analyzed, the external and internal forces, the displacement and the residual are vectors instead of scalars whereas the Jacobian is a matrix.

## 4.3 Implementation of 3D springpot model

The constitutive model of the springpot has been implemented in the commercial finite element software Abaqus/Standard through a user material subroutine UMAT. The implementation however is suitable for any finite element code that uses implicit or explicit integration schemes. The subroutine calculates the increment of stress at the end of each time increment and the material Jacobian to be used in the computation for the next increment. In this section we show only the implementation for the springpot model, the details for the other models are presented in Section 4.5.
When the routine is called, the following information is available as Input: the stress at the beginning of the increment, the strain at the beginning of the increment and the increment of strain. We need to have access to the history of strains i.e. the values of strains in all previous increments. We will give some details of how this can be achieved at the end of this section.
We start by evaluating the direct component of stress $\sigma_{11}$ at the end of increment $k$, which is the first component of the stress vector in Eq.(3.3); the equations for the evolution of the volumetric and the deviatoric parts of $\sigma_{11}$ are

$$\frac{I_1(t)}{3} = K_\beta \left( D^\beta \varepsilon_V \right)(t) \tag{4.33a}$$

$$\sigma_{11}^{(d)}(t) = \frac{4}{3} G_\alpha \left[ D^\alpha \left( \varepsilon_{11} - \frac{\varepsilon_{22} + \varepsilon_{33}}{2} \right) \right](t) \tag{4.33b}$$

where $I_1 = \sigma_{11} + \sigma_{22} + \sigma_{33}$, $\varepsilon_V = \varepsilon_{11} + \varepsilon_{22} + \varepsilon_{33}$ and $\sigma_{11}^{(d)} = \sigma_{11} - I_1/3$ is the deviatoric part of $\sigma_{11}$. Note that the fractional derivative in Eq. (4.33) is the Caputo's fractional derivative. By summing the two contributions we obtain:

$$\sigma_{11}(t) = K_\beta \left( D^\beta \varepsilon_V \right)(t) + \frac{4}{3} G_\alpha \left[ D^\alpha \left( \varepsilon_{11} - \frac{\varepsilon_{22} + \varepsilon_{33}}{2} \right) \right](t) \tag{4.34}$$

Note that Eq. (4.34) can be obtained also by direct evaluation of Eq. (3.3). Now, Eq. (4.34) is discretized by using the GL fractional operator; for numer-

ical implementation the GL operator is slightly modified:

$$\left({}_0^{GL}D_t^{\beta} f\right)(t) = \left({}_0^{GL}D_t^{\beta} f\right)((k+1)\Delta t) = \lim_{\Delta t \to 0} \Delta t^{-\beta} \sum_{j=1}^{k+1} \lambda_k f[t-(j-1)\Delta t] \tag{4.35a}$$

$$\lambda_{j+1} = \frac{j-1-\beta}{j}\lambda_j; \qquad \lambda_1 = 1 \tag{4.35b}$$

After discretization and rearranging Eq. (4.34) becomes:

$$\sigma_{11}^{(k+1)} = K_\beta \Delta t^{-\beta} \sum_{j=1}^{k+1} \lambda_k^{(\beta)} \varepsilon_V^{(k-j+2)} + \frac{4}{3} G_\alpha \Delta t^{-\alpha} \sum_{j=1}^{k+1} \lambda_k^{(\alpha)} \left(\varepsilon_{11} - \frac{\varepsilon_{22}+\varepsilon_{33}}{2}\right)^{(k-j+2)} \tag{4.36}$$

The other two direct components of stress can be found by simply rotating indexes. Eq. (4.36) can be directly implemented in the material subroutine. It is useful to distinguish the volumetric part, common to all direct components of stress, and the deviatoric part related to each direct component of strain; then a scalar quantity $V_\beta$ related to the first of these and a three component vector $S_\alpha$ related to the second are defined as:

$$V_\beta = K_\beta \Delta t^{-\beta} \sum_{j=1}^{k+1} \lambda_k^{(\beta)} \varepsilon_V^{(k-j+2)} \tag{4.37a}$$

$$S_{\alpha,r} = \frac{4}{3} G_\alpha \Delta t^{-\alpha} \sum_{j=1}^{k+1} \lambda_k^{(\alpha)} \varepsilon_r^{(k-j+2)}; \qquad r = 11, 22, 33 \tag{4.37b}$$

With these two quantities we are able to evaluate the direct components of stress as follows:

$$\sigma_r^{(k+1)} = V_\beta + S_{\alpha,r} - \frac{1}{2}\left(\sum_j S_{\alpha,j} - S_{\alpha,r}\right); \qquad r = 11, 22, 33 \tag{4.38}$$

In an analogous way it is possible to compute increments of the shear components of stress:

$$\tau_r^{(k+1)} = G_\alpha \Delta t^{-\alpha} \sum_{j=1}^{k+1} \lambda_k^{(\alpha)} \gamma_r^{(k-j+2)}; \qquad r = 12, 13, 23 \tag{4.39}$$

where $\tau$ is the shear stress and $\gamma$ is the engineering shear strain. These terms can be computed directly one by one.

At this point, by simply calculating differences between $\sigma_i^{(k+1)}$ and $\sigma_i^{(k)}$ with $i = 11, 22, 33$ and between $\tau_r^{(k+1)}$ and $\tau_r^{(k)}$ with $r = 12, 23, 13$, all increments of stress are easily evaluated, and determination of the Jacobian is straightforward:

$$\frac{\partial \Delta\sigma_{ij}^{(k+1)}}{\partial \Delta\varepsilon_{kh}^{(k+1)}} = \left( K_\beta \Delta t^{-\beta} - \frac{2}{3} G_\alpha \Delta t^{-\alpha} \right) \delta_{ij}\delta_{kh} + G_\alpha \Delta t^{-\alpha} \left( \delta_{ik}\delta_{jh} + \delta_{ih}\delta_{jk} \right) \tag{4.40}$$

Note that in Eq. (4.40) the substitution $\lambda_1^{(\alpha)} = \lambda_1^{(\beta)} = 1$ has been made. To code this, we need two quantities; one related to the volumetric relaxation function ($J_\beta$) and the other one related to the deviatoric function ($J_\alpha$)

$$J_\beta = K_\beta \Delta t^{-\beta} \tag{4.41a}$$

$$J_\alpha = G_\alpha \Delta t^{-\alpha} \tag{4.41b}$$

Then

$$\frac{\partial \Delta\sigma_{ij}^{(k+1)}}{\partial \Delta\varepsilon_{kh}^{(k+1)}} = \left( J_\beta - \frac{2}{3} J_\alpha \right) \delta_{ij}\delta_{kh} + J_\alpha \left( \delta_{ik}\delta_{jh} + \delta_{ih}\delta_{jk} \right) \tag{4.42}$$

It is to be noted that if routines for a different isotropic fractional viscoelastic model are needed the structure of Eqs. (4.38) and (4.42) remain the same and the coding can be done without any difficulties; in Section 4.5 some details are given for the fractional KV, fractional Maxwell and fractional SLS models, as illustrated in Fig. 3.5. These relationships also demonstrate how the use of GL fractional derivatives allow the unknown stresses to be determined from the derivative itself. In this way we avoid the implementation of convolution with Mittag-Leffler function kernels as done in [24]; moreover the evaluation of the components of the Jacobian is straightforward and leads to very simple expressions.

One of the issues in the implementation of the fractional viscoelasticity law is that we need to have access to the history of strains in order to obtain the increment of stress. To overcome this problem the values of the components of strain at each increment must be stored in an array to be updated at every increment and for each integration point. When working with Abaqus (as the author of the present work has done), the subroutine is written in Fortran or C language, then the storage of the values of strain/stress can be done simply by using a so-called "commonblock". Storing the history of strain of all

integration points of all elements can potentially lead to a huge memory requirement when running large models subjected to long histories of loading. This problem is not negligible, but sometimes can be reduced as shown in the section numerical tests.
The Newton-Raphson scheme has been proved to be very stable and accurate for this class of problem; furthermore the integration scheme proposed in this section is very stable and convergence is related only to the size of the time increment $\Delta t$, in fact fast convergence is ensured by the use of a sufficiently small $\Delta t$. The accuracy of this integration scheme in comparison with analytical results can be appreciated in the section Numerical tests. Some commercial FE codes that use an implicit Newton-Raphson integration scheme allow the time increment to be determined automatically to optimize the run time. The Grünwald-Letnikov formula for evaluation of the fractional derivatives has been derived assuming a constant independent variable increment (i.e. the time) and to the best of our knowledge a corresponding formulation for a variable increment is not available in the literature; furthermore, the automatic time increment requires the definition of a tolerance criterion, that is difficult to define without knowledge of the elastic and inelastic parts of the strain, contrary to that for plastic and classical viscoelastic materials. For these two reasons, until now, we have limited ourselves to use this model with a fixed time increment.
In situations where an explicit integration scheme is needed, we can simply use the formulation reported above, apart from computing the Jacobian which is not needed.

## 4.4 Numerical tests

In this section the results of simple analysis in Abaqus with the fractional viscoelastic material subroutine are reported. The purpose if this test is to investigate the accuracy of the subroutine for various $\Delta t$ and for various input on the system; moreover, in order to reduce the amount of memory needed for the analysis it is investigate the possibility to truncate the memory of the material.
In all the examples the model is a truss with length $L = 5\ m$, cross section $A = 10^{-4}\ m^2$; one end of the truss is fixed whereas on the other end a longitudinal force history $F(t)$ is applied which results in an applied stress $\sigma(t) = F(t)/A$ considered uniform over the truss. A 1D model has been

chosen because results are easily understandable and valid also for 3D model since here only the time integration scheme is analyzed; the truss is discretized with a single linear FE with two nodes and one Gauss point, that in case of application of one concentrated force gives the exact solution.
The mechanical model is the 1D springpot model with $C_\alpha = 10^9\ Pa\ sec^\alpha$ and $\alpha = 0.3$. The value of $C_\alpha$ is of the order of magnitude of the Young modulus of many common polymers.
Analysis are performed in quasi-static condition with implicit integration scheme and in dynamic condition with both implicit and explicit integration scheme. Implicit integration uses the Newton-Raphson iterative algorithm; in this case analysis with different value of $\Delta t$ have been performed; it is not possible to truncate the memory. Explicit integration scheme does not use the Newton-Raphson method and there is no check for the convergence; for this type of analysis the possibility to truncate the memory has been investigated. Furthermore, another strategy to reduce the amount of memory required has been tried, that is to use a variable $\Delta t$; some tests have been performed to explore the possibility to use this strategy in both implicit and explicit analysis, but results are not good and this strategy is abandoned for this work.
The analysis have been performed with three different applied stress history: constant (creep test), linear ramp, sinusoidal:

$$\sigma(t) = \frac{F_0}{A} U(t) \tag{4.43a}$$

$$\sigma(t) = \frac{F_0}{A} \frac{t}{T} \tag{4.43b}$$

$$\sigma(t) = \frac{F_0}{A} \sin(\omega t) \tag{4.43c}$$

where $F_0 = 1000\ N$, $T$ is the observation time and $\omega$ is the frequency of the sinusoidal load.

### 4.4.1 Implicit integration scheme

The implicit integration scheme is used at every time increment to evaluate the increment of stress from the knowledge of the the increment of strain; moreover the Jacobian is evaluated. The increment of stress together with the material Jacobian allow to evaluate the new increment of strain (for the next time increment or for the next iteration of the Newton-Raphson algorithm). This method can be used both in quasi-static analysis and in dynamic analysis.

### Quasi-static condition

In quasi-static condition the time variable is taken into account but inertia forces are neglected; the applied stress histories of Eqs. 4.43 are depicted in Fig. 4.4 for $T = 20\ s$ and $\omega = 1$.

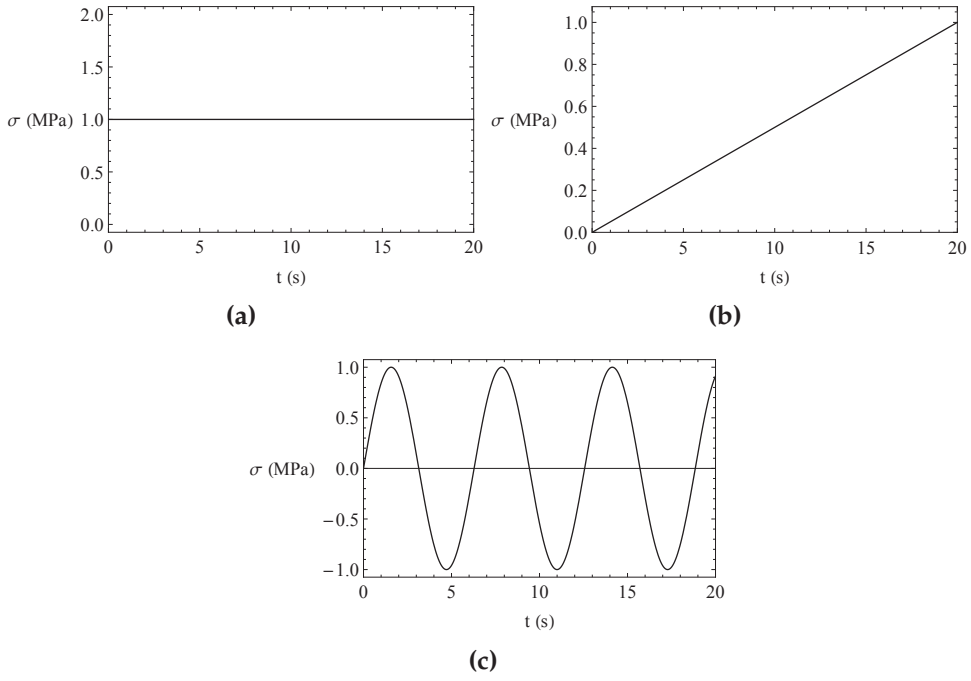


**Figure 4.4:** Applied history stresses for the quasi-static FEM tests: unitstep (a), linear ramp (b) and sinusoidal (c).

The analysis have been performed with different choices of the time increment $\Delta t = 0.1,\ 1,\ 2\ s$; for $\Delta t = 0.1\ s$ results coalesces with the analytical results. Fig. 4.5 shows the responses of the viscoelastic truss to the input of Fig. 4.4. From this figures it can be deduced that: the less demanding situation from the computational point of view is the case with ramp load (Fig. 4.5(b)), while the more demanding situation is that with the sinusoidal load (Fig. 4.5(c)); for the creep test (unitstep load), when $\Delta t$ assumes large values, the precision is low only at the beginning of the test, because the FE software can not apply the pure unitstep load, but it consider a linear ramp through the first time increment.

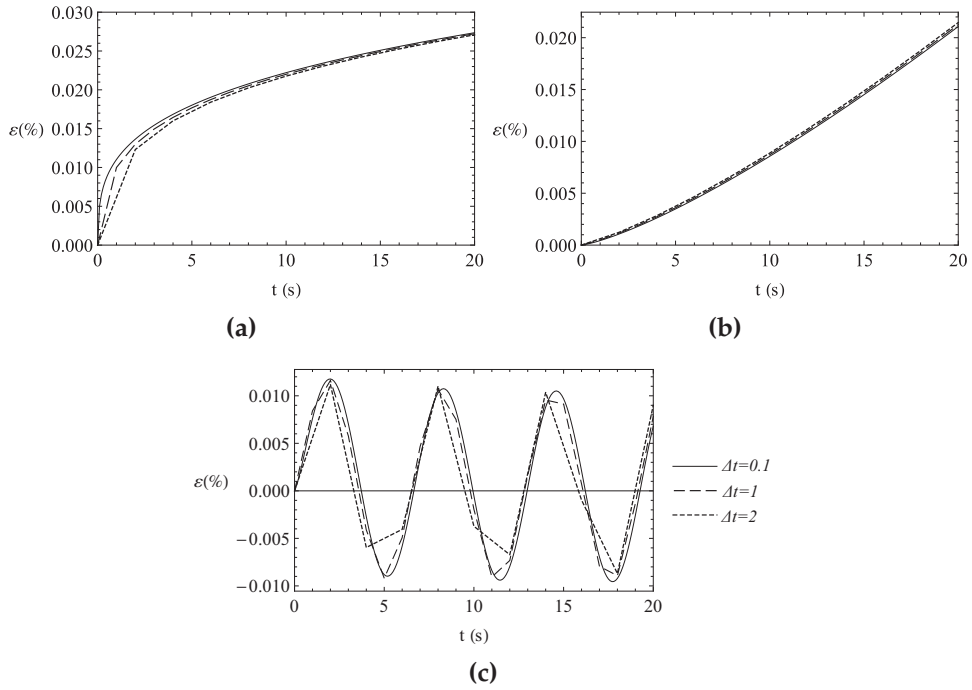


**Figure 4.5:** Responses of the viscoelastic truss in quasi static conditions for unitstep load (a), linear ramp load (b) and sinusoidal load (c).

It is to be noted that the precision is better than in the case that the Newton-Raphson algorithm is not used; this is evident especially when the sinusoidal load is applied: although the time resolution for $\Delta t = 1, 2\ s$ is not good to properly describe the applied load, the error is not big and it is at most 6 %.

### Dynamic conditions

The same numerical tests have been performed in dynamical conditions. For the chosen mechanical parameters, transitory dynamical effect are observable in a very small range of time; for this reason the time of observation has been set to $T = 0.2\ s$ and the frequency $\omega = 100$, resulting in the same applied stress histories of Fig. 4.4, in which the time scale has been reduced to have the maximum $t = 0.2\ s$. Results are shown in Fig. 4.6 for $\Delta t = 10^{-4}, 5 \cdot 10^{-3}, 10^{-2}\ s$.

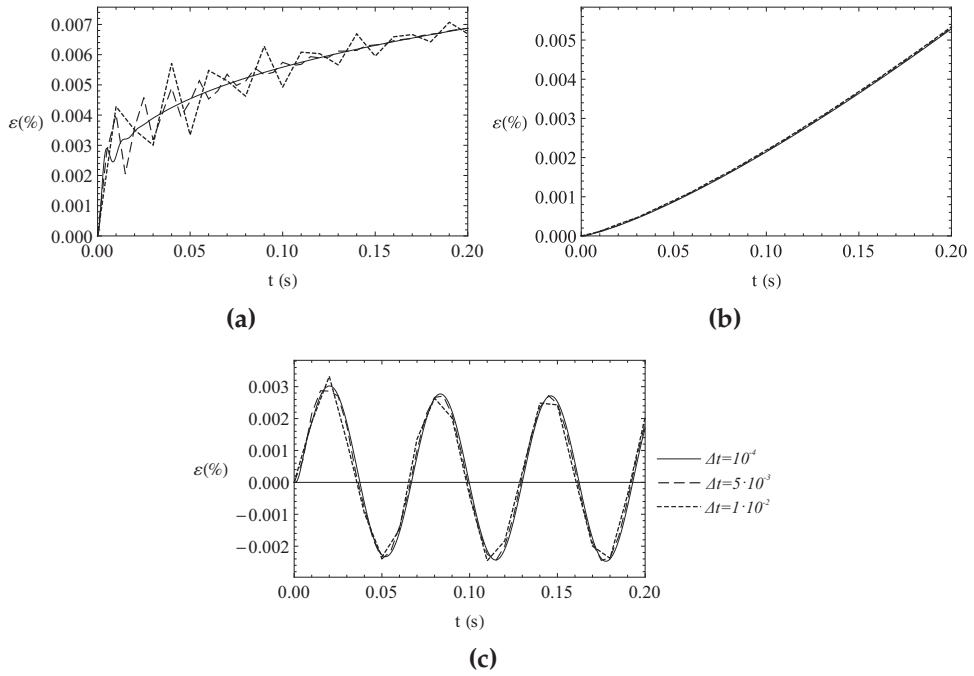


**Figure 4.6:** Responses of the viscoelastic truss in dynamic conditions for unitstep load (a), linear ramp load (b) and sinusoidal load (c) with implicit integration scheme.

Differently from the quasi-static conditions, the most demanding situation is the creep test; indeed in this case the load is applied suddenly (linear through a time increment) and very fast oscillations are inducted on the system. For the linear ramp and sinusoidal loads, the input change gradually from the value of 0 at $t = 0$, then a larger $\Delta t$ is able to reproduce the correct response. Good results with the constant and sinusoidal load are achieved also with $\Delta t = 10^{-3}$ (not present in Fig. 4.6), but in order to have a good resolution of the oscillations at the beginning of the creep test $\Delta t = 10^{-4}$ must be used. As in the quasi static conditions, results to the linear ramp applied stress are good also with very big time increments.

### 4.4.2 Explicit integration scheme

Explicit integration scheme is used when it is convenient to use a great number of small time increments; the integration for every time increment is much

faster than with implicit integration, because no Jacobian has to be evaluated and inverted; indeed in FE models with many DOFs, the Jacobian is a matrix which dimensions are equal to the number of integration points, than inverting the Jacobian is very time consuming.

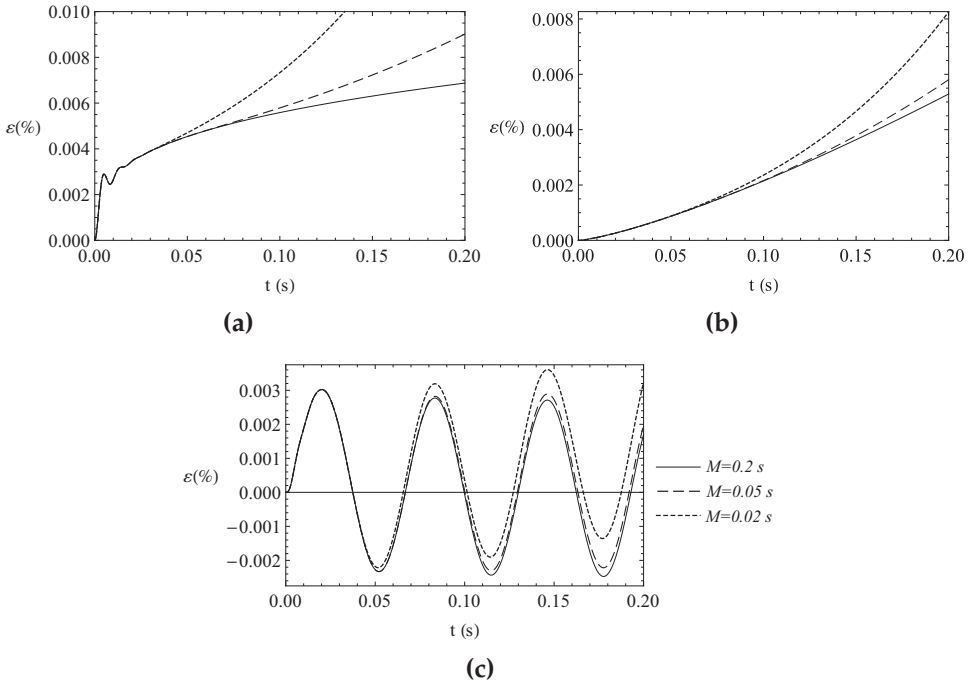


**Figure 4.7:** Responses of the viscoelastic truss in dynamic conditions for unitstep load (a), linear ramp load (b) and sinusoidal load (c) with explicit integration scheme.

Explicit integration schemes are conditionally stable; indeed, the size of the time increment has a maximum value $\Delta t_S$ that is the so called "stable time increment" determined as the time that a dilation wave employs to go through a single FE; when the model has FEs of different size and more then one material, $\Delta t_S$ is the smallest between the stable time increments of all the FEs. When the time increment is bigger than $\Delta t_S$, the response diverges; sometimes to obtain accurate results the time increment is even smaller than $\Delta t_S$. The truss of the previous sections has been used also for the test with explicit integration; the possibility to truncate the memory of the material is investi-

gated. In this case $\Delta t_S = 1,56 \cdot 10^{-3}$; however to obtain good results $\Delta t = 10^{-4}$ has been used. For each load history of the dynamic implicit conditions, the analysis has been performed with different length of the memory of the material $M = 0.2, 0.05, 0.02\ s$. Results are depicted in Fig. 4.7.
From this figure it is evident that when the memory of the material is truncated, at a certain time $t > M$ the response of the system starts to follow a wrong evolution; however, the response remain stable if the memory is truncated not too much: for the linear ramp and sinusoidal loads $M = 0.1\ s$ (not present in Fig. 4.7) ensure to obtain the correct response in an observation time $T = 0.2\ s$, while for the creep test the correct resposne is obtained with $M = 0.15\ s$ (not present in Fig. 4.7). As in the dynamic implicit analysis, the most demanding situation is the creep test.

## 4.5 Implementation of multi-element fractional models

In this section governing equations and Eqs. (4.37), (4.39) and (4.41) for the fractional multi-element models (fractional Maxwell, fractional KV, fractional SLS) are given.

**Fractional 3D Maxwell model**

The governing equation of the 1D fractional Maxwell (3.21a) is reported in the following:

$$\left(D^{\beta}\sigma\right)(t) + \frac{E}{C_{\beta}}\sigma(t) = E\left(D^{\beta}\varepsilon\right)(t) \tag{4.44}$$

From this equation it is evident that this model requires a knowledge of both strain and stress history to evaluate the new stresses; to avoid this, we simply perform an integration of order $\beta$ of the equation:

$$\sigma(t) + \frac{E}{C_{\beta}}\left(I^{\beta}\sigma\right)(t) = E\varepsilon(t) \tag{4.45}$$

In this way only the history of stress is required to evaluate the new stress at each increment. Then the volumetric and deviatoric parts of the governing equation are found by generalizing Eq. (4.45) and not Eq. (4.44); governing equations for volumetric and deviatoric parts of $\sigma_{11}(t)$ are

$$\frac{I_1}{3} + \frac{K}{K_{\beta}}\left(I^{\beta}\frac{I_1}{3}\right)(t) = K\varepsilon_V(t) \tag{4.46a}$$

$$\sigma_{11}^{(d)}(t) + \frac{G}{G_\alpha}\left(I^\alpha \sigma_{11}^{(d)}\right)(t) = \frac{4}{3}G\left(\varepsilon_{11}(t) - \frac{\varepsilon_{22}(t)+\varepsilon_{33}(t)}{2}\right) \tag{4.46b}$$

Terms for evaluating stresses:

$$V_\beta = \frac{KK_\beta}{K_\beta + K\Delta t^\beta}\left\{\varepsilon_V^{(k+1)} - \frac{\Delta t^\beta}{3K_\beta}\sum_{j=2}^{k+1}\lambda_j^{(\beta)} I_1^{(k+1)}\right\} \tag{4.47a}$$

$$S_{\alpha,r} = \frac{4}{3}\frac{GG_\alpha}{G + G_\alpha \Delta t^\alpha}\left\{\varepsilon_r^{(k+1)} - \frac{\Delta t^\alpha}{2G_\alpha}\sum_{j=2}^{k+1}\lambda_j^{(\alpha)}\sigma_r^{(k+1)}\right\}; \qquad r = 11, 22, 33 \tag{4.47b}$$

$$\tau_r^{(k+1)} = \frac{GG_\alpha}{G + G_\alpha \Delta t^\alpha}\left\{\gamma_r^{(k+1)} - \frac{\Delta t^\alpha}{G_\alpha}\sum_{j=2}^{k+1}\lambda_j^{(\alpha)}\tau_r^{(k-j+2)}\right\}; \qquad r = 12, 13, 23 \tag{4.48}$$

Terms for the evaluation of the Jacobian

$$J_\beta = \frac{KK_\beta}{K_\beta + K\Delta t^\beta} \tag{4.49a}$$

$$J_\alpha = \frac{GG_\alpha}{G + G_\alpha \Delta t^\alpha} \tag{4.49b}$$

**Fractional 3D KV model**

Governing equations for volumetric and deviatoric part of $\sigma_{11}(t)$:

$$\frac{I_1(t)}{3} = K\varepsilon_V(t) + K_\beta\left(D^\beta \varepsilon_V\right)(t) \tag{4.50a}$$

$$\sigma_{11}^{(d)}(t) = \frac{4}{3}G\left(\varepsilon_{11}(t) - \frac{\varepsilon_{22}(t)+\varepsilon_{33}(t)}{2}\right) + \frac{4}{3}G_\alpha\left[D^\alpha\left(\varepsilon_{11} - \frac{\varepsilon_{22}+\varepsilon_{33}}{2}\right)\right](t) \tag{4.50b}$$

Terms for evaluating stresses:

$$V_\beta = K\varepsilon_V^{(k+1)} + K_\beta \Delta t^{-\beta}\sum_{j=1}^{k+1}\lambda_j^{(\beta)}\varepsilon_V^{(k-j+2)} \tag{4.51a}$$

$$S_{\alpha,r} = \frac{4}{3}G\varepsilon_r^{(k+1)} + \frac{4}{3}G_\alpha \Delta t^{-\alpha}\sum_{j=1}^{k+1}\lambda_j^{(\alpha)}\varepsilon_r^{(k-j+2)}; \qquad r = 11, 22, 33 \tag{4.51b}$$

$$\tau_r^{(k+1)} = G\gamma_r^{(k+1)} + G_\alpha \Delta t^{-\alpha} \sum_{j=1}^{k+1} \lambda_j^{(\alpha)} \Delta\gamma_r^{(k-j+2)}; \qquad r = 12, 13, 23 \tag{4.52}$$

Terms for the evaluation of the Jacobian

$$J_\beta = K + K_\beta \Delta t^{-\beta} \tag{4.53a}$$

$$J_\alpha = G + G_\alpha \Delta t^{-\alpha} \tag{4.53b}$$

**Fractional 3D Zener model a)**

Governing equations for volumetric and deviatoric parts of $\sigma_{11}(t)$:

$$\frac{I_1}{3} + \frac{K_\beta}{K_2}\left(D^\beta \frac{I_1}{3}\right)(t) = K_1 \varepsilon_V(t) + \frac{(K_1 + k_2)K_\beta}{K_2}\left(D^\beta \varepsilon_V\right)(t) \tag{4.54a}$$

$$\sigma_{11}^{(d)}(t) + \frac{G_\alpha}{G_2}\left(D^\alpha \sigma_{11}^{(d)}\right)(t) = \frac{4}{3}G_1\left(\varepsilon_{11}(t) - \frac{\varepsilon_{22}(t) + \varepsilon_{33}(t)}{2}\right) + \\ + \frac{4}{3}\frac{(G_1 + G_2)G_\alpha}{G_2}\left[D^\alpha\left(\varepsilon_{11} - \frac{\varepsilon_{22} + \varepsilon_{33}}{2}\right)\right](t) \tag{4.54b}$$

By analizing Eqs. (4.54) it is immediately evident that this model requires a knowledge of both strain and stress histories; with this model, and also with more complicated models, this cannot be avoided and equivalent simplifications to that employed for the fractional Maxwell model are not available. Terms for evaluating stresses:

$$V_\beta = \frac{1}{K_2 + K_\beta \Delta t^{-\beta}}\left\{\varepsilon_V^{(k+1)}\left[K_1 K_2 + (K_1 + K_2)K_\beta \Delta t^{-\beta}\right] + \right. \\ \left. + K_\beta \Delta t^{-\beta} \sum_{j=2}^{k+1} \lambda_j^{(\beta)}\left[(K_1 + K_2)\varepsilon_V^{(k-j+2)} - \frac{I_1^{(k-j+2)}}{3}\right]\right\} \tag{4.55a}$$

$$S_{\alpha,r} = \frac{4}{3(G_2 + G_\alpha \Delta t^{-\alpha})}\left\{\varepsilon_r^{(k+1)}\left[G_1 G_2 + (G_1 + G_2)G_\alpha \Delta t^{-\alpha}\right] + \right. \\ \left. + G_\alpha \Delta t^{-\alpha} \sum_{j=2}^{k+1} \lambda_j^{(\alpha)}\left[(G_1 + G_2)\varepsilon_r^{(k-j+2)} - \frac{\sigma_r^{(k-j+2)}}{2}\right]\right\}; \\ r = 11, 22, 33 \tag{4.55b}$$

$$\tau_r = \frac{1}{G_2 + G_\alpha \Delta t^{-\alpha}} \Bigg\{ \gamma_r^{(k+1)} \left[ G_1 G_2 + (G_1 + G_2) G_\alpha \Delta t^{-\alpha} \right] + \\ + G_\alpha \Delta t^{-\alpha} \sum_{j=2}^{k+1} \lambda_j^{(\alpha)} \left[ (G_1 + G_2) \gamma_r^{(k-j+2)} - \tau_r^{(k-j+2)} \right] \Bigg\}; \\ r = 11, 22, 33 \quad (4.56)$$

Terms for the evaluation of the Jacobian

$$J_\beta = \frac{K_1 K_2 + (K_1 + K_2) + K_\beta \Delta t^{-\beta}}{K_2 + K_\beta \Delta t^{-\beta}} \quad (4.57a)$$

$$J_\alpha = \frac{G_1 G_2 + (G_1 + G_2) + G_\alpha \Delta t^{-\alpha}}{G_2 + G_\alpha \Delta t^{-\alpha}} \quad (4.57b)$$

**Fractional 3D Zener model b)**

Governing equations for volumetric and deviatoric parts of $\sigma_{11}(t)$:

$$\frac{I_1}{3} + \frac{K_\beta}{K_1 + K_2} \left( D^\beta \frac{I_1}{3} \right)(t) = \frac{K_1 K_2}{K_1 + K_2} \varepsilon_V(t) + \frac{K_1 K_\beta}{K_1 + K_2} \left( D^\beta \varepsilon_V \right)(t) \quad (4.58a)$$

$$\sigma_{11}^{(d)}(t) + \frac{G_\alpha}{G_1 + G_2} \left( D^\alpha \sigma_{11}^{(d)} \right)(t) = \frac{4}{3} \frac{G_1 G_2}{G_1 + G_2} \left( \varepsilon_{11}(t) - \frac{\varepsilon_{22}(t) + \varepsilon_{33}(t)}{2} \right) + \\ + \frac{4}{3} \frac{G_1 G_\alpha}{G_1 + G_2} \left[ D^\alpha \left( \varepsilon_{11} - \frac{\varepsilon_{22} + \varepsilon_{33}}{2} \right) \right](t) \quad (4.58b)$$

Terms for evaluating stresses:

$$V_\beta = \frac{1}{K_1 + K_2 + K_\beta \Delta t^{-\beta}} \Bigg\{ \varepsilon_V^{(k+1)} K_1 (K_2 + K_\beta \Delta t^{-\beta}) + \\ + K_\beta \Delta t^{-\beta} \sum_{j=2}^{k+1} \lambda_j^{(\beta)} \left( K_1 \varepsilon_V^{(k-j+2)} - \frac{I_1^{(k-j+2)}}{3} \right) \Bigg\} \quad (4.59a)$$

$$S_{\alpha,r} = \frac{4}{3(G_1 + G_2 + G_\alpha \Delta t^{-\alpha})} \Bigg\{ \varepsilon_r^{(k+1)} G_1 \left( G_2 + G_\alpha \Delta t^{-\alpha} \right) + \\ + G_\alpha \Delta t^{-\alpha} \sum_{j=2}^{k+1} \lambda_j^{(\alpha)} \left( G_1 \varepsilon_r^{(k-j+2)} - \frac{\sigma_r^{(k-j+2)}}{2} \right) \Bigg\}; \\ r = 11, 22, 33 \quad (4.59b)$$

$$\tau_r^{(k+1)} = \frac{1}{G_1 + G_2 + G_\alpha \Delta t^{-\alpha}} \Bigg\{ \gamma_r^{(k+1)} G_1 \left( G_2 + G_\alpha \Delta t^{-\alpha} \right) + \\ + G_\alpha \Delta t^{-\alpha} \sum_{j=2}^{k+1} \lambda_j^{(\alpha)} \left( G_1 \gamma_r^{(k-j+2)} - \tau_r^{(k-j+2)} \right) \Bigg\}; \qquad r = 12, 13, 23 \quad (4.60)$$

Terms for the evaluation of the Jacobian

$$J_\beta = \frac{K_1 \left( K_2 + K_\beta \Delta t^{-\beta} \right)}{K_1 + K_2 + K_\beta \Delta t^{-\beta}} \quad (4.61a)$$

$$J_\alpha = \frac{G_1 \left( G_2 + G_\alpha \Delta t^{-\alpha} \right)}{G_1 + G_2 + G_\alpha \Delta t^{-\alpha}} \quad (4.61b)$$

## 4.6 Conclusions

In this chapter the implementation of 3D fractional viscoelastic models in a finite element framework has been discussed; the fractional derivatives in the constitutive equations have been discretized by means of the GL definition. The routines have been tested in Abaqus and they resulted very fast and stable; however, the need to access to all history of stress and/or strain implies that a great amount of memory have to be used to analyze models with a great number of FEs and with many time increments; to decrease the amount of memory required one possible strategy is to truncate the memory of the materials, but this works only for explicit analysis; on the other hand, implicit analysis converge with larger time increment than explicit analysis, with consequent smaller amount of memory required, but in some cases, for example when contact are present in the model, explicit analysis converge more easily than implicit. Although in some cases truncate the memory is useful, it is believed that other strategy can be found to decrease the amount of memory required, for this reason in the future some efforts should be devoted to this purpose. In the next chapter an example of FE analysis with fractional viscoelastic material implemented with the formulation of this chapter is presented.

# Chapter 5

# Applications

In the previous chapters fractional viscoelasticity, 3D formulation of fractional viscoelasticity and its implementation in the finite element method has been discussed; in this chapter some engineering applications of these mechanical model are presented. In particular the following topics are discussed: the fractional Tajimi-Kanai model, that is a model useful to generate filtered white noise (as for example earthquakes) that has been modified with a fractional term; Euler-Bernoulli and Timoshenko beams made of fractional viscoelastic material; the formulation of a nonlocal fractional viscoelastic Timoshenko beam; FEM simulations of biomedical prosthesis constituted of a viscoelastic polymer.

## 5.1 The fractional Tajimi-Kanai model

The ground acceleration is usually modeled as a filtered Gaussian process. The most common model is a Tajimi-Kanai filter [62, 88] that is a classical viscoelastic Kelvin-Voigt unit carrying a mass excited by a white noise (acceleration at the bedrock). Based upon the observation that soils exhibit a power law trend in the creep test, it is proposed the substitution of the purely viscous element in the Kelvin Voigt element with the springpot. With this choice two main goals are reached: i) The viscoelastic behavior of the ground may be simply characterized by performing the creep (or the relaxation) test on a specimen of the ground at the given site; ii) The number of zero crossing of the absolute acceleration at the free field that for the classical Tajimi-Kanai model is $\infty$ for a true white noise acceleration, remains finite for the proposed model.

Results of this section have been already published in [6].
In the following the fractional Tajimi-Kanai model will be introduced in details, but for clarity's sake the classical Tajimi-Kanai model is first discussed.

### 5.1.1 The classical Tajimi-Kanai model

The Tajimi-Kanai (TK) model for the earthquake ground motion is based on the observation that the absolute acceleration of the ground may be sought as a white noise process (acceleration at bedrock) filtered through superimposed soil deposit modeled as a single degree of freedom oscillator as depicted in Fig. 5.1. Let us denote as $M_g$ the mass of the oscillator, $K_g$ the stiffness and

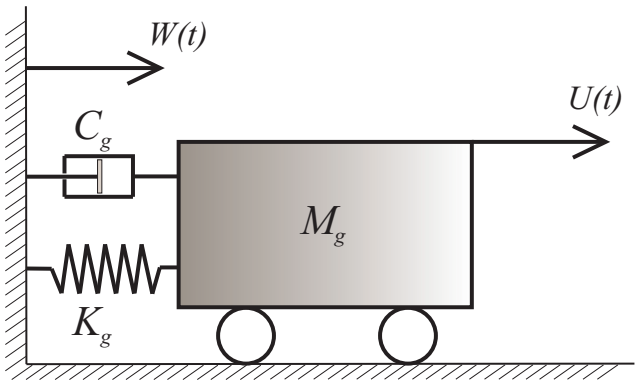


**Figure 5.1:** Classical Tajimi-Kanai model.

$C_g$ the damping coefficient of the dashpot connecting the mass $M_g$ and the bedrock, $U(t)$ is the absolute displacement of the mass $M_g$, $W(t)$ the absolute displacement of the bedrock and $X_g(t)$ the relative displacement between the mass $M_g$ and the bedrock ($X_g(t) = U(t) - W(t)$). Based on the above considerations, the dynamic equilibrium equation of the mass $M_g$ is given as:

$$M_g(\ddot{X}_g(t) + \ddot{W}(t)) + C_g\dot{X}_g(t) + K_gX(t) = 0 \tag{5.1}$$

and dividing by $M_g$ we get

$$\ddot{X}_g(t) + 2\zeta_g\omega_g\dot{X}_g(t) + \omega_g^2X(t) = -\ddot{W}(t) \tag{5.2}$$

where $\zeta_g$ and $\omega_g$ are the damping ratio and the circular natural frequency of the ground, respectively, whose values are generally $\omega_g = 5\pi$ (rad/sec),

$\zeta_g = 0.6$. Then since we are interested in absolute acceleration of the free field we may write

$$\ddot{U}(t) = \ddot{X}_g(t) + \ddot{W}(t) = -2\zeta_g\omega_g\dot{X}_g - \omega_g^2 X_g(t) \tag{5.3}$$

Now let us suppose that $\ddot{W}(t)$ is a normal white noise process characterized by the Power Spectral Density (PSD) level $S_0$ (constant at overall frequencies), then the PSD for $\ddot{U}(t)$ is given as

$$S_{\ddot{U}}(\omega) = 2\pi S_0 \frac{\omega_g^4 + 4\zeta_g^2\omega_g^2\omega^2}{(\omega_g^2 - \omega^2)^2 + 4\zeta_g^2\omega_g^2\omega^2} \tag{5.4}$$

Close inspection of Fig.5.1 reveals that the classical TK filter is neither else than a Kelvin-Voigt element carrying a mass $M_g$ in which the elastic and the viscous elements take into account the viscoelastic property of the soil deposit. In order to overcome the unrealistic value of $S_{\ddot{U}}(\omega)$ at $\omega = 0$ ($S_{\ddot{U}}(0) = 2\pi S_0$) in [19] is proposed a modification of the classical TK by inserting another oscillator (like a filter) avoiding the physical inconsistency. On the other hand in the previous section it has been shown that the correct interpretation of the viscoelastic property of the soil is a spring (like in the classical TK filter) and a fractional element characterized by the coefficients $\beta$ and $C_\beta$. This issue will be addressed in the following.

### 5.1.2 Fractional Tajimi-Kanai model

Once we know the local constitutive law of the ground, by knowing the depth and the local characteristics of the soil deposit by using a shear type beam model the acceleration at the free field may be obtained. However since our goal is to find a simplified model like the Tajimi-Kanai filter we assume that the dashpot in the TK is substituted by a fractional element characterized by $\beta$ and $C_g^{(\beta)}$, as depicted Fig. 5.2. Inspection of the above model reveals that the dashpot characterized by $C_g$ in the classical TK is substituted by a fractional element (Fig. 5.2b), usually termed as springpot because it is an element with an intermediate behavior between the purely elastic (SPRING) and a purely viscous one (dashPOT). As we assume that the term $C_g\dot{X}_g(t)$ in Eq. (5.1) is substituted by $C_g^{(\beta)}({}^C D_{0^+}^{\beta} X_g)(t)$ the equation of motion in canonical form is written as

$$\ddot{X}_g(t) + 2\bar{\zeta}_g\omega_g({}^C D_{0^+}^{\beta} X_g)(t) + \omega_g^2 X_g(t) = -\ddot{W}(t) \tag{5.5}$$

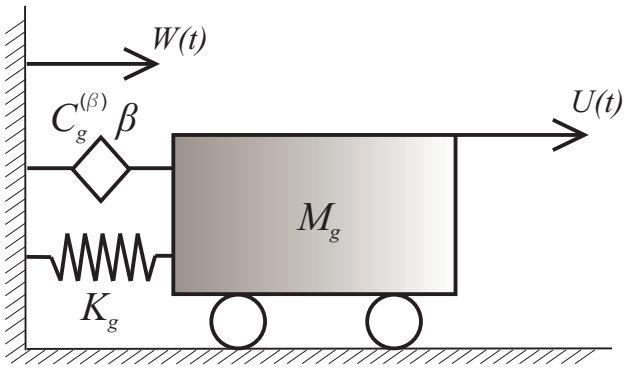


**Figure 5.2:** Fractional Tajimi-Kanai model.

where $\bar{\zeta}_g$ is an anomalous damping coefficient $[\bar{\zeta}_g] = [sec^{\beta-1}]$.
Since the Fourier transform of the Caputo's fractional derivative is given as

$$\mathcal{F}\left\{{}^{C}D^{\beta}_{0^+}X_g)(t);\omega\right\} = (i\omega)^{\beta}\hat{X}_g(\omega) = |\omega|^{\beta}\left(\cos\left(\frac{\beta\pi}{2}\right) + i\,\mathrm{sgn}(\omega)\sin\left(\frac{\beta\pi}{2}\right)\right)\hat{X}_g(\omega) \quad (5.6)$$

where $i = \sqrt{-1}$, $\mathrm{sgn}(\omega)$ is the signum function and $\hat{X}_g(\omega)$ is the Fourier transform of $X_g(t)$, then after some algebra we get the PSD of the absolute ground acceleration in the form

$$S_{\ddot{U}}(\omega) = 2\pi S_0 \frac{\omega_g^4 + 4\bar{\zeta}_g^2\omega_g^2\omega^{2\beta} + 4\bar{\zeta}_g\omega^{\beta}\omega_g^3\cos(\frac{\beta\pi}{2})}{(\omega_g^2-\omega^2)^2 + 4\bar{\zeta}_g^2\omega_g^2\omega^{2\beta} + 4\bar{\zeta}_g\omega^{\beta}\omega_g\cos(\frac{\beta\pi}{2})(\omega_g^2-\omega^2)} \quad (5.7)$$

It is worth stressing that as soon as we assume $\beta = 1$, then $\bar{\zeta}_g = \zeta_g$, and since $\cos(\beta\pi/2) = 0$ Eq.(5.7) reverts to Eq.(5.4). Also in the proposed model there is a physical inconsistency at $\omega = 0$, that is $S_{\ddot{U}}(0) = 2\pi S_0$ like in the classical filter. To avoid this problem, a similar strategy, like that one used in [19], may be also used for the FTK system. However for the sake of simplicity hereinafter this problem is not considered. To select the parameters $k_g$, $C_g^{(\beta)}$ and $\beta$ it is possible to perform a best fitting of experimental shear creep tests on sample of real ground. It can be easily demonstrated that for a fractional

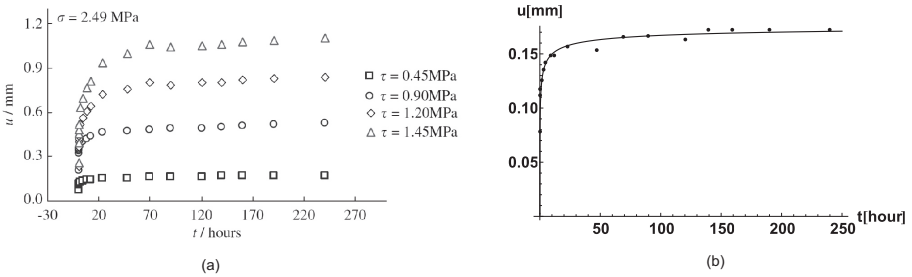


**Figure 5.3:** a) Typical visco-elastic shear test [91]; b) Shear creep test: experimental data (dots), theoretical result (solid line)

Kelvin-Voigt model the creep function is given in the form

$$J(t) = \frac{1}{k_g}\left(1 - E_\beta\left(-\frac{k_g}{C_g^{(\beta)}}t^\beta\right)\right) \tag{5.8}$$

where $E_{\beta,\beta+1}(\cdot)$ is the Mittag-Leffler defined in the Appendix. Inserting Eq. (5.8) into Eq. (2.6) it leads to

$$\gamma(t) = \sum_{k=0}^{\infty} \frac{k_g}{C_g^{(\beta)}}\left(I_{0^+}^{\beta k+1}\tau\right)(t) \tag{5.9}$$

The creep function for the ground are rare as in fact the tests performed on the specimen of ground are usually performed only to assess the ultimate load for the ground at hands and not for the characterization of the viscoelastic behavior. However recently [91] for shale located in Lougtan Hydropower project of China using shale sample size of 150mmx150mmx150mm the creep test are reported. Such a test have been performed for various shear stress levels and the results are depicted in Fig.5.3a A best fitting between experimental creep and theoretical ones obtained by Eq. (5.8) returns the parameters $k_g = 55 \cdot 10^6[N/m]$, $C_g^{(\beta)} = \gamma_1 k_g[Nsec^\beta/m]$, $\beta = 0.4$, for the minimum level stress $\tau = 0,45MPa$. The selection of the minimum stress level is made in order to ensure us that the ground behaves in the viscoelastic zone. The parameter $\gamma_1$ is a dimensional factor useful to give a numerical relation between $k_g$ and $C_g^{(\beta)}$; for the ground at hands it is $\gamma_1 = 20\,[sec^\beta]$. Like in the classical TK then the main assumption is that the ground deposit behaves linearly. This is reflected from the fact that the equation of the filter is ruled by

Caputo's fractional operators that are in fact linear ones. If the magnitude of earthquake grows then the Nutting law requires the dependence on the level of stress as well. As in fact the Nutting law is $\gamma(t) \propto \tau^{\alpha} t^{-\beta}$ (being $\alpha$ an indicator of nonlinearity) and the equation of the filter is non linear. Hereinafter the dependence on the stress level is eliminated in order to work with a linear model as the classical TK is. Once the parameters have been obtained by the best fitting the shear creep test curve obtained from experimental data is contrasted with the theoretical one expressed in Eq. 5.8 and plotted in Fig.5.3b. From the figures some considerations may be withdrawn: i) From the experimental tests it is apparent that the correct way to describe the soil constitutive law is involving power law in the kernel of Eqs. (2.6) and/or (2.8). ii) As a consequence of i) the proper constitutive model of soil deposit is not a classical Kelvin-Voigt or Maxwell element or more complex combination of such elementary units since a fractional constituitive law may be represented by $\infty$ Kelvin-Voigt elements. Now to study the PSD of the FTK the values of $\bar{\zeta}_g$ and $\omega_g$ have to be found; in order to do this, first a relation between $\bar{\zeta}_g$ and $\omega_g$ is found thanks to the relation between $k_g$ and $C_g^{(\beta)}$ as

$$\frac{C_g^{(\beta)}}{M_g} = \frac{\gamma_1 \, k_g}{M} = 2\bar{\zeta}_g \omega_g \tag{5.10}$$

and since

$$\frac{k_g}{M_g} = \omega_g^2 \tag{5.11}$$

we obtain

$$\bar{\zeta}_g = \frac{\gamma_1}{2} \, \omega_g \tag{5.12}$$

The values of $\bar{\zeta}_g$ and $\omega_g$ are then calibrated in order to have the PSD peak of the FTK at almost the same frequency of the peak of the TK PSD obtaining $\omega_g = 2\,[rad/sec]$ and $\bar{\zeta}_g = 20$. In Fig.5.4 the PSD for the classical TK filter is contrasted with that of the proposed FTK filter. From Fig.5.4 at first glance it seems that no substantial difference between the two PSD distributions is evidenced. It follows that up to now the only reason to prefer using the FTK is that it models the viscoelastic property of the soil in a more realistic way. As in fact the parameters $\zeta_g$ and $\omega_g$ of the classical TK are mainly determined by the zero crossing of historical data and other specific characteristics based upon the probability theory of stochastic processes. However there is another reason to prefer the FTK from a theoretical point of view that is not explicitely claimed in literature. This issue will be adressed in the next section.

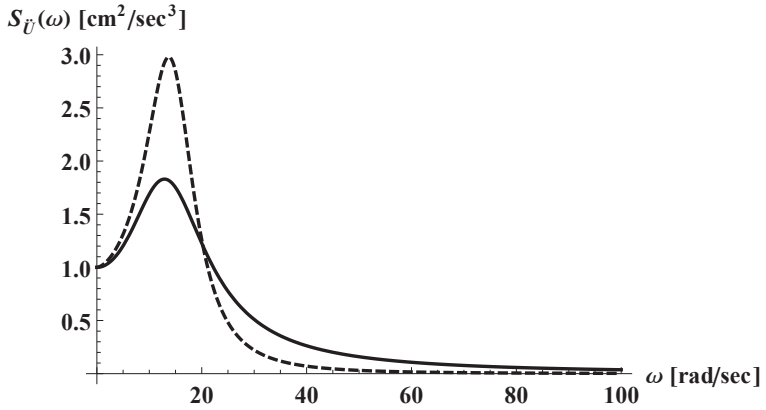


**Figure 5.4:** Power spectral densities of $\ddot{U}(t)$; classical TK (solid line): $\omega_g = 5\pi$, $\zeta_g = 0.6$, $S_0 = 1$; FTK (dashed line): $\omega_g = 2$, $\bar{\zeta}_g = 20$, $\beta = 0.4$, $S_0 = 1$

### 5.1.3 Zero crossings for TK and FTK model

The PSDs of the absolute acceleration $\ddot{U}(t)$ of TK and of FTK model are given in Eqs.(5.4) and 5.7, respectively. In order to match experimental data coming from historical earthquake model the zero crossings of the absolute acceleration at the free field has to be evaluated. It is well known that the mean number of zero crossings $\nu$ of the stationary Gaussian stochastic process $\ddot{U}(t)$ is given as [69]

$$\nu = \frac{1}{\pi}\left[\frac{\int_0^\infty S_{\dddot{U}}(\omega)d\omega}{\int_0^\infty S_{\ddot{U}}(\omega)d\omega}\right]^{1/2} = \frac{1}{\pi}\frac{\sigma_{\dddot{U}}}{\sigma_{\ddot{U}}} \tag{5.13}$$

where $S_{\dddot{U}}(\omega)$ is the power spectral density of the rate of acceleration $\dddot{U}$, $\sigma_{\dddot{U}}$ and $\sigma_{\ddot{U}}$ are the standard deviation of $\dddot{U}$ and $\ddot{U}$, respectively.
On the other hand since $S_{\dddot{U}}(\omega) = \omega^2 S_{\ddot{U}}(\omega)$, the number of zero crossings for the TK model and the FTK model is given by inserting the corresponding PSDs obtained by Eq.(5.4) (TK model) or Eq.(5.7) (FTK model). We preliminary observe that $S_{\dddot{U}}(\omega)$ for classical TK model is depicted in Fig.5.5 (solid line), in the same figure the $S_{\dddot{U}}(\omega)$ is plotted for FTK model (dashed line) for the selected parameters reported in previous sections and $S_0 = 1 cm^2/sec$. From this figure it is evident that for $\beta = 1$ (classical TK) the PSD of $\dddot{U}(t)$ for $\omega \to \infty$ is constant (for the case under exam the asymptotic value is $355\, cm^2/sec^5$). This may also be captured by making the limit for $\omega \to \infty$ of Eq.(5.4) multiplied by $\omega^2$.

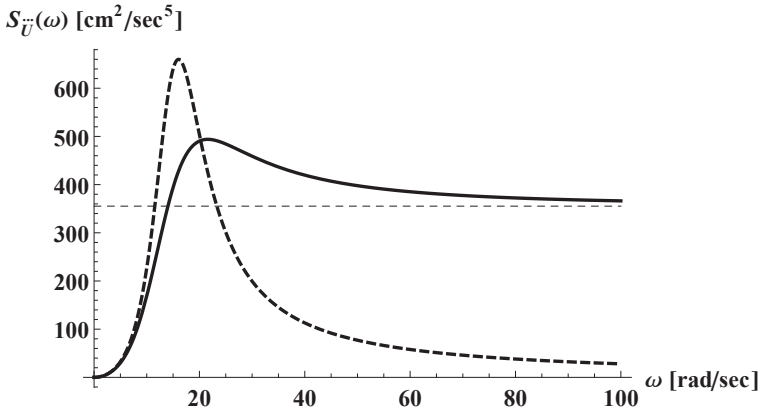


**Figure 5.5:** Power spectral densities of $\ddot{U}(t)$; classical TK solid line; FTK dashed line

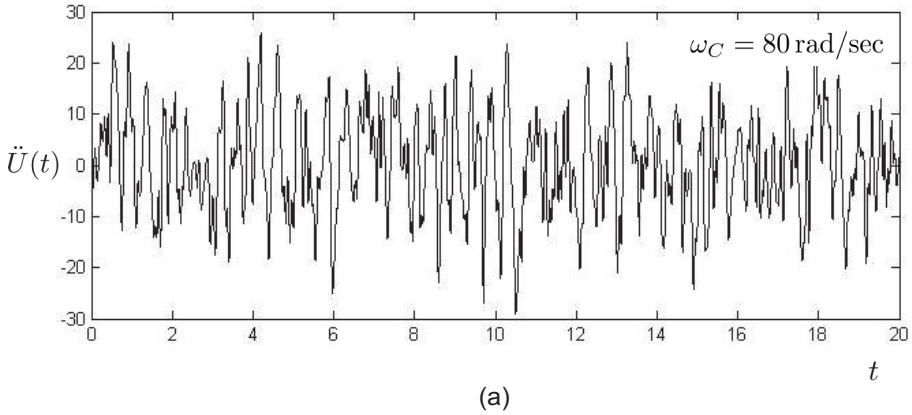


(a)

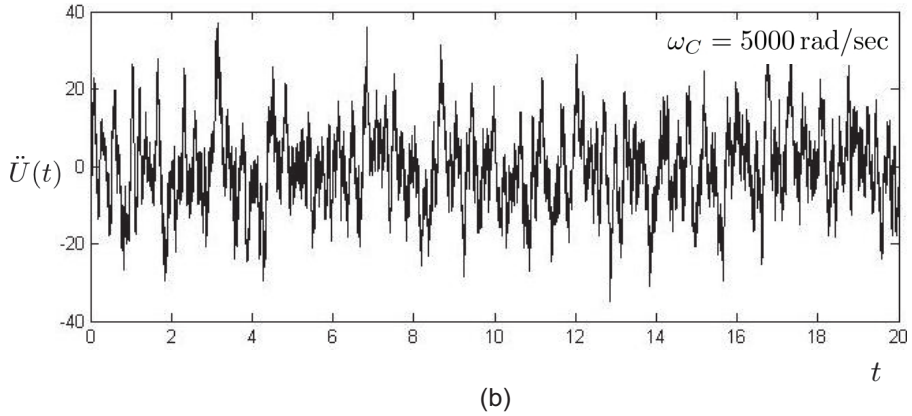


(b)

**Figure 5.6:** Sample functions of $\ddot{U}(t)$ for various values of the cut off frequency $\omega_c$ in the TK filter ($\omega_g = 5\pi$, $\zeta_g = 0.6$)

This means that as we assume that the PSD is that given in Eq.(5.4) the mean number of zero crossing per unit time is $\infty$. This fact is ignored in literature since usually people say that for $\omega > 80 - 100\, rad/sec$ the PSD is negligible. This means de facto that the stochastic process of input is band limited. If this assumptions is made then also the mean number of zero crossing does not diverge.

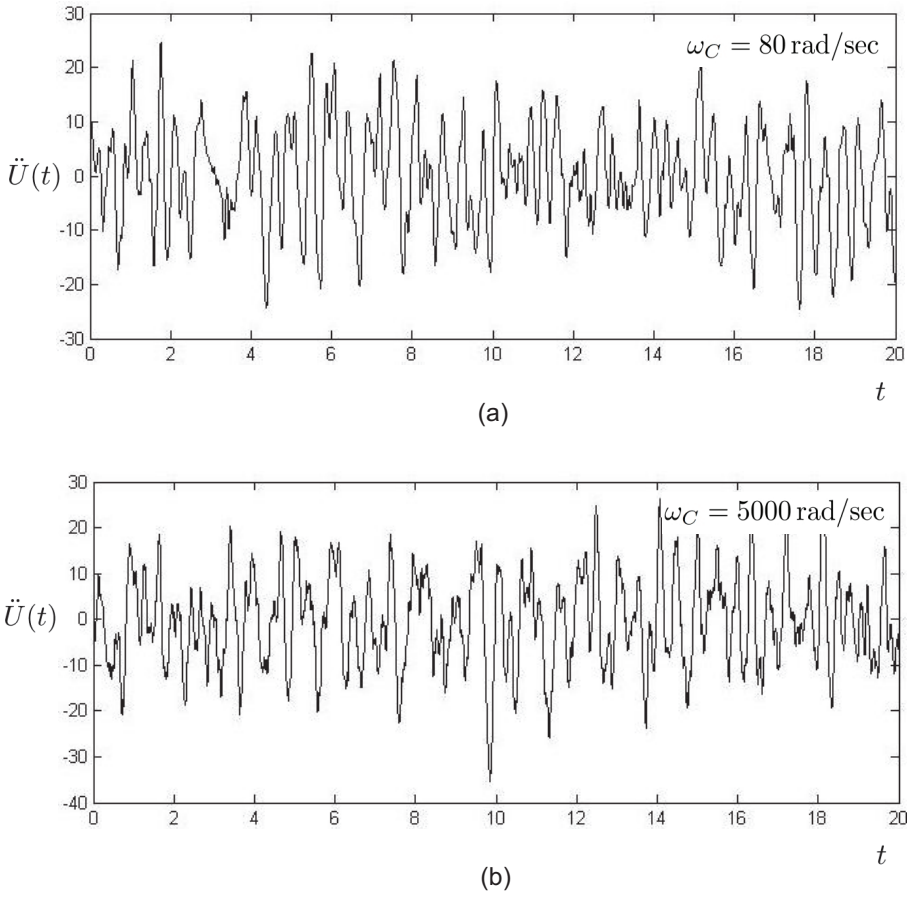


**Figure 5.7:** Sample functions of $\ddot{U}(t)$ for various values of the cut off frequency in the FTK filter ($\omega_g = 2$, $\bar{\zeta}_g = 20$, $\beta = 0.4$)

In Fig. 5.6 two sample functions of $\ddot{U}(t)$ are plotted with different clipping on the PSD of the classical TK filter. In Fig.5.6a the cut off frequency $\omega_C$ is 80 rad/sec and the number of zero crossings $\nu \simeq 8\, sec^{-1}$, in Fig.5.6b the cut

off frequency is 5000 rad/sec and $\nu \simeq 60\,sec^{-1}$. By increasing the cut off frequency $\nu$ increase without limit.

In Fig.5.5 something different happens for the FTK filter, that is the PSD of $\ddot{U}(t)$ goes to zero for $\omega \to \infty$. Moreover if $0 < \beta < 0.5$ also the area of the PSD reamains finite and then the mean number of zero crossings is finite. That is the FTK model may be enforced by a true white noise process, obtaining, for $\omega_c \to \infty$, a number of zero crossings $\nu \simeq 7.6\,sec^{-1}$. In Fig.5.7 two sample functions of $\ddot{U}(t)$ for the FTK with different values of $\omega_c$; in Fig.5.7 a the cut off frequency $\omega_C$ is 80 rad/sec and the number of zero crossings $\nu \simeq 5.7\,sec^{-1}$, in Fig.5.7b the cut off frequency is 5000 rad/sec and $\nu \simeq 7\,sec^{-1}$. This value remain stable also for higher values of the cut-off frequency and is $\nu \simeq 7.6\,sec^{-1}$ for $\omega_c \to \infty$. From the above considerations it follows that by using the FTK one may take profit of all tools of Itô$'s$ calculus that remains valid only if the input is a true white noise.

## 5.2 The fractional viscoelastic beams

In last years growing interest has been devoted to the use of polymers for structural applications; in particular, fiber reinforced composites with polymeric matrix are already widely used, as for example composite panel and pultruded elements. Fiber reinforced are more known as Fiber Reinforced Polymers (FRP). Many FRP are constituted by long fibers disposed along one or more direction; if for simplicity we refer to fibers along one direction only, it is reasonably expected that, since the fibers are often elastic, in the direction of the fibers the behavior is elastic while in the other direction the behavior is viscoelastic due to the viscoelasticity of the matrix. Viscoelastic effects occur also in the direction of the fibers because of the sliding of the fibers with respect to the matrix due to a non-perfect adhesion at fiber-matrix interface. For these reasons, when FRP elements are modeled as beams, it is necessary to include the viscoelastic constitutive laws in the beam model; with this strategy the elastic beam formulation can be modified to include fractional viscoelasticity. The fractional viscoelastic EB has been formulated and discussed in [33]; in the following the fractional viscoelastic Euler-Bernoulli is first reported for completeness and fractional viscoelastic Timoshenko beam is introduced; then a comparison between experimental result and the fractional viscoelastic Timoshenko beam is presented.

### 5.2.1 Fractional viscoelastic Euler-Bernoulli beam

In the classical elastic Euler-Bernoulli (EB) beam the main hypothesis is that the cross section of the beam remains perpendicular to the center of gravity line in the deformed configuration. This hypothesis, known as Bernoulli hypothesis, implies that there are not shear strain; this hypothesis is reasonable for slender beams in which the shear deformation in negligible respect to the flexural one. Slender beams are considered those with $L/H \geq 10$, where $L$ is the beam length and $H$ is the height of the cross section.
Consider an EB beam constituted of a viscoelastic material which corresponding model is the springpot model; the beam has the center of gravity line overlapping the $z$ axis, while the $x$ and $y$ axis are in the cross section plane. The equilibrium equations of the beam are given as:

$$\frac{\partial T_y(z,t)}{\partial z} = \rho A(z)\frac{\partial^2 v(z,t)}{\partial t^2} - q_y(z,t) \tag{5.14a}$$

$$\frac{\partial M_x(z,t)}{\partial z} = T_y(z,t) - m_x(z,t) + \rho I_x(z)\frac{\partial \varphi_x(z,t)}{\partial t^2} \tag{5.14b}$$

where $T_y$ is the shear in $y$ direction, $M_x(z,t)$is the bending moment around the $x$ axis, $v(z,t)$ is the displacement of the center of gravity of the cross section in the $y$ direction, $\varphi(z,t)$ is the rotation of the beam cross section around $x$ axis, $q_y(z,t)$ is the distributed load in the $y$ direction, $m_x(z,t)$ is the distributed

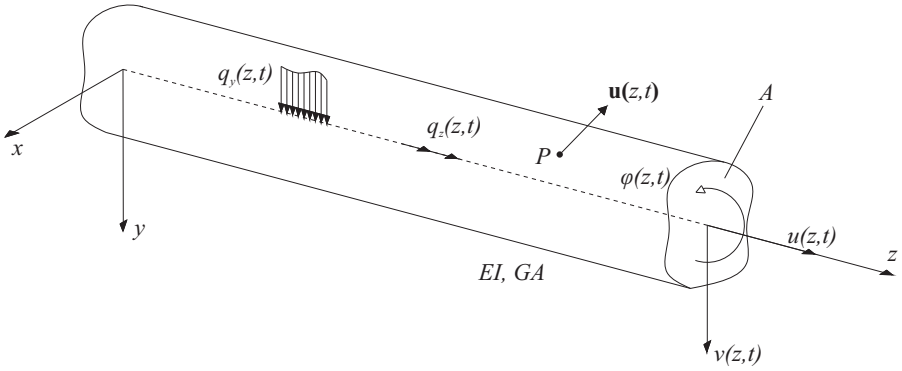


**Figure 5.8:** EB beam. Positive sign conventions are reported.

moment around $x$ axis, $I_x(z)$ is the second moment of the cross section about

$x$ axis and $\rho$ is the density of the beam. For the Bernoulli hypothesis:

$$\frac{\partial v(z,t)}{\partial z} = -\varphi(z,t) \tag{5.15}$$

With this assumption:

$$\varepsilon(y,z;t) = -y\frac{\partial^2 v(z,t)}{\partial z^2} \tag{5.16}$$

By considering the governing equation of the springpot (2.29) and considering that

$$\sigma(y,z;t) = \frac{M_x(z,t)}{I_x(z)}y \tag{5.17}$$

the following relationship is obtained:

$$M_x(z,t) = -C_\alpha I_x(z)\frac{\partial^2}{\partial z^2}(D^\alpha_{0^+}v(z,t)) \tag{5.18}$$

By differentiating (5.18) with respect to $z$ and taking into account Eq. (5.14b):

$$T_y(z,t) = -C_\alpha\frac{\partial}{\partial z}\left(I_x(z)\frac{\partial^2}{\partial z^2}(D^\alpha_{0^+}v(z,t))\right) \tag{5.19}$$

By substituting Eq. (5.19) in Eq. (5.14a) the fractional differential equation for the viscoelastic EB beam is obtained in this form:

$$\rho A(z)\frac{\partial^2 v(z,t)}{\partial t^2} + C_\alpha\frac{\partial^2}{\partial z^2}\left(I_x(z)\frac{\partial^2}{\partial z^2}(D^\alpha_{0^+}v(z,t))\right) = q_y(z,t) \tag{5.20}$$

Boundary condition can be superimposed by means of Eq. (5.18) and Eq. (5.19).
An analogous law can be obtained for viscoelastic EB beam which material is modeled as a fractional KV model with parameters $E$, $C_\alpha$ and $\alpha$; by making the same manipulations of above the following fractional differential equation is obtained:

$$\rho A(z)\frac{\partial^2 v(z,t)}{\partial t^2} + \frac{\partial^2}{\partial z^2}\left[I_x(z)\frac{\partial^2}{\partial z^2}\left(Ev(z,t) + C_\alpha(D^\alpha_{0^+}v(z,t))\right)\right] = q_y(z,t) \tag{5.21}$$

The solution to these equations can be fund by classical approach, as for example Galerkin approach or the Agrawal approach in the case that $I_x(z)$ is constant along $z$ (citare qualcosa).

### 5.2.2 Fractional viscoelastic Timoshenko beam

The fractional viscoelastic Timoshenko (TM) beam can be developed with the same approach used for the fractional viscoelastic EB beam. Differently from the EB beam the kinematics of the TM beam take into account of the shear strain for the evaluation of the deflection of the beam; this implies that the slope of the deflection has to be written as:

$$\frac{\partial v(z,t)}{\partial z} = \eta(z,t) - \varphi(z,t) \tag{5.22}$$

where $\eta(z,t)$ is the shear strain in the $y$ direction. The equilibrium equations (5.14) remain valid also in this case. In the viscoelastic Timoshenko beam two constitutive laws must be defined, one for the normal stress $\sigma(t)$ and one for the shear stress $\tau(t)$:

$$\sigma(t) = C_\alpha \left(D^\alpha_{0^+}\varepsilon\right)(t) \tag{5.23a}$$

$$\tau(t) = C_\beta \left(D^\beta_{0^+}\eta\right)(t) \tag{5.23b}$$

Note that $C_\alpha$ plays the role of $E$ (Young modulus) of the elastic case, while $C_\beta$ has the same role of $G$ (shear modulus), but $C_\alpha$ and $C_\beta$ are not related to each other as $E$ and $G$ are. This means that the mechanical model of the beam is transversally isotropic, because the constitutive law along $z$ is different from the constitutive law in the plane $xy$. Eq. (5.17) remains valid also in this case and moreover:

$$\tau(t) = \frac{T_y(z,t)}{\chi A} \tag{5.24}$$

where $\chi$ is the shear factor and $A$ is the area of the cross section. Eq. (5.16) is not valid for the TM beam then it is only possible to write:

$$\varepsilon(y,z;t) = y\frac{\partial \varphi(z,t)}{\partial z} \tag{5.25}$$

By using Eq. (5.17), Eq. (5.23a) and Eq. (5.25) the bending moment $M_x(z,t)$ is obtained as

$$M_x(z;t) = C_\alpha I_x(z)\frac{\partial}{\partial z}\left(D^\alpha_{0^+}\varphi\right)(z,t) \tag{5.26}$$

while using Eq. (5.23b) and Eq. (5.24) the shear $T_y(z,t)$ is

$$T_y(z;t) = \chi A(z) C_\beta \left[D^\alpha_{0^+}\left(\frac{\partial v(z,t)}{\partial z} + \varphi(z,t)\right)\right] \tag{5.27}$$

Spatial differentiation of both Eq. (5.26) and Eq. (5.27) and the use of equilibrium equations (5.14) leads to the coupled differential equation of the TM beam:

$$\rho I_x(z)\frac{\partial^2\varphi_x(z,t)}{\partial t^2} - C_\alpha I_x(z)\frac{\partial^2}{\partial z^2}\left(D^\alpha_{0^+}\varphi_x\right)(z,t) + \chi A C_\beta\left[D^\beta_{0^+}\left(\frac{\partial v(z,t)}{\partial z}+\varphi_x(z,t)\right)\right] = m_x(z,t) \quad (5.28a)$$

$$\chi A(z) C_\beta\frac{\partial}{\partial z}\left[D^\alpha_{0^+}\left(\frac{\partial v(z,t)}{\partial z}+\varphi(z,t)\right)\right] = -q_y(z,t)+\rho A(z)\frac{\partial^2 v(z,t)}{\partial z^2} \quad (5.28b)$$

If $I_x(z)$ and $A(z)$ are constant along $z$, by means of some manipulations Eqs. (5.28) can be reduced to a single equation:

$$C_\alpha I_x\frac{\partial^4\left(D^\alpha_{0^+}v\right)(z,t)}{\partial z^4}+\frac{\rho^2 I_x}{\chi C_\beta}\frac{\partial^4\left(I^\beta_{0^+}v\right)(z,t)}{\partial t^4}-\frac{C_\alpha I_x\rho}{\chi C_\beta}\frac{\partial^4\left(D^{\alpha-\beta}_{0^+}v(z,t)\right)}{\partial t^2\partial z^2}-$$
$$\rho I_x\frac{\partial^4 v(z,t)}{\partial t^2\partial z^2}+\rho A\frac{\partial^2 v(z,t)}{\partial t^2} = q_y(z,t)+\frac{\partial m_x(z,t)}{\partial z}+\frac{\rho I_x}{\chi A C_\beta}\frac{\partial\left(I^\beta_{0^+}q_y\right)(z,t)}{\partial t^2}+$$
$$\frac{C_\alpha I_x}{\chi A C_\beta}\frac{\partial^2\left(D^{\alpha-\beta}_{0^+}q_y\right)(z,t)}{\partial z^2} \quad (5.29)$$

Eq. (5.29) is the governing equation of a transversally isotropic fractional viscoelastic Timoshenko beam; by setting $\alpha = \beta = 0$ in Eqs. (5.28) and in Eq. (5.29) the classical elastic Timoshenko beam coupled equations or single equation are obtained. This model is more suitable to model fiber reinforce composites than the EB beam, because often FRP are well represented by transversally isotropic models due to the presence of a prevalent direction of the fiber orientation. Indeed, for long fiber composites, the viscoelasticity along the fiber direction can be captured by both the EB and TM beams, but the viscoelasticity in the cross section plane can not be represented by the EB beam that does not allow shear strain, but can be reproduced by the viscoelastic TM beam.
As longitudinal or transverse mechanical model for the beam, also other fractional viscoelastic mechanical models can be assumed, but they are not reported here for brevity.

### 5.2.3 Fitting of experimental results with fractional viscoelastic Timoshenko beam

The mechanical parameters of viscoelastic beams can be obtained by the best fitting on experimental test. To show that the models introduced above are good to reproduce the behavior of viscoelastic beams, a three point relaxation bending test has been performed on a specimen obtained from a pultruded beam. In the middle of the specimen a displacement is applied and corresponding force is monitored. The machine is a Zwick Roell Z005, with a load cell of 5 $kN$. In Fig. 5.9 the experimental setup is depicted. The beam has

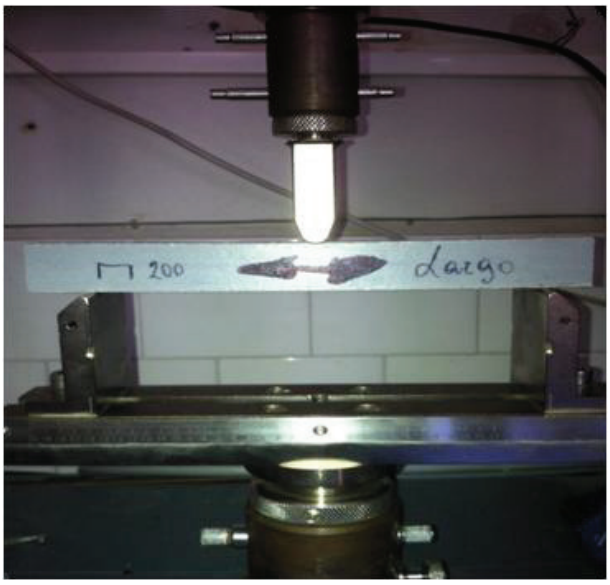


**Figure 5.9:** Experimental setup for the 3-points bending test on a pultruded bar.

length $L_0 = 200\ mm$, the distance between the supports is $L = 160\ mm$, the height is $h = 24,4mm$ and the width is $b = 9,7\ mm$; for the rectangular section the shear factor is $\chi = 5/6$. The mechanical scheme of the beam is of simply-supported beam of length $L$ with a concentrated force at $z = L/2$, but because of the symmetry, it has been considered half beam, as shown in Fig. 5.10.

Previous axial test on similar specimen resulted in the evidence that the longitudinal behavior of the beam, and then of the specimen, is elastic; this means that in Eq. (5.29) $\alpha = 0$. With this assumptions, neglecting inertia forces and

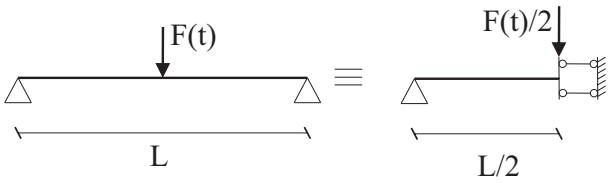


**Figure 5.10:** Mechanical scheme for the 3-points bending relaxation test.

considering that $q_y(z,t) = 0$ and $m_x(z,t) = 0$, Eq. (5.29) reduces to:

$$C_\alpha I_x \frac{\partial^4 v(z,t)}{\partial z^4} = 0 \tag{5.30}$$

With the equivalent scheme of Fig. 5.10 it is needed to integrate Eq. (5.30) only for half beam and then only four constant of integration have to be found; indeed if we perform integration with respect of $z$ of Eq. (5.30) the following equation is obtained

$$v(z,t) = c_1(t)\frac{z^3}{6} + c_2(t)\frac{z^2}{2} + c_3(t)z + c_4(t) \tag{5.31}$$

Note that the constant of integration are constant only in the $z$ variable but not in the $t$ variable; the following boundary conditions can be einforced:

$$\begin{aligned} v(0,t) &= 0 \\ M(0,t) &= 0 \\ \varphi(L/2,t) &= 0 \\ M(L/2,t) &= F(t)L/4 \end{aligned} \tag{5.32}$$

From Eq. (5.32) descends that:

$$\begin{aligned} c_1(t) &= -\frac{F(t)}{2C_\alpha I_x} \\ c_2(t) &= 0 \\ c_3(t) &= \frac{\left(I^\beta_{0^+} F\right)(t)}{2C_\beta \chi A} + \frac{FL^2}{2C_\alpha I_x} \\ c_4(t) &= 0 \end{aligned} \tag{5.33}$$

The governing equation for half beam is then:

$$v(z,t) = -\frac{F(t)}{2C_\alpha I_x}\frac{z^3}{6} + \left(\frac{\left(I^\beta_{0+}F\right)(t)}{2C_\beta \chi A} + \frac{FL^2}{2C_\alpha I_x}\right) z \tag{5.34}$$

that particularized in $z = L/2$ gives

$$v(L/2,t) = F(t)\frac{L^3}{48C_\alpha I_x} + \left(I^\beta_{0+}F\right)(t)\frac{L}{4C_\beta \chi A} = \bar{\delta} \tag{5.35}$$

where $\bar{\delta} = 0.5\ mm$ is the superimposed displacement in the relaxation test. Eq. (5.35) can be solved for $F(t)$ in Laplace domain; the solution in the time domain is:

$$F(t) = \frac{\bar{\delta}L^3}{48C_\alpha I_x} E_\beta\left(-\frac{12C_\alpha I_x}{L^2 C_\beta \chi A}t^\beta\right) \tag{5.36}$$

The fitting has been performed with Eq. (5.36) and gave the following results:

$$\beta = 0,19 \qquad C_\alpha = 13290\ MPa \qquad C_\beta = 29140\ MPa\, s^\beta \tag{5.37}$$

Fig. 5.11 shows the experimental curve and a comparison between the data and the theoretical curve (5.36) with the parameters of Eq. (5.37); from this figure it is possible to appreciate the fractional viscoelastic Timoshenko beam model is able to reproduce the experimental behavior both in short and long term behavior.

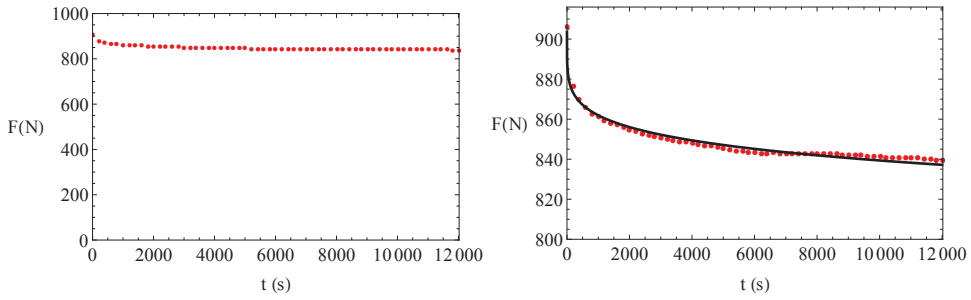


**Figure 5.11:** Experimental and theoretical results for a 3 points bending relaxation test: experimental data (a); comparison with fitting curve (b).

## 5.3 The fractional viscoelastic non-local Timoshenko beam

In last decades, increasing importance of micro- and nano-technologies has recently drawn a considerable attention to the need of mathematical models capable of capturing the effects of micro- structure and long-range intermolecular forces. For this purpose, a classical local continuum modeling has been proved soon inadequate owing to its inherent free-scale formulation, while molecular simulations, although may seem a most appropriate way to model microstructural effects, involve as a major drawback a considerable computational effort. For these reasons, and on account of the fact that even to build a molecular model some theoretical assumptions are still needed, researchers have preferred the formulation of "enriched" continua, i.e. continua where the effects of microstructure and long-range intermolecular forces are modeled, in an average sense, by introducing appropriate nonlocal terms. The preference accorded to the formulation of these "nonlocal continua" is motivated by the fact that conventional numerical solution methods can be applied, with considerable advantages for design and verification purposes.
Several well-established theories of nonlocal continua exist in the scientific literature: Eringen's integral theory [44, 45]; gradient elasticity theories [3, 18]; the peridynamic theory [84]; the micropolar "Cosserat" theory [22] and the couple-stress theory [72]. Great importance assume nonlocal beam theories because of the need for adequate and computationally-efficient modeling of microstructural effects in beam-like micro- and nano-devices ([2, 9, 65, 77]). Indeed, these effects, which have been revealed by experimental tests on materials such as graphite [87], copper [76], epoxy ([66]) and polypropylene ([70]), cannot be described by the intrinsically free-scale classical continuum approach while, on the other hand, could be captured only at the expense of computationally intensive and, in some cases, almost prohibitive atomistic/molecular simulations ([90]).
A further important application of non-local beam theories is at a macroscopic scale, whenever an intrinsic dependence exists between the response at a given point and the response at surrounding points of a beam. Such a dependence may arise as a result of external patches, long adhesive joints in composites, surface treatments using fluids, or fibers in fiber-reinforced composites. In these cases, instead of modeling all components of the system, as beam and external patch, or composite matrix and embedded fibers, a simpler yet accurate solution can be obtained from 1D equilibrium equations of the beam, where coupling between responses at non-adjacent points is accounted

for by appropriate non-local terms. Non-local beam theories are also suitable for modeling effects produced, at a given point, by the complex deformations of non-adjacent beam cross sections, as these effects cannot be captured by classical beam models where cross section remain planes ([16, 17, 67]).
In order to model damping effects in nano-beams, EB beam models with non-local viscoelastic behavior have been proposed in [68], with applications on single walled carbon nanotubes. The torsional behavior of functionally-graded nano-beams, including non-local viscoelasticity, has been studied in [13]. In the last few years, the authors have proposed non-local EB and TM beam models ([7, 31, 32, 48]), within a mechanically-based approach to non-locality, which treats non-local effects as long-range interactions resulting from relative motion of non-adjacent volume elements ([29, 30, 40, 46, 47]). In these non-local beam models, in particular, long-range interactions are volume forces/moments resulting from a differential motion of non-adjacent beam segments, measured by the pure deformation modes of the beam ([51, 52]), i.e. a "pure axial" symmetric mode, a "pure bending" symmetric mode and a "pure shear" asymmetric mode. The analytical form of the long-range volume forces/moments is built as linearly depending on the product of the volumes of the interacting beam segments, and the pure deformation modes, through pertinent attenuation functions governing the space decay of the non-local effects. In previous studies, elastic and viscous long-range interactions have been considered, either separately or simultaneously ([7, 31, 32, 48]).
In the following, the displacement-based non-local fractional viscoelastic TM beam is introduced; then the FEM formulation of this model is discussed; finally some ideal creep tests are performed in order to show the influence of the mechanical parameters on th response of the beam. The concepts and results of this section have already been published in [7, 8].

### 5.3.1 The displacement-based non-local fractional viscoelastic Timoshenko beam

The kinematics of the classical elastic TM beam is used, then Eq. (5.22) and Eq. (5.25) remain valid. The local stress resultant are expressed as usual as:

$$N^{(l)}(z,t) = EA\varepsilon_z(z,t) \tag{5.38a}$$

$$T_y^{(l)}(z,t) = \chi AG\gamma(z,t) \tag{5.38b}$$

$$M_x^{(l)}(z,t) = EI_x\frac{\partial\varphi_x(z,t)}{\partial z} \tag{5.38c}$$

**Non-local resultants**

Long-range interactions are modeled on a mechanical basis. The fundamental assumption is that two non-adjacent beam segments of volume $\Delta V(z_i)$ and $\Delta V(\xi_k)$ located, respectively, at $x = x_i$ and $x = \xi_k$ on the beam axis, mutually exert long-range volume forces/moments as a result of their relative motion measured in terms of the "pure axial", "pure bending" and "pure shear" deformation modes of a TM beam ([51, 52]). It is assumed that the long-range volume forces/moments are self-equilibrated interactions, which counteract the relative motion of the beam segments. The analytical form is built as linearly depending on the product of the volumes of the interacting beam segments, through appropriate attenuation functions governing the space decay of non-local effects. Purely elastic and fractional-order viscoelastic long-range volume forces/moments are considered, the latter modeled by the Caputo's fractional derivative. A mechanical description of the long-range interactions is shown in Figs. 5.12, 5.13, 5.14.
In the pure axial deformation mode, two non-adjacent beam segments of volume $\Delta V(z_i)$ and $\Delta V(\xi_k)$ exchange long-range volume axial forces as a result of the relative axial displacement:

$$\eta(z_i, \xi_k, t) = u(\xi_k, t) - u(z_i, t) \tag{5.39}$$

The specific volume axial forces exchanged by unit volumes $\Delta V(z_i) = 1$ and $\Delta V(\xi_k) = 1$, due to the pure axial deformation (9), are given by

$$q_z(z_i, \xi_k, t) = r_z(z_i, \xi_k, t) + d_z(z_i, \xi_k, t) \tag{5.40a}$$

$$r_z(z_i, \xi_k, t) = g_z(z_i, \xi_k)\eta(z_i, \xi_k, t)\Delta V(z_i)\Delta V(\xi_k) \tag{5.40b}$$

$$d_z(z_i, \xi_k, t) = \tilde{g}_z(z_i, \xi_k) D_{0^+}^{\alpha}[\eta(z_i, \xi_k, t)]\Delta V(z_i)\Delta V(\xi_k) \tag{5.40c}$$

In the pure bending mode, two non-adjacent beam segments of volume $\Delta V(x_i)$ and $\Delta V(\xi_k)$ exchange long-range volume moments as a result of the relative rotation:

$$\theta(z_i, \xi_k, t) = \varphi(\xi_k, t) - \varphi(z_i, t) \tag{5.41}$$

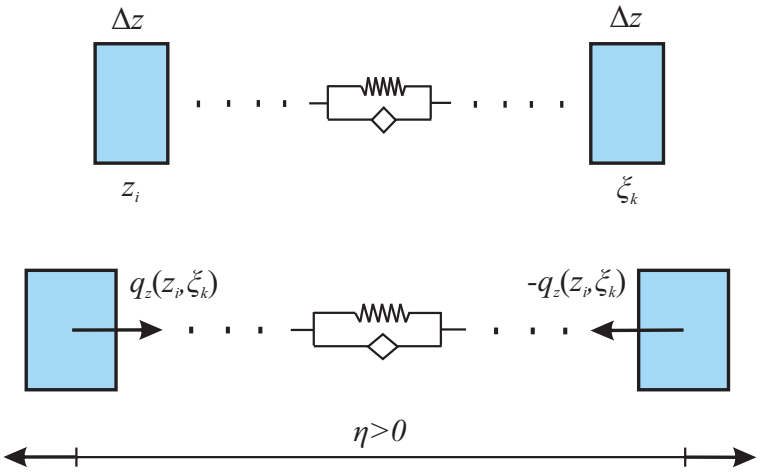


**Figure 5.12:** Pure axial long-range interactions.

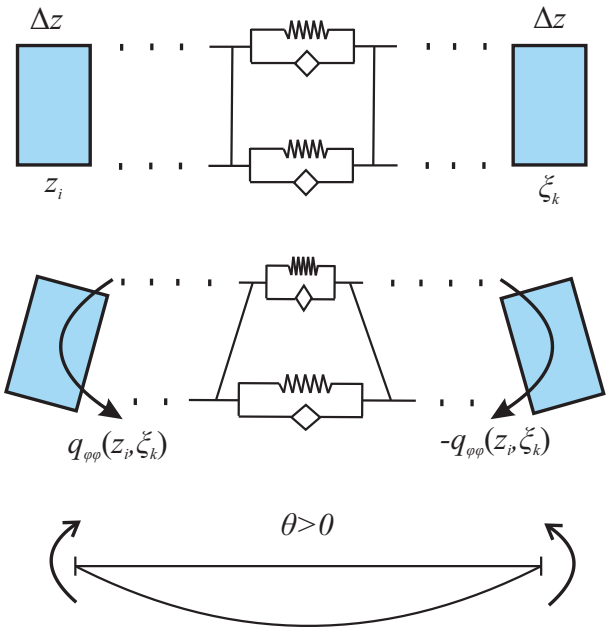


**Figure 5.13:** Pure bending long-range interactions.

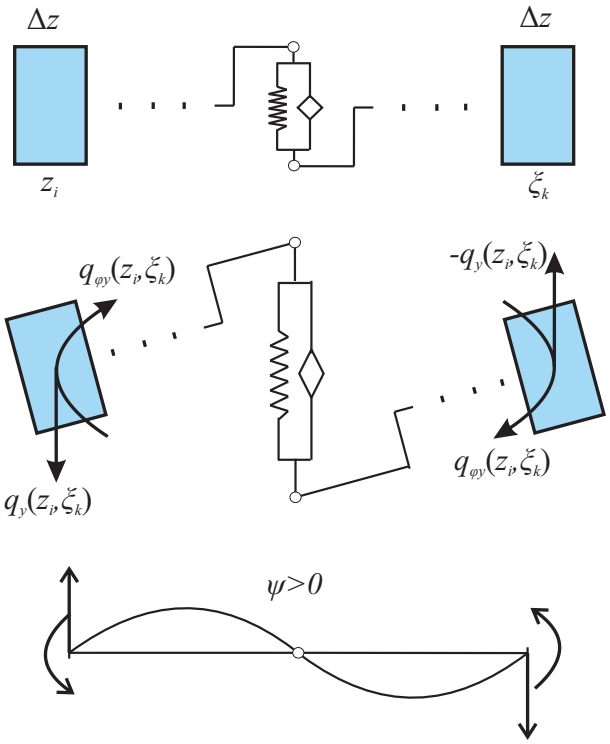


**Figure 5.14:** Pure shear long-range interactions.

The specific volume moments exchanged by $\Delta V(z_i) = 1$ and $\Delta V(\xi_k) = 1$ are given as

$$q_{\varphi\varphi}(z_i,\xi_k,t) = r_{\varphi\varphi}(z_i,\xi_k,t) + d_{\varphi\varphi}(z_i,\xi_k,t) \tag{5.42a}$$

$$r_{\varphi\varphi}(z_i,\xi_k,t) = g_{\varphi}(z_i,\xi_k)\theta(z_i,\xi_k,t)\Delta V(z_i)\Delta V(\xi_k) \tag{5.42b}$$

$$d_{\varphi\varphi}(z_i,\xi_k,t) = \tilde{g}_{\varphi}(z_i,\xi_k)D^{\alpha}_{0^+}[\theta(z_i,\xi_k,t)]\Delta V(z_i)\Delta V(\xi_k) \tag{5.42c}$$

In the pure shear mode, two non-adjacent beam segments of volume $\Delta V(z_i)$ and $\Delta V(\xi_k)$ exchange volume transverse forces and moments, as a result of their rotations with respect to the line given by the relative transverse displacement, that is

$$\psi(z_i,\xi_k,t) = \left[\frac{v(\xi_k,t) - v(z_i,t)}{\xi_k - z_i} + \varphi(\xi_k,t)\right] + \left[\frac{v(\xi_k,t) - v(z_i,t)}{\xi_k - x_i} + \varphi(z_i,t)\right] \tag{5.43}$$

The specific volume transverse forces exchanged by $\Delta V(z_i) = 1$ and $\Delta V(\xi_k) = 1$ are given by

$$q_y(z_i, \xi_k, t) = r_y(z_i, \xi_k, t) + d_y(z_i, \xi_k, t) \tag{5.44a}$$

$$r_y(z_i, \xi_k, t) = \frac{1}{|z_i - \xi_k|} g_y(z_i, \xi_k) \psi(z_i, \xi_k, t) \Delta V(z_i) \Delta V(\xi_k) \tag{5.44b}$$

$$d_y(z_i, \xi_k, t) = \frac{1}{|z_i - \xi_k|} \tilde{g}_y(z_i, \xi_k) D^{\alpha}_{0^+}[\psi(z_i, \xi_k, t)] \Delta V(z x_i) \Delta V(\xi_k) \tag{5.44c}$$

whereas the moments are

$$q_{\varphi y}(z_i, \xi_k, t) = r_{\varphi y}(z_i, \xi_k, t) + d_{\varphi y}(z_i, \xi_k, t) \tag{5.45a}$$

$$r_{\varphi y}(z_i, \xi_k, t) = g_y(z_i, \xi_k) \psi(z_i, \xi_k, t) \Delta V(z_i) \Delta V(\xi_k) \tag{5.45b}$$

$$d_{\varphi y}(z_i, \xi_k, t) = \tilde{g}_y(z_i, \xi_k) D^{\alpha}_{0^+}[\psi(z_i, \xi_k, t)] \Delta V(z_i) \Delta V(\xi_k) \tag{5.45c}$$

In Eqs. (5.40), (5.42), (5.44) and (5.45) $g_s(z, \xi)$ and $\tilde{g}_s(z, \xi)$ with $s = z,\ \varphi,\ y$ are attenuation functions governing the space decay of purely elastic and purely viscoelastic long-range interactions. They shall be positive definite and must be taken as symmetric with respect to arguments $x$ and $\xi$, to ensure that the long-range resultants exchanged by the interacting beam segments are mutual, according to Newton's third law. Further, notice that they are introduced as independent functions. That is, by $g_s(z, \xi) \neq \tilde{g}_s(z, \xi)$ for $s = z,\ \varphi,\ y$ a different spatial decay can be considered for purely elastic and purely viscoelastic long-range interactions, while $g_z(z, \xi) \neq g_\varphi(z, \xi) \neq g_y(z, \xi)$ and $\tilde{g}_z(z, \xi) \neq \tilde{g}_\varphi(z, \xi) \neq \tilde{g}_y(z, \xi)$ mean that spatial decay may vary depending on pure axial, pure bending and pure shear effects. This choice is made for the model to be as versatile as possible for experimental data fitting. A possible choice could be adopting the same mathematical model for the attenuation functions but with different parameters. Attenuation functions can be exponential, Gaussian or power law for both elastic and viscoelastic effects.

### Equilibrium equations

Dividing the beam in $N$ segments of length $\Delta z$ , the equations of motion of the beam segment of volume $\Delta V(z_i) = A\Delta z$ at $z = z_i$, for $i = 0, 1, ...N - 1$ ($z_0 = 0$, $z_N = L$), are written in the form (see Fig. 5.15):

$$N^{(l)}(z_i + \Delta z) - N^{(l)}(z_i) + R_z(z_i, t) + q_z(z_i, t)\Delta z - \rho(x_i) A \ddot{u}(z_i, t) \Delta z = 0 \tag{5.46a}$$

$$T^{(l)}(z_i+\Delta z)-T^{(l)}(z_i)+R_y(z_i,t)+q_y(z_i,t)\Delta z-\rho(x_i)A\ddot{v}(z_i,t)\Delta z=0 \quad (5.46b)$$

$$M^{(l)}(z_i+\Delta z)-M^{(l)}(z_i)+R_\varphi(z_i,t)\Delta z-\rho I_x\ddot{\varphi}(z_i,t)\Delta z=0 \quad (5.46c)$$

Eqs. (5.46) state that the equilibrium of the beam segment of volume $\Delta V(z_i)$, at $x=x_i$, is attained due to the local stress resultants (5.39) exerted by the adjacent beam segments, and the resultants $R_z$, $R_y$ and $R_\varphi$ of the volume forces/moments exerted by all the non-adjacent beam segments of volume $\Delta V(\xi_k)$ at $z=\xi_k$, $\xi_k\neq x_i$ , given as

$$R_z(z_i,t)=\sum_{k=0,k\neq i}^{N-1}q_z(z_i,\xi_k,t) \quad (5.47a)$$

$$R_y(z_i,t)=\sum_{k=0,k\neq i}^{N-1}q_y(z_i,\xi_k,t) \quad (5.47b)$$

$$R_\varphi(z_i,t)=\sum_{k=0,k\neq i}^{N-1}q_{\varphi\varphi}(z_i,\xi_k,t)+q_{\varphi z}(z_i,\xi_k,t) \quad (5.47c)$$

By using Eqs. (5.40), (5.42), (5.44) and (5.45), dividing Eqs. (5.46) by $\Delta z$ and taking the limit $\Delta z\to 0$ leads t the following equations:

$$EA\frac{\partial^2u(z,t)}{\partial z^2}+q_z(z,t)+A^2\int_0^L\left\{g_z(z,\xi)\eta(z,\xi,t)+\tilde{g}_z(z,\xi)D_{0^+}^{\alpha}\left[\eta(z,\xi,t)\right]\right\}dz=\rho A\ddot{u}(z,t) \quad (5.48a)$$

$$\chi GA\left[\frac{\partial^2u(z,t)}{\partial z^2}+\frac{\partial\varphi(z,t)}{\partial z}\right]+q_y(z,t)+\int_0^L\frac{2}{\xi-z}\left\{g_y(z,\xi)\psi(z,\xi,t)+\tilde{g}_y(z,\xi)D_{0^+}^{\alpha}\left[\psi(z,\xi,t)\right]\right\}dz=\rho A\ddot{v}(x,t) \quad (5.48b)$$

$$EI_x\frac{\partial^2\varphi(z,t)}{\partial z^2}+\chi GA\left[\frac{\partial u(z,t)}{\partial z}+\varphi(z,t)\right]+A^2\int_0^L\left\{g_\varphi(z,\xi)\theta(z,\xi,t)+\tilde{g}_\varphi(z,\xi)D_{0^+}^{\alpha}\left[\theta(z,\xi,t)\right]\right\}dz+A^2\int_0^L\left\{g_y(z,\xi)\psi(z,\xi,t)+\tilde{g}_y(z,\xi)D_{0^+}^{\alpha}\left[\psi(z,\xi,t)\right]\right\}dz=\rho I_x\ddot{\varphi}(z,t) \quad (5.48c)$$

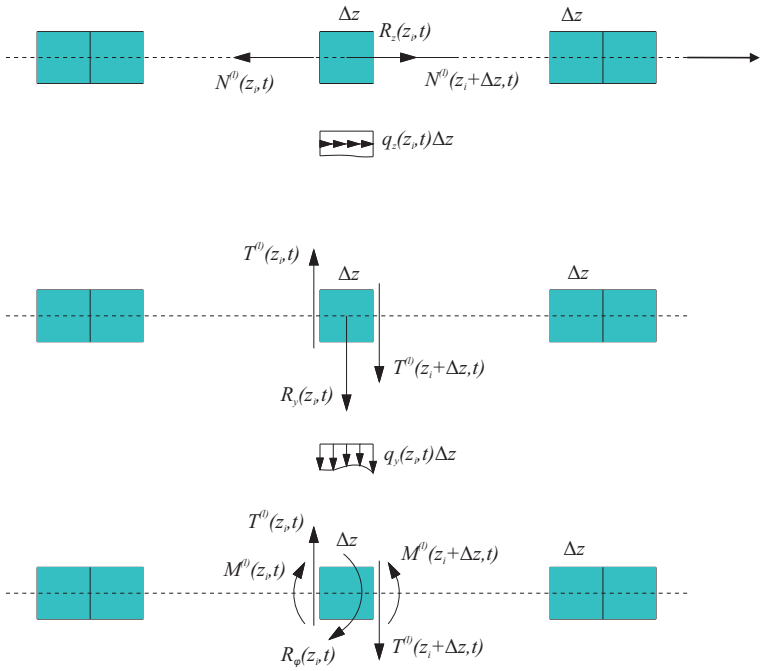


**Figure 5.15:** Axial, bending and shear equilibrium of a beam segment.

where the constitutive local laws Eqs. (5.39) have been introduced, and $\Delta V(z) = A\Delta z$, $\Delta V(\xi) = A\Delta xi$ for the volumes of the interacting beam segments. As for the boundary conditions (B.C.), it can readily be seen that the mechanical B.C. hold the classical form of local theory. This is true because, in the equilibrium equations at the beam ends, the long-range resultants Eq. (5.47) are infinitesimal of higher order with respect to the local stress resultants (e.g., see [29]). Also, time independent kinematic B.C. are considered. Therefore, the B.C. are given as:

$$EA\,\frac{\partial u(z,t)}{\partial z}\bigg|_{z=z_i} = \mp N_i(t) \quad or \quad u(z_i,t) = u_i \tag{5.49a}$$

$$\chi GA\left[\frac{\partial u(z,t)}{\partial z} + \varphi(z,t)\right]_{z=z_i} = \mp T_i(t) \quad or \quad v(z_i,t) = v_i \tag{5.49b}$$

$$EI_x\,\frac{\partial \varphi(z,t)}{\partial z}\bigg|_{z=z_i} = \mp M_i(t) \quad or \quad \varphi(z_i,t) = \varphi_i \tag{5.49c}$$

The equilibrium equations Eqs. (5.48) clearly show that the non-local beam model is a displacement-based model, with long-range volume forces/moments that arise from relative displacements/rotations between non-adjacent beam segments, as given by the pure deformation modes (5.39), (5.41), (5.43). On the contrary, if the long-range volume transverse forces/moments were taken as depending on the relative transverse displacement and not on the pure shear deformation (5.43), long-range volume transverse forces/moments would erroneously arise from a relative transverse displacement induced, for instance, by a rigid rotation of the beam. That is, the non-local beam model is invariant with respect to rigid body motion and axial, bending and shear non-local behaviors are mechanically consistent.
The integral terms on the l.h.s. of Eqs. (5.48) are the long-range resultants per unit length. Interestingly, the viscoelastic long-range axial force in Eq. (5.48a) and moment in Eq. (5.48b), specifically the part due to the pure bending deformation mode (5.41), correspond to those introduced by Russell [80] in his non-local damping model for a bar and a EB composite beam with longitudinal embedded fibers. Unlike the model proposed in [80], however, the proposed model includes long-range transverse forces/moments due to the asymmetric "pure shear" deformation mode between non-adjacent beam segments, and mechanical B.C. identical to those of classical local theory.
Finally, recognize that the non-local damping model is not proportional, as the fractional-order viscoelastic terms do not have the analytical form of the elastic ones, to which contribute both local and non-local terms.

### 5.3.2 The FE formulation of the displacement-based non-local Timoshenko beam

Following a standard approach of the FE method, consider a mesh with $n$ disjointed elements of the same length, along the beam axis. Points shared by contiguous elements are mesh nodes. Abscissas of the nodes of the $i^{th}$ element are denoted as $\hat{x}_i$ and $\hat{x}_{i+1}$, with $\hat{x}_1 = 0$ and $\hat{x}_{n+1} = L$ (symbol $''\hat{}''$ is introduced to avoid confusion with abscissas $x_i$ used in previous sections), and $l$ denotes the length of the $i^{th}$ element. The displacement field within the $i^{th}$ element is given the following form

$$\boldsymbol{u}_i(z,t) = \boldsymbol{N}_i(z)\boldsymbol{d}_i(t) \quad i = 1,2,\ldots,n \tag{5.50}$$

In Eq. (5.50), $\boldsymbol{u}_i(z,t) = [u(x,t)v(x,t)\varphi(x,t)]^T$ is the vector of displacements/rotation within the $i^{th}$ element, $\boldsymbol{d}_i(t)$ is the vector of the unknown nodal displacements

of the $i^{th}$ element,i.e.,

$$\boldsymbol{d}_i(t) = \left[u_{(i)1}(t)\ v_{(i)1}(t)\ \varphi_{(i)1}(t)\ u_{(i)2}(t)\ v_{(i)2}(t)\ \varphi_{(i)2}(t)\right] \tag{5.51}$$

where subscript $(i)$ indicates $i^{th}$ element, where subscript $1,2$ denote first and second node of the element. $\boldsymbol{N}_i(z)$ is the matrix collecting the shape functions taken, in this paper, as the standard $1^{st}$ order and $3^{rd}$ order polynomial shape functions of the two-node TM beam element, for the axial and flexural response respectively. That is, $\boldsymbol{N}_i(z)$ is given as

$$\boldsymbol{N}_i(z) = \begin{bmatrix} \frac{\hat{z}_{i+1}-z}{l} & 0 & 0 \\ 0 & \frac{(l-y_i)\left(l^2(1+12\Omega)+(l-2y_i)y_i\right)}{l^3(1+12\Omega)} & \frac{6(l-y_i)y_i}{l^3(1+12\Omega)} \\ 0 & -\frac{(l-y_i)(l+6l\Omega-y_i)y_i}{l^2(1+12\Omega)} & \frac{(l+12l\Omega-3y_i)(l-y_i)}{l^2(1+12\Omega)} \\ \frac{z-\hat{z}_{i+1}}{l} & 0 & 0 \\ 0 & \frac{y_i(12l^2\Omega+3ly_i-2y_i^2)}{l^3(1+12\Omega)} & \frac{6(y_i-l)y_i}{l^3(1+12\Omega)} \\ 0 & \frac{(l-y_i)(6l\Omega+y_i)y_i}{l^2(1+12\Omega)} & \frac{(2l(1-6\Omega)+3y_i)y_i}{l^2(1+12\Omega)} \end{bmatrix} \tag{5.52}$$

where $y_i = z - \hat{z}_i$ and $\Omega = EI_x/GAl^2$.
Letting $\boldsymbol{d} = [u_1 v_1 \varphi_1 \dots u_n v_n \varphi_n 1]^T$ the vector collecting all nodal displacements of the mesh, the nodal displacements of the $i^{th}$ element are written as

$$\boldsymbol{d}_i(t) = \boldsymbol{C}_i \boldsymbol{d}(t) \tag{5.53}$$

where $\boldsymbol{C}_i$ are the connectivity matrix. Next, following a standard Galerkin approach, the following equations can be derived:

$$\boldsymbol{M}\ddot{\boldsymbol{d}}(t) + \boldsymbol{C}^{(nl)}\left[D_{0^+}\boldsymbol{d}(t)\right] + \boldsymbol{K}\boldsymbol{d}(t) = \boldsymbol{F}(t) \tag{5.54}$$

In Eq. (5.54), $\boldsymbol{K}$ is the $3(n+1) \times 3(n+1)$ global stiffness matrix, given as

$$\boldsymbol{K} = \boldsymbol{K}^{(l)} + \boldsymbol{K}^{(nl)} = \sum_{i=1}^{n} \boldsymbol{K}_i^{(l)} + \sum_{i=1}^{n} \boldsymbol{K}_i^{(nl)} \tag{5.55}$$

where $\boldsymbol{K}_i^{(l)}$ is the local stiffness matrix

$$\boldsymbol{K}^{(l)} = \int_{\hat{x}_i}^{\hat{x}_{i+1}} \left[\boldsymbol{B}_i(z)\boldsymbol{C}_i\right]^T \boldsymbol{D}\boldsymbol{B}_i(z)\boldsymbol{C}_i dz \tag{5.56}$$

where $\boldsymbol{D} = \mathrm{D}iag\,[EA \;\; EI_x \;\; \chi GA]$ and $\boldsymbol{B}_i(z)$ is the derivative of the shape functions matrix, whikle $\boldsymbol{K}_i^{(nl)}$ are the local and non-local stiffness given as

$$\boldsymbol{K}_i^{(nl)} = \boldsymbol{K}_i^{(nl,\eta)} + \boldsymbol{K}_i^{(nl,\theta)} + \boldsymbol{K}_i^{(nl,\psi)} = \sum_{j=1}^{n} \boldsymbol{K}_{ij}^{(nl,\eta)} + \sum_{j=1}^{n} \boldsymbol{K}_{ij}^{(nl,\theta)} + \sum_{j=1}^{n} \boldsymbol{K}_{ij}^{(nl,\psi)} \quad (5.57)$$

In Eq. (5.57), matrices $\boldsymbol{K}_{ij}^{(nl,\eta)}$, $\boldsymbol{K}_{ij}^{(nl,\theta)}$ and $\boldsymbol{K}_{ij}^{(nl,\psi)}$ include the nonlocal stiffness contributions due to the long-range interactions between the differential volumes $dV(z) = Adz$ inside the $i^{th}$ element ($\hat{z}_i \leq z \leq \hat{z}_{i+1}$) and the differential volumes $dV(\xi) = Adz$ inside the $i^{th}$ element ($\hat{z}_i \leq \xi \leq \hat{z}_{i+1}$), namely

$$\boldsymbol{K}_{ij}^{(nl,\eta)} = \frac{A^2}{2} \int_{\hat{x}_i}^{\hat{x}_{i+1}} \int_{\hat{x}_j}^{\hat{x}_{j+1}} \left[\boldsymbol{N}_j^{(u)}(\xi)\boldsymbol{C}_j - \boldsymbol{N}_i^{(u)}(z)\boldsymbol{C}_i\right]^T g_z(z,\xi) \left[\boldsymbol{N}_j^{(u)}(\xi)\boldsymbol{C}_j - \boldsymbol{N}_i^{(u)}(z)\boldsymbol{C}_i\right] dzd\xi \quad (5.58a)$$

$$\boldsymbol{K}_{ij}^{(nl,\theta)} = \frac{A^2}{2} \int_{\hat{x}_i}^{\hat{x}_{i+1}} \int_{\hat{x}_j}^{\hat{x}_{j+1}} \left[\boldsymbol{N}_j^{(\varphi)}(\xi)\boldsymbol{C}_j - \boldsymbol{N}_i^{(\varphi)}(z)\boldsymbol{C}_i\right]^T g_\varphi(z,\xi) \left[\boldsymbol{N}_j^{(\varphi)}(\xi)\boldsymbol{C}_j - \boldsymbol{N}_i^{(\varphi)}(z)\boldsymbol{C}_i\right] dzd\xi \quad (5.58b)$$

$$\boldsymbol{K}_{ij}^{(nl,\psi)} = \frac{A^2}{2} \int_{\hat{x}_i}^{\hat{x}_{i+1}} \int_{\hat{x}_j}^{\hat{x}_{j+1}} \left[2\frac{\boldsymbol{N}_j^{(v)}(\xi)\boldsymbol{C}_j - \boldsymbol{N}_i^{(v)}(z)\boldsymbol{C}_i}{\xi - z} + \boldsymbol{N}_j^{(\varphi)}(\xi)\boldsymbol{C}_j + \boldsymbol{N}_i^{(\varphi)}(z)\boldsymbol{C}_i\right]^T g_y(z,\xi) \left[2\frac{\boldsymbol{N}_j^{(v)}(\xi)\boldsymbol{C}_j - \boldsymbol{N}_i^{(v)}(z)\boldsymbol{C}_i}{\xi - z} + \boldsymbol{N}_j^{(\varphi)}(\xi)\boldsymbol{C}_j + \boldsymbol{N}_i^{(\varphi)}(z)\boldsymbol{C}_i\right] dzd\xi \quad (5.58c)$$

where $\boldsymbol{N}_i^{(u)}$, $\boldsymbol{N}_i^{(v)}$ and $\boldsymbol{N}_i^{(\varphi)}$ are row vectors corresponding to the first, second and third column of the shape functions matrix (5.52). Furthermore in Eq. (5.54) $\boldsymbol{C}^{(nl)}$ is the $3(n+1) \times 3(n+1)$ global viscoelastic matrix. It is to recognize that $\boldsymbol{C}^{(nl)}$ has the same mathematical form as the nonlocal stiffness matrix $\boldsymbol{K}^{(nl)}$ where, however, $g_s(z,\xi)$ are replaced by $\tilde{g}_s(z,\xi)$ for $s = z, \varphi, v$. Further, in Eq. (5.54) matrix $\boldsymbol{M}$ is the $3(n+1) \times 3(n+1)$ global consistent mass matrix [79], while vector $\boldsymbol{F}(t)$ is the load vector given as:

$$\boldsymbol{F}(t) = \sum_{i=1}^{n} \boldsymbol{F}_i(t) \quad (5.59)$$

with

$$\boldsymbol{F}_i(t) = \int_{V_i} \left[\boldsymbol{N}_i(z)\boldsymbol{C}_i\right]^T \bar{\boldsymbol{F}}(z,t)dV_i(z) + \left[\boldsymbol{N}_i(0)\boldsymbol{C}_i\right]^T \bar{\boldsymbol{F}}_0(t) + \left[\boldsymbol{N}_i(L)\boldsymbol{C}_i\right]^T \bar{\boldsymbol{F}}_L(t) \tag{5.60}$$

being $\bar{\boldsymbol{F}}(z,t) = \begin{bmatrix} F_z(z,t) & F_y(z,t) & 0 \end{bmatrix}^T$, $\bar{\boldsymbol{F}}_i(t) = [N_i(t) \;\; T_i(t) \;\; M_i(t)]$, $i = 0, L$. Finally, two important remarks are in order. Unlike the local stiffness matrix $\boldsymbol{K}^{(l)}$, the non-local stiffness matrix $\boldsymbol{K}^{(nl)}$ and the viscoelastic matrix $\boldsymbol{C}^{(nl)}$ are fully-populated. Also, closed-form solutions for the elements of $\boldsymbol{K}^{(nl)}$ and $\boldsymbol{C}^{(nl)}$ can be obtained for attenuation functions $g_s(z,\xi)$ and $\tilde{g}_s(z,\xi)$ of common use in non-local theories, such as exponential or power-law functions. Details can be found in a previous study by the author [7] and are not reported here, for brevity.

### 5.3.3 The elastic static solution

In order to better understand the behavior of the model, it is useful first to focus only on the response of the elastic non-local TM beam. Here a simply-supported TM epoxy micro-beam with rectangular cross section is considered; the material properties are the following: Young's modulus $E = 1.4\ GPa$, Poisson's ratio $\nu = 0.35$. It is assumed that pure bending and shear behaviors are governed by the same attenuation functions $g_s(z,\xi) = g(z,\xi)$:

$$g(z,\xi) = \frac{C}{h^2} \exp\left(-|z-\xi|/\lambda\right) \tag{5.61}$$

where $\lambda$ is an internal length. The larger is the internal length $\lambda$, the wider is the so-called influence distance, i.e. the maximum distance beyond which the attenuation functions and therefore the nonlocal effects become negligible. The nonlocal parameters $C$ and $\lambda$ in Eq. (5.61) are set on a theoretical basis, in order to enhance nonlocal effects and assess how they affect the response. Specifically, $C = 10^{11}\ Nm^{-6}$ and different values of the internal length $\lambda$ are considered. The beam has the following geometry: length $L = 300\ \mu m$, width $b = 30\ \mu m$ and thickness $h = 30\ \mu m$; the beam is loaded by a uniformly distributed load $p = 1\ Nm^{-1}$. In Fig. 5.16 the non dimensional deflection of the beam for different values of the internal length $\lambda$ is shown; it can be seen that the nonlocal deflection is smaller than the local counterpart. This stiffening effect is not surprising and may be explained by considering that the nonlocal model is a displacement-based model, where the elastic long-range interactions counteract the relative motion between non-adjacent beam segments; as

such, they provide additional stiffness with respect to the stiffness of the classical local TM terms; the larger is $\lambda$, the smaller is the non local deflection: in fact a larger internal length $\lambda$ corresponds to a larger amount of mutually interacting non-adjacent beam segments, with a consequent stiffening of the solution. To have a further insight into the response of the nonlocal TM

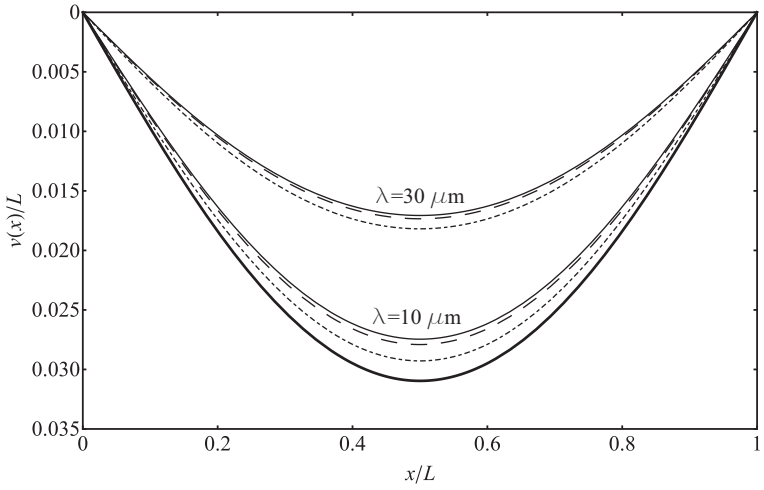


**Figure 5.16:** Static deflection of an epoxy micro beam for different values of $\lambda$ and different number of FEs: local response (thick continuous line), non local response with 10 FEs (dotted line), 20 FEs (dashed line), 30 FEs (thin continuous line).

beam model, Fig. 5.17 shows the nonlocal deflection to local deflection ratio, $v_{max}/v_{max}^{(l)}$, versus the thickness to length ratio, $h/L$, for fixed values of $L$ and $b$, i.e. $L = 300\ \mu m$, $b = 30\ \mu m$, different values of thickness $h$ and internal length $\lambda$ (30 $\mu m$ and 10 $\mu m$). For a given value of $\lambda$, the smaller $h$, the smaller the ratio $v_{max}/v_{max}^{(l)}$ is, i.e. the nonlocal effects become more significant and, consequently, the deviation from the corresponding classical local TM beam response. Again, such a behavior can be explained in recognition of the fact that the nonlocal TM beam model is displacement based: for $L = cost$ and $b = cost$ the deformability of the beam increases as $h$ decreases, with a consequent increasing relative motion between the beam segments that produces an increasing "weight" of the nonlocal terms with respect to that of the local ones. Fig. 5.18 instead shows the nonlocal deflection to local deflection ratio, $v_{max}/v_{max}^{(l)}$, versus the beam thickness, $h$, for fixed values of the ratio $L/h = 10$,

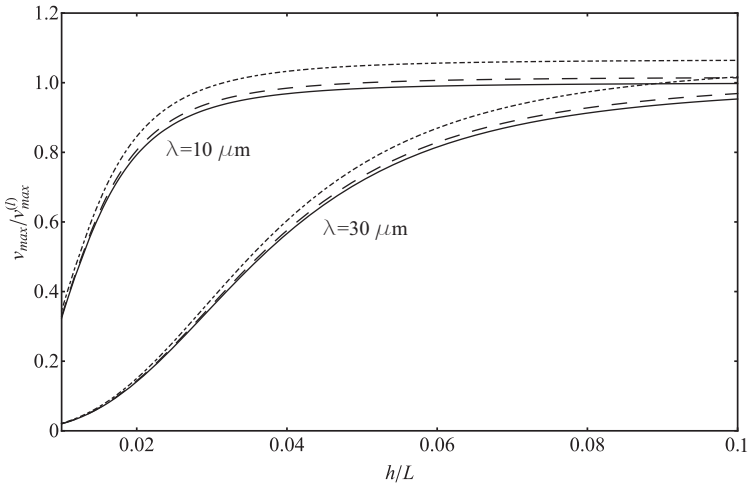


**Figure 5.17:** Nonlocal to local maximum deflection ratio of a simply-supported beam for $L = cost$, $b = cost$, variable $h$ and different $\lambda$ and number of FEs:10 FEs (dotted line), 20 FEs (dashed line), 30 FEs (thin continuous line).

$b = 30\ \mu m$, and different values of the internal length $\lambda$ (30 $\mu m$ and 10 $\mu m$). It can be seen that the smaller is $h$ (i.e. the smaller is also $L$, being $L/h = cost$), the smaller is the nonlocal deflection, i.e. the nonlocal effects are more significant. Such a behavior, for a given value of the internal length $\lambda$, can be expected in consideration of the fact that $L$ decreases with $h$ ($L/h = cost$): as the beam becomes shorter while the internal length $\lambda$ is fixed, each beam segment interacts with a relatively increasing number of beam segments (i.e., relatively to the total number of interacting beam segments) and, as a consequence, the "weight" of the nonlocal terms does increase with respect to that of the local ones. Fore more details see [7].

### 5.3.4 The viscoelastic response

The viscoelastic behavior of the non-local fractional viscoelastic TM beam proposed above is investigated through the simulation of a creep test. In this case the solution can be obtained in a closed form as shown in the following. If inertial terms are neglected in Eq. (5.54), it can be recast as follows:

$$\mathbf{\Lambda}\left(D^{\alpha}_{0^+}\boldsymbol{z}\right)(t) + \mathbf{\Omega}\boldsymbol{z}(t) = \mathbf{\Phi}^T\boldsymbol{F}(t) \tag{5.62}$$

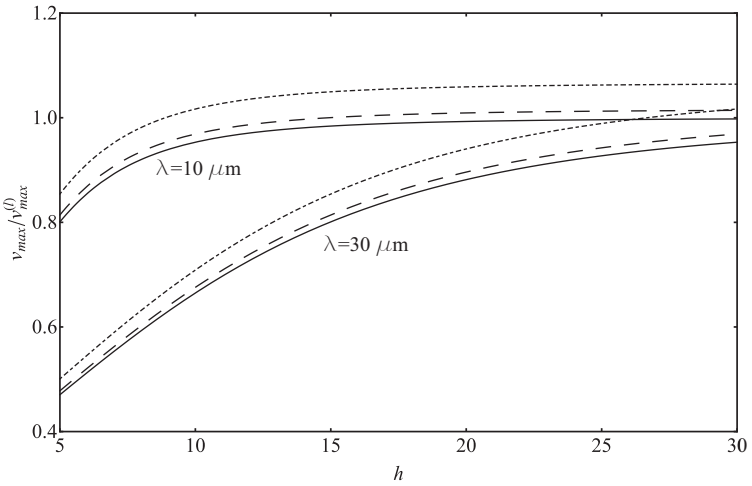


**Figure 5.18:** Nonlocal to local maximum deflection ratio of a simply-supported beam for $L/h = cost$, $b = cost$, variable $h$ and different $\lambda$ and number of FEs:10 FEs (dotted line), 20 FEs (dashed line), 30 FEs (thin continuous line).

where $\boldsymbol{z}(t) = \boldsymbol{\Phi}^{-1}\boldsymbol{d}(t)$, while $\boldsymbol{\Lambda}(t) = \boldsymbol{\Phi}^T\boldsymbol{C}^{(nl)}\boldsymbol{\Phi}$ and $\boldsymbol{\Omega}(t) = \boldsymbol{\Phi}^T\boldsymbol{K}\boldsymbol{\Phi}$ are diagonal matrices and $\boldsymbol{\Phi}$ is the eigenvectors matrix of $\boldsymbol{A} = \boldsymbol{K}^{-1}\boldsymbol{C}^{(nl)}$. For instance, if the load vector $\boldsymbol{F}(t)$ is given the analytical form $\boldsymbol{F}(t) = \boldsymbol{F}t/t_0 + \boldsymbol{F}U(t - t_0)(1 - t/t_0)$, exact closed-form solutions for components can be obtained for load cases of particular interest in viscoelasticity. For a typical creep test under a constant load distributed over the beam, $\boldsymbol{F}(t) = \boldsymbol{F}U(t)$, it yields

$$\lambda_j \left(D_{0^+}^{\alpha} z_j\right)(t) + \omega_j z_j(t) = f_j \frac{t}{t_0} + f_j U(t - t_0)\left(1 - \frac{t}{t_0}\right) \tag{5.63}$$

where $f_j = \boldsymbol{\Phi}_j^T\boldsymbol{F}$, $\lambda_j$ and $\omega_j$ are the $j$-th elements of matrices $\lambda_j$ and $\omega_j$, while $z_j(t)$ is given by a Mittag-Leffler function as follows

$$z_j(t) = \frac{f_j t}{t_0\omega_j}\left[1 - E_{\alpha,2}\left(-\frac{\omega_j}{\lambda_j}t^{\alpha}\right)\right] - \frac{f_j(t - t_0)U(t - t_0)}{t_0\omega_j}\left[1 - E_{\alpha,2}\left(-\frac{\omega_j}{\lambda_j}(t - t_0)^{\alpha}\right)\right] \tag{5.64}$$

As in the previous section, an epoxy micro-beam with length $L = 300\ \mu m$, width $b = 30\ \mu m$, thickness $h = 15\ \mu m$, Young's modulus $E = 1.4\ GPa$ and

Poisson's ratio $\nu = 0.35$ is considered. As for the long-range interactions, it is assumed that pure bending and shear behaviors are governed by the same attenuation functions, i.e. $g_s(z,\xi) = g(z,\xi)$, $\tilde{g}_s(z,\xi) = \tilde{g}(z,\xi)$ with the following exponential forms:

$$g(z,\xi) = \frac{C}{h^2}\exp\left(-|z-\xi|/\lambda\right) \tag{5.65a}$$

$$\tilde{g}(z,\xi) = \frac{C_\alpha}{h^2}\exp\left(-|z-\xi|/\lambda_\alpha\right) \tag{5.65b}$$

With these attenuation functions terms in the non-local stiffness matrix and viscoelastic matrix can be built in a closed form (Alotta et al. 2014). A uniformly distributed load

$$p(t) = p_0\frac{t}{t_0} + p_0 U(t-t_0)\left(1-\frac{t}{t_0}\right); \quad p_0 = 1\ Nm^{-1}, \quad t_0 = 10\ s \tag{5.66}$$

is applied. In Figs. 5.19, 5.20 and 5.21 the midspan deflection to the local elastic midspan deflection as the time elapses is plotted for different values of $\alpha$, for different values of $C\alpha$ and for different values of $\lambda_\alpha$. In Fig. 5.19 the midspan deflection tends to the purely elastic non-local counterpart as time elapses, and more rapidly as the fractional order $\alpha$ increases; in Figs. 5.20 and 5.21 it is clear that viscoelastic effects do increase with increasing $C_\alpha$ and $\lambda_\alpha$.

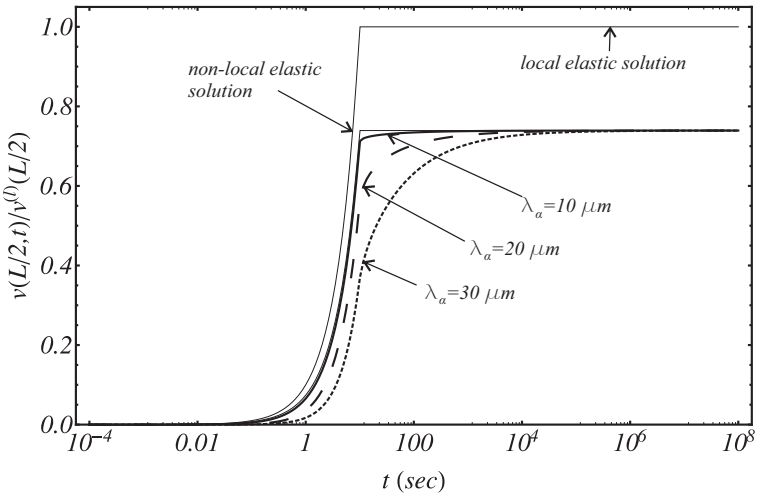


**Figure 5.20:** Simply-supported beam midspan deflection under the uniformly distributed load given in Eq. (5.66), for $\alpha = 0.5$, $\lambda_\alpha = 30\ \mu\, m$ and different values of $C_\alpha$.

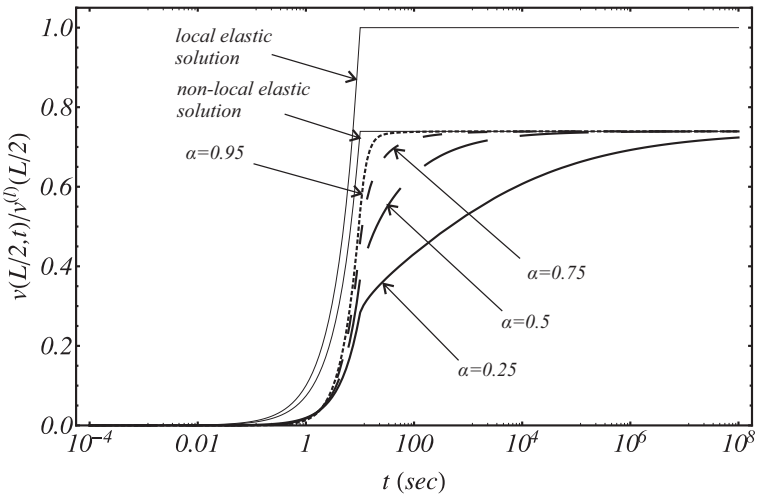


**Figure 5.19:** Simply-supported beam midspan deflection under the uniformly distributed load given in Eq. (5.66), for different fractional orders $\alpha$.

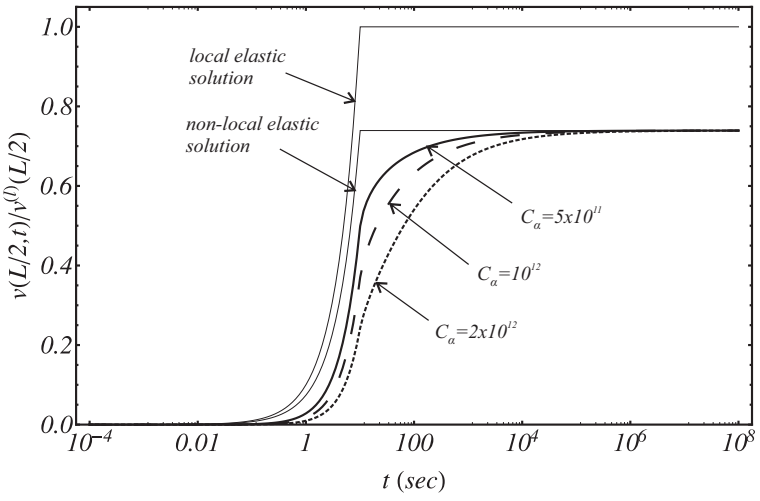


**Figure 5.21:** Simply-supported beam midspan deflection under the uniformly distributed load given in Eq. (5.66), for $\alpha = 0.5$, $C_\alpha = 10^{12}\ Nm^{-1}$ and different values of $\lambda_\alpha$.

## 5.4 A study on a polyethylene knee replacement

In the last decades large diffusion have had human joint replacements; the most diffused are knee, hip and shoulder replacements, see Fig. 5.22. Usually they are constituted by two parts that are coupled together to reproduce the original mode of operation of the joint.

**(a)** **(b)**

**(c)**

**Figure 5.22:** Examples of joint replacement devices: total knee replacement (a), partial (or one-sided) knee replacement (b) and hip replacement (c).

The parts are fixed to the bones at hands and the coupling has to be re-

alized in such a way that the relative motion between the two parts is guaranteed; indeed, the original coupling "devices", made of cartilage, are able to guarantee the separation between the two bones, guarantee the motion thanks to very low friction coefficients and moreover they absorb shocks due to impact or sudden motions (think for example to the knee or the hip that are always very stressed). The most used material used in place of cartilages is the *Ultra-High Molecular Weight PolyEthylene* (UHMWPE); the part constituted of polyethylene is usually called bearing. This polymer (the plastic parts in Fig.5.22) is characterized by:

- very high molecular weight due to the very long chain;
- resistance to UV radiation, to micro-organism and no water absorption;
- it is isotropic, it has high tensile strength, low friction coefficient together with high wear resistance;
- power law viscoelasticity.

The other parts of the replacements are usually made of a titanium alloy; it is clear that, since the titanium alloy have very high mechanical properties, the weak part of these replacements is the bearing. Typical problems are the wear due to the motion of the joint and the fracture that is believed is due to fatigue. The life of these replacements are then limited and when they are out of order they need to be substituted. Of course, the substitution of the replacement needs a surgery with very high costs for the health insurances or for the national health systems and also with consequences for the person to which the replacement is applied. At this point it is clear that a longer life of these joint replacements is desirable for both economic and human aspects.
For the reasons explained above a considerable effort is devoted by research centers and manufacturers to improve the life of the UHMWPE components of the substitution; to obtain such an improvement the right prevision of the fatigue and wear life of the polyethylene component needs a correct definition of the level of stress and strain and to do so it is not possible to disregard the real mechanical behavior of the material that exhibits power law viscoelasticity especially if it is considered that they are in order for years; however often researchers do not consider viscoelasticity and model the UHMWPE as elasto-plastic or as hyperelastic (see [78]).

(a) (b)

**Figure 5.23:** Oxford partial knee replacement (a), side view (b) and application (c).

Experimental results revealed that viscoelastic behavior of UHMWPE is well fitted by power law type functions, as shown in [56, 57] and in the following section. To show how power law viscoelasticity affects the behavior of these polyethylene components a knee substitution has been considered; in particular it has been studied an innovative one-sided (that is substitution of half joint) knee replacement designed in Oxford, depicted in Fig. 5.23. The reason to design a one-sided prosthesis is that often only one side of the meniscus is damaged; then, since the application of complete knee replacement implies the elimination of the cruciate ligament that it is not desirable, the use of a one-sided devices permit instead to maintain it with considerable advantages for the functionality of the knee.
Firstly, the viscoelastic properties of the UHMWPE have been investigated by means of creep-recovery tests; then a FEM model has been run in order to compare results between analysis using an elasto-plastic model and analysis using a fractional viscoelastic model which parameters have been calibrated by experimental tests.

### 5.4.1 Viscoelastic characterization of UHMWPE

The characterization of the viscoelastic behavior of the UHMWPE has been performed by means of creep-recovery test in tension on simple shaped specimens. The tests have been performed in the Material teaching lab of the En-

gineering Science Department of the University of Oxford; the machine is an Instron model 5582. Since Digital Image Correlation (DIC) has been used in

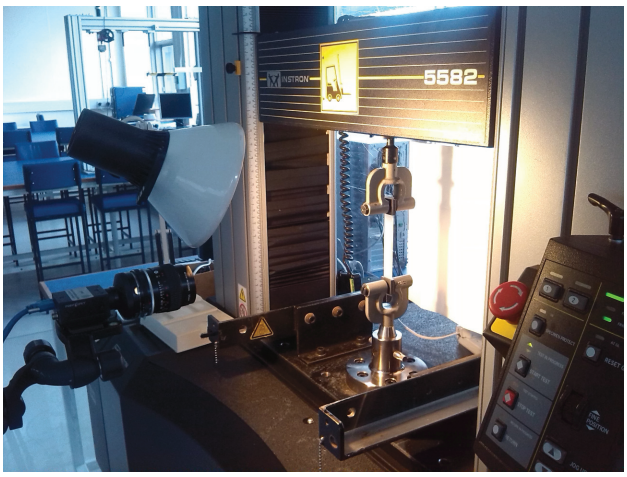


**Figure 5.24:** Experimental setup for the viscoelastic characterization of UHMWPE for knee replacement.

order to measure the strain, there was no reason to give a particular shape to the specimens, as for example dog-bones; indeed with DIC it is possible to measure the strain in a region of the specimen where the stress it is for sure uniform; the extension of this region can be estimated by FE simulation. For this reason specimens are rectangle shaped with dimensions $180 \times 20 \times 1$ $mm$. The experimental setup is depicted in Fig. 5.24. The DIC technique was originally chosen in order to measure both the longitudinal and transverse strain; indeed, if a material is isotropic only two creep functions are needed to completely characterize the 3D viscoelastic behavior and with two measures of strain in the creep test it is theoretically possible to obtain the parameters of both function. However, the transverse strain measurement were difficulty interpretable, then the complete 3D characterization has been postponed in the future. The creep-recovery tests have been performed for a duration of $6 + 6$ $h$; the final value of the stress was reached with a linear ramp of 4 minutes; after 6 hours, the load has been reduced to zero by a linear ramp of 4 minutes. The applied stress was $\sigma = 3\,MPa$, then a load cell of 100 $N$ was sufficient for the dimensions of the specimens at hand; on the other hand, in the paper [71] it has been shown that to a level of stress of 10 $MPa$ the UHMWPE is linear, then results can be considered valid for a large range of stress. Fol-

lowing the work in [56, 57] the fractional Maxwell model has been selected as model for the UHMWPE. The applied history of stress is depicted in Fig. 5.25(a); in Fig. 5.25(b), instead, the measured longitudinal strain and the fitting curve are depicted.

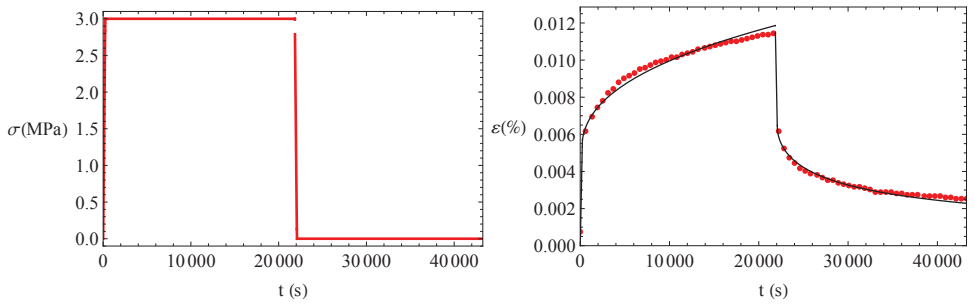


**Figure 5.25:** Creep recovery test of UHMWPE: applied stress history (a); fitting of obtained strain history (b), (red dots are experimental data, black line is the theoretical curve).

The best fitting of creep tests has given the following mechanical parameter values:

$$\bar{\alpha} = 0.4; \quad C_{\bar{\alpha}} = 24553\, MPas^{\bar{\alpha}} \quad E = 561\, MPa \tag{5.67}$$

It is to be specified that these are the parameters relative to a 1D fractional Maxwell model.

### 5.4.2 FEM simulation

In order to show how fractional viscoelasticity affects the behavior of the UHMWPE bearing, a FEM model has been analyzed in Abaqus 6.14 by considering once the UHMWPE as elasto-plastic with isotropic hardening and once by considering it as fractional viscoelastic, with the mechanical model selected as the fractional Maxwell. It is well known that a plastic model is not adequate for polymers, but many researchers in the field have used this constitutive law to model the UHMWPE in the past (e.g., see[55]). The FEM model of the knee replacement is depicted in Fig. 5.26(a). The analysis simulates the loading phase of the bearing due to the normal functionality of the leg; the load is ramped up linearly to the final load $F = 1200\ N$ in $0.2\ s$. This value of load has been obtained by experimental measurement [42, 43] and

of course it includes also the inertial forces due to accelerations of the other parts of the human body. Usually this kind of analysis is compared with

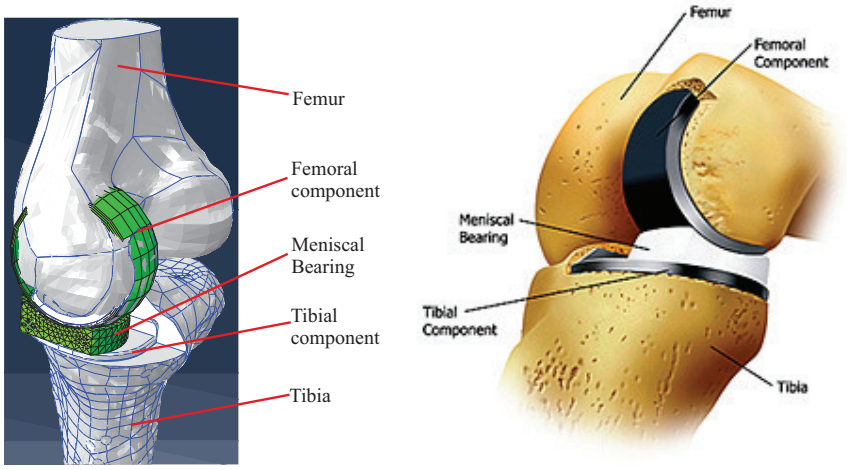


(a) (b)

**Figure 5.26:** Oxford partial knee replacement: FE model (a) and illustrative chart (b).

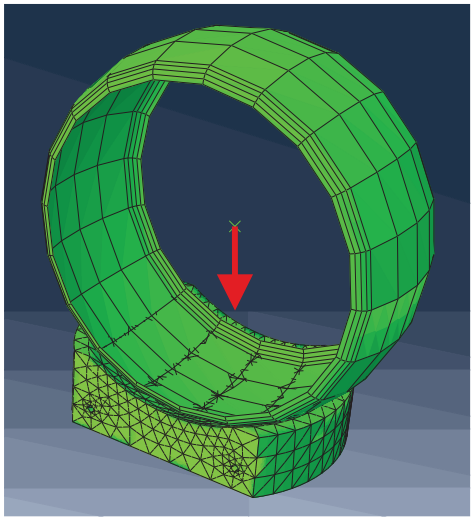

**Figure 5.27:** Parts considered in the FE analysis; in red the force applied to the femoral component.

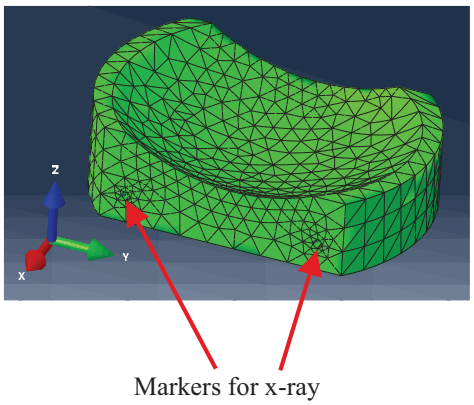


**Figure 5.28:** Mesh of the meniscal bearing.

experimental test on the component, see for example [78], in order to validate mechanical modeling by comparing stresses and area of contact at the interface bearing-femoral component; indeed, in the initial (unloaded) configuration the area of contact is small and limited to the central part of the bearing, but when the femoral component is pressed against the bearing, the area of contact increases. In the FE model of Fig. 5.26(a) only two components are really taken into account for the analysis: the meniscal bearing and the femoral components (see Fig. 5.27). The first is modeled with 5312 C3D10M finite elements, that are tetrahedral elements with four nodes and four Gauss points; the second is modeled as rigid body. The lower base of the bearing has been constrained in the $z$ direction. As it is possible to see in Fig. 5.28, there are two refined zone of the mesh in the side of the bearing; these correspond to two metal marker inserted to be seen in x-ray exams, because UHMWPE is transparent to x-ray; the markers are cylinder shaped and are long as the bearing width. The force is applied in the center of the femoral component along the $z$ direction as depicted in Fig. 5.27.

### Analysis with elasto-plastic model

The mechanical parameters of the elasto-plastic model have been taken from the papers [55, 78]; the elastic parameters are the following:

$$E = 575\ MPa \quad \nu = 0.46 \tag{5.68}$$

while to model plasticity an isotropic hardening model has been considered, with an initial yield stress of 15 $MPa$ and hardening parameters from the pa-

pers [55]. The contact between the two surfaces has been modeled as a simple contact master-slave, in which the master surface is the one of the femoral component; the friction coefficient has been assumed $\mu = 0.08$. The analysis has been run with explicit integration and with an imposed time increment $\Delta t = 4 \times 10^{-6}$.

**Analysis with fractional viscoelastic model**

The mechanical parameters have been derived from the experimental results and are those of Eq. (5.67); note that the Young modulus is almost identical to that one of the elasto-plastic model. Since a complete 3D viscoelastic characterization is missing, the parameters $K$ and $G$ (parameters of the elastic part of the 3D Maxwell model) and the parameters $G_\alpha$ and $K_\beta$ (parameters of the springpot in the 3D Maxwell model) are derived by considering $\alpha = \beta = \bar{\alpha}$ and a constant Poisson's ratio $\nu = 0.46$; the parameters are then the following:

$$\begin{gathered} K = 2338\ MPa \quad G = 192\ MPa \\ K_\beta = 102304\ MPa\, s^\beta \quad G_\alpha = 8408\ MPa\, s^\alpha \quad \alpha = \beta = 0.4 \end{gathered} \tag{5.69}$$

The definition of the contact is the same as the elasto-plastic model. The analysis has been run with explicit integration and with an imposed time increment $\Delta t = 4 \times 10^{-6}$.

**Comparison of results**

Results of the two analysis are here compared in terms of:

- contact pressure at the interface bearing-femoral component, shown in Fig. 5.29;
- stress along the $z$ axis in the lower face of the bearing, shown in Fig. 5.30.

In the map of Fig. 5.29(a) related to the analysis with elasto-plastic model the maximum contact pressure is about 7 $MPa$; in the map of Fig. 5.29(b) related to analysis with fractional Maxwell model the maximum contact pressure is about 25 $MPa$. The difference between the maximum pressure values it is easily explained by the contact areas that can be noted in Fig. 5.29.
In the maps of Fig. 5.30 the values of maximum stress along $z$ axis are very similar to those of Fig. 5.29; the area of the surface that effectively reacts is

smaller in the analysis with fractional viscoelastic model than in the analysis with elasto-plastic model.
First of all, it should be noted the bearing has not experienced plastic deformation, since the stress is under the yielding stress; this means that the bearing has simply behaved as elastic. Then in order to explain this different values

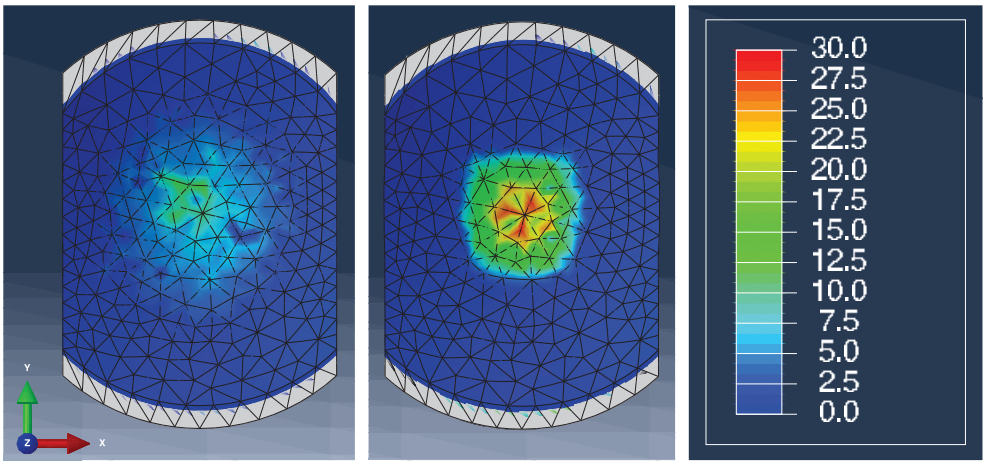


**(a)** **(b)** **(c)**

**Figure 5.29:** Contact pressure at the interface bearing-femoral component for different constitutive model of the bearing: elasto-plastic model (a); fractional Maxwell model (b); legend in *MPa* (c).

of stress, it should be considered that in a viscoelastic material when a force is applied the consequent deformation appears with a certain delay. Then, in the case that fractional viscoelastic model is considered the surface changes configuration with a certain delay in comparison with the case when an elastic model is considered. For this reason the surface contact area remains small in the first instants.
At this point many unexpected and premature break of the bearing can be explained by considering that elasto-plastic models underestimate the stress when the load is applied suddenly; of course higher stresses reduce the fatigue life and for this reason many of this component are substituted before the predicted life. On the other hand the improvement of the fatigue life of such a kind of component can be performed correctly if the right field f stresses and strains are predicted. Of course this analysis alone it is not exhaustive for the study of the behavior of a component such as the bearing,

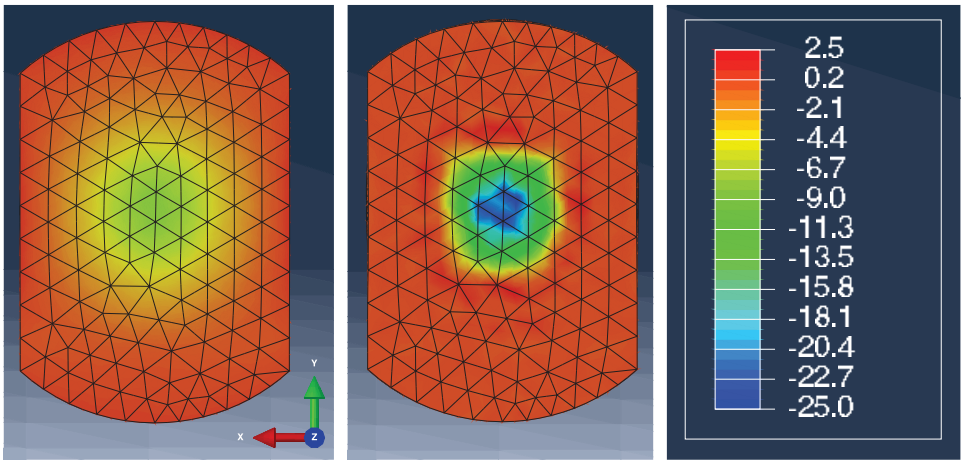


(a) (b) (c)

**Figure 5.30:** Stress along $z$ axis on the lower face of the bearing for different constitutive model of the bearing: elasto-plastic model (a); fractional Maxwell model (b); legend in $MPa$ (c).

but with this example it has been shown that fractional viscoelasticity can capture complex behaviors of materials that other models neglect; sometimes this behaviors can help to understand some unexpected phenomena in the mechanics of the materials.

## 5.5 Conclusions

In this chapter some applications of fractional viscoelasticity have been introduced; these applications clearly demonstrate the fractional viscoelasticity is a really useful tool to describe mechanical behavior of real materials. In particular fitting of experimental test have been successfully performed for a soil, for a simple polymer and for pultruded bar with epoxy resin matrix.
Another important fact is that classical mathematical theories of the single degree of freedom oscillator, Euler-Bernoulli and Timoshenko beams and also of non-local beam theories can be easily modified to include fractional viscoelasticity; resulting governing equation can be manipulated, also when multi-degree of freedom systems with discrete parameters are considered [10, 35].
Moreover, it has been shown from the fractional Tajimi-Kanai filter that in

stochastic dynamics applications fractional viscoelasticity does not lead to mathematically inconsistent results as classical viscoelastic modeling does. Finally it has been demonstrated that 3D fractional viscoelasticity can be successfully applied in a finite element analysis and that the design of engineering component can be helped by the modeling with fractional viscoelasticity.

# Concluding remarks

In this thesis a useful tool for the analysis viscoelastic material have been developed. First the fractional calculus and linear viscoelasticity have been introduced; then, in the frame of linear viscoelasticity, fractional viscoelasticity has been derived introducing power law type creep and relaxation functions in the Boltzmann superposition principle. The mechanical element corresponding to the fractional constitutive law is labeled springpot and reduces to the spring (purely elastic element) or the dashpot (purely viscous element) when the order of the derivative (or of the integral) in the constitutive law reaches the limiting values of zero and one, respectively. The physical meaning of the springpot model can be explained by means of hierarchical mechanical models made of many (theoretically infinite) elementary elastic and viscous elements; this results have been found by different authors in literature and with different mechanical scheme; this means that the accuracy of fractional viscoelasticity in the modeling of real materials can be achieved with classical viscoelastic models only if a prohibitive number of mechanical parameters is considered, with consequent great difficulty in the fitting experimental results. This fact alone is already enough to prefer fractional viscoelasticity instead of classical viscoelasticity.
In order to allow researcher of the field to use fractional viscoelasticity a 3D fractional viscoelastic models has been formulated in terms of deviatoric and volumetric relaxation (or creep) functions; the functions are those of the springpot and the order of the power law are independent from each other. The 3D behavior of this model has been investigated by evaluating the Poisson's ratio in creep and in relaxation and also by analyzing the response in terms of longitudinal and transverse strains/stresses in creep/relaxation tests. Moreover the 3D fractional viscoelasticity has been extended to those cases in which the relaxation (or creep functions) for both volumetric and deviatoric contributions are related to fractional models with more than one element: fractional

Maxwell model, fractional Kelvin-Voigt model and fractional Standard Linear Solid models. Some difference are evidenced between the springpot and the multi-element fractional models in terms of instantaneous and long term behavior of the creep and relaxation functions.
The 3D fractional viscoelastic models have been implemented in the finite element software Abaqus 6.14 by means of user material (UMAT) subroutine written in Fortran language. The routine is suitable for both implicit and explicit analysis; it is very fast and the only inconvenient is that for very large models (that is models with a very large number of finite elements) and for large number of time increments it needs to use a great amount of memory; however it is already possible to successfully run analysis with some thousand of finite elements and with some tenth of thousands of time increment in common machines.
The applications shown in the last Chapter clearly demonstrate that fractional viscoelasticity is desirable for the mechanical description of soils, pultruded bar with polymeric matrix, to model the damping in non-local beams and also to analyze complex shaped engineering components made of viscoelastic materials. Also stochastic dynamics analysis enjoy some advantages from the modeling of damping with fractional viscoelasticity. For these reasons it is believed that more and more effort should be devoted in the field of solid mechanics in order to obtain an even better comprehension of viscoelasticity phenomena and to refine these already good tools for the mechanical modeling.

# Appendix A

# Integral transforms and special functions

In this appendix some specials functions and some integral transforms used in the previous chapters are introduced.
Integrals transforms are common tools of classical differential calculus and for this reason they need to be introduced in the frame of fractional calculus. Here some informations are given about Fourier transform, Laplace transform and Mellin transform.
Special functions are those functions that usually do not appear when dealing with classical differential calculus and equations, but that are very common working with fractional calculus. We give here informations about the Euler-Gamma function, the beta function and the Mittag-Leffler function.

## A.1 Laplace transform

The Laplace transform $F_{\mathcal{L}}(s)$, with $s = \gamma + i\eta \in \mathbb{C}$, of a function $f(t)$ is defined as:

$$F_{\mathcal{L}}(s) = \mathcal{L}\{f(t); s\} = \int_0^{\infty} e^{-st} f(t) dt \tag{A.1}$$

The integral in Eq. (A.1) exists if the function $f(t)$ does not grow faster then a certain exponential function when $t \to \infty$, in other words two positive constants $M$ and $\alpha$ satisfying the following relationship must exist

$$e^{-\alpha t}|f(t)| \leq M \quad t \to \infty$$

The original function $f(t)$ can be restored from its Laplace transform $F(t)$ by using the inverse Laplace transform

$$f(t) = \mathcal{L}^{-1}\{F_{\mathcal{L}}(s); t\} = \int_{c-i\infty}^{c+i\infty} e^{st} F(s) ds, \quad c = Re(s) > c_0 \tag{A.2}$$

where $c_0$ is the lower value of the right half plane of the absolute convergence of the Laplace integral (A.1).

### A.1.1 Property of the Laplace transform

The fundamental properties of the Laplace transform are listed in the following:

- *Linearity.* If $f(t)$ and $g(t)$ are Laplace transformable and $\lambda, \mu \in \mathbb{C}$, then

$$\mathcal{L}\{\lambda f(t) + \mu g(t); s\} = \lambda F_{\mathcal{L}}(s) + \mu G_{\mathcal{L}}(s) \tag{A.3}$$

- *Retardation formulas.* Consider the Laplace transformable function $f(t)$. The Laplace transform of the function $f(t-a)$, with $a > 0$, is obtained by performing the change of variable $\tau = t - a$

$$\mathcal{L}\{f(t-a); s\} = \int_0^\infty e^{-st} f(t-a) dt = \int_0^\infty e^{-s(\tau+a)} f(\tau) d\tau = e^{-sa} F_{\mathcal{L}}(s) \tag{A.4}$$

  Eq. (A.4) is known as *time shifting* formula. Now consider the Laplace transform of the function $g(t) = e^{at} f(t)$:

$$\mathcal{L}\{g(t); s\} = \int_0^\infty e^{(a-s)t} f(t) dt = F_{\mathcal{L}}(s-a) \tag{A.5}$$

  Eq. (A.5) is known as *frequency shifting* formula.

- *Laplace transform of derivatives.* Let $f(t)$ be a derivable function and $f'(t)$ a Laplace transformable function, then

$$\mathcal{L}\{f'(t); s\} = sF_{\mathcal{L}}(s) - f(0) \tag{A.6}$$

where integration by parts has been used. If $f(t)$ is $n$-times derivable and $f^{(n)}(t)$ is Laplace transformable, then integrating by parts it is possible to demonstrate that

$$\mathcal{L}\left\{f^{(n)}(t);s\right\} = s^n F_{\mathcal{L}}(s) - \sum_{k=0}^{n-1} s^{n-k-1} f^{(k)}(0) = s^n F_{\mathcal{L}}(s) - \sum_{k=0}^{n-1} s^k f^{(n-k-1)}(0) \tag{A.7}$$

- *Laplace transform of a primitive.* Let $F(t)$ be the primitive of the function $f(t)$ defined as

$$F(t) = \int_0^t f(t)dt \tag{A.8}$$

If $f(t)$ is Laplace transformable then $F(t)$ is Laplace transformable and the following relationship hold

$$\mathcal{L}\left\{F(t);s\right\} = \frac{F_{\mathcal{L}}(s)}{s} \tag{A.9}$$

- *Laplace transform of a convolution.* Consider two functions $f(t)$ and $g(t)$ that are equal to zero for $t < 0$. The convolution between these two functions is defined as

$$(f \star g)(t) = \int_0^t f(t-\tau)g(\tau)d\tau = \int_0^t f(\tau)g(t-\tau)d\tau \tag{A.10}$$

If the Laplace transforms of $f(t)$ and $g(t)$ exists then the Laplace transform of the convolution (A.10) is equal to the product of the Laplace transforms of the two functions:

$$\mathcal{L}\left\{(f \star g)(t);s\right\} = F_{\mathcal{L}}(s)G_{\mathcal{L}}(s) \tag{A.11}$$

- *Derivative of Laplace transform.* A useful relationship can be found by considering the derivative of the Laplace transform of a function $f(t)$:

$$\frac{d}{ds}\mathcal{L}\left\{f(t);s\right\} = \frac{d}{ds}\int_0^\infty e^{-st}f(t)dt = \int_0^\infty \frac{d}{ds}e^{-st}f(t)dt =$$

$$-\int_0^\infty e^{-st}tf(t)dt = \mathcal{L}\left\{-tf(t);s\right\} \tag{A.12}$$

By considering higher order derivative of the Laplace transform and generalizing:

$$\mathcal{L}\left\{(-1)^n t^n f(t); s\right\} = \frac{d^n}{ds^n} F_{\mathcal{L}}(s) \tag{A.13}$$

- *Transform of a function with scaled variable.* The last useful property of the Laplace transform reads

$$\mathcal{L}\left\{f(at); s\right\} = \frac{1}{a}\mathcal{L}\left\{f(t); \frac{s}{a}\right\} = \frac{1}{a} F_{\mathcal{L}}(\frac{s}{a}), \quad a > 0 \tag{A.14}$$

### A.1.2 Application to the resolution of differential equations

Laplace transform is very useful to find solution to ordinary differential equations with constant coefficients and assigned initial conditions; it allows to transform a differential equation into an algebraic one, that is much easier to solve.
Consider for example a non-homogeneous differential equation of order $n$ forced by a function $f(t)$:

$$\sum_{k=0}^{n} C_k x^{(k)}(t) = f(t) \tag{A.15}$$

with initial conditions of the type:

$$x(0) = x_0; \;\; x'(0) = x'_0; \;\; \ldots \;\; ; x^{(n-1)}(0) = x_0^{(n-1)} \tag{A.16}$$

that for the uniqueness of the solution must be $n$. By applying Laplace transform to Eq. (A.15) and taking into account for the rule of the Laplace transform of derivatives, the following equation in the Laplace domain is obtained:

$$\sum_{k=0}^{n} C_k s^k X_{\mathcal{L}}(s) - I_0(s) = F_{\mathcal{L}}(s) \tag{A.17}$$

where $I_0(s)$ is a polynomial that contains the contributions due to all initial conditions. The solution in the Laplace domain is readily found because the equation (A.17) is algebraic and not differential:

$$X_{\mathcal{L}}(s) = \frac{F_{\mathcal{L}}(s) + I_0(s)}{\sum_{k=0}^{n} C_k s^k} \tag{A.18}$$

To find the solution in the time domain it is sufficient to apply the inverse Laplace transform operator (A.2); however it is to be noted that often the application of the inverse Laplace transform to Eq. (A.17) is complicated and then this method is not resolutive of all the problems involving differential equations.

## A.2 Fourier transform

The Fourier transform $F_{\mathcal{F}}(\omega)$ of a function $f(t)$ is defined as:

$$F_{\mathcal{F}}(\omega) = \mathcal{F}\{f(t);\omega\} = \int_{-\infty}^{\infty} e^{j\omega t} f(t)dt \tag{A.19}$$

where $j$ is the imaginary unit. Once the function $F_{\mathcal{F}}(\omega)$ is known, the original function $f(t)$ can be restored by means of the inverse Fourier transform operator:

$$f(t) = \mathcal{F}^{-1}\{F_{\mathcal{F}}(\omega);t\} = \frac{1}{2\pi}\int_{-\infty}^{\infty} e^{-j\omega t} F_{\mathcal{F}}(\omega)d\omega \tag{A.20}$$

Fourier transform is very similar to Laplace transform; in fact it can be obtained from Laplace transform by setting the lower bound of integration equal to $-\infty$ (instead of 0) and $s = -j\omega$.
Fourier transform is useful to study dynamical systems in the frequency domain and then to study dynamical properties of system ruled by differential equations.
An important characteristic of the Fourier transform operator is that it is able to distinguish between the even and odd part of a function $f(t)$; in fact, using Euler formula $e^{jx} = \cos(x) + j\sin(x)$

$$F_{\mathcal{F}}(\omega) = \int_{-\infty}^{\infty} e^{j\omega t} f(t)dt = \int_{-\infty}^{\infty} \cos(\omega t)u(t)dt + j\int_{-\infty}^{\infty} \sin(\omega t)v(t)dt =$$

$$u_{\mathcal{F}}(\omega) + jv_{\mathcal{F}}(\omega) \tag{A.21}$$

where $u(t)$ and $v(t)$ are the even and odd parts of $f(t)$, respectively, defined as:

$$u(t) = \frac{f(t) + f(-t)}{2} \tag{A.22a}$$

$$v(t) = \frac{f(t) - f(-t)}{2} \tag{A.22b}$$

and $u_{\mathcal{F}}(\omega)$ and $v_{\mathcal{F}}(\omega)$ are the real and imaginary parts of the Fourier transform of $f(t)$ and related respectively to $u(t)$ and $v(t)$. Then the Fourier transform of an even function in real and even, the Fourier transform of an odd function is imaginary and odd while the Fourier transform of a generic function has both real and imaginary parts.

### A.2.1 Properties of the Fourier transform

Since the Fourier transform is similar to Laplace transform, they have some properties in common. The most important properties of the Fourier transform are listed in the following:

- *Linearity.* Let $f(t)$ and $g(t)$ be Fourier transformable functions and $\lambda, \mu \in \mathbb{C}$; then
$$\mathcal{F}\{\lambda f(t) + \mu g(t); \omega\} = \lambda F_{\mathcal{F}}(\omega) + \mu G_{\mathcal{F}}(\omega) \tag{A.23}$$
- *Retardation formulas.* Consider the Fourier transformable function $f(t)$; the Fourier transform of the function $f(t - t_0)$, with $t_0 \in \mathbb{R}$ reads
$$\mathcal{F}\{f(t - t_0); \omega\} = \int_{-\infty}^{\infty} e^{j\omega t} f(t - t_0) dt = \int_{-\infty}^{\infty} e^{j\omega(\tau + t_0)} f(\tau) d\tau = e^{j\omega t_0} F_{\mathcal{F}}(\omega) \tag{A.24}$$
where the change of variable $\tau = t - t_0$ has been performed. Now consider $\omega_0 \in \mathbb{C}$:
$$\mathcal{F}\left\{e^{j\omega_0 t} f(t); \omega\right\} = \int_{-\infty}^{\infty} e^{j(\omega + \omega_0)t} f(t) dt = F_{\mathcal{F}}(\omega + \omega_0) \tag{A.25}$$
Eq. (A.24) and (A.25) are the *time shifting* and *frequency shifting* retardation formulas, respectively, and they are formally identical to the analogous formulas for the Laplace transform.
- *Fourier transform of derivatives.* Consider a $n$ times derivable function $f(t)$, then integrating by parts the following property is obtained
$$\mathcal{F}\left\{f^{(n)}(t); \omega\right\} = (-j\omega)^n F_{\mathcal{F}}(\omega) \tag{A.26}$$

Property (A.26) is similar to property (A.7) of the Laplace transform, but in this case the value in zero of the function $f(t)$ and of its derivatives do not appear.

- *Derivatives of the Fourier transform.* If the function $F_{\mathcal{F}}(\omega)$ admits $n-th$ derivative, then

$$\mathcal{F}\{t^n f(t);\omega\} = (-j)^n \frac{d^n}{d\omega^n} F_{\mathcal{F}}(\omega) \tag{A.27}$$

- *Fourier transform of convolution.* Consider the Fourier transformable functions $f(t)$ and $g(t)$ and their convolution defined as:

$$(f \star g)(t) = \int_{-\infty}^{\infty} f(\tau) g(t-\tau) d\tau \tag{A.28}$$

Fourier transform of the convolution (A.28) is

$$\mathcal{F}\{(f \star g)(t);\omega\} = F_{\mathcal{F}}(\omega) G_{\mathcal{F}}(\omega) \tag{A.29}$$

There exists also a reciprocal property:

$$\mathcal{F}\{f(t)g(t);\omega\} = (F_{\mathcal{F}} \star G_{\mathcal{F}})(\omega) \tag{A.30}$$

- Finally the following property holds

$$\mathcal{F}\{f(at);\omega\} = \frac{1}{|a|}\mathcal{F}\left\{f(t);\frac{\omega}{a}\right\} = \frac{1}{|a|}F_{\mathcal{F}}\left(\frac{\omega}{a}\right) \tag{A.31}$$

### A.2.2 Application to the solution of differential equations

The Fourier transform can be used in a similar way the Laplace transform is used in section 1.1.2. To this purpose, consider Eq. (A.15), with the initial conditions (A.16) and here reported for simplicity of reading

$$\sum_{k=0}^{n} C_k x^{(k)}(t) = f(t) \tag{A.32}$$

$$x(0) = x_0;\ \ x'(0) = x'_0;\ \ \ldots\ \ ; x^{(n-1)}(0) = x_0^{(n-1)} \tag{A.33}$$

By performing Fourier transform of Eq. (A.32) an algebraic equation in the variable $\omega$ is obtained:

$$\sum_{k=0}^{n} C_k(-j\omega)^k X_{\mathcal{F}}(\omega) = F_{\mathcal{F}}(\omega) \tag{A.34}$$

As in the case of Laplace transform the solution in the $\omega$ domain is readily found:

$$X_{\mathcal{F}}(\omega) = \frac{F_{\mathcal{F}}(\omega)}{\sum_{k=0}^{n} C_k(-j\omega)^k} \tag{A.35}$$

The function

$$H_{\mathcal{F}}(\omega) = \frac{1}{\sum_{k=0}^{n} C_k(-j\omega)^k} \tag{A.36}$$

is called *transfer function* and assume a great importance in the study of dynamical systems because it contains all relevant features in the frequency domain of the dynamical system at hand.
Once $X_{\mathcal{F}}(\omega)$ is known the solution in the time domain can be found by applying the inverse Fourier transform operator (A.20), but as in the case of Laplace transform this operation is not always feasible. Note that, differently from the case of the Laplace transform, the solution with the Fourier transform does not involve initial conditions.

## A.3 Mellin transform

Mellin transform is another integral transform defined in the interval $0 \div \infty$ as:

$$F_{\mathcal{M}}(\gamma) = \mathcal{M}\{f(t);\gamma\} = \int_0^{\infty} t^{\gamma-1} f(t)dt \tag{A.37}$$

with $\gamma = \rho + i\eta \in \mathbb{C}$. To ensure the existence of $F_{\mathcal{M}}(\gamma)$, the real part of $\gamma$ must lie in the so called *Fundamental Strip* (FS), that is

$$-\rho_1 < \rho < -\rho_2 \tag{A.38}$$

Some informations about the fundamental strip are given in the following subsection.

The original function $f(t)$ can be restored by applying the inverse Mellin transform operator

$$f(t) = \frac{1}{2\pi i} \int_{\rho - i\infty}^{\rho + i\infty} F_{\mathcal{M}}(\gamma) t^{-\gamma} d\gamma, \quad 0 < t < \infty \tag{A.39}$$

Note that integration is performed along the imaginary axis, therefore Eq. (A.39) can be rewritten as

$$f(t) = \frac{1}{2\pi i} \int_{-\infty}^{\infty} F_{\mathcal{M}}(\gamma) t^{-\gamma} d\eta, \quad 0 < t < \infty \tag{A.40}$$

This means that the inverse Mellin transform does not depend on the value of $\rho$, provided that it belongs to the FS.
With the proper choice of $\rho$ (in the FS) $F_{\mathcal{M}}(\gamma)$ decays very fast for $t \to \infty$; this allows to define a discretized version of integral (A.40) with a reasonable number of terms:

$$f(t) = \frac{\Delta\eta}{2\pi} \sum_{k=-m}^{m} F_{\mathcal{M}}(\gamma_k) t^{-\gamma_k}, \quad 0 < t < \infty \tag{A.41}$$

where $\Delta\eta$ is the step of discretization of the imaginary axis in the Mellin domain, $\gamma_k = \rho + ik\Delta\eta$ and $m = \eta_c / \Delta\eta$ is such that beyond the cut-off value $\eta_c$ the contribution of other terms are negligible.
Note that the inverse Mellin transform of Eqs. (A.39), (A.40) and (A.41) is able only to restore the function $f(t)$ in the range $0 < t < \infty$; the value of the function at the origin is not restored by the inverse Mellin transform because $t^{-\gamma}$ (or $t^{-\gamma_k}$) diverges at $t = 0$. It is also possible to work with Mellin transform in the whole real axis; in order to do this, it is necessary to split the function $f(t)$ in its even and odd parts $u(t)$ and $v(t)$, respectively:

$$\begin{gathered} u(t) = \frac{f(t) + f(-t)}{2}, \quad v(t) = \frac{f(t) - f(-t)}{2} \\ f(t) = u(t) + v(t) \end{gathered} \tag{A.42}$$

Then we evaluate separately the Mellin transforms of $u(t)$ and $v(t)$:

$$U_{\mathcal{M}}(\gamma) = \mathcal{M}\{u(t); \gamma\} = \int_0^{\infty} t^{\gamma - 1} u(t) dt \tag{A.43a}$$

$$V_{\mathcal{M}}(\gamma) = \mathcal{M}\{v(t);\gamma\} = \int_0^\infty t^{\gamma-1} v(t) dt \tag{A.43b}$$

And finally we restore the whole function $f(t)$ as it follows

$$f(t) = \frac{1}{2\pi i}\left[\int_{-\infty}^{\infty} U_{\mathcal{M}}(\gamma) t^{-\gamma} d\eta + \mathrm{sgn}(t)\int_{-\infty}^{\infty} V_{\mathcal{M}}(\gamma) t^{-\gamma} d\eta\right] \qquad t \neq 0 \tag{A.44}$$

or in discretized form

$$f(t) = \frac{\Delta\eta}{2\pi}\sum_{k=-m}^{m}\left[U_{\mathcal{M}}(\gamma_k) + \mathrm{sgn}(t) V_{\mathcal{M}}(\gamma_k)\right] t^{-\gamma_k} \qquad t \neq 0 \tag{A.45}$$

In Eqs. (A.44) and (A.45) the value at $t = 0$ is excluded because in it divergence occurs because of the presence of $t^{-\gamma}$ (or $t^{-\gamma_k}$).
In the very recent past this discretized form of inverse Mellin transform has proved to be very useful and effective to solve systems of fractional differential equations [14, 15], diffusive equations [4, 28], to characterize random processes [34] and in wavelet analysis [5].

### A.3.1 The Fundamental Strip

The integral in Eq. (A.38) converges and therefore exists if the value of $\Re(\gamma) = \rho$ lies in the so called *Fundamental Strip*; this represents a portion of the complex plane bounded by two values in the real axis. The values of these bounds depend only on the asymptotic behavior of the function $f(t)$; in particular $\rho_1$ is related to the behavior of the function for $t \to 0$, while$\rho_2$ is related to the behavior of $f(t)$ for $t \to \infty$:

$$\lim_{t\to 0} f(t) = \mathcal{O}(t^{\rho_1}) \tag{A.46a}$$

$$\lim_{t\to \infty} f(t) = \mathcal{O}(t^{\rho_2}) \tag{A.46b}$$

Moreover if there is a constant $A > 0$ such that it is possible to write

$$\int_{-\infty}^{\infty} |F_{\mathcal{M}}(\gamma)| d\eta < A; \qquad (-\rho_1 < \rho < -\rho_2) \tag{A.47}$$

then the inverse Mellin transform exist and can be evaluated with Eq. (A.40).

**Example of FS** To show how to find the FS of a function, consider the following function:

$$f(t) = \frac{1}{1+t^2} \tag{A.48}$$

In order to find the behavior for $t \to 0$ and for $t \to \infty$ we evaluate the limits:

$$\lim_{t\to 0} \frac{1}{1+t^2} = 1 \quad \Rightarrow \quad t^{\rho_1} = 1 \quad \Rightarrow \quad \rho_1 = 0 \tag{A.49a}$$

$$\lim_{t\to \infty} \frac{1}{1+t^2} = \frac{1}{\infty^2} \quad \Rightarrow \quad t^{\rho_2} = \infty^{-2} \quad \Rightarrow \quad \rho_2 = -2 \tag{A.49b}$$

Then the FS is comprised in the range $0 \div 2$.

### A.3.2 Properties of Mellin transform

The main and most useful properties of Mellin transform are listed in the following.

- The first useful property comes directly from the definition;

$$\mathcal{M}\{t^a f(t); \gamma\} = \int_0^\infty t^{\gamma+a-1} f(t) dt = F_{\mathcal{M}}(\gamma + a) \tag{A.50}$$

- *Mellin transform of the convolution.* The Mellin convolution between two functions $f(t)$ and $g(t)$ is defined as

$$(f \star g)(t) = \int_0^\infty f(t\tau) g(\tau) d\tau \tag{A.51}$$

  The Mellin transform of convolution (A.51) is

$$\mathcal{M}\{(f \star g)(t); \gamma\} = F_{\mathcal{M}}(\gamma) G_{\mathcal{M}}(1-\gamma) \tag{A.52}$$

  Combining properties (A.50) and (A.52) the following relationship is found

$$\mathcal{M}\left\{t^\lambda \int_0^\infty \tau^\mu f(t\tau) g(\tau) d\tau; \gamma\right\} = F_{\mathcal{M}}(\gamma+\lambda) G_{\mathcal{M}}(1-\gamma-\lambda+\mu) \tag{A.53}$$

- *Melin transform of derivatives.* If $f(t)$ admit $n-th$ derivative, by integrating repeatedly by parts, the following relationship is obtained

$$\begin{aligned}\mathcal{M}\left\{f^{(n)}(t);\gamma\right\} &= \int_0^\infty f^{(n)}(t)t^{\gamma-1}dt \\ &= \left[f^{(n-1)}(t)t^{\gamma-1}\right]_0^\infty - (\gamma-1)\int_0^\infty f^{(n-1)}(t)t^{\gamma-2}dt \\ &= \left[f^{(n-1)}(t)t^{\gamma-1}\right]_0^\infty - (\gamma-1)\mathcal{M}\left\{f^{(n-1)}(t);\gamma-1\right\} \\ &= \dots \\ &= \sum_{k=0}^{n-1}(-1)^k\frac{\Gamma(\gamma)}{\Gamma(\gamma-k)}\left[f^{(n-k-1)}(t)t^{\gamma-k-1}\right]_0^\infty + \\ &\quad (-1)^k\frac{\Gamma(\gamma)}{\Gamma(\gamma-k)}F_{\mathcal{M}}(\gamma-n) \\ &= \sum_{k=0}^{n-1}\frac{\Gamma(1-\gamma+k)}{\Gamma(1-\gamma)}\left[f^{(n-k-1)}(t)t^{\gamma-k-1}\right]_0^\infty + \\ &\quad \frac{\Gamma(1-\gamma+n)}{\Gamma(1-\gamma)}F_{\mathcal{M}}(\gamma-n)\end{aligned} \tag{A.54}$$

  where $\Gamma(\cdot)$ is the Euler Gamma function introduced in the next section. Under some conditions on the behavior of $f(t)$ and on the value of $\Re(\gamma)$, the terms in square brackets of Eq. (A.54) become zero, then Eq. (A.54) becomes

$$\mathcal{M}\left\{f^{(n)}(t);\gamma\right\} = \frac{\Gamma(1-\gamma+n)}{\Gamma(1-\gamma)}F_{\mathcal{M}}(\gamma-n) \tag{A.55}$$

  Another useful property involving the first derivative of the function $f(t)$ is

$$\mathcal{M}\left\{tf'(t);\gamma\right\} = -\gamma F_{\mathcal{M}}(\gamma) \tag{A.56}$$

- *Derivative of the Mellin transform.* The integer order derivative of the Mellin transform can be obtained in the following way:

$$\mathcal{M}\left\{\log(t)^n f(t);\gamma\right\} = F_{\mathcal{M}}^{(n)}(\gamma) \tag{A.57}$$

- *Mellin transform of the Fourier transform.* The Mellin transform is related to the Fourier transform:

$$\mathcal{M}\left\{\mathcal{F}\left\{f(t);\omega\right\};\gamma\right\} = 2\Gamma(\gamma)\cos\left(\frac{\gamma\pi}{2}\right)F_{\mathcal{M}}(1-\gamma) \tag{A.58}$$

If we are working with a function $f(t)$ in the whole real axis, the relationship is obtained by considering separately for the even and the odd part $u(t)$ and $v(t)$, respectively:

$$\mathcal{M}\left\{\mathcal{F}\left\{f(t);\omega\right\};\gamma\right\} = \mathcal{M}\left\{\mathcal{F}\left\{u(t)+v(t);\omega\right\};\gamma\right\} = 2\Gamma(\gamma)\left[\cos\left(\frac{\gamma\pi}{2}\right)U_{\mathcal{M}}(1-\gamma)+\sin\left(\frac{\gamma\pi}{2}\right)V_{\mathcal{M}}(1-\gamma)\right] \quad \text{(A.59)}$$

- *Other useful properties.* For $a > 0$ the following equalities hold true

$$\mathcal{M}\left\{f(at);\gamma\right\} = a^{-\gamma}F_{\mathcal{M}}(\gamma) \quad \text{(A.60)}$$

$$\mathcal{M}\left\{f(t^{\pm a});\gamma\right\} = \frac{1}{a}F_{\mathcal{M}}(\pm\frac{\gamma}{a}) \quad \text{(A.61)}$$

$$\mathcal{M}\left\{t^{\alpha}f(t^{\pm a});\gamma\right\} = \frac{1}{a}F_{\mathcal{M}}(\pm\frac{\gamma+\alpha}{a}) \quad \text{(A.62)}$$

## A.4 The Euler-Gamma function

The Euler-Gamma function is with any doubt the basic function of the fractional calculus and was defined by the young mathematician Leonhard Euler in the 18th century; it is the generalization of factorials $n!$ and allow $n$ to assume real or complex values.
Gamma function is denoted as $\Gamma(z)$ and is defined as

$$\Gamma(z) = \int_0^{\infty} e^{-t}t^{z-1}dt; \quad z \in \mathbb{C} \quad \text{(A.63)}$$

The integral in Eq. (A.63) converge in all the half plane $\Re(z) > 0$. This can be easily proved by substituting $z = x + iy$, with $x, y \in \mathbb{R}$ and $i$ is the imaginary unit:

$$\Gamma(x+iy) = \int_0^{\infty} e^{-t}t^{x+iy-1}dt = \int_0^{\infty} e^{-t}t^{x-1}e^{iy\log t}dt = \int_0^{\infty} e^{-t}t^{x-1}\left[\cos\left(y\log t\right)+i\sin\left(y\log t\right)\right]dt \quad \text{(A.64)}$$

The expression in square brackets contains only trigonometric functions, then

is bounded for all $t$; convergence at infinity is provided by the exponential function $e^{-t}$, while the convergence at $t = 0$ is guaranteed if $x = \Re(z) > 1$. Note that the integral in Eq. (A.63) corresponds to the Mellin transform of the function $e^{-t}$; therefore the Euler Gamma function can be defined as the Mellin transform of $e^{-t}$ The Gamma function can be also defined with the following limit representation:

$$\Gamma(z) = \lim_{n\to\infty} \frac{n! n^z}{z(z+1)\cdots(z+n)} \tag{A.65}$$

The proof of the equivalence between Eq. (A.63) and Eq.(A.65) can be found in [75]. Finally the Gamma function diverges at the points $z = -n$ (with $n \in \mathbb{N}$), as it is possible to appreciate in Fig. A.1 and in Fig. A.2.

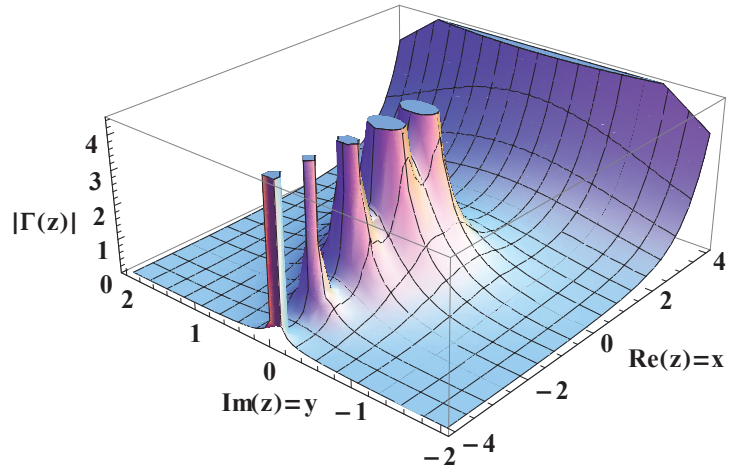


**Figure A.1:** Absolute value of the Euler gamma function on the Gauss plane ($|\Gamma(z)|$ for $z \in \mathbb{C}$).

### A.4.1 Properties of Gamma function

Some basic properties of the Gamma function are listed in the following:

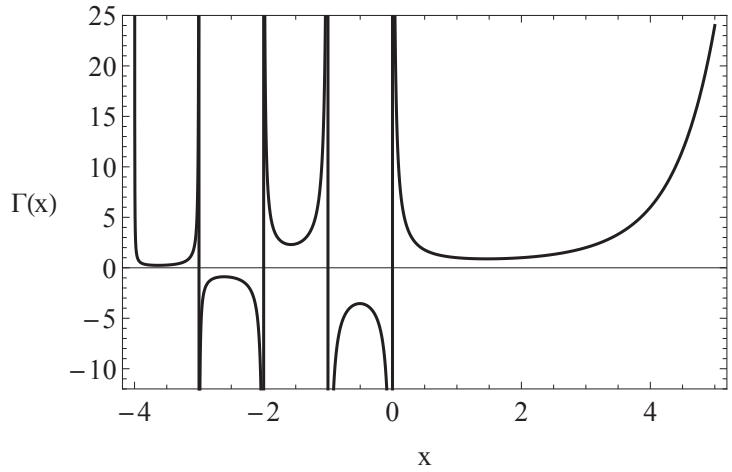


**Figure A.2:** Euler Gamma function for $\Im(z) = y = 0$.

- The first properties reads

$$\Gamma(z+1) = z\Gamma(z) \tag{A.66}$$

This property can be easily proved by integrating by parts:

$$\Gamma(z+1) = \int_0^\infty e^{-t}t^z dt = \left[-e^{-t}t^z\right]_0^\infty + z\int_0^\infty e^{-t}t^{z-1}dt = z\Gamma(z) \tag{A.67}$$

It can be easily found that $\Gamma(1) = 1$, then using the property (A.66):

$$\begin{aligned}
\Gamma(2) &= 1\cdot\Gamma(1) = 1 = 1! \\
\Gamma(3) &= 2\cdot\Gamma(2) = 2\cdot 1! = 2! \\
\Gamma(4) &= 3\cdot\Gamma(3) = 3\cdot 2! = 3! \\
&\cdots \quad \cdots \quad \cdots \quad \cdots \quad \cdots \\
\Gamma(n+1) &= n\cdot\Gamma(n) = n\cdot(n-1)! = n!
\end{aligned} \tag{A.68}$$

- *Euler reflection formula.*

$$\Gamma(z)\Gamma(1-z) = \frac{\pi}{\sin(\pi z)} \tag{A.69}$$

This relationship allows to easily evaluate the value of the Gamma function for $z = 1/2$

$$\Gamma(\frac{1}{2}) = \sqrt{\pi} \tag{A.70}$$

- *Legendre formula.*

$$\Gamma(z)\Gamma(z+\frac{1}{2}) = \sqrt{\pi}2^{2z-1}\Gamma(2z) \qquad 2z \neq 0, -1, -2, ... \tag{A.71}$$

Eq. (A.71) is also known as *duplication formula* and is a particular case of the more general *multiplication theorem*:

$$\prod_{k=1}^{m}\Gamma(z+\frac{k-1}{m}) = (2\pi)^{\frac{m-1}{2}}m^{\left(\frac{1}{2}-mz\right)}\Gamma(mz) \tag{A.72}$$

### A.4.2 Euler Beta function

This function is strictly related to the Gamma function; it is defined by:

$$\beta(z,w) = \int_0^1 \tau^{z-1}(1-\tau)^{w-1}d\tau \quad \Re(z), \Re(w) > 0 \tag{A.73}$$

By means of some manipulations it can be demonstrated that

$$\beta(z,w) = \frac{\Gamma(z)\Gamma(w)}{\Gamma(z+w)} \tag{A.74}$$

The definition (A.74) provides the analytical continuation of the beta function for the entire complex plane. Relationships (A.69) and (A.71) can be demonstrated by means of the use of the Beta function.

## A.5 Mittag-Leffler function

The one parameter Mittag-Leffler (M-L) functions was introduced by G. M. Mittag-Leffler in 1985; it is a very useful function in the frame of fractional calculus because it is the one parameter generalization of the function $e^z$, that

plays very important role in the solution of ordinary differential equations. The definition is given as:

$$\mathrm{E}_{\alpha}(z) = \sum_{k=0}^{\infty} \frac{z^k}{\Gamma(\alpha k + 1)} \tag{A.75}$$

As $e^z$ is important on the solution of ordinary differential equations, it will be shown in the subsequent sections of this thesis that $\mathrm{E}_{\alpha}(z)$ is very important on the solution of fractional differential equations.
A more general definition was given by Agrawal, that introduced the two parameters M-L function:

$$\mathrm{E}_{\alpha,\beta}(z) = \sum_{k=0}^{\infty} \frac{z^k}{\Gamma(\alpha k + \beta)} \quad \alpha > 0, \beta > 0 \tag{A.76}$$

It is obvious that the one parameter Mittag-Leffler function is a special case of the two parameters Mittag-Leffler function in which $\beta = 1$.
Another definition of the two parameters ML function is provided by the following Mellin-Barnes integral:

$$\mathrm{E}_{\alpha,\beta}(z) = \frac{1}{2\pi i} \int_{c-i\infty}^{c+i\infty} \frac{\Gamma(\gamma)\Gamma(1-\gamma)}{\Gamma(\beta - \alpha\gamma)} (-z)^{-\gamma} d\gamma \tag{A.77}$$

Comparing Eq. (A.77) with (A.39)it can be stated that ML function is related to the inverse Mellin transform of a certain combination of Euler gamma functions; obviously, the one parameter ML function is obtained by setting $\beta = 1$ in Eq. (A.77).

### A.5.1 Properties of the Mittag-Leffler function

In this subsection some equivalence of ML functions with other known functions and some other properties are listed.

- *Relationship with exponential function.* As already mentioned above, the ML function is the generalization of the exponential function:

$$\mathrm{E}_{1,1}(z) = \sum_{k=0}^{\infty} \frac{z^k}{\Gamma(k+1)} = \sum_{k=0}^{\infty} \frac{z^k}{k!} = e^z \tag{A.78}$$

$$\mathrm{E}_{1,2}(z) = \sum_{k=0}^{\infty} \frac{z^k}{\Gamma(k+2)} = \sum_{k=0}^{\infty} \frac{z^k}{(k+1)!} = \frac{1}{z} \sum_{k=0}^{\infty} \frac{z^{k+1}}{(k+1)!} = \frac{e^z - 1}{z} \quad \text{(A.79)}$$

$$\mathrm{E}_{1,3}(z) = \sum_{k=0}^{\infty} \frac{z^k}{\Gamma(k+3)} = \sum_{k=0}^{\infty} \frac{z^k}{(k+2)!} = \frac{1}{z^2} \sum_{k=0}^{\infty} \frac{z^{k+2}}{(k+2)!} = \frac{e^z - 1 - z}{z^2} \quad \text{(A.80)}$$

and in general:

$$\mathrm{E}_{1,m}(z) = \frac{1}{z^{m-1}} \left\{ e^z - \sum_{k=0}^{m-2} \frac{z^k}{k!} \right\} \quad \text{(A.81)}$$

- *Relationship with hyperbolic functions.* The hyperbolic sine and cosine can be also defined as particular cases of the two parameters M-L functions:

$$\mathrm{E}_{2,1}(z^2) = \sum_{k=0}^{\infty} \frac{z^{2k}}{\Gamma(2k+1)} = \sum_{k=0}^{\infty} \frac{z^{2k}}{2k!} = \cosh(z) \quad \text{(A.82)}$$

$$\mathrm{E}_{2,2}(z^2) = \sum_{k=0}^{\infty} \frac{z^{2k}}{\Gamma(2k+2)} = \frac{1}{z} \sum_{k=0}^{\infty} \frac{z^{2k+1}}{(2k+1)!} = \frac{\sinh(z)}{z} \quad \text{(A.83)}$$

- *Relationship with error function complement.* The M-L function is related also to the error function complement $\mathrm{erfc}(z)$ defined as

$$\mathrm{erfc}(z) = \frac{2}{\sqrt{\pi}} \int_z^{\infty} e^{-t^2} dt \quad \text{(A.84)}$$

In fact by setting $\alpha = 1/2$ and $\beta = 1$:

$$\mathrm{E}_{1/2,1}(z) = \sum_{k=0}^{\infty} \frac{z^k}{\Gamma(\frac{k}{2}+1)} = e^{z^2}\mathrm{erfc}(-z) \quad \text{(A.85)}$$

- *Derivatives of ML function.*

$$\left(\frac{d}{dt}\right)^m \left( t^{\alpha k+\beta-1} \mathrm{E}^{(k)}_{\alpha,\beta}(\lambda t^\alpha) \right) = t^{\alpha k+\beta-m-1} \mathrm{E}^{(k)}_{\alpha,\beta-m}(\lambda t^\alpha) \quad \text{(A.86)}$$

- *Laplace transform of ML function*

$$\mathcal{L}\left\{t^{\alpha k+\beta-1}E_{\alpha,\beta}(\pm at^{\alpha});s\right\}=\frac{k!s^{\alpha-\beta}}{(s^{\alpha}\mp a)^{k+1}} \tag{A.87}$$

  where $k$ is the integer order of derivation.

- *Other useful relationships.*

$$\mathrm{E}_{\alpha,\beta}=z\mathrm{E}_{\alpha,\alpha+\beta}+\frac{1}{\Gamma(\beta)} \tag{A.88}$$

$$\mathrm{E}_{\alpha,\beta}=\beta\mathrm{E}_{\alpha,\beta+1}+\alpha z\frac{d}{dz}\mathrm{E}_{\alpha,\beta+1} \tag{A.89}$$

### A.5.2 Wright function

Another important function, useful in the study of fractional differential equations, is the Wright function that is reported here because it is strictly related to the two parameters ML function; it is defined as:

$$W(z;\alpha,\beta)=\sum_{k=0}^{\infty}\frac{z^k}{k!\Gamma(\alpha k+\beta)} \tag{A.90}$$

For $\alpha=0$ and $\beta=1$ the Wright function reduces to the exponential function $e^z$:

$$W(z;0,1)=\sum_{k=0}^{\infty}\frac{z^k}{k!\Gamma(1)}=\sum_{k=0}^{\infty}\frac{z^k}{k!}=e^z \tag{A.91}$$

For particular values of the parameters the Wright function becomes the *Mainardi* function, denoted as $M(z;\alpha)$:

$$W(-z;-\alpha,1-\alpha)=M(z;\alpha)=\sum_{k=0}^{\infty}\frac{(-1)^k z^k}{k!\Gamma\left[-\alpha(k+1)+1\right]} \tag{A.92}$$

## A.6 Bessel functions

Bessel functions are involved in the solution of some problem of fractional viscoelasticity that will be described ahead in this work. For this reason, and in order to avoid confusion later in the text, they are introduced in this section.

### A.6.1 First and second kind Bessel functions

First and second kind Bessel functions are the solutions to this ordinary differential equation:

$$z^2\frac{d^2y(z)}{dz^2} + z\frac{dy(z)}{dz} + (z^2 - \nu^2)y(z) = 0 \tag{A.93}$$

where $\nu$ is the "order" of the Bessel equation and functions. Since Eq. (A.93) is a second order differential equation, two linearly independent solutions must be found. The Bessel functions of the first kind is defined as:

$$J_\nu(z) = \left(\frac{z}{2}\right)^\nu \sum_{n=0}^{\infty} \frac{(-1)^n}{n!\Gamma(n+\nu+1)} \left(\frac{z}{2}\right)^{2n} \tag{A.94}$$

If $\nu$ is not real then $J_\nu(z)$ and $J_{-\nu}(z)$ are independent and then the general solution can be obtained by linear combination of them; if, instead, $\nu$ is integer $J_{-\nu}(z) = (-1)^\nu J_\nu(z)$, then another particular solution is needed, that is the second kind Bessel function

$$N_\nu(z) = J_\nu(z)\cos(\nu\pi) - J_{-\nu}(z)\sin(\nu\pi) \tag{A.95}$$

Then the general solution can be obtained as a linear combination of $J_\nu(z)$ and $N_\nu(z)$. These functions are strictly related to trigonometric functions, indeed:

$$J_{\frac{1}{2}}(z) = \frac{\cos(z)}{\sqrt{z}}, \quad N_{\frac{1}{2}}(z) = \frac{\sin(z)}{\sqrt{z}} \tag{A.96}$$

The behavior of the Bessel functions can be observed in Fig. A.3

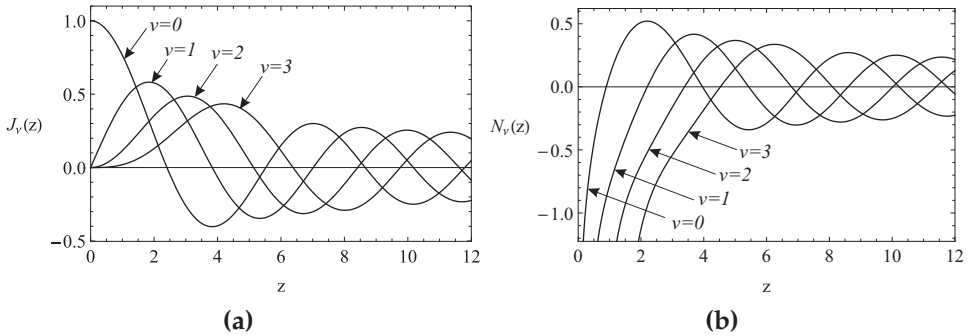


**Figure A.3:** Bessel functions of the first kind (a) and of the second kind (b).

### A.6.2 Modified Bessel functions

Modified Bessel functions are the solutions of the modified Bessel equation:

$$z^2\frac{d^2y(z)}{dz^2}+z\frac{dy(z)}{dz}-(z^2+\nu^2)y(z)=0 \tag{A.97}$$

One solution to Eq. (A.97)is the modified first kind Bessel function:

$$I_\nu(z)=e^{-j\frac{\pi}{2}\nu}J_\nu(ze^{j\frac{\pi}{2}})=\sum_{k=0}^{\infty}\frac{(\frac{z}{2})^{\nu+2k}}{k!\Gamma(k+\nu+1)} \tag{A.98}$$

If $\nu$ is non-integer, then $I_{-\nu}(z)$ is independent of $I_\nu(z)$, otherwise as second particular solution the modified second kind Bessel function can be used:

$$K_\nu(z)=\frac{\pi\left(I_{-\nu}(z)-I_\nu(z)\right)}{2\sin(\pi\nu)} \tag{A.99}$$

The functions $I_\nu(z)$ and $K_\nu(z)$ are related to the hypergeometric functions cosh(z) and sinh(z). The behavior of the modified Bessel functions can be observed in Fig. A.4

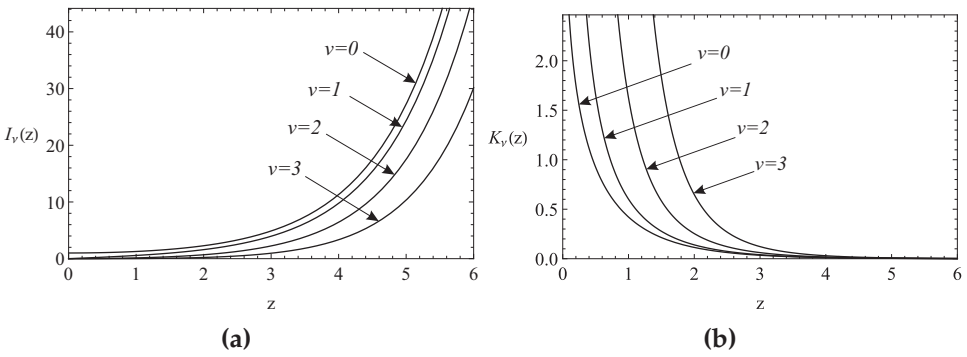


**Figure A.4:** Modified Bessel functions of the first kind (a) and of the second kind (b).

# Bibliography

[1] Adolfsson K, Enelund M, Olsson P, *On the Fractional Order Model of Viscoelasticity*, Mechanics of Time Dependent Materials, 9:15–34, 2005

[2] Aifantis EC, *Gradient effects models at macro, micro and nanoscales*, Journal of Mechanical Behavior of Materials, 5(3): 355–375, 1994.

[3] Aifantis EC, *Gradient deformation models at nano, micro, and macroscales*, Journal of Engineering Materials and Technologies – Transaction ASME, 121: 189–202, 1999.

[4] Alotta G, Di Paola M, *Probabilistic characterization of nonlinear systems under α-stable white noise via complex fractional moments*, Physica A: Statistical Mechanics and its Applications, 420: 265–276, 2015.

[5] Alotta G, Di Paola M, Failla G, *A Mellin transform approach to wavelet analysis*, Communications in Nonlinear Science and Numerical Simulations, 28(1–3): 175–93, 2015.

[6] Alotta G, Di Paola M, Pirrotta A, *Fractional Tajimi-Kanai model for simulating earthquake ground motion*, Bulletin of Earthquake Engineering, 12: 2495–2506, 2014.

[7] Alotta G, Failla G, Zingales M, *Finite element method for a nonlocal Timoshenko beam model*, Finite Elements in Analysis and Design, 89: 77–92, 2014.

[8] Alotta G, Failla G, Zingales M, *Finite element formulation of a nonlocal hereditary fractional-order Timoshenko beam*, Journal of Engineering Mechanics (ASCE), 10.1061/(ASCE)EM.1943-7889.0001035, 2015.

[9] Arash B, Wang Q, *A review on the application of nonlocal elastic models in modeling of carbon nanotubes and graphenes*, Computational Materials Science, 51(1): 303–313, 2012.

[10] Bagley RL, Torvik PJ, *Fractional Calculus - A Different Approach to the Analysis of Viscoelastically Damped Structures*, AIAA Journal, 21 (5): 741–748, 1983.

[11] Bagley RL, Torvik PJ, *On the Appearance of the Fractional Derivative in the Behavior of Real Materials*, Journal of Applied Mechanics, 51: 294–298, 1984.

[12] Bagley RL, Torvik PJ, *On the fractional calculus model of viscoelastic behaviour*, Journal of Rheology, 30(1): 133–55, 1986.

[13] Barretta R, Feo L, Luciano R, *Torsion of functionally graded nonlocal viscoelastic circular nanobeams*, Composites Part B Engineering, 72: 217–222, 2015.

[14] Butera S, Di Paola M, *Fractional differential equations solved by using Mellin transform*, Communications in Nonlinear Science and Numerical Simulations, 19(7): 2220–27, 2014.

[15] Butera S, Di Paola M, *Mellin transform approach for the solution of coupled systems of fractional differential equations* , Communications in Nonlinear Science and Numerical Simulations, 20(1): 32–38, 2015.

[16] Challamel N, *Higher-order shear beam theories and enriched continuum*, Mechanics Research Communications, 35(5): 388–392, 2011.

[17] Challamel N, *Variational formulation of gradient or/and nonlocal higher-order shear elasticity beams*, Computers and Structures, 105: 351–368, 2013.

[18] Chang CS, Askes H, Sluys LJ, *Higher-order strain/higher-order stress gradient models derived from a discrete microstructure, with application to fracture*, Engineering Fracture Mechanics, 69: 1907–924, 2002.

[19] Clough R, Penzien J, *Dynamics of Structures*, Computers and Structures, Berkeley, 1995.

[20] Craiem DO, Rojo FJ, Atienza JM, Guinea GV, Armentano RL, *Fractional calculus applied to model arterial viscoelasticity*, Latin American Applied Research, 38:141–45, 2008.

[21] Coleman BD, *Thermodynamics of materials with memory*, Archive for Rational Mechanics and Analysis, 17: 1–46, 1964.

[22] Cosserat E, Cosserat F, *ThÃ©orie des corps dÃ©formables*, Hermann, Paris, 1909.

[23] Day WA, *Restrictions on relaxation functions in linear viscoelasticity*, The Quarterly Journal of Mechanics and Applied Mathematics, 23: 1–15, 1970.

[24] Demirci N, Tonuk E, *Non-integer viscoelastic constitutive law to model soft biological tissues to in-vivo indentation*, Acta Bioengineering Biomechanics 2014; 16(4): 13–21.

[25] Deseri L, Di Paola M, Zingales M, *Free energy and states of fractional-order hereditariness*, International Journal of Solids and Structures 2014; 51:3156–67.

[26] Deseri L, Di Paola M, Zingales M, Pollaci P, *Power-law hereditariness of hierarchical fractal bones*, International Journal of Numerical Methods Biomedical Engineering, 29(12):1338–60, 2013

[27] Di Mino G, Airey G, Di Paola M, Pinnola FP, D'Angelo G, Lo Presti D, *Linear and non linear fractional hereditary constitutive laws of asphalt mixture*, Journal of Civil Engineering and Management 2013; doi:10.3846/13923730.2014.914104.

[28] Di Paola M, *Fokker–Planck equation solved in terms of complex fractional moments*, Probabilisitic Engineering Mechanics, 38: 70–76, 2014.

[29] Di Paola M, Failla G, Zingales M, *Physically-based approach to the mechanics of strong non-local linear elasticity theory*, Journal of Elasticity, 97:103–130, 2009.

[30] Di Paola M, Failla G, Zingales M, *The mechanically-based approach to 3D non-local linear elasticity theory: Long-range central interactions*, International Journal of Solids and Structures, 47: 2347–2358, 2010.

[31] Di Paola M, Failla G, Zingales M, *Non-local stiffness and damping models for shear-deformable beams*, European Journal of Mechanics A/Solids, 40:69–83, 2013.

[32] Di Paola M, Failla G, Zingales M, *Mechanically based nonlocal Euler-Bernoulli beam model*, Journal of Nanomechanics and Micromechanics, 4(1): A4013002, 2014.

[33] Di Paola M, Heuer R, Pirrotta A, *Fractional visco-elastic Euler-Bernoulli beam*, International Journal of Solids and Structures, 50:3505–10, 2013.

[34] Di Paola M, Pinnola FP, *Riesz Fractional Integrals and Complex Fractional Moments for the Probabilistic Characterization of Random Variables*, Probabilistic Engineering Mechanics, 29: 149–156, 2012.

[35] Di Paola M, Pinnola FP, Spanos PD, *Analysis of multi-degree-of-freedom systems with fractional derivative elements of rational order*, International Conference on Fractional Differentiation and its Applications – ICFDA'14 Catania, 23–25 June 2014.

[36] Di Paola M, Pinnola, FP, Zingales M, *Fractional multi-phase hereditary materials: Mellin transform and multi-scale fractances*, European Congress on Computational Methods in Applied Sciences and Engineering (ECCOMAS 2012), e-Book Full Papers, 4735–4745, 2012.

[37] Di Paola M, Pinnola FP, Zingales M, *A Discrete Mechanical Model of Fractional Hereditary Materials*, Meccanica: an International Journal of Theoretical and Applied Mechanics, 48 (7): 1573–1586, 2013.

[38] Di Paola M, Pinnola FP, Zingales M, *Fractional differential equations and related exact mechanical models*, Computers and Mathematics with Applications, 66 (5): 608–620, 2013.

[39] Di Paola M, Pirrotta A, Valenza A, *Visco-elastic behavior through fractional calculus: An easier method for best fitting experimental results*, Mechanics of Materials, 43: 799–806, 2011.

[40] Di Paola M, Pirrotta A, Zingales M, *Mechanically-based approach to non-local elasticity: Variational principles*, International Journal of Solids and Structures, 47: 539–548, 2010.

[41] Di Paola M, Zingales M, *Exact mechanical models of fractional hereditary materials*, Journal of Rheology, 56 (5): 983–1004, 2012.

[42] D'Lima DD, Steklov N, Fregly BJ, Banks SA, Colwell CW, *In vivo contact stresses during activities of daily living after knee arthroplasty*, Journal of Orthopaedic Research, 26: 1549–1555, 2008.

[43] D'Lima DD, Steklov N, Patil S, Colwell CW, *The Mark Coventry Award: in vivo contact stresses during recreation and exercise activities after knee arthroplasty*, Clinical Orthopaedics and Related Research, 46: 2605–611, 2008.

[44] Eringen AC, *Linear theory of nonlocal elasticity and dispersion of plane waves*, International Journal of Engineering Science, 10: 425–435, 1972.

[45] Eringen AC, *On differential equations of nonlocal elasticity and solutions of screw dislocation and surface waves*, Journal of Applied Physics, 54: 4703–710, 1983.

[46] Failla G, Santini A, Zingales M, *Solution strategies for 1D elastic continuum with long-range interactions: Smooth and fractional decay*, Mechanics Research Communications, 37:13–21, 2010.

[47] Failla G, Santini A, Zingales M, *A non-local two-dimensional foundation model*, Arch. Appl. Mech, 83(2): 253–272, 2013.

[48] Failla G, Sofi A, Zingales M, *A new displacement-based framework for non-local Timoshenko beams*, Meccanica, doi: 10.1007/s11012-015-0141-0, 2015.

[49] Flugge W, *Viscoelasticity*, Massachusetts: Blaisdell Publishing Company; 1967.

[50] Freed AD, Diethelm K, *Fractional calculus in biomechanics: a 3D viscoelastic model using regularized fractional derivative kernels with application to the human calcaneal fat pad*, Biomechanics and Modeling in Mechanobiology, 5:203–15, 2006.

[51] Fuchs MB, *Unimodal beam elements*, International Journal of Solids and Structures, 27(5): 533–545, 1991.

[52] Fuchs MB, *Unimodal formulation of the analysis and design problems for framed structures*, Computer and Structures, 63(4): 739–747, 1997.

[53] Fukunaga M, Shimizu N, *Fractional derivative constitutive models for finite deformation of viscoelastic materials*, Journal of Computational and Nonlinear Dynamics, 10:061002, 2015.

[54] Gerasimov AN, *A generalization of linear laws of deformation and its application to inner friction problems*, Prikl. Mat. Mekh., 12: 251-259, 1949, (in Russian).

[55] Godest AC, Beaugonin M, Haug E, Taylor M, Gregson PJ, *Simulation of a knee joint replacement during a gait cycle using explicit finite element analysis*, Journal of Biomechanics, 35: 267–275, 2002.

[56] Guedes RM, *A viscoelastic model for a biomedical ultra-high molecular weight polyethylene using the time-temperature superposition principle*, Polymer Testing, 30: 294–30, 2011.

[57] Guedes RM, *Analysis of temperature and aging effects on biomedical ultra-high molecular weight polyethylene's grades using a viscoelastic model*, Polymer Testing, 30: 641–650, 2011.

[58] Heymans N, Bauwens JC, *Fractal rheological models and fractional differential equations for viscoelastic behavior*, Rheological Acta, vol. 33, pp. 210-219, 1994.

[59] Hilton HH, *Generalized Fractional Derivative Anisotropic Viscoelastic Characterization*, Materials, 5:169–191, 2012.

[60] Kilbas AA, Srivastave HM, Trujillo JJ, *Theory and Applications of Fractional Differential Equations*, Elsevier, Amsterdam, 2006.

[61] Kobayashi Y, Kato A, Watanabe H, Hoshi T, Kawamura K, Fujie MG, *Modeling of viscoelastic and nonlinear material properties of liver tissue using fractional calculations*, Journal of Biomechanical Science and Engineering, 7(2):117–87, 2012.

[62] Kanai K, *Semi empirical formula for the seismic characteristics of the ground motion*, Bulletin of the Earthquake Research Institute, 35: 309–325, 1957.

[63] Lakes RS, *The time-dependent Poisson's ratio of viscoelastic materials can increase or decrease*, Cellular Polymers, 11:466-469, 1992.

[64] Lakes RS, Wineman A, *On Poisson's ratio in linearly viscoelastic solids*, Journal of Elasticity, 85: 45–63, 2006.

[65] Lakes RS, *Experimental micro mechanics methods for conventional and negative Poisson's ratio cellular solids as Cosserat continua*, Journal of Engineering Materials and Technologies, 113: 144–155, 1991.

[66] Lam DCC, Yang F, Chong ACM, Wang J, Tong P, *Experiments and theory in strain gradient elasticity*, Journal of Mechanics and Physics of Solids, 51: 1477–1508, 2003.

[67] Lei Y, Friswell MI, Adhikari S, *A Galerkin method for distributed systems with non-local damping*, International Journal of Solids and Structures, 43: 3381–3400, 2006.

[68] Lei Y, Murmu T, Adhikari S, Friswell MI, *Dynamic characteristics of damped viscoelastic nonlocal Euler-Bernoulli beams*, European Journal of Mechanics A/Solids, 42:125–136, 2013.

[69] Lin Y, *Probabilistic theory of structural dynamics*, McGraw-Hill, New York, 1967.

[70] McFarland AW, Colton JS, *Role of material microstructure in plate stiffness with relevance to microcantilever sensors*, Journal of Micromechanics and Microengineering, 15: 1060–1067, 2005.

[71] Mourad AHI, Fouad H, Elleithy R, *Impact of some environmental conditions on the tensile, creep-recovery, relaxation, melting and crystallinity behaviour of UHMWPE-GUR 410-medical grade*, Materials and Design, 30: 4112–19, 2009.

[72] Nowacki W, *Theory of asymmetric elasticity*, Pergamon Press, Oxford, Polish Scientific Publishers, Warsaw, 1986.

[73] Nutting PG, *A New General Law of Deformation*, Journal of the Franklin Institute, 191: 679–685, 1921.

[74] Oldham KB, Spainer J, *The Fractional Calculus: Theory and applications of differentiation and integration to arbitrary order*, Academic Press, New York, 1974.

[75] Podlubny I, *Fractional differential equations*, Academic Press, San Diego, 1999.

[76] Poole WJ, Ashby MF, Fleck NA, *Micro-hardness of annealed and work-hardened copper polycrystals*, Scripta Materialia, 34(4): 559–564, 1996.

[77] Qian D, Wagner GJ, Liu WK, Yu MF, Ruoff RS, *Mechanics of carbon nanotubes*, Applied Mechanics Revisions, 55(6): 495-533, 2002.

[78] Quinci F, Dressler M, Strickland AM, Limbert G, *Towards an accurate understanding of UHMWPE visco-dynamic behaviour fornumerical modelling of implants*, Journal of the Mechanical Behavior of Biomedical Materials, 32: 62–75, 2014.

[79] Reddy JN, *An introduction to finite element method*, McGraw Hill, New York, 2006.

[80] Russel DL, *On mathematical models for the elastic beam with frequency-proportional damping*, Control and Estimation in Distributed Parameters Systems, HT Banks, ed, SIAM, Philadelphia, 125–169, 1992.

[81] Samko SG, Kilbas AA, Marichev O.I., *Fractional Integrals and Derivatives - Theory and Applications*, Gordon and Breach Science Publishers.

[82] Schiessel H, Blumen A, *Hierarchical Analogues to Fractional Relaxation Equations*, Journal of Physics A: Mathematical and General, 26: 5057-5069, 1993.

[83] Scott Blair GW, Caffyn JE, *An application of the theory of quasi-properties to the treatment of anomalous strain-stress relations*, The Philosophical Magazine, 40 (300): 80–94, 1949.

[84] Silling SA, Zimmermann M, Abeyaratne R, *Deformation of peridynamic bar*, Journal of Elasticity, 73: 173–190, 2003.

[85] Slonimsky GL, *On the law of deformation of highly elastic polymeric bodies*, Dokl. Akad. Nauk SSSR, vol. 140 (2), pp. 343-346, 1961, (in Russian).

[86] Spanos PD, Evangelatos GI, *Response of a non-linear system with restoring forces governed by fractional derivatives–Time domain simulation and statistical linearization solution*, Soil Dynamics and Earthquake Engineering: 30:811–21, 2010.

[87] Tang PY, *of bend strength increase of graphite by the couple stress theory*, Computers and Structures, 16: 45-49, 1983.

[88] Tajimi H, *A statistical method of determining the maximum response of a building structure during an earthquake*, Proceedings of the 2nd World Conference on Earthquake Engineering, Tokyo, 2: 781–798, 1960.

[89] Tschoegl NW, Knauss WG, Emri I, *Poisson's ratio in linear viscoelasticity - A critical review*, Mechanics of Time-Dependent Materials, 6: 3–51, 2002.

[90] Wang LF, Hu HY, *Flexural wave propagation in single-walled carbon nanotube*, Physical Review B, 71, 195412–195418, 2005.

[91] Yang SQ, Chen L, *Non-stationary and non-linear visco-elastic shear creep model for shale*, International Journal of Rock Mechanics and Mining Science, 48: 1011–20, 2011.

# Acknowledgements

I am enormously grateful to my supervisor, Prof. Mario Di Paola, for his wise guide and his ability to stimulate my curiosity and my desire to study, to improve my knowledge and my ability to solve problems. Many times his help has been very important to simplify problems and to motivate me and my efforts.

A great thanks goes to Dr. Olga Barrera and Prof. Alan C.F. Cocks of the University of Oxford, for their hospitality during my time in Oxford, that was essential to complete my path and to write this thesis.

I wish to thank Prof. Giuseppe Failla, Prof. Antonina Pirrotta and Prof. Massimiliano, Zingales, for their support and their patience in many occasions. Thanks to my colleagues Francesco, Pietro, Gianluca, Salvo, Emma, Natalia, Alberto, Mahdi and Matthew for the friendly moment that helped against many difficulties. I am also thankful to all Ph.D. advisor board and to the members of the Department of Civil, Environmental, Aerospace, and Materials Engineering and to Ruggero Garaffa and Maria Rita Cinà of the Department Library.

An important thanks is addressed to the members of my family and Grazia, that always supported me during difficult periods.

Gioacchino Alotta
Palermo, January 2016